ICACCHE

2nd International Conference on Applications
in Chemistry and Chemical Engineering

BOOK OF PROCEEDINGS

10 - 14 October 2018 **Belgrade**

www.icacche.com

Organized by

Partners

INTERNATIONAL CONFERENCE ON APPLICATION IN CEHMISTRY AND CHEMICAL ENGINEERING (ICACCHE)

ISBN 978-605-67917-2-7

BOOK OF FULL TEXTS OF THE INTERNATIONAL CONFERENCE ON APPLICATION IN CEHMISTRY AND CHEMICAL ENGINEERING (ICACCHE) 10-14 OCTOBER 2018, BELGRADE

Edited by
Prof. Dr. Ömer Şahin

Published, 2018

info@icacche.com
www.icacche.com

SCIENTIFIC COMMITTEE

1. Prof. Dr. İbrahim DİNÇER-University of Ontario
2. Prof. Dr. Gülhayat NASÜN SAYGILI - İstanbul Technical University
3. Prof Dr. İnci EROĞLU- Middle East Technical University
4. Prof. Dr. Mustafa BÖYÜKATA - Bozok University
5. Prof. Dr. Ferdinand Bego - University of Tirana, Albania
6. Prof. Dr. M. Salih AĞIRTAŞ - Yüzüncü Yıl University
7. Prof. Dr. Spiro Drushku - University of Tirana, Albania
8. Prof. Dr. Mahmut DOĞRU - Fırat University
9. Prof. Dr. Ahmet ÖZER - Fırat University
10. Prof. Dr. Muhtar KOCAKERİM - Çankırı University
11. Prof. Dr. Sinan YAPICI - İnonu University
12. Prof. Dr. Tahir Arbneshi - University of Pristina
13. Prof. Dr. İbrahim DİNÇER - Yıldız Teknik Üniversity
14. Prof. Dr. İsmail ÇAKMAK - Kafkas University
15. Prof. Dr. Ahmet KILIÇ - Harran University
16. Prof. Dr. Ahmet Duran ŞAHİN - İstanbul Technical University
17. Prof. Dr. Mustafa DEĞİRMENCİ - Harran University
18. Prof. Dr. Kozeta Vaso - University of Tirana, Albania
19. Prof. Dr. Zübeyde BAYSAL - Dicle University
20. Prof. Dr. Hasan TOĞRUL - Eskişehir Osmangazi University
21. Prof. Dr. Filiz KARAOSMANOĞLU - İstanbul Technical University
22. Prof. Dr. Fikret AKDENİZ - Kafkas University
23. Prof. Dr. Sermet KABASAKAL - Eskişehir Osmangazi University
24. Prof. Dr. Handan KAMIŞ - Selçuk University
25. Prof. Dr. Ülker BEKER - Yildiz Technical University
26. Prof. Dr. Mahmut KUŞ - Selçuk University
27. Prof. Dr. Hafız ALİSOY - Namık Kemal University
28. Prof. Dr. Ömer YAVUZ - Dicle University
29. Prof. Dr. Mesut AKGÜN - Yildiz Technical University
30. Prof. Dr. Birsen Şengul OKSAL - Giresun University
31. Assoc. Prof. Dr.Koray KÖKSAL - Bitlis Eren University
32. Assoc. Prof. Dr. Naser Troni - University of Pristina
33. Assoc. Prof. Dr. Nasrettin GENLİ - Dicle University
34. Assoc. Prof. Dr. M. Zafer KÖYLÜ - Dicle University
35. Assoc. Prof. Dr. Cafer SAKA - Siirt University
36. Assoc. Prof. Dr. Abdurrahman ASAN - Hitit University
37. Assoc. Prof. Dr. Halil DEMİR - Siirt University
38. Assoc. Prof. Dr. A.Abdullah CEYHAN - Selçuk University
39. Assist. Prof. Dr. Yunus ÖNAL - İnönü University
40. Assist. Prof. Dr. Vedat ADIGÜZEL - Kafkas University
41. Assist. Prof. Dr. Mustafa ÖZDEMİR - Süleyman Demirel University

ORGANIZATION COMMITTEE

Honorary Chairs
Prof. Dr. Murat ERMAN – Rector – Siirt University

Conference Chairman
Prof. Dr. Ömer ŞAHİN – Vice Rector– Siirt University

Members of the Committee

- Assist. Prof. Dr. Orhan BAYTAR - Siirt University
- Assist. Prof. Dr. M. Sait İZGİ - Siirt University
- Assist. Prof. Dr. Sabit HOROZ - Siirt University
- Assist. Prof. Dr. Sinan KUTLUAY - Siirt University
- Assist. Prof. Dr. Arzu EKİNCİ - Siirt University
- Assist. Prof. Dr. Dilek KILINÇ - Siirt University
- Teaching assistant Amra Banda - University of Sarajevo
- Teaching assistant Amina Sivac - University of Sarajevo
- Teaching assistant Boris Avdic - University of Sarajevo
- Teaching assistant Edin Hrelja - University of Sarajevo

Secretariat of the Committee

- Research assistant Yavuz KIRIM-Siirt University
  Tel: +90 541 592 38 60 - yavuzkirim@siirt.edu.tr
- Research assistant Tülin Avcı HANSU - Siirt University
  Tel: +90 539 666 00 69 - tulinn_avci@hotmail.com

WELCOME TO ICACCHE 2018

On behalf of the organizing committee, we are pleased to announce that the International Conference on Application in Chemistryand Chemical Engineering (ICACCHE-2018) is heldfrom October 10 to 14, 2018 in Belgrade-SERBİA. ICACCHE 2018 provides an ideal academic platform to present the latest research finding on design, manufacture and operation of plants and machinery, the development of new materials or substances, developing novel materials and processes, analyzing substances, measuring the physical properties of substances and testing theories. This event gives a chance for all the professionals to gain and share information on Chemistry and Chemical Engineering and other related science branches issues and research.

Chemistry and Chemical engineering are multidisciplinary branchs of applied engineering and science consisting of the application of physical science (Chemistry & Physics), life sciences including biochemistry with applied mathematics and economics to produce transform and use of chemicals, molecules materials, energy to make the whole production process successful with economic benefits.

Over the last 50 years, the discoveries in the basic sciences and the engineering of these inventions have been targeted at the development of applied technology and the prosperity of mankind and the distant and high quality of life away from environmental destructions for a sustainable future. Mathematics, physics, chemistry, and biology, which are accepted as basic sciences, and their engineering applications are now accepted in the scientific circles that have been intertwined and one of which is not worthless. It is foreseen by sectoral and academic stakeholders that these interdisciplinary relationships will continue to increase over the next several years.

The ability to identify, model, and solve engineering problems, and the ability to apply engineering knowledge develops with the knowledge of basic sciences. So, in terms of engineering education and the application of the engineering profession, the basic sciences have an important place and the necessary importance should be given.

Our goal is to transform this conference into an exchange of views on future vision and scenarios in chemistry, chemical engineering and related sciences, and to make science a tool of peace and justice.

Best regards,

Prof. Dr. Ömer ŞAHİN

ICACChE
2nd International Conference on Applications in Chemistry and Chemical Engineering
10 - 14 October 2018 Belgrade

The Use of Carbon Nanotube-Supported Co-Cu-B Catalyst in the Hydrolysis of Sodium Borohydride

Orhan Baytar[1], Ömer Şahin, Mehmet Gürsoy

Abstract

The carbon nanotube (CNT) synthesized by the chemical vapor deposition method was used as support material for the Co-Cu-B catalyst. Then, the effect of CNT supported Co-Cu-B catalyst on sodium borohydride hydrolysis was investigated. The effects of CNT/catalyst ratio, $NaBH_4$ concentration, catalyst amount and temperature parameters were investigated in sodium borohydride hydrolysis studies. It was determined that sodium borohydride hydrolysis rate increased with increasing catalyst amount and temperature. The initial hydrogen production rates for carbon nanotube-supported Co-Cu-B and unsupported Co-Cu-B catalyst catalysts were 6325 and 1533 $ml*min^{-1}*g^{-1}$, respectively. Decomposition kinetics and activation energy of sodium borohydride were determined. The order of kinetic and activation energy of sodium borohydride hydrolysis were determined as 0.14 and 53.5 $kj*mol^{-1}$ respectively. The carbon nanotube synthesized by us was found to increase the active surface area of the Co-Cu-B catalyst used in the hydrolysis of sodium borohydride and to be used in applications

Keywords: sodium borohydride, carbon nanotubes supported

1. GİRİŞ

Mevcut olan fosil yakıtların tükenmesi ve aynı zamanda neden olduğu küresel ısınma ve çevre kirliliği temiz ve sürdürülebilir bir enerji sistemine olan talebi artırmaktadır [1]. Alternatif bir yakıt olarak hidrojen düşünülebilir çünkü hidrojen enerjisi temiz ve sıfır emisyon nedeniyle geleceğin enerjisi olarak bakılmaktadır [2]. Bu yüzden güvenli ve pratik kullanışlı bir hidrojen üretim sistemine ihtiyaç vardır. Hidrojenin yanabilirliği ve depolama problemi nedeniyle üretimi, depolanması ve tüketimi oldukça zordur. Bunun için metal hidritin kararlı hale getirilmiş sulu bir çözeltisi, hidrojen depolanması için uygun bir malzeme olarak düşünülebilir [3]. Metal hidritler $NaBH_4$, NaH, CaH_2, MgH_2, $LiAlH_2$ gibi bileşiklerdir [4]. Bu metal hidritler arasında en avantajlı ve dikkat çekici olan NaBH4 dür ve bu avantajlar şunlardır; (i) yüksek hidrojen depolama kapaistesi(%10,8), (ii) yüksek pH'lerde yüksek stabilitesi ve yanmazlığı, (iii) destekli katalizörler ile hidrojen üretim hızı üzerindeki optimum kontrol, (iv) düşük sıcaklıkta bile kabul edilebilr hidrojen üretim hızı, (v) kullanılabilirlik ve kullanım kolaylığı[5], (vi) Elde edilen 4 mol hidrojenin 2 molunun sudan gelmesi ve aşağıdaki reaksiyon ile hidrojen elde edilecektir[6].

$NaBH_4(aq) + 2\ H_2O(l) \rightarrow NaBO_2 + 4\ H_2(g)$

Sodyum bor hidrürün kendi kendine hidrolizi yüksek pH değerlerinde olmamaktadır. Bu yüzden sodyum bor hidrür hidrolizi uygun katalizör varlığında gerçekleşmektedir. Sodyum bor hidrür hidrolizinde Co-B-P[7], Co-W-B[8], Co-Cu-B[9], $Ce_{0.05}$-Ni-W-B[10], Karbon nanotüp destekli CoB[11], Karbon destekli Ru[12] gibi birçok katalizör kullanılmaktadır. Katalizörlerin aktivitesi partikül boyutu ve yüzey alanıyla doğrudan bağlantılı olup küçük partikül boyutu ve yüksek yüzey alanına sahip katalizör reaktant ile daha çok temas ettiğinden dolayı daha etkilidir.

[1] Corresponding author: Siirt University, Faculty of Engineering, 56100 Siirt, Turkey. baytarorhan@gmail.com

Reaksiyon hızını önemli derecede arttırmak için yüksek miktarda katalizör kullanılması gerekmektedir. Bu yüzden yüksek yüzey alana sahip bazı materyaller destek malzemesi olarak kullanılmaktadır [13].

2. DENEYSEL

Katalizör Hazırlanması

Karbon nanotüp destekli Co-Cu-B katalizörü kimyasal emdirme ve indirgenme metoduyla hazırlandı. Katalizör hazırlanma prosedürü; belli bir miktarda $CoCI_2.6H_2O$ ve $CuCI_2.2H_2O$ 50 ml etil alkol çözündü daha sonra gerekli miktar karbon nanotüp eklenip 24 saat oda sıcaklığında metallerin karbon nanotüp'e emdirilmesi sağlandı. Daha sonra ortamdaki etil alkol 50 ^oC'de uzaklaştırıldı ve metal emdirilmiş karbon nanotüp üzerine 50 ml saf su eklenerek buz banyosunda bırakıldı. Toplam metal mollerinin 5 katı kadar olacak şekilde hazırlanan $NaBH_4$ çözeltisi metal emdirilmiş karbon nanotüp üzerine azot gazı ortamında damla damla eklendi. Elde edilen katalizör süzüldü ve birkaç kez saf su en son olarak ta susuz etil alkol ile yıkandı. Sentezlenen katalizör azot ortamında 80 ^oC de 6 saat boyunca kurutuldu. Elde edilen katalizör $NaBH_4$ hidrolizinde kullanılmak için kapalı bir kapta azot ortamında muhafaza edildi.

3. BULGULAR VE TARTIŞMA

Metal/aktif karbon Oranı Etkisi

Co-Cu-B/aktif karbon oranı (%5-20 Co-Cu-B yüklenmiş) etkisi; 10 ml çözelti %2,5 $NaBH_4$+%2 NaOH, 30 ^oC sıcaklıkta ve 100 mg katalizör varlığında incelenmiştir. Hidrojen başlangıç hızının % Co-Cr-B ile değişimi Şekil 1'de verilmiştir.

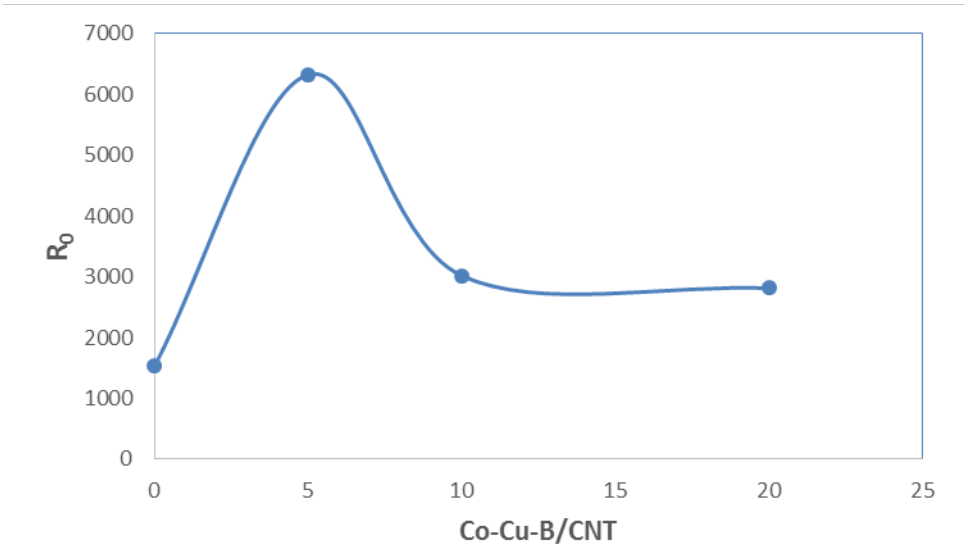

Şekil 1: Hidrojen başlangıç üretim hızının CNT üzerine yüklenmiş Co-Cu-B miktarı ile değişimi

Şekil 1'ten $NaBH_4$ hidrolizinde desteksiz üretilen Co-Cu-B katalizörün hidrojen başlangıç üretim hızının 1533 $mlg^{-1}.dk.^{-1}$ iken %5 Co-Cu-B yüklenmiş karbon nanotüp destekli katalizörün hidrojen üretim hızının ise 6325 $mlg^{-1}.dk.^{-1}$ olduğu görülmektedir. Bu durumun muhtemel nedeni aktif olan Co-Cu-B katalizörünün destekli karbon nanotüp ile yüzey alanının artması ve karbon nanotüp yüzeyinde aktif bölgelerin artmasıdır. % 5'den daha büyük miktarlarda hidrojen başlangıç üretim hzıının azaldığı görülmektedir. Bu durumun muhtemel nedeni Co-Cu-B miktarı arttıkça karbon nanotüp yüzeyinde çok tabakalı katalizör katmanları olmasından kaynaklanmaktadır.

$NaBH_4$ Konsantrasyonu Etkisi

Sodyum borhidrürün hidrolizi sadece katalizör etkinliğine bağlı değil aynı zamanda $NaBH_4$ konsantrasyonu, katalizör miktarı ve sıcaklık gibi faktörlere de bağlıdır. 10 ml çözelti ortamında %2 NaOH konsantrasyonu,

100 mg karbon nanotüp destekli Co-Cu-B katalizör (%5 Co-Cu-B yüklenmiş) ve 30 ºC sıcaklık ortamında farklı konsantrasyonlarda $NaBH_4$ hidrolizi incelenmiştir. Farklı $NaBH_4$ konsantrasyonlarda zaman ile açığa çıkan hidrojen hacmi Şekil 2 te verilmiştir.

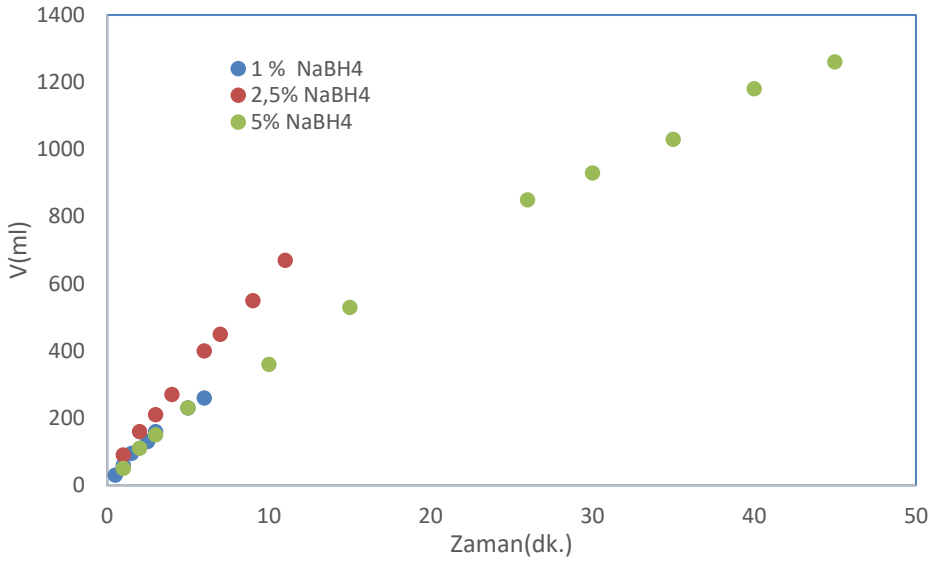

Şekil 2: Farklı NaBH4 konsantrasyonları için zamanla hidrojen hacminin değişim grafiği

Şekil 2'den görüldüğü gibi $NaBH_4$ konsantrasyonu arttıkça hidrojen üretim başlangıç hızı azaltmaktadır. Özellikle $NaBH_4$ konsantrasyonu %5 olduğunda hidrojen üretim hızında çok ciddi bir azalma söz konusudur. Bu durumun muhtemel nedeni $NaBH_4$ ve $NaBH_4$'ün hidrolizinde yan ürün olan $NaBO_2$ sudaki çözünürlülüğün sınırlı olmasıdır. Bu durumun diğer bir nedeni ise ortamda bulunan $NaBH_4$ ve $NaBO_2$ konsantrasyonlarının yüksek olması sonucu çözeltinin vizkositenin artması buda çözelti ortamında bulunan sodyum borhidrürün katalizör yüzeyine olan kütle transferini yavaşlatmaktadır.

Katalizör Miktarı Etkisi

Sodyum borhidrür hidrolizine 10 ml çözelti %2,5 $NaBH_4$ + %2 NaOH konsantrasyonunda 30 ºC sıcaklıkta farklı miktarlarda katalizör etkisi incelenmiştir. Farklı katalizör miktarı için zaman ile üretilen hidrojen hacmi Şekil 3'de verilmiştir.

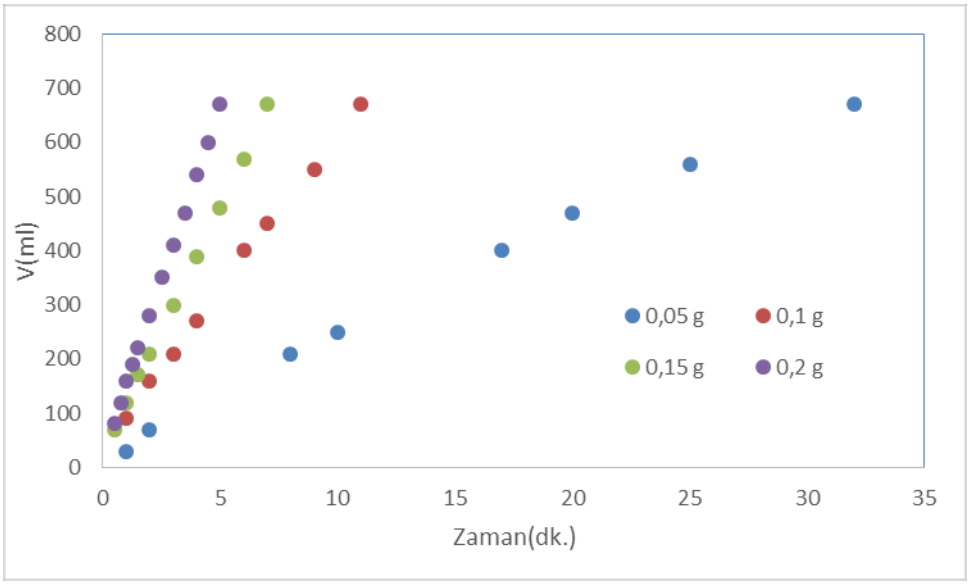

Şekil 3: Farklı katalizör miktarların için zaman ile hidrojen hacminin değişim grafiği

Şekil 4'den görüldüğü gibi katalizör miktarı arttıkça hidrojen hızı da artmaktadır. Bu sonuçta sodyum borhidrürün hidrolizinin katalizör kontrollü olduğunu göstermektedir.

Çözelti Sıcaklığının Etkisi

Sodyum borhidrür hidrolizine sıcaklığın etkisi 20-50 °C aralığında 10 ml çözelti %2,5 $NaBH_4$ + %2 NaOH konsantrasyonu ve 100 mg karbon nanotüp destekli Co-Cu-B(%5 Co-Cu-B yüklenmiş) katalizör varlığında incelenmiştir. Farklı sıcaklıklarda zamanla üretilen hidrojen hacminin değişimi şekil 4'te verilmiştir.

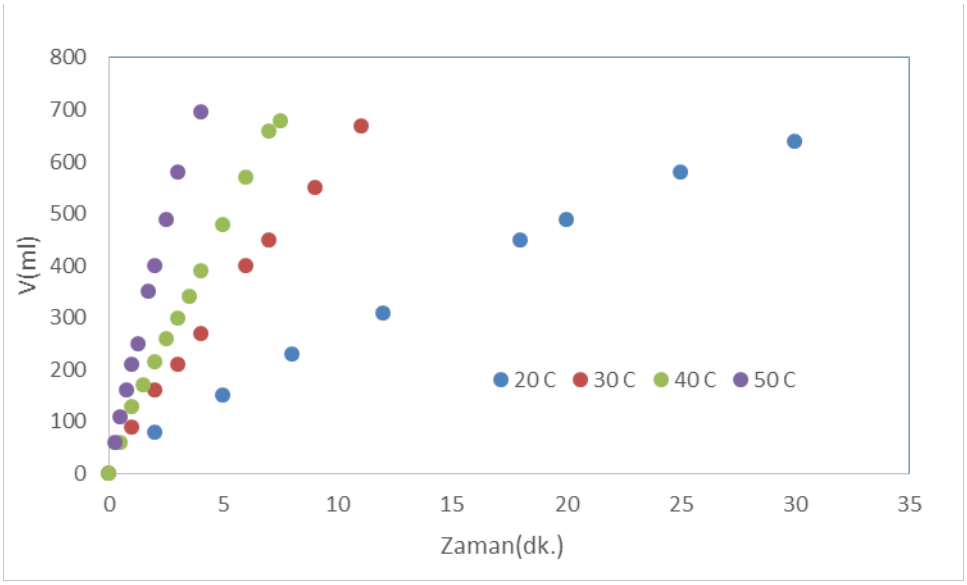

Şekil 4: Farklı sıcaklıklar için zaman ile hidrojen hacminin değişim grafiği

Şekil 4'den görüldüğü gibi sıcaklık arttıkça sodyum bor hidrürün hidrolizinde elde edilen hidrojen hacminde ciddi bir artış olmaktadır. Şekil 4'ten görüldüğü gibi %2,5'lik sodyum bor hidrür hidrolizi 20 °C de 30 dakikada 30 °C 'de 12 dakikada ve 50 °C de 4 dakika zarfında reaksiyon tamamen gerçekleşmektedir.

Farklı sıcaklıklarda herhangi bir reaksiyonun yürüyüşünü ölçülmesindeki en temel sebeplerden bir tanesi de reaksiyon hız sabitinin belirlenmesi ve buna bağlı olarak reaksiyonun gerçekleşmesi için gerekli olan aktivasyon enerjisinin belirlenmesidir. Bu nedenle öncelikle farklı sıcaklıklardaki hız sabitlerini belirlemek üzere n. derecede bir reaksiyon baz alınmış olup bu reaksiyona ait reaksiyon hız sabiti aşağıda verilen eşitlikle belirlenmiştir.

$$\frac{1}{n-1}\left(\frac{1}{C_A^{n-1}}-\frac{1}{C_{A_0}^{n-1}}\right)=kt \qquad 1$$

Eşitlik 1 düzenlenirse Eşitlik 2 elde edilir.

$$\frac{1}{C_A^{n-1}}=(n-1)kt+\frac{1}{C_{A_0}^{n-1}} \qquad 2$$

Eşitlik 2'ye göre $\frac{1}{C_A^{n-1}}$ karşın t grafiğinde eğimden reaksiyon hız sabiti k farklı sıcaklıklar için bulunur. Fakat bu eşitlik uygulanırken n değerleri o şeklide seçilir ki regrasyon katsayısı 1'e yakın olana kadar değiştirilir. En uygun n değeri belirlendikten sonra elde edilen eğrinin eğiminden k bulunur.

Yukarıdaki prosedür dahilinde en uygun hız derecesi 0.14 olarak belirlenmiştir. Farklı sıcaklıklarda bulunan hız sabitleri aşağıdaki tabloda verilmiştir. Farklı sıcaklıklarda bulunan bu hız sabitleri aşağıda verilen arhenius eşitliği ile aktivasyon enerjisi belirlenmiştir.

Sıcaklık(°C)	Hız sabiti,k($mlg^{-1}.dk.^{-1}$)	Derece
20	0.0246	0.14
30	0.0688	0.14
40	0.1058	0.14
50	0.2148	0.14

$$k=Ae^{\frac{-E}{RT}} \qquad 3$$

Eşitlik lineerleştirildiğinde Eşitlik 4 elde edilir.

$$\ln(k) = lnA - \frac{E}{RT} \quad (4)$$

Eşitlik 4'e göre ln(k)-1/T grafiği(Şekil 5) çizildiğinde elde edilen doğrunun eğiminden $NaBH_4$'ün karbon nanotüp destekli Co-Cu-B katalizörü varlığındaki hidrolizi için gerekli olan aktivasyon enerjisinin 53.5 kj/mol olduğu belirlenmiştir.

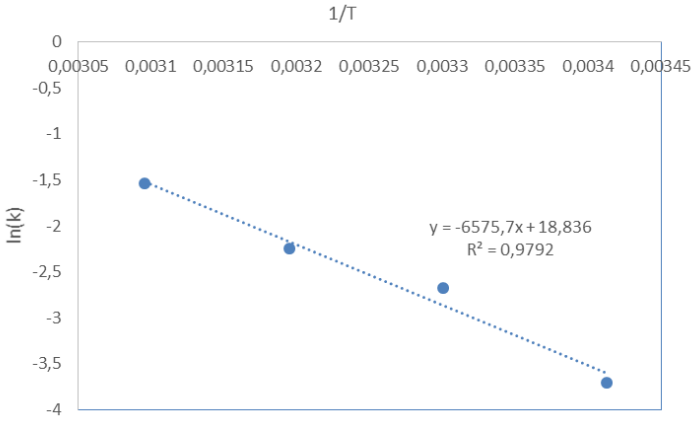

Şekil 5: ln(k)-1/T ile değişim grafiği

4. SONUÇLAR

Bu çalışmada NaBH4'ün hidrolizinde kullanılmak için karbon nanotüp destekli Co-Cu-B katalizörü hazırlanmıştır. Sentezlenen karbon nanotüp destekli Co-Cu-B katalizörün hidrojen üretim 6325 $mlg^{-1}.dk.^{-1}$ iken desteksiz Co-Cu-B katalizörün hidrojen üretim hızı ise 1533 $mlg^{-1}.dk.^{-1}$ olduğu tespit edilmiştir. Co-Cu-B katalizörünün karbon nanotüp yüzeyine tutulmasıyla aktivitesinin yaklaşık olarak 4 kat arttığı belirlenmiştir. Karbon nanotüp destekli Co-Cu-B katalizörün $NaBH_4$ hidrolizinde kullanılmasında; Co-Cu-B/aktif karbon oranı, $NaBH_4$ konsantrasyonu, katalizör miktarı ve sıcaklığın etkisi incelenmiştir. %5 Co-Cu-B yüklenmiş katalizörün hidrojen üretim hızının daha iyi olduğu belirlenmiştir. Artan NaBH4 konsatrasyonu ile hidrojen üretim hızının azalırken artan katalizör miktarı ile hidrojen üretim hızının arttığı tespit edilmiştir. Artan sıcaklık ile hidrojen üretim hızının çok ciddi şekil arttığı belirlenmiştir. $NaBH_4$ hidrolizinin karbon nanotüp destekli Co-Cu-B katalizör varlığında bozunma kinetiğinin 0.14. olduğu ve aktivasyon enerjisinin ise 53,5 kJ/mol olduğu belirlenmiştir.

KAYNAKLAR

1. Zhu J., Li R., Niu W., Wu Y., Gou X., Facile hydrogen generation using colloidal carbon supported cobalt to catalyze hydrolysis of sodium borohydride, Journal of Power Sources 211 (2012) 33-39.
2. Luo W., Campbell P. G., Zakharov L. N., Liu S., A Single-Component Liquid-Phase Hydrogen Storage Material, Journal of the American Chemical Society, 133 (48) (2011) 19326–19329.
3. Crisafulli C., Scire` S., Zito R., Bongiorno C., Role of the Support and the Ru Precursor on the Performance of Ru/Carbon Catalysts Towards H_2 Production Through $NaBH_4$ Hydrolysis, Catalysis Letters, 142 (2012) 882–888.
4. Rakap M., Kalu E. E., Özkar S., Cobalt–nickel–phosphorus supported on Pd-activated TiO2 (Co–Ni–P/Pd-TiO_2) as cost-effective and reusable catalyst for hydrogen generation from hydrolysis of alkaline sodium borohydride solution, Journal of Alloys and Compounds 509 (2011) 7016–7021.
5. Lee J., Kong K. Y., Jung C. R., Cho E., Yoon S. P., Han J., A structured Co–B catalyst for hydrogen extraction from $NaBH_4$ solution, Catalysis Today, 120 (2007) 305–310.
6. Şahin Ö., Karakas D., Kaya M., Saka C., The effects of plasma treatment on electrochemical activity of Co-B-P catalyst for hydrogen production by hydrolysis of $NaBH_4$, Journal of the Energy Institute, 90 (2016) 1-10.
7. Ekinci A., Şahin Ö., Saka C., Avci T., The effects of plasma treatment on electrochemical activity of Co-W-B catalyst for hydrogen production by hydrolysis of $NaBH_4$, international journal of hydrogen energy, 38 (2013) 15295 -15301.
8. Izgi M. S., Şahin Ö., Saka C., Hydrogen production from $NaBH_4$ using Co-Cu-B catalysts prepared in methanol: Effect of plasma treatment, international journal of hydrogen energy, 41 (2016) 1600-1608.

9. Saka C., Ekinci A., Şahin Ö., Balbay A., Influence of plasma treatment on $Ce_{0.05}$-Ni-W-B catalyst for hydrogen production by hydrolysis of $NaBH_4$, Journal of the Energy Institute, 89 (2016) 190-198.
10. Huang Y., Wang Y., Zhao R.,, Shen P. K., Wei Z., Accurately measuring the hydrogen generation rate for hydrolysis of sodium borohydride on multiwalled carbon nanotubes/Co–B catalysts, International Journal of Hydrogen Energy, 33 (2008) 7110 – 7115.
11. Crisafulli C., Scire S., Zito R., Bongiorno C., Role of the Support and the Ru Precursor on the Performance of Ru/Carbon Catalysts Towards H_2 Production Through $NaBH_4$ Hydrolysis, Catalysis Letters, 142 (2012) 882–888.
12. Xu D., Dai P., Guo Q., Yue X., Improved hydrogen generation from alkaline $NaBH_4$ solution using cobalt catalysts supported on modified activated carbon" International Journal of Hydrogen Energy, 33 (2008) 7371–7377.
13. Ye W., Zhang H., Xu D., Ma L., Yi B., Hydrogen Generation Utilizing Alkaline Sodium Borohydride Solution and Supported Cobalt Catalyst, Journal of Power Sources, 164 (2007) 544–548.

ICACChE
2nd International Conference on Applications in Chemistry and Chemical Engineering
10 - 14 October 2018 Belgrade

The Synthesis the Active Carbon from the Beech Wood and Investigatıon of Its Effect on the Cr (VI) Adsorption by Surface Response Method

Orhan Baytar[1], Ömer Şahin, A. Abdullah Ceyhan

Abstract

In this study, activated carbon was synthesized from beech wood by chemical activation method using $ZnCl_2$ activator. The effect of impregnation rate, impregnation time, activation temperature and activation time parameters were investigated in the synthesis of activated carbon. Iodine numbers of synthesized activated carbons were determined. Characterization of activated carbon-containing high iodine number was determined by BET, SEM and FTIR devices. The surface area of activated carbon was determined as 908 m^2/g. Adsorption of Cr (VI) using the synthesized activated carbon was investigated by experiment design. Experimental design was performed with Box-Behnken design model of Surface Response Method in Dizayn Expert package program. The effects of temperature, time and initial concentration parameters were investigated in the experimental design. In the surface response method, the experimental design was carried out by selecting the adsorption capacity (qe) response parameter. It was determined that the best model was quadratic by using Box- Behnken design model. The ANOVA table was created and 3D graphics were plotted to examine the effect of the selected parameters on Cr (VI) adsorption. According to the ANOVA table, the initial concentration of the solution was determined as the most effective parameter for Cr (VI) adsorption. According to ANOVA table, it was determined that single parameters were more effective than binary parameters. As a result of the analysis, Box-Behnken model was suitable and regression equation was obtained by regression process with this model. The values of the selected parameters have been optimized with the Box-Behnken design model.

Keywords: Activated carbon, Experiment design, Cr (VI) adsorption

1. GİRİŞ

Boyalar anyonik, katyonik ve iyonik olmayan olarak gruplandıralabilir. Boyalar biyolojik olarak bozundurulmayan organik kompleks bileşiklerdir. Boyaların uzaklaştırılması zor bir işlemdir. Boyar maddelerin sulardan giderilmesi için adsorpsiyon, çöktürme, membran filtrasyonu ve iyon değişimi gibi teknolojiler kullanılmaktadır. Atık sulardan ağır metallerin, organik kirleticilerin ve boyarmaddelerin giderilmesinde hem ekonomik olması hem de etkin giderim sağlaması açısından adsorpsiyon işlemi önemli bir alternatiftir. Suların temizlenmesi işleminde, aktif karbon, silica ve grafen gibi farklı adsorbentler yaygın biçimde kullanılmaktadır [1]. Yüksek yüzey alanı ve gözenekli yapısının yanı sıra yapısında bulunan fonksiyonel gruplar nedeniyle aktif karbon diğer adsorbentlerden çok daha avantajlıdır. Aktif karbon hazırlanmasında iki yöntem vardır. Bunlar, fiziksel aktivasyon ve kimyasal aktivasyondur. Fiziksel aktivasyon, hammaddenin CO_2 veya su buharı ile aktivasyon işlemidir [2]. Kimyasal aktivasyon tek basamaktan oluşur ve $ZnCl_2$, KOH, K_2CO_3, H_3PO_4 gibi aktifleştiricilerin kullanıldığı yöntemdir. Kimyasal aktivasyon yönteminin karbon yüzdesi fiziksel aktivasyondan daha yüksektir. En iyi gelişmiş gözenekli aktif karbonlar kimyasal aktivasyon ile elde edilmektedir [3]. Aktif karbon birçok hammaddeden üretilmektedir.

2. DENEYSEL

Kimyasallar

Deneysel çalışmalarda kullanılan bütün kimyasal malzemeler merck firmasından temin edilmiş ve analitik saflıktadır. Deneysel çalışmalarda deiyonize saf su kullanılmıştır. Aktif karbon üretilmesinde kullanılan kayın ağacı talaşı Konya mobilyacılar sanayisinden temin edilmiştir.

Aktif karbon hazırlanması

Kayın ağacı talaşından $ZnCl_2$ aktifleştiricisi kullanılarak kimyasal aktivasyon yöntemiyle aktif karbon elde edilmiştir. Kayın ağacı talaşı öğütülmüş ve elenmiştir. Kayın ağacı talaşının -500+250 μm partikül boyut aralığındaki kısımları aktif karbon hazırlanmasında kullanılmıştır.

[1] Corresponding author: Siirt University, Faculty of Engineering, 56100 Siirt, Turkey. baytarorhan@gmail.com

Elenen kayın ağacı talaşı kullanılmadan önce de-iyonize saf su ile yıkanarak 80 ^{o}C'deki etüvde 24 saat kurutulmuştur. Kayın ağacı kimyasal aktivasyon ile aktif karbon hazırlanmasında aşağıdaki parametreler incelenmiştir.

- Aktifleştirici/hammadde oranı (impragnasyon oranı) (% 30, 50, 90, 150, 200)
- İmpragnasyon süresi (24 ve 48 saat)
- Aktivasyon sıcaklığı (400, 500, 600 ^{o}C)
- Aktivasyon süresi (30, 60, 90 dk.)

Kimyasal madde emdirilmiş her bir hammadde 24 ve 48 saat bekletildikten sonra süzülmüş ve 80 ^{o}C'de 4 saat kurutulmuştur. Kimyasal emdirilmiş numune aktivasyon için 400, 500, 600 ^{o}C sıcaklık ve 30, 60, 90 dk. süreleri için azot ortamında bekletilerek aktifleştirilmiştir. Oda sıcaklığına kadar soğuyan numune fırından alındıktan sonra öncelikle 0.5 M HCI çözeltisi ile daha sonra ise pH değeri 6-6.5 oluncaya kadar sıcak de-iyonize saf su ile yıkanmıştır. Elde edilen her bir aktif karbonun iyot sayısı belirlenmiştir.

Adsorpsiyonun deney tasarımı ile modellenmesi

Cr(VI) adsorpsiyonu için seçilen yüksek yüzey alanına sahip aktif karbon kullanıldığı adsorpsiyon çalışmaları deney tasarımı kullanılarak modellenmiştir. Deney tasarımında en çok tercih edilen yöntemlerden birisi olan Yüzey Yanıt Yöntemi ve Yüzey Yanıt Yöntemi içerisinde bulunan Box-Behnken tasarım modeli kullanılmıştır. Seçilen aktif karbonlar kullanılarak Cr(VI) birim adsorbent başına adsorplanan madde miktarı (qe) cevap parametresi seçilerek deney tasarımı gerçekleştirilmiştir. İncelenen parametreler ve seviyeleri Çizelge 1 de verilmiştir.

Çizelge 1.Yüzey Yanıt Yönteminde kullanılan faktörlerin etkinlik aralıkları

Parametreler	Kod	En düşük değer	En yüksek değer
Zaman(dk.)	A	60	150
Sıcaklık(^{o}C)	B	20	50
Çözelti başlangıç derişimi(ppm)	C	50	500

Box-Behnken tasarım modeline göre tasarlanan deney koşulları Çizelge 2'de verilmiştir. Yönteme göre 15 faklı deneyden oluşan bir set ortaya çıkmıştır. Her bir deney en az 2 defa tekrarlanarak deney sonuçlarının ortalaması alınmıştır.

Çizelge 2.Yüzey Yanıt Yöntemiyle Box-Behnken tasarımına göre tasarlanan deneysel koşullar

Deney No	Zaman	Sıcaklık	Konsantrasyon	qe
1	105	50	50	33
2	150	50	275	45
3	105	35	275	57
4	150	35	50	33
5	105	20	50	22
6	60	35	50	33
7	60	50	275	29
8	105	35	275	58
9	150	35	500	87
10	105	35	275	58
11	105	20	500	64
12	105	50	500	146
13	60	20	275	37
14	60	35	500	107
15	150	20	275	72

3. BULGULAR VE TARTIŞMA

Aktif karbon karakterizasyonu

Kayın ağacı talaşından $ZnCI_2$ aktifleştiricisi ile hazırlanan aktif karbonların iyot sayıları yüksek olanlar seçilerek BET yüzey alanları tespit edilmiştir. Seçilen aktif karbonlar, yüzey alanları ve gözenek dağılımları Çizelge 3 verilmiştir.

Çizelge 3:.Kayın ağacı talaşından $ZnCI_2$ aktifleştiricis ile üretilen aktif karbonların yüzey alanı ve gözenek dağılımları

Aktif Karbon	Yüzey Alanı(m^2/g)	Toplam Gözenek Hacmi (cc/g)	Mikro Gözenek Hacmi(cc/g)	Ortalama Gözenek Çap Dağılımı(nm)	BJH Adsorpsiyon Ortalaması(nm)
KÇAC85	908	0.463	0.43	1.02	1.497
KÇAC87	868	0.426	0.429	1.02	2.87

$ZnCI_2$ aktifleştiricisi ile hazırlanan KÇAC85 ve KÇAC87 kodlu aktif karbonların yüzey alanlarının sırasıyla 908 ve 868 m^2/g ve toplam gözenek hacmi, mikro gözenek hacmi ve BJH adsorpsiyon ortalaması sırasıyla 0.42-0.465 cc/g, 0.43 cc/g ve 1.496-2.87 nm aralığında değişmektedir. Ortalama gözenek çap dağılımı 1.02 nm olduğu tespit edilmiştir. Bu sonuç hazırlanan aktif karbonların mikro gözenekli yapıda olduğunu göstermektedir.

Şekil 1'da herhangi bir işleme tabi tutulmamış kayın ağacı talaşının(a), % 200 oranında $ZnCI_2$ aktifleştirici ilave edilerek 24 saat bekletilen ancak henüz aktivasyon işlemi uygulanmamış karışımın(b) ve % 200 oranında aktifleştirici emdirilerek 24 saat bekletilen numunenin 500 ^oC sıcaklıkta 90 dakika süre ile aktivasyon işlemine tabi tutulması sonrası ele geçen aktif karbonun(c) SEM görüntüsü verilmektedir.

a

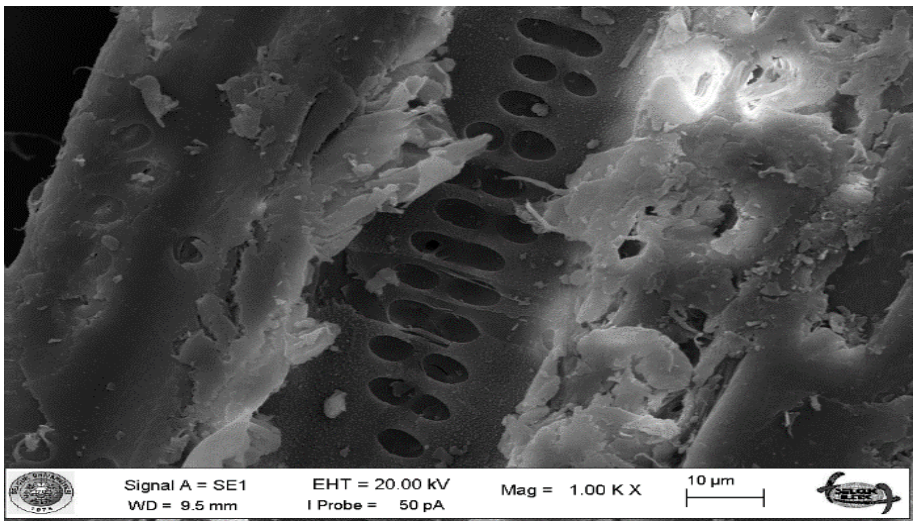

b

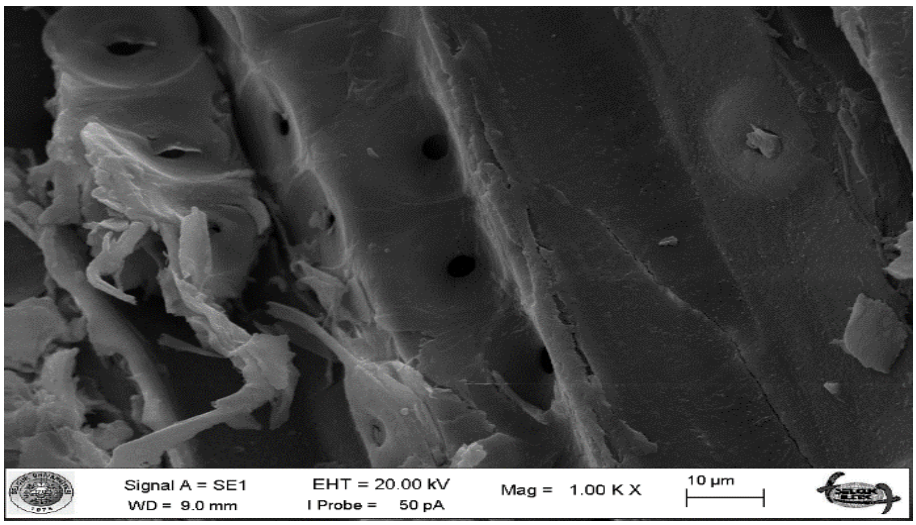

c

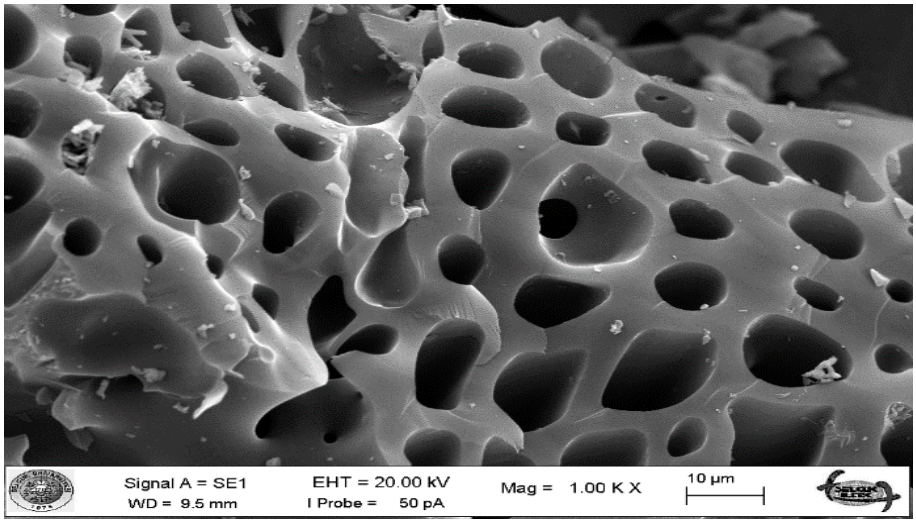

Şekil1: .a-)Kayın ağaçı talaşının b-)% 200 oranında $ZnCI_2$ aktifleştiricisi ile işlem görmüş hammaddenin c-) KÇAC85 kodlu aktif karbonun SEM görüntüleri

Şekil 1(a)'dan görüldüğü gibi kayın ağacı talaşının yüzeyi pürüzlü ve yüzeysel gözeneklere sahiptir. % 200 oranında $ZnCI_2$ aktifleştirici ile işlem görmesinin ardından yüzeyindeki boşlukların aktifleştirici ile dolduğu ve daha pürüzsüz bir şekilde olduğu görülmektedir (Şekil 1(b)). % 200 oranında aktifleştirici emdirilerek 24 saat bekletilen numunenin 500 ^oC sıcaklıkta 90 dakika süre ile aktivasyon işlemine tabi tutulması sonrası hazırlanan aktif karbonun (KÇAC85) homojen gözenek dağılımına ve pürüzsüz bir yüzeye sahip olduğu görülmektedir. Aynı zamanda aktif karbon yüzeyinde çok sayıda mikro ve az sayıda mezo gözeneklerin varlığı da görülmektedir.

Kayın ağacı talaşının, % 200 oranında $ZnCI_2$ aktifleştirici ile karıştırılarak 24 saat emdirilme işlemine tabi tutulan kayın ağacı talaşının ve % 200 oranında $ZnCI_2$ aktifleştiricisi ile 24 saat emdirilme işleminin ardından 500 ^oC'de 90 dakika aktivasyona tabi tutularak hazırlanan aktif karbonun (KÇAC85) 4000-400 cm^{-1} dalga sayısı aralığında taranarak elde edilen FT-IR spektrumları Şekil 2'de verildiği gibidir.

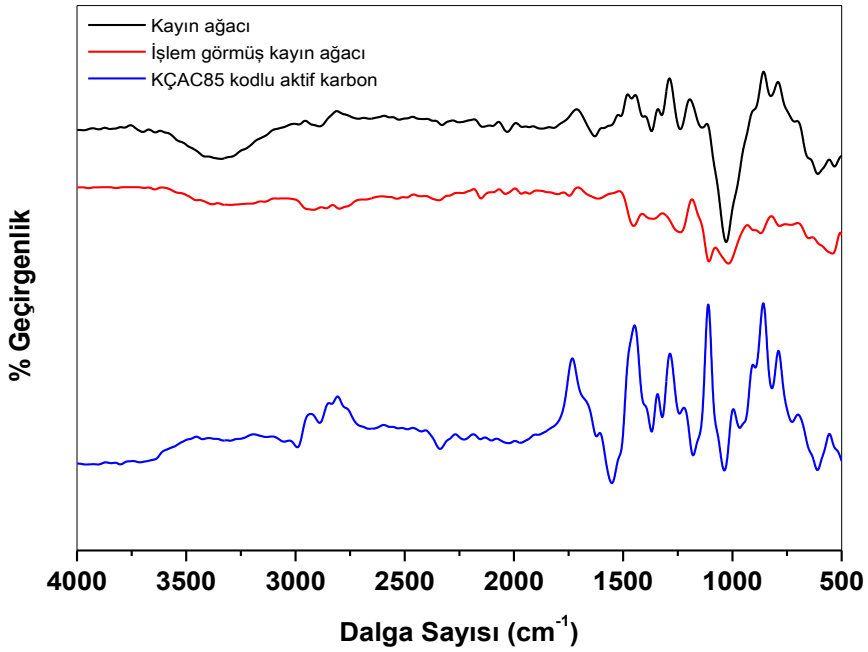

Şekil 2: KÇAC85 kodlu aktif karbonun FT-IR analizi

Şekilde 2'den görüldüğü gibi, işlem görmemiş kayın ağacı talaşının yapısında, 3400-3200 cm^{-1} dalga sayısı aralığında maksimum 3333 cm^{-1} dalga sayısında hidrojen bağlarıyla bağlı hidroksil (–OH) fonksiyonel gruplarından kaynaklanan, 1627 cm^{-1} dalga sayısında olefenik gruplardan kaynaklanan C-C fonksiyonel gruplarının, 1506 cm^{-1} dalga sayısında karboksilik veya lakton gruplarından kaynaklanan C=O fonksiyonel

gruplarınının, 1368 cm^{-1} dalga sayısında aromatik bileşiklerin yapısında bulunan C-C gruplarından kaynaklanan pikler bulunmaktadır. 1000-1300 cm^{-1} dalga sayısı aralığında bulunan sönük pikler yapıda asit, alkol, fenol, ester ve eter gibi gruplarda bulunan C-C ve C-O gruplarının ve 1027 cm^{-1} dalga sayısındaki keskin pik yapıda C-O-C fonksiyonel grubun olduğunu göstermektedir. Şekil 2'den, % 200 oranında aktifleştirici emdirilmesinin ardından kayın ağacı talaşının yapısında yeni fonksiyonel grupların oluştuğu, bazı grupların belirgin hale geldiği ve bazı fonksiyonel grupların da yok olduğu görülmektedir. 3333 cm^{-1} dalga sayısındaki pikin (hidroksil(–O-H) grubundan kaynaklanan) yok olduğu ve 2919 cm^{-1} dalga sayısında C-H grubunun varlığını gösteren pikin daha da belirginleştiği görülmektedir. 2341-2151 cm^{-1} dalga sayısı aralığındaki C=C ve –COOH varlığını gösteren pikler yeni oluşmuş ve sönük bir şekilde olan 1018 cm^{-1} dalga sayısında –C-OH grubunun varlığını gösteren pik keskinleşmiştir. 1018 cm^{-1} dalga sayısında C-O-C fonksiyonel grubunun varlığını gösteren pik de daha keskinleşmiştir. Şekil 2'den görüldüğü gibi, % 200 oranında aktifleştirici emdirilerek 48 saat bekletilen numunenin 500 ^oC sıcaklıkta, 90 dakika süre ile aktivasyon işlemine tabi tutulması sonrası ele geçen aktif karbonun yapısında yeni fonksiyonel grupların oluştuğu, bazı grupların belirgin hale geldiği ve bazı fonksiyonel grupların da yok olduğu görülmektedir. 2919 cm^{-1} dalga sayısında C-H grubunun varlığını gösteren pik belirginleşmiştir. 2332 cm^{-1} dalga sayısında –COOH fonksiyonel gruplarının, 1623 ve 1549 cm^{-1} dalga sayılarında sırasıyla amit ve C=O (karboksilik ve lakton gruplarından kaynaklanan) fonksiyonel gruplarının, 1366 cm^{-1} dalga sayısında –C-CH_3 fonksiyonel gruplarının varlığı görünmektedir. 124 5cm^{-1} dalga sayısındaki pik, karboksilik asitlerin bozulmasıyla oluşan C-O fonskiyonel gruplarının ve 1037 cm^{-1} dalga sayısındaki pik ise –C-OH fonsksiyonel gruplarının varlığını göstermektedir.

Aktif karbon hazırlanmasında parametrelerin etkisi

Kayın ağacı talaşından aktif karbon üretiminde farklı oranlarda $ZnCl_2$/hammadde (% 30, % 50, % 90, % 150 ve % 200) etkisi incelenmiştir. İyot sayılarında artan emdirilme oranı ile birlikte önemli bir artışın olduğu tespit edilmiştir(Tablo gösterilmemiştir). 48 saat emdirilme zamanı, 500 ^oC aktivasyon sıcaklığı ve 90 dakika aktivasyon süresi için emdirilme oranı % 30 olduğunda iyot sayısı 188 mg/g iken, % 200 emdirilme oranı için ise iyot sayısının 1177 mg/g olduğu görülmektedir. Emdirilme oranın artması ile iyot sayısında ortaya çıkan artışın yeni mikro gözeneklerin oluşması ve mevcut mikro gözeneklerin iç yüzeylerinin genişleyerek mezo gözenek formuna geçmesi sebebiyle olduğu düşünülmektedir.

Emdirilme oranının belirlemesinin ardından emdirilme süresinin etkisi de 24 ve 48 saatlik bekleme zamanları için ayrı ayrı incelenmiştir. Emdirilme süresinin uzaması ile iyot sayılarında belirgin bir azalış söz konusu olduğu belirlenmiştir. 500 ^oC aktivasyon sıcaklığı, 90 dakika aktivasyon süresi ve % 200 emdirilme oranında 24 saat emdirilme süresi sonrasında iyot sayısı 898 mg/g iken, emdirilme süresi 48 saat olduğunda iyot sayısı 878 mg/g olarak bulunmuştur. Bu sonuç emdirilme süresinin kısa tutulmasınının gereğini ortaya koymaktadır.

Kayın ağacı talaşından $ZnCI_2$ aktifleştiricisi kullanılarak aktif karbon hazırlanmasında aktifleştirici emdirilmiş maddelerin aktivasyonu 400, 500 ve 600 ^oC olmak üzere 30, 60 ve 90 dakika aktivasyon süreleri için gerçekleştirilmiştir. Aktivasyon sıcaklığının 400 ^oC den 500 ^oC artması ile birlikte iyot sayısının arttığı ve aktivasyon sıcaklığının 600 ^oC olması durumunda ise iyot sayısının azaldığı tespit edilmiştir. 24 saat emdirilme süresi, % 200 emdirilme oranı ve 90 dakika aktivasyon süresi için aktivasyon sıcaklığı 400, 500 ve 600 ^oC'de gerçekleştirilen aktivasyon sonrası bulunan iyot sayılarının sırasıyla 580, 899 ve 687 mg/g olduğu tespit edilmiştir. Kayın ağacı talaşından $ZnCI_2$ aktileştiricisi ile aktifleştirme sonrasında hazırlanan aktif karbon için 400 ^oC'de bulunan iyot sayısının düşük olmasının muhetemel sebebi, mevcut gözeneklerin tam açılması ve yeni gözeneklerin oluşması için aktivasyon sıcaklığının yetersiz kalması olduğu düşünülmektedir. Aktivasyon sıcaklığının 500 ^oC'ye yükselmesi ile mevcut gözenekler gelişmeye ve yeni mikro gözenekler oluşmaya başlamıştır. 600 ^oC'de ise mikro gözenekler genişleyerek mezo gözeneklere dönüşmekte ve mevcut gözenek yapıları çökmektedir.

Kayın ağacı talaşından $ZnCI_2$ aktifleştiricisi kullanılarak aktif karbon hazırlanmasında aktifleştirici emdirilmiş maddelerin aktivasyonu 400, 500 ve 600 ^oC olmak üzere 30, 60 ve 90 dakika aktivasyon süresi için gerçekleştirilmiştir. İyot sayılarının aktivasyon süresinin artması ile birlikte azalış gösterdiği belirlenmiştir. 24 saat emdirilme süresi, % 150 emdirilme oranı ve 600 ^oC aktivasyon sıcaklığında aktivasyon süresi 30, 60 ve 90 dakika olması halinde iyot sayıları sırasıyla 773, 668 ve 664 mg/g olarak bulunmuştur. Kayın ağacı talaşından $ZnCI_2$ aktifleştiricisi ile aktif karbon hazırlanırken yeni gözeneklerin oluşması ve mevcut gözeneklerin gelişmesi için 30 dakika aktivasyon süresi yeterli iken, aktivasyon süresinin artırılması mevcut gözeneklerin genişlemesine ve çökmesine sebep olmaktadır. Bu durum iyot sayısının azalmasına neden olmaktadır.

Kayın ağacı talaşından $ZnCI_2$ aktifleştiricisi ile aktif karbon hazırlanması için maksimum iyot sayısı; % 200 emdirilme oranı, 24 saat emdirilme zamanı, 500 ^oC aktivasyon sıcaklığı ve 90 dakika aktivasyon süresi olduğu şartlarda 898 mg/g olarak belirlenmiştir.

Cr(VI) adsorpsiyonunun Deney Tasarımı ile modellenmesi

Kayın ağacından elde edilen aktif karbon kullanılarak Cr(VI) adsorpsiyon işleminin Yüzey Yanıt Yöntemi ile sayısal modellenmesi gerçekleştirilmiştir. Sayısal modelleme Dizayn Expert paket programı ile tasarlanmıştır. Cr(VI) adsorpsiyon çalışmalarında elde edilen adsorpsiyon kapasitesi sonuçları Çizelge 2'de verildiği gibidir.

Çizelge 2'deki sonuçları verilen her bir deney en az iki kez gerçekleştirilmiş olup sonuçların ortalamaları alınarak kullanılmıştır. Sonuçların Design Expert programı içerisinde yer alan Yüzey Yanıt Yöntemi (Box-

Behnken modelleri) kullanılarak modellenmesinin uygunluğu regresyon katsayıları (R^2) ile değerlendirilmiştir. Elde edilen regresyon katsayıları Çizelge 4'de verildiği gibidir.

Çizelge 0: Cr(VI) adsorpsiyonu için önerilen modellerin uygunluğunun test edilmesi amacıyla verilen regresyon katsayıları

	Doğrusal	İki Faktörlü Etkileşim	Kuadratik	Kübik
R^2	0,5569	0,5352	0,5292	0,9997

Kübik model haricinde, seçilen tüm aktif karbonlar için, en yüksek R^2 değeri doğrusal modele aittir.

Aktif karbon kullanılarak Cr(VI) adsorpsiyon kapasitesi qe'nin, zaman, sıcaklık ve başlangıç derişimi parametrelerinin tekli ve çoklu etkileri altındaki değişimini ifade eden model denklemi doğrusal model yardımıyla çıkartılmış olup Eşitlik 1 'de verildiği gibidir.

$$q_e = -16.53320 + 0{,}130759 * \mathrm{A} + 0{,}483333 * \mathrm{B} + 0{,}166152 * \mathrm{C} \qquad 1$$

Eşitlikte, zaman: A, sıcaklık: B, başlangıç derişimi: C ile verilmektedir. Eşitlik 1 kullanılarak tahmin edilen Cr(VI) adsorpsiyon kapasitesi ile deney sonucu bulunan adsorpsiyon kapasitesi arasındaki ilişki Şekil 3'da verildiği gibidir.

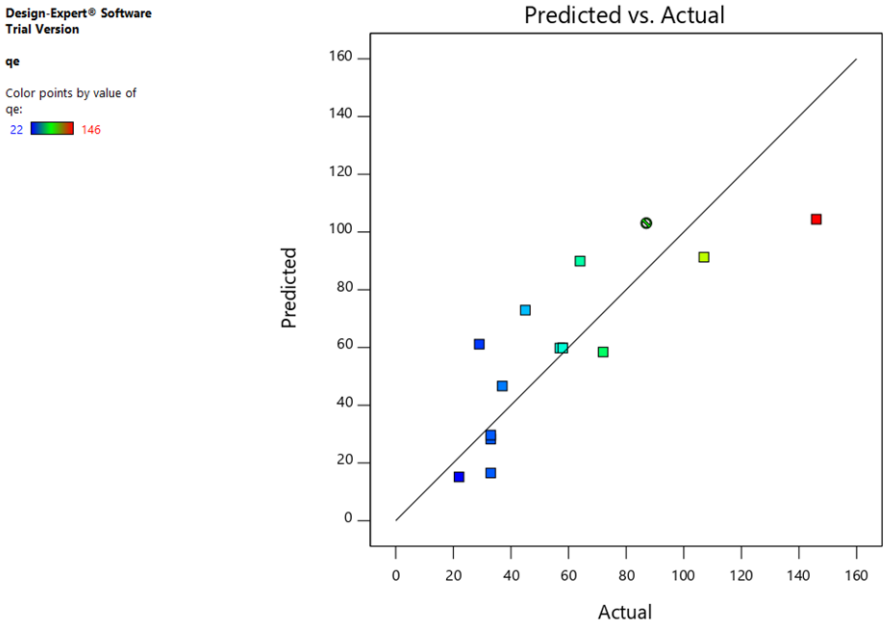

Şekil 3: Cr(VI) adsorpsiyon kapasitesi için deney sonuçları ve model sonuçlarının karşılaştırılması

Şekil 3'den doğrusal model ile tahmin edilen sonuçlarının gerçek deney sonuçlarına yakın olduğu görülmektedir. Bu sonuç, aktif karbonun Cr(VI) adsorpsiyonu işlemi için Eşitlik 1'de verilen model denklemin güvenle kullanılabileceğini göstermektedir.
Seçilen her bir parametrenin tek başına veya birlikte Cr(VI) adsorpsiyon kapasitesine etkilerini belirlemek için doğrusal model içerisinde ANOVA çizelgesi oluşturulmuştur. Elde edilen sonuçlar Çizelge 5'da verildiği gibidir.

Çizelge 5: *Cr(VI) adsorpsiyon kapasitesi için ANOVA tablosu- doğrusal model*

Kaynak	Kareler Toplamı	S.S	Karelerin Ortalaması	F Değeri	p > F	
Model	9872,21	3	3290,74	6,45	0,0105	significant
A-Zaman	234,15	1	234,15	0,4587	0,5136	
B-sıcaklık	420,50	1	420,50	0,8238	0,3854	
C-başlangıç konsantrasyonu	9451,64	1	9451,64	18,52	0,0016	
Residual	5104,65	10	510,46			
Lack of Fit	5103,98	8	638,00	1913,99	0,0005	significant
Pure Error	0,6667	2	0,3333			
Cor Total	14976,86	13				

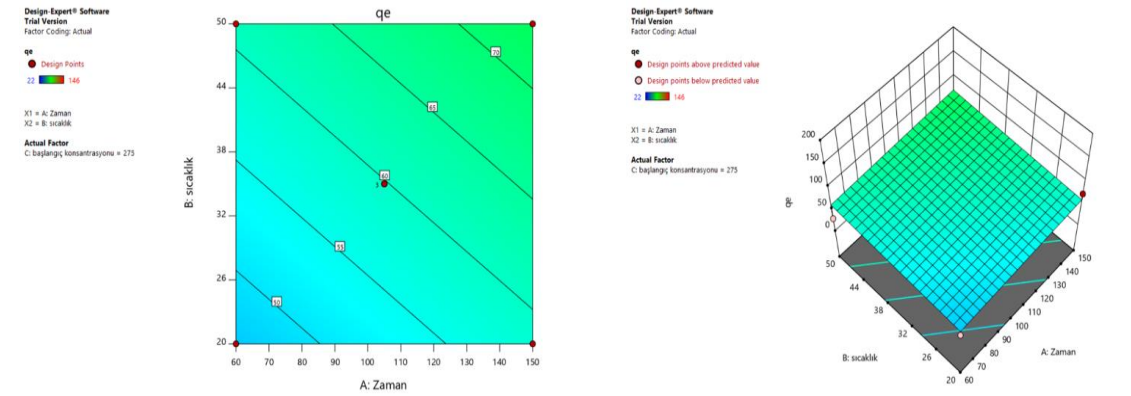

a) zaman-sıcaklık

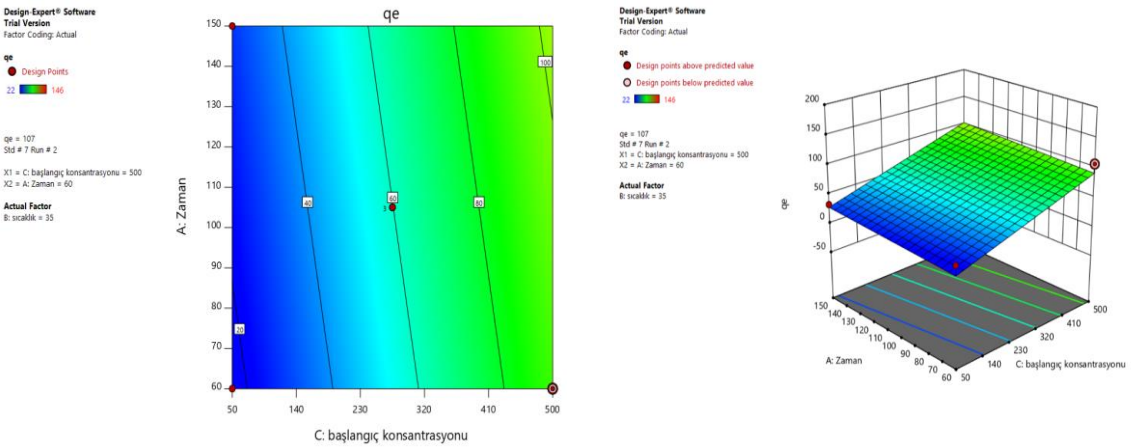

b) zaman-başlangıç derişimi

Şekil 0. *Seçilen parametrelerin aktif karbonun Cr(VI) adsorpsiyon kapasitesine tekli etkisi*

Çizelge 5'dan görüldüğü gibi F değeri en yüksek olan değişken, başlangıç derişimi değişkenidir. Zaman ve sıcaklık F değerleri de dikkate alınacak büyüklüktedir. ANOVA tablosuna göre en etkin parametre başlangıç derişimi olup ve başlangıç derişimi değişkenin değişmesi adsorpsiyon kapasitesinin önemli oranda değişmesine yol açmaktadır. Parametrelerin tekli etkilerine ait 3 boyutlu-kontur grafikleri Şekil 4'de verildiği gibidir. Şekil 4(a)'dan sabit başlangıç derişimi için artan zaman ve sıcaklık ile birlikte Cr(VI) adsorpsiyon kapasitesinde çok değişiklik olmadığı görülmektedir. Bu sonuç ANOVA tablosunda verilen başlangıç derişiminin F değeri ile ilişkili olmaktadır. Cr(VI) adsorpsiyon kapasitesini etkileyen parametre olan başlangıç derişiminin sabit olduğu durumda, artan sıcaklık ve adsorpsiyon zamanının adsorpsiyon kapasitesi üzerine belirgin bir etkisi bulunmamaktadır.

4. SONUÇLAR

Kayın ağacından $ZnCl_2$ aktifleştiricisi kullanılarak kimyasal aktivasyon yöntemiyle aktif karbon sentezlenmiştir. Kayın ağacı talaşından $ZnCI_2$ aktifleştiricisi ile aktif karbon hazırlanmasında maksimum iyot sayısı ve BET yüzey alanı; %200 kimyasal emdirilme oranı, 24 saat emdirilme süresi, 500 ^oC aktivasyon sıcaklığı ve 90 dakika aktivasyon süresi şartlarında 898 mg/g ve 908 m^2/g olarak tespit edilmiştir. Elde edilen yüksek yüzey alanına sahip aktif karbon kullanılarak Cr(VI) adsorpsiyonu deney tasarımı ile incelenmiştir. Deney tasarımı Dizayn Expert programı içerisindeki Yüzey Yanıt Yöntemi Box-Behnken tasarım modeli ile sayısal olarak modellenmiştir. Adsorpsiyon işleminin doğrusal model ile tanımlanmasının uygunluğu tespit edilmiştir. Adsorpsiyon işlemi üzerine en etkin parametrenin ise çözelti başlangıç konsantrasyonu olduğu belirlenmiştir.

KAYNAKLAR

1. Baytar, O. 2015, "İğde Çekirdeği Ve Kayin Ağacindan Üretilen Aktif Karbonun Ağir Metal Ve Boyarmadde Gideriminde Kullanilmasi", Doktora, Selçuk Üniversitesi, Konya
2. Baytar, O., Şahin Ö., Saka C., 2018, "Sequential application of microwave and conventional heating methods for preparation of activated carbon from biomass and its methylene blue adsorption", Applied Thermal Engineering, (138) 542–551.
3. Şahin Ö., Saka C., Ceyhan A. A., Baytar O., 2016," The pyrolysis process of biomass by two-stage chemical activation with different methodolog and iodine adsorption", Energy Sources, Part A: Recovery, Utilization, and Environmental Effects, 12(38), 1756-1762.

ICACChE
2nd International Conference on Applications in Chemistry and Chemical Engineering
10 - 14 October 2018 Belgrade

Comparison of properties of Eu(2+) doped ZnS and Eu(3+) doped ZnS quantum dots

***Sabit HOROZ*[1]**

Abstract

In this study, x-ray diffraction (XRD) and ultraviolet-visible region (UV-Vis) spectroscopy were used to investigate the structural and optical properties of Eu doped ZnS quantum dots synthesized using the wet-chemical method. In the XRD data obtained, it was determined that the Eu doped ZnS quantum dots were in a cubic structure. Furthermore, in the presence of Eu additive, it has been observed that the bandgap energy of the Eu doped ZnS quantum dots is wider than the un-doped ZnS.

Keywords: Characterization, doping, rare-earth ions, synthesis

Eu (2+) katkılı ZnS ve Eu (3+) katkılı ZnS kuantum noktalarının özelliklerinin karşılaştırılması

Özet

Bu çalışmada ıslak-kimyasal yöntemi kullanılarak sentezlenen Eu katkılı ZnS kuantum noktalarının yapısal ve optiksel özelliklerinin incelenmesi için sırasıyla x-ray kırınımı (XRD) ve ultraviolet görünür bölge (UV-Vis) spektroskopisi kullanılmıştır. Elde edilen XRD verilerinde Eu katkılı ZnS kuantum noktalarının kübik yapıda olduğu tespit edilmiştir. Ayrıca Eu katkı maddesinin varlığında Eu katkılı ZnS kuantum noktalarının yasak enerji band aralığının katkısız ZnS'ye oranla daha geniş olduğu gözlemlenmiştir.

Keywords: Karakterizasyon, katkılama, nadir toprak

1. GİRİŞ

Geçmiş yıllarda, II-VI yarıiletken kuantum noktalarının (QD) hazırlanması ve karakterizasyonu, indirgenmiş boyutlarda yeni fiziği ortaya çıkarmış ve yeni materyaller üretme olanağı sağlamıştır. ZnS, optoelektronik ve fotovoltaik enerji uygulamaları için, daha iyi kimyasal stabilitesi ve çevre dostu olması nedeniyle diğer malzemelere kıyasla önemli bir fosfor olarak yaygın kullanılan ve her yerde bulunan yarı iletken malzemelerden biridir [1-2]. Katkılı yarı iletken nanokristaller / QD'ler, yeni bir araştırma alanı ve aynı zamanda nanoyapılı malzemelerin uygulanması için yeni fırsatlar yaratan yeni bir lüminesan materyal sınıfıdır. ZnS nanoparçacıklarının geçiş metali iyonları ile katkılanması, (örneğin Mn^{2+}, Cu^{2+} ve nadir toprak iyonları olan Eu^{3+} / Eu^{2+}) seyreltik manyetik yarıiletkenlere (DMS) neden olabilir. Bu iyonlar manyetik olmayan ev sahibi yarı iletkenin örgü kafesinde rastgele dağılır ve birbirleriyle uzun menzilli değişim etkileşimi ile yerel manyetik momentler oluşturabilir. Böylece, katkılama tipine bağlı olarak ZnS yarı iletken malzemeler paramanyetik veya ferromanyetik davranış gösterebilmektedir [3-5].

Bu çalışmada ıslak-kimyasal yöntemi kullanılarak sentezlenen Eu katkılı ZnS kuantum noktalarının yapısal ve optiksel özelliklerinin incelenmesi için sırasıyla x-ray kırınımı (XRD) ve ultraviolet görünür bölge (UV-Vis) spektroskopisi kullanılmıştır. Elde edilen XRD verilerinde Eu katkılı ZnS kuantum noktalarının kübik yapıda olduğu tespit edilmiştir. Ayrıca Eu katkı maddesinin varlığında Eu katkılı ZnS kuantum noktalarının yasak enerji band aralığının katkısız ZnS'ye oranla daha geniş olduğu gözlemlenmiştir.

[1] Corresponding author: Siirt University, Faculty of Engineering, 56100 Siirt, Turkey. sabithoroz@siirt.edu.tr

2. DENEYSEL YÖNTEM

Eu katkılı ZnS kuantum noktaları ıslak-kimyasal bir yöntem kullanılarak sentezlenmiştir. Zn kaynağı olarak ticari çinko asetat, Eu kaynağı olarak evropiyum klorür ve S kaynağı olarak sodyum sülfür kullanılmıştır. Tipik bir prosedürde, uygun miktarlarda Zn (CH_3COO) $.2H_20$, $EuCl_2$ ve Na_2S sulu çözeltileri, metakrilik asit ve sitrik asit içeren bir çözeltiye eklenmiştir. Daha sonra, sonuçtaki çözelti N_2 altında birkaç saat geri akıtıldı ve oda sıcaklığına kadar soğutuldu. Elde edilen tozlar santrifüj ile ayrıldı ve oda sıcaklığında vakumda kurutuldu. Bu işlem sonucunda Eu^{3+} katkılı ZnS kuantum noktaları sentezlenmiştir. Daha sonra, elde edilen Eu^{3+} katkılı ZnS kuantum noktaları 500 ^{0}C lik sıcaklıkta 2 saat boyunca kalsine edilerek Eu^{2+} katkılı ZnS kuantum noktaları sentezlenmesi gerçekleştirilmiştir.

3. BULGULAR VE TARTIŞMA

Şekil 1 ıslak-kimyasal yöntemi ile sentezlenen ZnS, Eu^{3+} katkılı ZnS ve Eu^{2+} katkılı ZnS kuantum noktalarına ait XRD desenlerini göstermektedir.

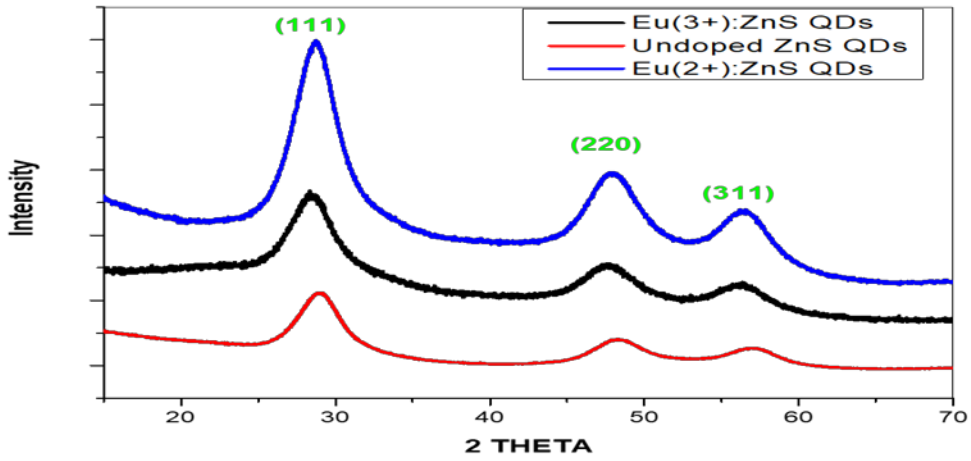

Şekil 1. ZnS, Eu^{3+} katkılı ZnS ve Eu^{2+} katkılı ZnS kuantum noktalarına ait XRD desenleri.

Elde edilen üç geniş kırınım desenlerinin (111), (220) ve (311) düzlemlerine karşılık gelmektedir. XRD kütüphanesinde var olan ZnS'ye ait standart veriler ile elde edilen veriler kıyaslandığında sentezlenen her üç numunenin kübik yapıda olduğu tespit edilmiştir. Eu^{3+} katkılı ZnS ve Eu^{2+} katkılı ZnS kuantum noktalarına ait XRD desenlerinde herhangi bir ekstra piklerinin gözlemlenmemesi sentezleme işleminin başarılı bir şekilde yapıldığının bir göstergesi kabul edilebilir.

ZnS, Eu^{3+} katkılı ZnS ve Eu^{2+} katkılı ZnS kuantum noktalarının parçacık boyutları Eşitlik (1)'de verilen Scherrer bağıntısı kullanılarak belirlenmiştir.

$$d = (k * \lambda)/B * cos\theta \qquad (3.3.1)$$

Burada, d= nanopartikül boyutu nanometre cinsinden, k=yüzey faktörü (genellikle 0.9 olarak kullanılır.), λ= kullanılan XRD cihazının dalga boyu, B= elde edilen pikin yarı yükseklikteki genişliği ve θ= düzlemin gözlendiği Bragg açısıdır. Böylece, ZnS, Eu^{3+} katkılı ZnS ve Eu^{2+} katkılı ZnS kuantum noktalarının parçacık boyutları sırasıyla 3.04 nm, 2.7 nm and, 2.6 nm olarak tespit edilmiştir. Katkılama işleminin bir yarı iletkenin parçacık boyutunun değiştirilmesinde etkin bir rol oynadığı bu sonuç ile gösterilmiştir. Eu katkılı ZnS kuantum noktalarının optik özelliklerini incelemek için ultraviolet görünür bölge $(UV - Vis)$ spektroskopisi kullanılarak optik absorpsiyon ölçümleri yapılmıştır. ZnS, Eu^{3+} katkılı ZnS ve Eu^{2+} katkılı ZnS kuantum noktaları için kaydedilen optik absorpsiyon spektrumları Şekil 2'de gösterilmektedir.

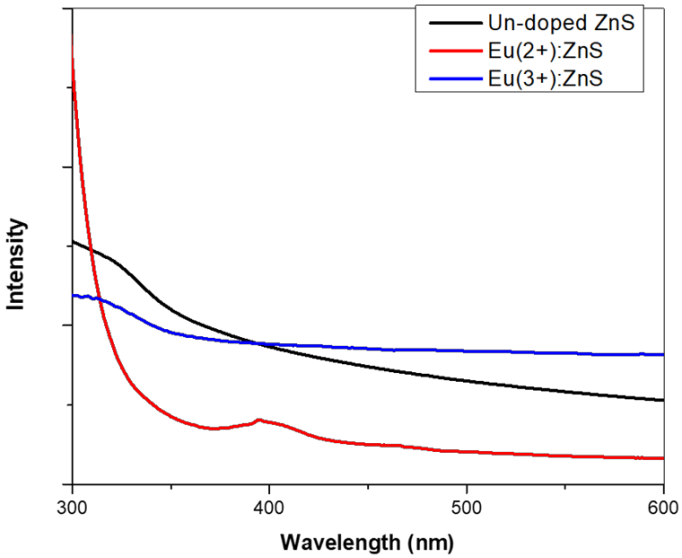

Şekil 2. ZnS, Eu^{3+} katkılı ZnS ve Eu^{2+} katkılı ZnS kuantum noktaları için oda sıcaklığında kaydedilen optik absorpsiyon spektrumları.

Saf ZnS kuantum noktalarına ait optik absorpsiyon spektrumumun 310 nm (4 eV) olduğu gözlemlenmiştir. Bu enerji band aralık değeri bulk ZnS (3.67 eV)'nin enerji band aralığından daha geniştir. Bu durumum muhtemel sebebi kuantum sınırlandırma etkisi ile açıklanabilir. Çünkü kuantum sınırlandırma etkisinde bir yarı iletkenin parçacık boyutu küçüldükçe o yarı iletkenin enerji band aralığı artış göstermektedir. Eu^{3+} katkılı ZnS ve Eu^{2+} katkılı ZnS kuantum noktalarına ait opitk absorpsiyon spektrumları ile saf ZnS kuantum noktalarına ait optik absorpsiyon spektrumu kıyaslandığında parçacık boyutundan dolayı Eu katkılı ZnS kuantum noktalarının saf ZnS'ye nazaran daha geniş bir enerji aralığına sahip oldukları gözlemlenmiştir.

4. SONUÇLAR

Bu çalışmada ZnS, Eu^{3+} katkılı ZnS ve Eu^{2+} katkılı ZnS kuantum noktaları ıslak-kimyasal tekniği kullanılarak sentezlenmiştir. Sentezlenen ZnS, Eu^{3+} katkılı ZnS ve Eu^{2+} katkılı ZnS kuantum noktalarının yapısal ve optik özellikleri sırasıyla XRD ve UV-Vis spektroskopisi kullanılarak incelenmiştir. Elde edilen XRD desenleri sonucunda tüm numunelerin kübik yapıda olduğu tespit edilmiştir. Ayrıca XRD verileri kullanılarak ZnS, Eu^{3+} katkılı ZnS ve Eu^{2+} katkılı ZnS kuantum noktalarının parçacık boyutları sırasıyla 3.04 nm, 2.7 nm and, 2.6 nm olarak hesaplanmıştır. Bu sonuç ile katkılama işleminin kuantum noktalarının parçacık boyutundaki etkisi açıkça görülmüştür. UV-Vis spektroskopisi kullanılarak optik absorpsiyon spektrumları elde edilmiştir. Bu spektrumlar baz alındığında, Eu^{3+} katkılı ZnS ve Eu^{2+} katkılı ZnS kuantum noktalarının saf ZnS kuantum noktalarına kıyasla daha geniş enerji band aralıklarına sahip oldukları tespit edilmiştir. Böylece bu çalışma ile katkılama işleminin ZnS kuantum noktalarının hem parçacık boyutu hem enerji band aralığı üzerindeki etkisi incelenmiştir.

5. KAYNAKÇALAR

[1]- A. L. Rogach, A. Kornowski, M. Gao et al.,J. Phys. Chem. B **103**, 3065 (1999).
[2]- A. P. Alivisatos, Science **271**, 933 (1996).
[3]- L. Wang, X. Xu, X. Yuan, Journal of Luminescence 130, 137 (2010).
4- H.Yang, S.Santra, and P. Holloway, Journal of Nanoscience and Nanotechnology 5, 1364 (2005).
5- W.Q. Peng, S.C. Qu, G.W. Cong, Z.G. Wong, J. Cryst. Growth 282, 179 (2005).
6- W. Chen, J. O. Malm, V. Zwiller, R. Wallenberg and J. O. Bovin, Journal of Applied Physics 89, 2671 (2001).

Biyografi:

1986 yılında Hatay ilinin İskenderun ilçesinde doğdum. Lisans eğitimini 2008 yılında Sivas Cumhuriyet Üniversitesi Fizik Bölümünde tamamladım. Yüksek Lisans ve Doktora eğitimimi 2010-2015 yılları arasında University of Wyoming (A.B.D.) Fizik Bölümünde tamamladım. Halen Siirt Üniversitesi Elektrik-Elektronik Mühendisliği Bölümünde Öğretim Üyesi olarak çalışmaktayım. İlgili Konular; Yoğun madde fiziği, güneş pilleri, yarı iletkenlerin sentezlenmesi ve onların karakterizasyonu.

ICACChE
2nd International Conference on Applications in Chemistry and Chemical Engineering
10 - 14 October 2018 Belgrade

Investigation of the Effect of Synthesis Temperature on the Band Energy of Cds Nanoparticles

Sabit Horoz[1], Ömer Şahin, Arzu Ekinci

Abstract

In our study, we reported the synthesis of un-doped CdS nanoparticles. Samples were prepared by wet-chemical method using 1-thioglycerol as a capping agent at different temperatures. We studied the structural and optical properties of un-doped CdS nanoparticles synthesized at different temperatures. The effect of synthesis temperature on optical properties were discussed.

Keywords: Synthesis, nanoparticles, cadmium sulfide, optical properties

Sentezleme Sıcaklığının CdS Nanopartiküllerin Bant Enerjisine Etkisinin İncelenmesi

Özet

Çalışmamızda, katkısız CdS nanopartiküllerinin sentezini bildirdik. Numuneler, farklı sıcaklıklarda bir ajan maddesi olarak 1-tiyogliserol kullanılarak ıslak-kimyasal yöntemle hazırlandı. Farklı sıcaklıklarda sentezlenen katkısız CdS nanopartiküllerin yapısal ve optik özellikleri incelendi. Sentez sıcaklığının optik özellikler üzerindeki etkisi tartışıldı.

Keywords: Sentez, nanopartiküller, kadmiyum sülfit, optik özellikler

1. GİRİŞ

Son zamanlarda, II-IV bileşiklerinin mono dispersiyonlu nanopartiküllerinin sentezi ve karakterizasyonunda büyük dikkat çekilmiştir. Bunun nedeni, nanometre aralığındaki parçacıkların optik, elektronik ve termodinamik özelliklerinin, genellikle kuantum sınırlandırma etkisine bağlı olarak bulk malzemelerin optik, elektronik ve termodinamik özelliklerinden farklı olmasıdır. Bu benzersiz özelliklerinden dolayı nanopartiküller Teknolojik uygulamalarda büyük potansiyele sahiptirler. Örneğin; bu benzersiz özellikler, düzensiz DNA yapıları için optoelektronik problar, peptidlerde floresan probları gibi ilginç doğrusal ve doğrusal olmayan optik özelliklere neden olabilir [1-3]. Bu II-VI yarı iletkenler arasında, kadmiyum sülfür (CdS), 515 nm'de optik bir kesime karşılık gelen 2.42 eV'lik bir doğrudan bant boşluğuna sahiptir. Bu özelliğinden dolayı CdS'ler fotonik, fotovoltaik ve fotokatalizde gibi farklı uygulamalarda katalizör olarak geniş bir şekilde kullanılmaktadır.

CdS nanopartiküller bulk CdS'lerekıyasla farklı fiziksel, optiksel, kimyasal ve yapısal özellikler göstermektedirler. Bu özellikler, parçacık büyüklüğünden kuantum hapsi etkisinden etkilenir. Örneğin, bant boşluğu ve böylece bant kenarı emilimi doğrudan parçacık büyüklüğü tarafından kontrol edilir [4-5].

Çalışmamızda, katkısız CdS nanopartiküllerinin sentezini bildirdik. Numuneler, farklı sıcaklıklarda bir ajan maddesi olarak 1-tiyogliserol kullanılarak ıslak-kimyasal yöntemle hazırlandı. Farklı sıcaklıklarda sentezlenen katkısız CdS nanopartiküllerin yapısal ve optik özellikleri incelendi. Sentez sıcaklığının optik özellikler üzerindeki etkisi tartışıldı.

[1]Corresponding author: Siirt University, Faculty of Engineering, 56100 Siirt, Turkey. sabithoroz@siirt.edu.tr

2. DENEYSEL YÖNTEM

Katkısız CdS nanopartikülleri sentezlemek için ticari Cd $(CH_3COO)_2$. $2H_2O$ ve Na_2S kullanıldı. Sentezlenmiş nanopartiküllerin herhangi bir kümeleşmesini önlemek için, başlık ajanı olarak 1-tiyogliserol kullanılmıştır. Tipik bir ıslak-kimyasal yöntemde, 0.1 M Cd $(CH_3COO)_2$. $2H_2O$, 40 ml dimetil sülfoksit (DMSO) içine çözülmüş, daha sonra karışıma 0.5 ml 1-tiyogliserol damla damla eklenmiştir. Reaksiyon karışımı, 55-130 °C aralığındaki istenen sıcaklıkta ısıtıldı ve sonra 10 ml sulu Na2S çözeltileri, yukarıdaki çözeltiye enjekte edildi. Çözelti, birkaç saat boyunca sabit bir sıcaklıkta geri akışa alındıktan ve oda sıcaklığına kadar soğutulduktan sonra, CdS nanopartiküller, aseton ilave edilerek çözeltiden ayrıldı. Daha sonra numuneler santrifüj edildi ve kümelerin dışında kalan reaksiyona girmemiş iyonlardan kurtulmak için birkaç kez durulandı.

3. BULGULAR VE TARTIŞMA

Şekil 1 farklı sıcaklıklarda ıslak-kimyasal yöntemi ile sentezlenen CdS nanopartiküllere ait x-ray kırınım (XRD) desenlerini göstermektedir.

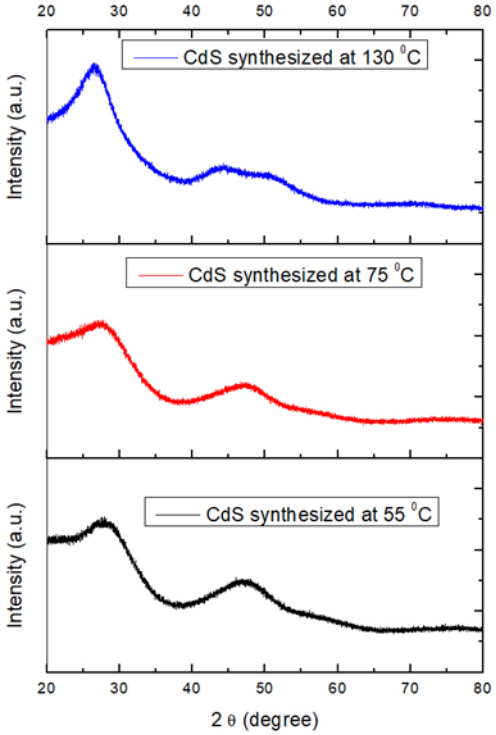

Şekil 1. Farklı sıcaklıklarda sentezlenen CdS nanopartiküllere ait kaydedilen XRD desenleri.

130 ^{0}C'de hazırlanan CdS nanopartiküllerin XRD desenleri, kübik fazın (111), (220) ve (311) kafes düzlemlerinden üç geniş tepe noktası gösterirken, 55 ^{0}C ve 75 ^{0}C'de hazırlanan numuneler sadece iki geniş difraksiyonun tepe noktasını göstermektedir. Sentezleme sıcaklığı düştükçe (220) ve (311) düzlemlerine karşılık gelen XRD piklerinin birleştiği gözlemlenmiştir. Bunun muhtemel sebebi sentezlenme sıcaklığındaki düşüşün parçacık boyutunda ki düşüşe sebep olmasıdır. Farklı sıcaklıklarda sentezlenen CdS nanopartiküllerin parçacık boyutu XRD verileri taban alınarakEşitlik (1)'de verilen Scherrer bağıntısı kullanılarak belirlenmiştir.

$$d = (k * \lambda)/B * cos\theta \qquad (3.3.1)$$

Burada, d= nanopartikül boyutu nanometre cinsinden, k=yüzey faktörü (genellikle 0.9 olarak kullanılır.), λ= kullanılan XRD cihazının dalga boyu, B= elde edilen pikin yarı yükseklikteki genişliği ve θ= düzlemin gözlendiği Bragg açısıdır. 55 °C, 75 °C ve 130 °C'de hazırlanan numuneler için ortalama parçacık boyutu sırasıyla 1.7 nm, 2.1 nm ve 2.7 nm olarak tespit edilmiştir.

CdS nanopartiküllerin optik özelliklerini incelemek için ultraviolet görünür bölge $(UV - Vis)$ spektroskopisi kullanılarak optik absorpsiyon ölçümleri yapılmıştır. Farklı sıcaklıklarda

sentezlenen CdS nanopartiküller için kaydedilen optik absorpsiyon spektrumları Şekil 2'de gösterilmektedir.

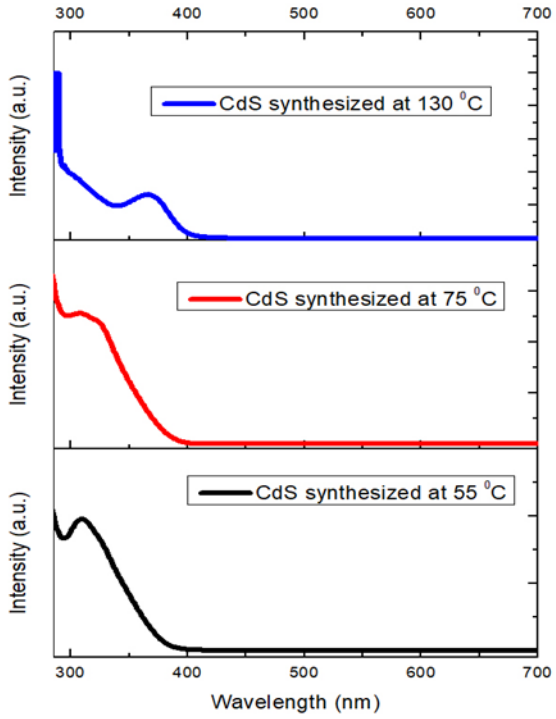

Şekil 2. Farklı sıcaklıklarda sentezlenen CdS nanopartiküller için oda sıcaklığında kaydedilen optik absorpsiyon spektrumları. Sentez sıcaklığı azaldıkça spektrumların tepe pozisyonlarında (392 nm'den 310 nm'ye) sistematik bir kayma olduğu gözlemlenmiştir. Bu kayma literatürde mavi kayma olarak adlandırılmaktadır. Elde edilen spektrumlar baz alınarak, 55 °C, 75 °C ve 130 °C'de hazırlanan CdS nanopartiküller için belirlenen yasak enerji değerleri sırasıyla 4, 3.94 ve 3.38 eV'dir. Sıcaklık arttıkça yasak enerji değerlerindeki azalışın muhtemel sebebi sıcaklık arttıkça parçacık boyutlarında gözlemlenen artış olabilmektedir.

4. SONUÇLAR

Bu çalışmada farklı sentezlenme sıcaklığı kullanılarak saf CdS nanopartiküller ıslak-kimyasal tekniği kullanılarak sentezlenmiştir. Sentezlenme sıcaklığı sırasıyla 55 °C, 75 °C ve 130 °C olarak belirlenmiştir. Farklı sıcaklıklarda sentezlenen CdS nanopartiküllerin yapısal ve optik özellikleri sırasıyla XRD ve UV-Vis spektroskopisi kullanılarak incelenmiştir. Elde edilen XRD desenleri sonucunda tüm numunelerin kübik yapıda olduğu tespit edilmiştir. Ayrıca XRD verileri kullanılarak 55 °C, 75 °C ve 130 °C sıcaklığında sentezlenen CdS nanopartiküller parçacık boyutları sırasıyla 1.7 nm, 2.1 nm ve 2.7 nm olarak hesaplanmıştır. Bu sonuç ile sentezlenme sıcaklığının nanopartiküllerin parçacık boyutundaki etkisi açıkça görülmüştür. UV-Vis spektroskopisi kullanılarak optik absorpsiyon spektrumları elde edilmiştir. Bu spektrumlar baz alınarak 55 °C, 75 °C ve 130 °C sıcaklığında sentezlenen CdS nanopartiküllerin yasak enerji aralıkları sırasıyla 4, 3.94 ve 3.38 eV olarak tespit edilmiştir. Böylece bu çalışma ile sentezlenme sıcaklığının CdS nanopartiküllerinin hem parçacık boyutu hem yasak enerji aralığı üzerindeki etkisi incelenmiştir.

KAYNAKÇALAR

[1] Horoz S., Lu L., Dai Q., Chen J., Yakami B., Pikal J.M., Wang W., Tang J., Applied Physics Letters, 101: 223902 (2012).

[2] Tilley R.D., Chemistry in New Zealand, 146-150 (2008).

[3] Xu X., Hu L., Gao H., liu S., Wageh S., Al-Ghamdi A.A., Alshahrie A., Fang X.,Advanced Functional Materials, 25 (3): 445-454 (2015).

[4] A.Khosravi, F.B. Bigdeli, M. Yousefi, M.S. Abdikhani, and S.M. Taheri Otaqsara, Environmental Progress & Sustainable Energy 33, 1194 (2014).

[5] A. Dumbrava, Badea, C. Badea, Prodan, G. Prodan, Ciupina, V. Ciupina, Chalcogenide

Letters **7**, 111 (2010)

Biyografi:

1986 yılında Hatay ilinin İskenderun ilçesinde doğdum. Lisans eğitimini 2008 yılında Sivas Cumhuriyet Üniversitesi Fizik Bölümünde tamamladım. Yüksek Lisans ve Doktora eğitimimi 2010-2015 yılları arasında University of Wyoming (A.B.D.) Fizik Bölümünde tamamladım. Halen Siirt Üniversitesi Elektrik-Elektronik Mühendisliği Bölümünde Öğretim Üyesi olarak çalışmaktayım. İlgili Konular; Yoğun madde fiziği, güneş pilleri, yarı iletkenlerin sentezlenmesi ve onların karakterizasyonu

ICACChE
2nd International Conference on Applications in Chemistry and Chemical Engineering
10 - 14 October 2018 Belgrade

Hydrogen Production via TiO_2 Based Fe (II)–Schiff Base Complex

Dilek Kılınç [1], Ömer Şahin

Abstract

This work present to use the Fe-Schiff Base complex that we previously synthesized [1] to support titanium dioxide and to research catalytic effects on $NaBH_4$ hydrolysis reaction to hydrogen production. The prepared catalyst was characterized with some of analyzed technique. Titanium dioxide supported Fe-Schiff Base complex catalyzed $NaBH_4$ hydrolysis reaction study depend on many parameters. Activation energy that belongs to hydrolysis reaction is 29.266 kJ.mol^{-1} and H_2 generation rates are 13892 and 31084 mL $H_2/g_{cat.}$min in order of 30°C and 50°C for this reaction.

Keywords: Hydrogen generation, Catalyst, Hydrolysis, Schiff Base, Complex

1. Introduction

Hydrogen is a wonderful energy source and a notable clean energy carrier, attracting great interest all over the world [2]. That's why to improve the hydrogen economy, scientists make an effort to find effective hydrogen storage materials with provide safe and green hydrogen production techniques. Recently, H_2 is mainly stored in a lot of form like metal hydrides, liquefied hydrogen, organic hydrides, etc. Between them, H_2 stored in the form of complex hydrides especially sodium borohydrides has been widely studied because of its specific suitability for all applications [3]. Schlesinger et al. [4] indicated that the hydrogen generation from sodium borohydride with this reaction:

$$NaBH_4 + 2\ H_2O \longrightarrow 4H_2 + NaBO_2 + Q\ (217\ kj\ ) \qquad (1)$$

With present study we utilized 4,4-methylenebis(2,6-diethyl)aniline-3,5-di-tert-butylsalisilaldimine-Fe(II) complex [1] to supported on TiO_2 and it was used as a catalyst to hydrogen generation from $NaBH_4$ hydrolysis with based on some parameters as temperature, concentration of Fe complex, $NaBH_4$, NaOH, and amount of catalyst. Catalyst was also analyzed with FT-IR, XRD, SEM and BET. As a result it was seen that TiO_2 supported Fe(II) complex is effective catalyst in $NaBH_4$ hydrolysis reaction for H_2 production.

2. Experimental Study

Preparation of TiO_2 supported-Fe (II)-Schiff Base Complex Catalyst

The TiO_2 supported4,4-methylenebis(2,6-diethyl)aniline-3,5-di-tert-butylsalisilaldimine-Fe(II)-Schiff Base complex catalysts were prepared by mechanical mixing method With different percentages 4,4-methylenebis (2,6-diethyl)aniline-3,5-di-tert-butyl salisilaldimine-Fe(II) complex was dissolved in ethanol (10 mL) and stirred. After this, 100 milligram powdered TiO_2 was added and stirred about 72 hour then filtered.

[1]*Corresponding author: Department of Chemistry, Faculty of Science and Letters, Siirt University, 56100 Siirt, Turkey, dkilinc@siirt.edu.tr*

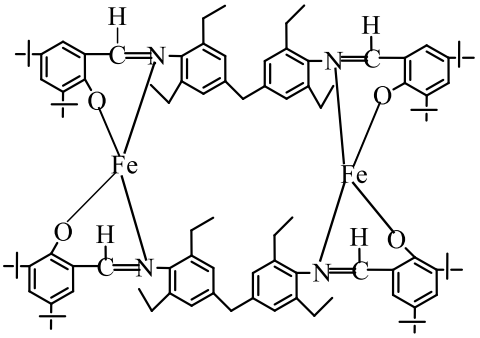

Fig.1. Structure of 4,4-methylenebis(2,6-diethyl)aniline-3,5-di-tert-butylsalisilaldimine-Fe(II) complex

Hydrogen Generation

For Sodium borohydride hydrolysis, reaction system consist from 10 % NaOH, 2.0 % $NaBH_4$ and different amounts of catalyst in 10 mL solution with using a 100 mL flask. The predicted hydrogen volume is 560 mL at 30 ˚C.

Effect of NaOH concentration

Fig. 2. displayed that the hydrolysis reaction rates changing with 0 %, 5 %, 7 %, 10 % NaOH concentrations, with 5 %-Fe-Schiff Base complex in 15 mg of TiO_2 supported-Fe (II)-Schiff Base complex in 2.0 % $NaBH_4$ solution at 30 ℃.

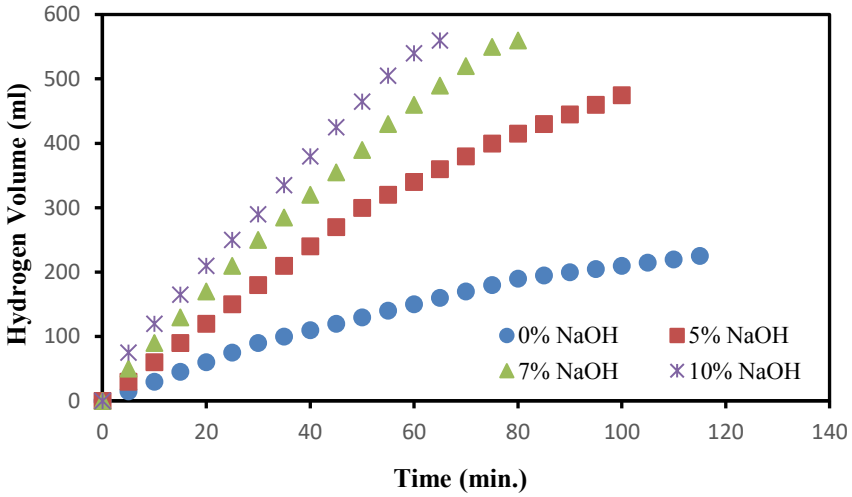

Fig. 2. Effect of NaOH concentration on the hydrogen generation rate

Effect of Fe(II)-complex percentage in total TiO_2 supported complex

Fig. 3. displayed that the hydrolysis reaction rates changing with several Fe(II)-Schiff Base complex concentrations like 1 %, 5 %, 7 %, 10 % in 2.0 % $NaBH_4$ solution with 10 %-NaOH, 15 mg of TiO_2 supported-Fe (II)-Schiff Base complex catalyst at 30 ℃.

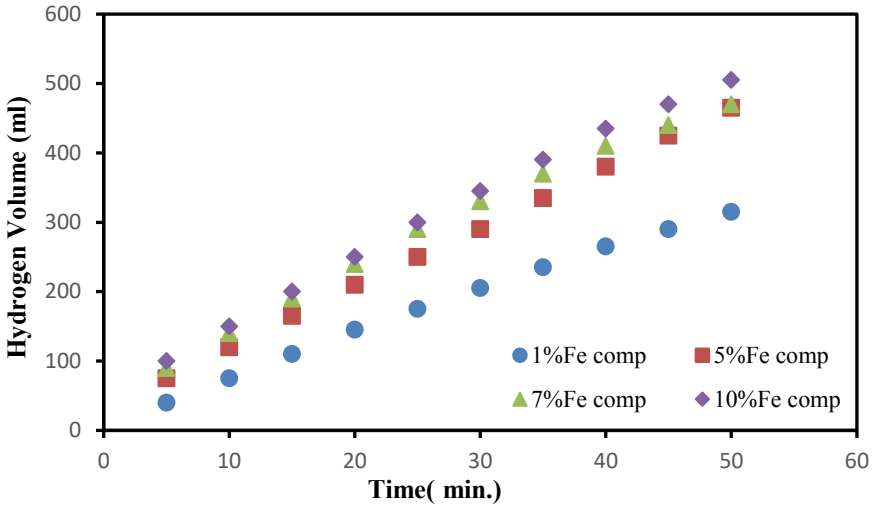

Fig.3. Effect of Fe (II)-complex ratio in total polymer supported complex

Effect of catalyst amount

Fig. 4. displayed that the hydrolysis reaction rates changing with several amounts of TiO_2 supported-Fe (II)-Schiff Base complex catalyst concentrations like 5, 15, 25, and 50 mg with 5% Fe (II)-Schiff Base complex in 2.0 % $NaBH_4$ solution and 10 % NaOH at 30 ℃.

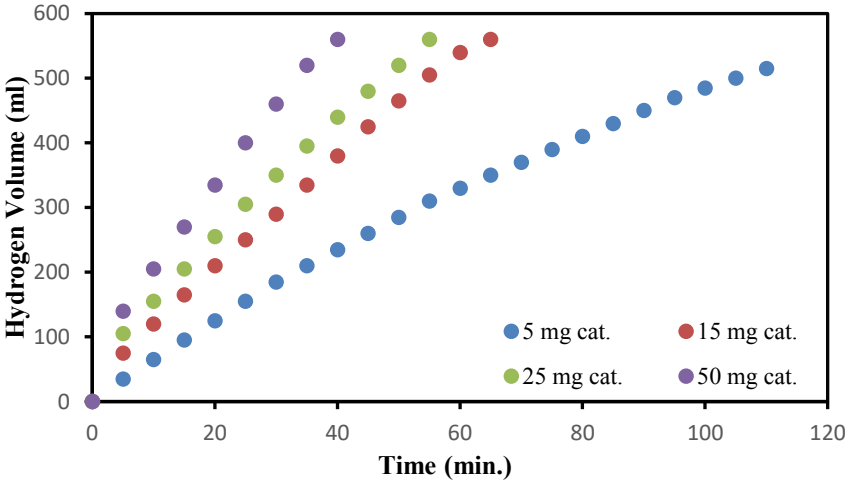

Fig.4. Effect of catalyst amount on hydrogen generation

Effect of $NaBH_4$ Percentage

Fig. 4. displayed that the hydrolysis reaction rates changing with several percentages of $NaBH_4$ as 2, 5, 7 and 10 % with using 5 %-Fe-Schiff Base complex in 15 mg of TiO_2 supported-Fe (II)-Schiff Base in 10 % NaOH solutions at 30 °C.

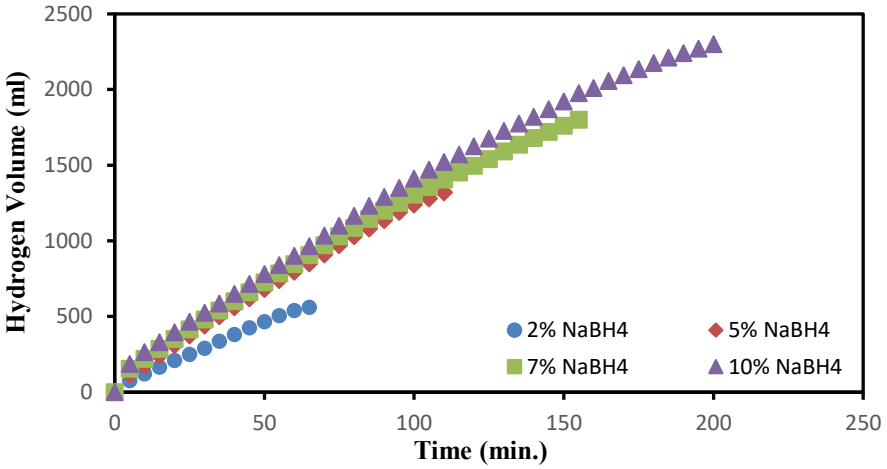

Fig.5. Effect of NaBH4 concentration on the hydrogen generation rate

Effect of Temperature

Fig. 6. displayed that the hydrolysis reaction rates changing with several temperatures as 20, 30, 40, 50 °C with using 5 %-Fe-Schiff Base complex in 15 mg of TiO_2 supported-Fe (II)-Schiff Base complex in 10 % NaOH solutions and 2 % $NaBH_4$.

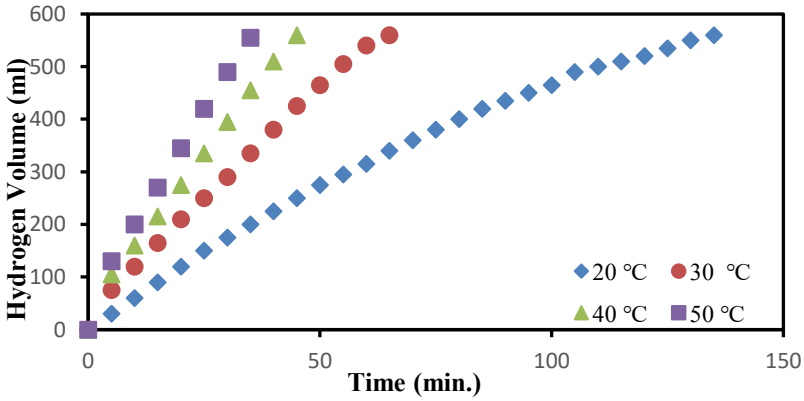

Fig.6. Effect of temperature on the hydrogen generation rate

Conclusion

TiO_2 supported-Fe (II)-Schiff Base complex was prepared to investigate its catalytic activity in $NaBH_4$ hydrolysis reaction for hydrogen production. TiO_2 supported-Fe (II)-Schiff Base complex was studied with based on temperature, Fe-complex concentration in catalyst and TiO_2 supported-Fe (II)-Schiff Base catalyst amount, Fe-complex in total complex catalyst, TiO_2 supported-Fe (II)-Schiff Base catalyst amount, NaOH concentration and $NaBH_4$ concentration. Activation energy that belongs to hydrolysis reaction is 29.266 $kJ.mol^{-1}$ and H_2 generation rates are 13892 and 31084 mL $H_2/g_{cat}.min$ in order of 30 °C and 50 °C for this reaction. And if all of the results are examined, seen that TiO_2 supported-Fe (II)-Schiff Base complex catalyst is highly active catalyst in $NaBH_4$ hydrolysis reaction to hydrogen production.

References

[1] Sahin Omer, Kilinc Dilek, Saka Cafer. Hydrogen production by catalytic hydrolysis of sodium borohydride with a bimetallic solid-state Co-Fe complex catalyst. Separation Science and Technology 2015; 50:2051-9.
[2] Mattos LV, Jacobs G, Davis BH, Noronha FB. Production of Hydrogen from Ethanol: Review of Reaction Mechanism and Catalyst Deactivation. Chem Rev 2012; 112:4094-123.
[3] Schlapbach L, Zuttel A, Zu¨ttel a. Hydrogen-storage materials for mobile applications. Nature 2001; 414:353-8.
[4] H. I., Schlesinger, H. C., Brown, A. E., Finholt, J. R., Gilbreath, H. R., Hoekstra, E. K., Hyde, The Preparation of Other Borohydrides by Metathetical Reactions Utilizing the Alkali Metal Borohydrides. J. Am. Chem. Soc. 1953;75:215-219.

ICACChE
2nd International Conference on Applications in Chemistry and Chemical Engineering
10 - 14 October 2018 Belgrade

Adsorption of Gas-Phase Benzene onto Formaldehyde-Treated Walnut shells: Kinetics, Equilibrium and Thermodynamics

***Sinan Kutluay*[1]**

Abstract

In this paper, formaldehyde-treated walnut shells were used as biosorbent for the adsorption of gas-phase benzene. The adsorption process was carried out using a laboratory-scale fixed-bed reactor, under atmospheric pressure. According to the knowledge published hitherto, there is no research on adsorption of gas-phase benzene onto formaldehyde-treated walnut shells, in a dynamic system. For this reason, within the context of the main purpose of this research, the adsorption process was investigated depending on the nitrogen (N_2) flow rate (50-120 mL min^{-1}) as the gas-phase benzene carrier, formaldehyde-treated walnut shells amount (0.25-1.00 g), gas-phase benzene concentration at the inlet (10-15 mg L^{-1}) and temperature (20-50°C). The adsorption process of gas-phase benzene onto formaldehyde-treated walnut shells can be well represented by the pseudo-second-order kinetic model. Equilibrium isotherm data were analyzed by Langmuir and Freundlich isotherm models and results indicated that the adsorption process was described well by the Langmuir isotherm model. Thermodynamic parameters, $\Delta G° = -7.99$ kJ mol^{-1}, $\Delta H° = -11.87$ kJ mol^{-1}, $\Delta S° = -0.008$ kJ mol^{-1} K^{-1}, showed that the adsorption process of gas-phase benzene onto formaldehyde-treated walnut shells was spontaneous exothermic and physical. The maximum monolayer adsorption capacity (q_{max}) of formaldehyde-treated walnut shells was determined to be 14.48 mg g^{-1} for 303 K. The results suggested that formaldehyde-treated walnut shell was an efficient adsorbent for the adsorption of gas-phase benzene.

Keywords: Benzene Adsorption; Kinetics; Isotherms; Thermodynamics; Walnut shells

1. INTRODUCTION

Air pollution, which is a very important environmental problem and which affects human health in particular, first begins with the change of the compounds forming the atmosphere. In recent years, many different types of Volatile Organic Compounds (VOCs) have been used in daily life as a result of advances in petrochemical and related industries. However, there are a number of sources that cause VOCs to be generated and introduced into the atmosphere. It is known that VOCs have various effects on human health [1, 2]. VOCs delivered from many sources to the atmosphere have direct or indirect negative effects on the human health, as well as on the natural composition of other living things and the atmosphere. (Among VOCs, the most notable because of their health risks; benzene, toluene, ethylbenzene, xylene and styrene. Benzene is even more prominent in terms of health effects. Respiratory benzene is easily absorbed by the lungs. The most important health effect of this component is that it causes cancer [3, 4]. VOCs, their number and diversity, is particularly noteworthy in scientific fields due to their own resources and potential harmful effects on human health. Because of their carcinogenicity and frequent occurrence, VOC sampling and analysis are very common in both indoor and outdoor air. [5]. Developed countries have determined the maximum permissible concentration values in the air of VOCs with harmful environmental effects by environmental policies. As a result, sanctions have been imposed on industrial processes to reduce the pollutants released to the environment to the determined concentration values during production [6, 7]. In the literature, the methods developed for the removal of VOCs in the environment are collected in two classes as oxidation and bio-filtration. The chemical structure of VOC is completely degraded by the process applied in the removal method. Recovery methods can be collected under absorption, condensation, membrane separation and adsorption. Among the VOCs removal and recovery techniques, the adsorption process using high surface area adsorbents with many advantages in terms of process conditions and applicability is the most preferred method [6, 8, 9]. Adsorption is usually carried out on a fixed bed filled with adsorbents. Some solids used as adsorbents in the adsorption process have a porous structure and the inner surface areas are larger than the outer surface areas. The adsorption on the inner surface of the layer does not occur as easily as the outer surface.

[1] *Corresponding author: Siirt University, Faculty of Engineering, Department of Chemical Engineering, Siirt, Turkey. kutluays2012@gmail.com*

Because gas molecules interact with atoms, molecules or ions when entering. In this case, condensation occurs in the inner spaces called capillary condensation. Adsorption may take place in the form of physical adsorption (or van der Waals adsorption) or chemical adsorption (or chemisorption). In the physical adsorption, the forces holding the adsorbed substance bound to the adsorbent surface are van der Waals forces. Van der Waals forces are effective from a long distance but are weak forces. The enthalpy of the physical adsorption is typically about 20 kJ/mol. Such a small enthalpy change is insufficient to cause ligation and therefore a physically adsorbed molecule protects its identity. Physical adsorption is observed at low temperatures and the amount of adsorption usually decreases when the temperature is increased [10]. There are many studies on fixed bed modeling in literature [5, 10]. Allen et al. [11] revealed theoretical mathematical equations for the adsorbed particles in the adsorbent particles given by injection to a gas stream. Equations in the same study were solved in parameters such as different gas flow rate and adsorbent feed rate and the results were analyzed. In the other studies, theoretical and experimental results were evaluated together [12, 13].

In this study, the adsorption of gas-phase benzene onto formaldehyde-treated walnut shells was performed using a laboratory-scale fixed-bed reactor, under atmospheric pressure. The effects of nitrogen (N_2) flow rate as the gas-phase benzene carrier, amount of formaldehyde-treated walnut shells, concentration of gas-phase benzene at the inlet and the adsorption temperature on adsorption process were investigated separately. For the analysis of adsorption kinetics, pseudo-first-order and pseudo-second-order models were applied. Equilibrium isotherm data were analysed by Langmuir and Freundlich models. Thermodynamic parameters such as Gibbs free energy ($\Delta G°$), enthalpy change ($\Delta H°$) and entropy change ($\Delta S°$) were also calculated using van't Hoff equation to characterize the adsorption process.

2. MATERIALS AND METHODS

In this study, the samples of walnut shells were obtained from the province of Siirt which is located in the South-East of Turkey. Walnut shells were ground in a mortar and sieved to a particle size of -850+500 μm. The obtained samples were stored in closed containers. In order to be used as an adsorbent in the process of gas-phase benzene adsorption, walnut shells were treated with 1% formaldehyde solution at a ratio of 1:5 (walnut shells: formaldehyde; w/v) at room temperature for 24 h. The walnut shells were then removed by filtration and washed with hot deionized water to remove formaldehyde in the medium. Washed walnut shells at 80°C for 24 hours after drying the adsorption experiments were taken to be used in closed containers. The adsorbate used in this study is gas-phase benzene at analytical grade (Sigma Aldrich, 99.0%). The experimental setup used in gas-phase benzene adsorption studies is schematically shown in Figure 1. Adsorption experiments of gas-phase benzene onto formaldehyde-treated walnut shells were performed in the fixed bed of a Pyrex-glass reactor with the height of 16 cm and an internal diameter of 0.9 cm. To determine the effects of adsorption conditions, the study was carried out under atmospheric pressure at different N_2 flow rates (50-120 mL min^{-1}) as a gas-phase benzene carrier, amounts of formaldehyde-treated walnut shells (0.25-1.00 g), concentrations of gas-phase benzene at the inlet (10.00-15.00 mg L^{-1}) and adsorption temperatures (20-30°C). For this purpose, 300 mL of the benzene solution to be subjected to the dynamic adsorption was placed in a 500 mL glass balloon and then placed in the thermostat set to the study temperature. Gas-phase benzene was introduced into the fixed bed by using N_2 as a carrier gas and it was continuously adsorbed onto formaldehyde-treated walnut shells. The internal temperature of the jacketed adsorbent, in which the adsorption is carried out, and the gas-pahse benzene temperature was kept constant by using the thermostat connected to both the adsorber and the heat exchanger. The concentration of gas-phase benzene at the inlet of the adsorber was analyzed while the valve-2 line was closed and the valve-1 bypass line was open. When the concentration of gas-phase benzene at the inlet of the adsorber reached the steady state, about 0.50 g of formaldehyde-treated walnut shells was weighed out and formaldehyde-treated walnut shells ged into the adsorption column and then the experiments were carried out by turning the valve-1 line to closed and the valve-2 line to the open position. The concentrations of gas-phase benzene at the inlet and outlet (after adsorption) of the adsorber were produced using a PID controlled heated thermostat at 20, 30, 40 and 50°C, respectively. The formaldehyde-treated walnut shells particles were supported by microsieve at the outlet of the adsorber. Then, the carrier gas containing a previously arranged concentration of gas-phase benzene was passed through the column until the gas-phase benzene concentration become constant and stable. The concentrations of gas-phase benzene at the inlet and outlet of the adsorber were measured by a Gas Chromatograph equipped with a Flame Ionization Detector (GC-FID, GC 910, Buck Scientific) and recorded by a computer.

The dynamic adsorption capacity was determined using the following equation [14]:

$$q = \frac{F}{m}\int_0^t (C_{in} - C_{eff})dt \quad (1)$$

The integrated form of Eq. (1), which was used in this study to determine the adsorption capacity of gas-phase benzene onto formaldehyde-treated walnut shells, can be defined as:

$$q_t = \sum_0^n \left[\frac{F}{m}(C_{in} - C_{eff})\Delta t\right] \quad (2)$$

Where, q_t (mg g^{-1}) is the gas-phase benzene adsorption capacity, as shown in Eq. (1), which is integrated from t=0 to t (min), m (g) is the amount of adsorbent, F (L min^{-1}) is the gas flow rate, n is the number of samples taken, C_{in} (ppm) and C_{eff} (ppm) are the concentrations of gas-phase benzene at the inlet and outlet (after adsorption) of the adsorber, respectively. In the adsorption process, q_t=qe is achieved when the equilibrium time (t_e) is reached and refers to the adsorption capacity at equilibrium.

The adsorption efficiency of gas-phase benzene onto formaldehyde-treated walnut shells is defined as below:

$$Adsorption\ efficiency\ (\%) = \frac{C_{in} - C_e}{C_{in}} \times 100 \quad (3)$$

Where, C_{in} ($mg\ L^{-1}$) and C_e ($mg\ L^{-1}$) are the concentrations of gas-phase benzene at the inlet and equilibrium, respectively.

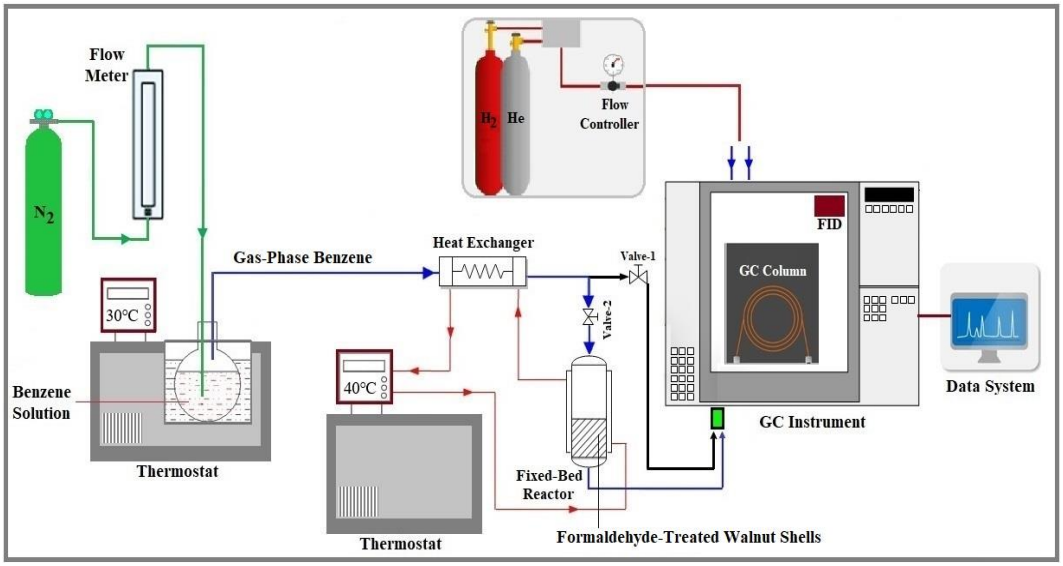

Figure 1. Experimental setup for the adsorption of gas-phase benzene onto formaldehyde-treated walnut shells

3. RESULTS AND DISCUSSION

In the study, the effects of adsorption conditions such as nitrogen (N_2) flow rate as the gas-phase benzene carrier, amount of formaldehyde-treated walnut shells, concentration of gas-phase benzene at the inlet and the adsorption temperature on the adsorption process of gas-phase benzene onto formaldehyde-treated walnut shells were determined, in a continuous system. In addition, adsorption kineticss, isotherms and thermodynamics of adsorption process were investigated.

Effect of Flow Rate on Adsorption Process

To determine the effect of the flow rate on both the adsorption capacity and the adsorption efficiency of gas-phase benzene onto formaldehyde-treated walnut shells, the experiments were performed at different flow rates (50, 75, 100 and 120 mL min^{-1}), and the results are given in Figure 2. To determine the equilibrium time of the adsorption, the adsorption capacity was investigated depending on the time (0-120 min) (Figure 2a). As shown in Figure 2a, depending on the increase in the flow rate, the adsorption capacity is increased and the maximum adsorption capacity is achieved in a shorter time. However, in Figure 2b, the adsorption capacity at equilibrium is increased with increasing flow rate, while the adsorption efficiency is not changed. This result means that the flow rate in the equation (Eq. 2), in which the adsorption capacity is determined, changes the adsorption capacity in proportion to the numerical value it has. In other words, it has been observed that the amount of gas-phase benzene adsorbed onto formaldehyde-treated walnut shells does not increase at higher flow rates.

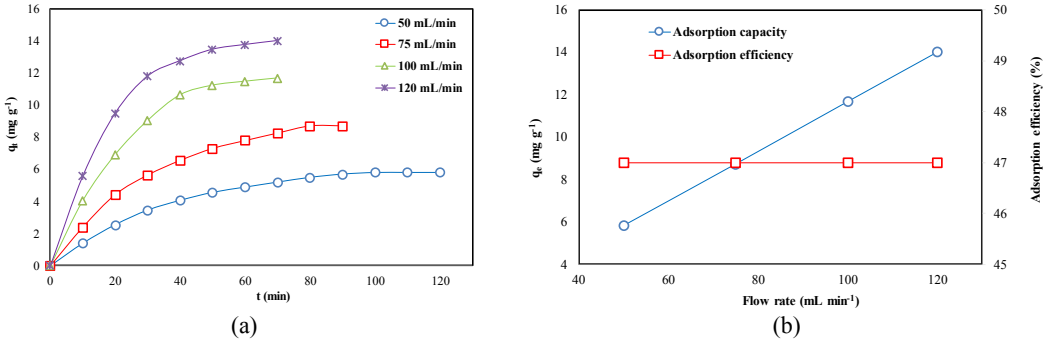

(a) (b)

Figure 2. Effect of flow rate of N_2 as the carrier gas on the adsorption capacity with time (a) and the adsorption capacity at equilibrium and the adsorption efficiency (b) of gas-phase benzene (conditions: amount of formaldehyde-treated walnut shells 0.50 g, concentration of gas-phase benzene at the inlet 12.50 mg L^{-1} and temperature 30°C)

Effect of the Amount of Formaldehyde-Treated Walnut Shells on Adsorption Process

The amount of adsorbent is one of the important parameters for the adsorption process. To determine the effect of the formaldehyde-treated walnut shells amount on both the adsorption capacity and the adsorption efficiency of gas-phase benzene onto formaldehyde-treated walnut shells, the experiments were performed at

different formaldehyde-treated walnut shells amounts (0.25, 0.50, 0.75 and 1.00 g), and the results are in Figure 3. To determine the adsorption equilibrium time, the adsorption capacity was investigated based on time (0-90 min) (Figure 3a). Figure 3a shows that an increase in the amount of formaldehyde-treated walnut shells causes a decrease in the adsorption capacity. As seen in Figure 3b, it was observed that the adsorption capacity at equilibrium decreased with the increasing amount of formaldehyde-treated walnut shells, the adsorption efficiency increased up to 0.50 g of formaldehyde-treated walnut shells, and did not change with higher amounts of formaldehyde-treated walnut shells. In this work, the minimum amount of adsorbent corresponding to maximum adsorption for formaldehyde-treated walnut shells is 0.50 g.

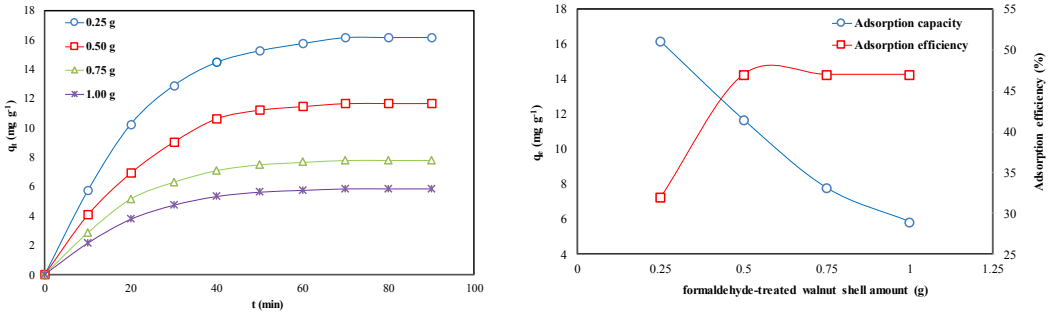

(a) (b)

Figure 3. Effect of formaldehyde-treated walnut shells amount on the adsorption capacity with time (a) and the adsorption capacity at equilibrium and the adsorption efficiency (b) of gas-phase benzene (conditions: gas flow rate 100 mL min^{-1}, concentration of gas-phase benzene at the inlet 12.50 mg L^{-1} and temperature 30°C)

Effect of Concentration of Gas-Phase Benzene at the inlet on Adsorption Process

In order to investigate the effect of concentration of gas-phase benzene at the inlet on both the adsorption capacity and the adsorption efficiency of gas-phase benzene onto formaldehyde-treated walnut shells, the experiments were performed at different concentrations of gas-phase benzene at the inlet (10.00, 12.50, 13.50, 15.00 mg L^{-1}), and the results are shown in Figure 4. To determine the adsorption equilibrium time, the adsorption capacity was investigated based on time (0-100 min) (Figure 4a). As shown in Figure 4a, it was observed that the adsorption capacity increased up to 12.50 mg L^{-1} and did not change at higher concentrations due to the increase in gas-phase benzene concentration at the influent. In addition, the increase in the concentration of gas-phase benzene at the inlet shows that equilibrium adsorption capacity has been reached in a shorter time. In Figure 4b, the increase in the concentration of gas-phase benzene at the inlet shows that the adsorption capacity at equilibrium increases up to 12.50 mg L^{-1} and does not change at higher concentrations. However, the adsorption efficiency was observed to decrease at concentrations greater than 12.50 mg L^{-1} (Figure 4b). For all these evaluations, the concentration of gas-phase benzene at the inlet was taken as 12.50 mg L^{-1} in other adsorption experiments.

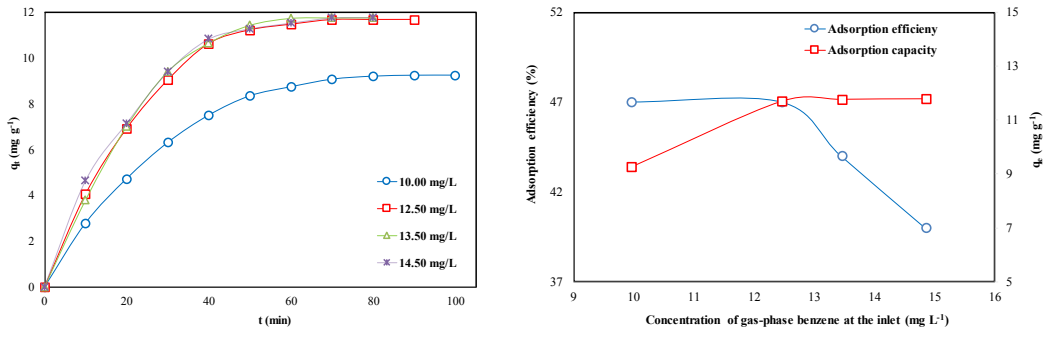

(a) (b)

Figure 4. Effect of concentration of gas-phase benzene at the inlet on its adsorption capacity with time (a) and the adsorption capacity at equilibrium and the adsorption efficiency (b) of gas-phase benzene (conditions: amount of formaldehyde-treated walnut shells 0.50 g, gas flow rate 100 mL min^{-1} and temperature 30°C)

Effect of Temperature on Adsorption Process

In the adsorption process, temperature plays an important role in adsorption behavior. To illustrate the effect of adsorption temperature on both the adsorption capacity and the adsorption efficiency of gas-phase benzene onto formaldehyde-treated walnut shells, the experiments were performed at different adsorption temperatures (20, 30, 40 and 50°C), and the results are shown in Figure 5. To determine the adsorption equilibrium time, the adsorption capacity was investigated based on time (0-90 min) (Figure 5a). Figure 5a shows that, depending on the increase in adsorption temperature, the adsorption capacity does not change up to 30°C and decreases at higher temperatures. As shown in Figure 5b, both the adsorption capacity at equilibrium and the adsorption efficiency did not change up to 30°C, while decreasing at higher temperatures with the increase in temperature. Since gas adsorption is an exothermic process, the adsorption capacity

decreases with the increasing temperature. This result shows that physical adsorption is a mechanism that separates the vapor [15].

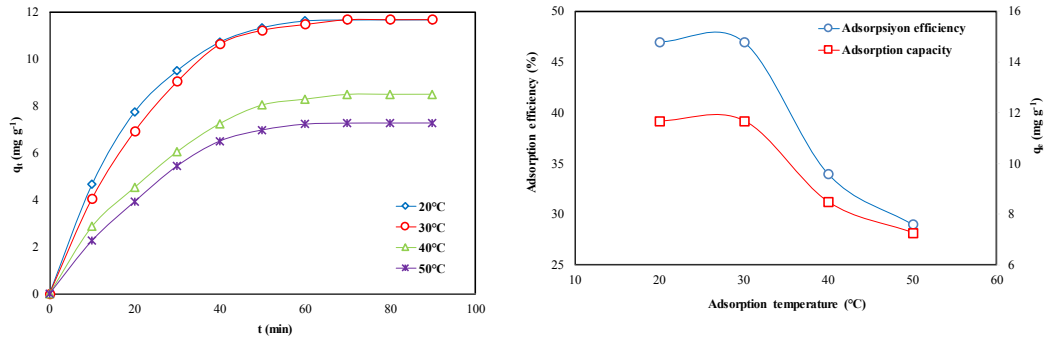

(a) (b)

Figure 5. Effect of adsorption temperature on the adsorption capacity with time (a) and the adsorption capacity at equilibrium and the adsorption efficiency (b) of gas-phase benzene (conditions: amount of formaldehyde-treated walnut shells 0.50 g, gas flow rate 100 mL min^{-1} and concentration of gas-phase benzene at the inlet 12.50 mg L^{-1})

Adsorption Kinetics

In order to understand the adsorption process of gas-phase benzene onto formaldehyde-treated walnut shells, pseudo-first-order and pseudo-second-order kinetics models were applied to experimental data obtained at different temperatures. The pseudo-first-order and pseudo-second-order kinetics models are shown in Figure 6. Figure 6a shows that the pseudo-first-order kinetics model not give beneficient results for adsorption of gas-phase benzene onto formaldehyde-treated walnut shells, indicating that it is not in good agreement with adsorption data. On the other hand, Figure 6b shows that the pseudo-second-order kinetics model gives beneficient results for adsorption of gas-phase benzene onto formaldehyde-treated walnut shells and shows a satisfactory agreement with experimental adsorption data.

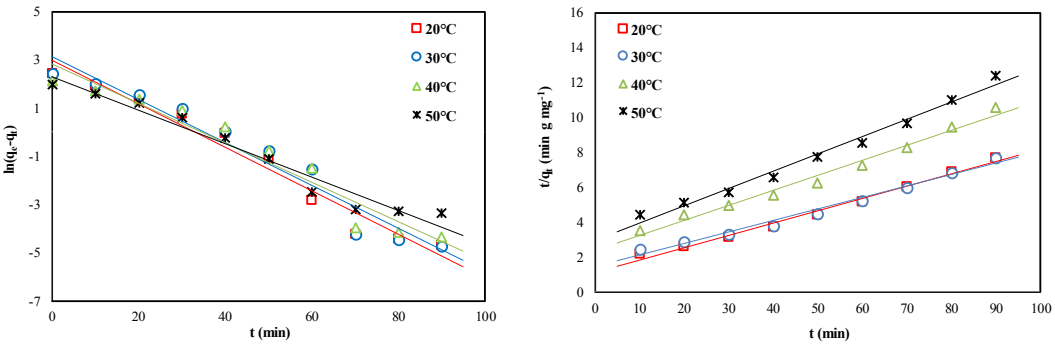

(a) (b)

Figure 6. Pseudo-first-order (a) and pseudo-second-order (b) kinetic models for adsorption of gas-phase benzene onto formaldehyde-treated walnut shells

Adsorption Isotherms

In order to be able to analyse the adsorption process of gas-phase benzene onto formaldehyde-treated walnut shells, experimental adsorption equilibrium data obtained at different temperatures were evaluated by applying Langmuir and Freundlich isotherm models. Adsorption tendencies are investigated as the functions of equilibrium concentration. Plots of Langmuir and Freundlich isotherm models are presented in Figure 7. As can be seen from Figure 7a and 7b, it is clear that the plots of the Langmuir isotherm model fit well with the experimental data, while the plots of Freundlich isotherm models do not fit. The compatibility of adsorption equilibrium data with the Langmuir isotherm suggests that the surface of the formaldehyde-treated walnut shells has a homogeneous structure and identical active sites. In addition, this result indicates that the surface energy is homogeneously distributed and that single-plate adsorption occurs [16]. The maximum monolayer adsorption capacity (q_{max}) of formaldehyde-treated walnut shells was calculated to be 14.48 mg g^{-1} for 30°C.

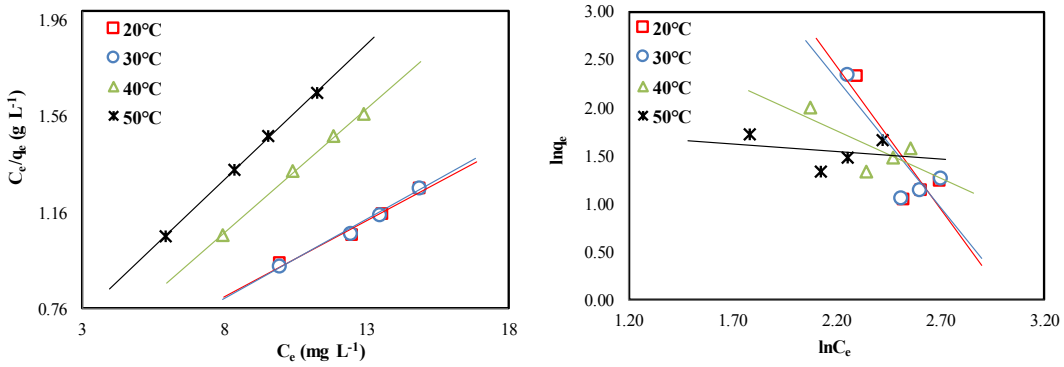

Figure 7. Langmuir (a) and Freundlich (b) isotherm models for adsorption of gas-phase benzene onto formaldehyde-treated walnut shells

Adsorption Thermodynamics

In an adsorption study, the determination of the adsorption mechanism is rather essential [17]. Adsorption mechanism can be explained by thermodynamic parameters such as Gibbs free energy change (*ΔG°)*, enthalpy change (*ΔH°)* and entropy change (*ΔS°*) [18]. In order to determine the thermodynamic parameters, experiments were carried out at four different temperatures (20, 30, 40 and 50°C). The negative sign of *ΔG°* (-7.986 kJ mol^{-1}) indicates that the adsorption process of gas-phase benzene onto formaldehyde-treated walnut shells was appropriate and spontaneous [19]. The *ΔG°* values between -20 kJ mol^{-1} and 0 kJ mol^{-1} were reduced to the physical adsorption range [20]. This result shows that physical adsorption was the dominant mechanism for adsorption of gas-phase benzene onto formaldehyde-treated walnut shells. The *ΔH°* value for gas-phase benzene was calculated as -11.872 kJ mol^{-1}. The negative value of the calculated *ΔH°* indicates that the adsorption process was exothermic. This means that the energy in the form of heat was released to the environment during the adsorptive process as new bonds were formed. Furthermore, the magnitude of *ΔH°* (<20 kJ mol^{-1}) indicates that physical adsorption was predominant [21]. The negative value of *ΔS°* (-0.008 kJ mol^{-1} K^{-1}). indicates that the entropy of the system decreases. This means that the disorder of the system during the adsorption process and the randomization of the adsorbate at the solid/gas interface were reduced [22]. That is, gas-phase benzene molecules pass from a random step to a regular step (on the surface of the adsorbent).

4. CONCLUSİONS

In this study, the adsorption of gas-phase benzene onto formaldehyde-treated walnut shells was performed, under atmospheric pressure. Adsorption parameters such as N_2 flow rate as the gas-phase benzene carrier, amount of formaldehyde-treated walnut shells, concentration of gas-phase benzene at the inlet, and adsorption temperature are effective on both the adsorption capacity and the adsorption efficiency of gas-phase benzene onto formaldehyde-treated walnut shells. Experimental results were showed that the adsorption capacity decreases with increasing temperature and amount of formaldehyde-treated walnut shells, while increasing with gas flow rate and the concentration of gas-phase benzene at the inlet. The results indicated that the adsorption process follows pseudo-second-order kinetics model in the most efficient way. It was observed that the data obtained for the adsorption of gas-phase benzene onto formaldehyde-treated walnut shells were in a good fitting with the Langmuir isotherm. Thermodynamic parameters, ΔG° = -7.99 kJ mol^{-1}, ΔH°= -11.87 kJ mol^{-1}, ΔS°= -0.008 kJ mol^{-1} K^{-1}, showed that the adsorption process of gas-phase benzene onto formaldehyde-treated walnut shells was spontaneous exothermic and physical. The maximum monolayer adsorption capacity (q_{max}) of formaldehyde-treated walnut shells was determined to be 14.48 mg g^{-1} for 303 K. The results suggested that formaldehyde-treated walnut shell was an efficient adsorbent for the adsorption of gas-phase benzene.

REFERENCES

[1] H. Guo, S. Lee, W.M. Li, J. Cao, Source characterization of BTEX in indoor microenviroments in Hong Kong, Atmospheric Environment 37 (2003) 73-82.
[2] A.L. Hinwood, C. Rodriguez, T. Runnion, D. Farrar, F. Murray, A. Horton, D. Glass, V. Sheppeard, J.W. Edwards, L. Denison, T. Whitworth, C. Eiser, M. Bulsara, R.W. Gillett, J. Powell, S. Lawson, I. Weeks, I. Galbally, Risk factors for increased BTEX exposure in four Australian cities, Chemosphere 66 (2007) 533-541.
[3] J.N. Cape, D. Fowler, A. Davison, Ecological effects of sulfur dioxide, fluorides, and minor air pollutants: recent trends and research needs, Environment International 29 (2003) 201-211.
[4] Delia M. Pinto, James D. Blande, Silvia R. Souza, Anne-Marja Nerg, J.K. Holopainen, Plant Volatile Organic Compounds (VOCs) in Ozone (O3) Polluted Atmospheres: The Ecological Effects, Journal of Chemical Ecology 36 (2010) 22-34.
[5] M.A. Parra, D. Elustondo, R. Bermejo, J.M. Santamaría, Quantification of indoor and outdoor volatile organic compounds (VOCs) in pubs and cafés in Pamplona, Spain, Atmospheric Environment 42 (2008) 6647-6654.

[6] V.K. Gupta, N. Verma, Removal of volatile organic compounds by cryogenic condensation followed by adsorption, Chemical Engineering Science 57 (2002) 2679-2696.
[7] W.-T. Tsai, A review of environmental hazards and adsorption recovery of cleaning solvent hydrochlorofluorocarbons (HCFCs), Journal of Loss Prevention in the Process Industries 15 (2002) 147-157.
[8] K.S. Hwang, C. Dae Ki, G. Sung Yong, C. Sung Yong, Adsorption and thermal regeneration of methylene chloride vapor on an activated carbon bed, Chemical Engineering Science 52 (1997) 1111-1123.
[9] F.I. Khan, A. Kr. Ghoshal, Removal of Volatile Organic Compounds from polluted air, Journal of Loss Prevention in the Process Industries 13 (2000) 527-545.
[10] D.M. Ruthven, Principles of Adsorption and Adsorption Processes, John Wiley, New York, 1984.
[11] R.W.K. Allen, E. D Archer, J. MacInnes, Adsorption by Particles Injected into a Gas Stream, Chemical Engineering Journal - CHEM ENG J 83 (2001) 165-174.
[12] R.W.K. Allen, E.D. Archer, J.M. MacInnes, Theoretical account of a dry sorption injection experiment, AIChE 47 (2001) 2684-2695.
[13] E.D. Archer, R.W.K. Allen, J.M. MacInnes, Measurements of VOC take-up by adsorbing particles in a gas stream, Filtration & Separation 37 (2000) 32-39.
[14] Z. Zhao, S. Wang, Y. Yang, X. Li, J. Li, Z. Li, Competitive adsorption and selectivity of benzene and water vapor on the microporous metal organic frameworks (HKUST-1), Chemical Engineering Journal 259 (2015) 79-89.
[15] D. Ramirez, S. Qi, M.J. Rood, K.J. Hay, Equilibrium and Heat of Adsorption for Organic Vapors and Activated Carbons, Environmental Science & Technology 39 (2005) 5864-5871.
[16] Y. Guo, Y. Li, T. Zhu, J. Wang, M. Ye, Modeling of dioxin adsorption on activated carbon, Chemical Engineering Journal 283 (2016) 1210-1215.
[17] H.N. Tran, S.-J. You, H.-P. Chao, Thermodynamic parameters of cadmium adsorption onto orange peel calculated from various methods: A comparison study, Journal of Environmental Chemical Engineering 4 (2016) 2671-2682.
[18] P. Ammendola, F. Raganati, R. Chirone, CO2 adsorption on a fine activated carbon in a sound assisted fluidized bed: Thermodynamics and kinetics, Chemical Engineering Journal 322 (2017) 302-313.
[19] J. He, S. Hong, L. Zhang, F. Gan, Y.-S. Ho, Equilibrium and Thermodynamic Parameters of Adsorption of Methylene Blue onto Rectorite, Fresenius Environmental Bulletin 19 (2010) 2651–2656.
[20] D. Duranoğlu, A.W. Trochimczuk, U. Beker, Kinetics and thermodynamics of hexavalent chromium adsorption onto activated carbon derived from acrylonitrile-divinylbenzene copolymer, Chemical Engineering Journal 187 (2012) 193-202.
[21] A.A. Adelodun, J.C. Ngila, D.-G. Kim, Y.M. Jo, Isotherm, Thermodynamic and Kinetic Studies of Selective CO2 Adsorption on Chemically Modified Carbon Surfaces, Aerosol and Air Quality Research (2016) 3312–3329.
[22] A. Gürses, Ç. Doğar, M. Yalçın, M. Açıkyıldız, R. Bayrak, S. Karaca, The adsorption kinetics of the cationic dye, methylene blue, onto clay, Journal of Hazardous Materials 131 (2006) 217-228.

BIOGRAPHY

Sinan KUTLUAY was born in 1988 in Ağrı/Tutak. He graduated from Yildiz Technical University, Faculty of Chemistry-Metallurgy, Department of Chemical Engineering in 2010. Between the years 2010-2012, he completed his master's degree at Yıldız Technical University, Graduate School of Natural Sciences, Department of Chemical Engineering. Between the years 2014-2018, he completed his doctorate's degree at Selçuk University, Graduate School of Natural Sciences, Department of Chemical Engineering. In 2011, he was appointed as research assistant at Siirt University, Department of Chemical Engineering. He is currently working as Assist. Prof. Dr. in the same department. Sinan KUTLUAY is married and has one child.

ICACChE
2nd International Conference on Applications in Chemistry and Chemical Engineering
10 - 14 October 2018 Belgrade

Investigation of Adsorption Kinetics, Equilibrium and Thermodynamics of Toluene Vapor onto Formaldehyde-Treated Walnut Shells

Orhan Baytar, Ömer Şahin, Sinan Kutluay[1]

Abstract

In this study, the adsorption kinetics, equilibrium and thermodynamics of toluene vapor onto formaldehyde-treated walnut shells were investigated. The effects of nitrogen (N_2) flow rate (50-120 mL min^{-1}) as the toluene vapor, amount of formaldehyde-treated walnut shells (0.25-1.00 g), concentration of toluene vapor at the inlet (10-15 mg L^{-1}) and temperature (20-50°C) on adsorption process were investigated separately, under atmospheric pressure. The results indicated that the adsorption process follows pseudo-second order kinetic model in the most efficient way. It was observed that the data obtained for the adsorption of toluene vapor onto formaldehyde-treated walnut shells were in a good fitting with the Langmuir isotherm. Thermodynamic parameters, $\Delta G° = -8.67$ kJ mol^{-1}, $\Delta H° = -16.04$ kJ mol^{-1}, $\Delta S° = -0.024$ kJ mol^{-1} K^{-1}, showed that the adsorption process of toluene vapor onto formaldehyde-treated walnut shells was spontaneous exothermic and physical. The maximum monolayer adsorption capacity (q_{max}) of formaldehyde-treated walnut shells was determined to be 19.15 mg g^{-1} for 30°C.

Keywords: Kinetics; Isotherms; Thermodynamics; Toluene Adsorption; Walnut shells

1. INTRODUCTION

Volatile organic compounds (VOCs) are important air pollutant components found in the atmosphere originating from all municipal and industrial areas [1]. VOCs are pollutants that are given to the environment from the chemical, petrochemical and many other industries. Evaporation of chemicals such as solvents, thinners, scrubbers and lubricants, flue gas emissions from the burning of fossil fuels for industrial and urban activities, incineration of wastes resulting from urban life, oil refineries and stations, etc. there are numerous sources of VOCs [2-5]. VOCs, which are not removed before being released to the environment in their source, have serious detrimental effects on the environment and thus on living things. Global warming is a significant environmental problem [6]. VOCs, which can be readily mixed with direct evaporation into air, can lead to fatal degrees by inhalation. Some VOCs can cause persistent health problems due to their irritating properties. VOCs accumulate on the leaves and refine crops with a degree of influence that affects photosynthesis. Some other volatile organic compounds, which are carcinogenic, can lead to death by toxin [3]. Among VOCs, the most notable because of their health risks; toluene, benzene, ethyltoluene, xylene and styrene. Toluene is a VOC within the risk group of components that do not carry cancer risk. The most important health effect of toluene is its acute and chronic effects on the central nervous system [7, 8]. VOCs, their number and diversity, is particularly noteworthy in scientific fields due to their own resources and potential harmful effects on human health. Because of their carcinogenicity and frequent occurrence, VOC sampling and analysis are very common in both indoor and outdoor air. [9]. In the literature, the methods developed for the removal of VOCs in the environment are collected in two classes as oxidation and bio-filtration. The chemical structure of VOC is completely degraded by the process applied in the removal method. Recovery methods can be collected under absorption, condensation, membrane separation and adsorption.

Among the VOCs removal and recovery techniques, the adsorption process using high surface area adsorbents with many advantages in terms of process conditions and applicability is the most preferred method [3, 10, 11]. Adsorption is usually carried out on a fixed bed filled with adsorbents. There are many studies on fixed bed modeling in literature [9, 12]. Allen et al. [13] revealed theoretical mathematical equations for the adsorbed particles in the adsorbent particles given by injection to a gas stream.

[1] *Corresponding author: Siirt University, Faculty of Engineering, Department of Chemical Engineering, Siirt, Turkey. kutluays2012@gmail.com*

Equations in the same study were solved in parameters such as different gas flow rate and adsorbent feed rate and the results were analyzed. In the other studies, theoretical and experimental results were evaluated together [14, 15].

In this study, the adsorption kinetics, equilibrium and thermodynamics of toluene vapor onto formaldehyde-treated walnut shells was performed using a laboratory-scale fixed-bed reactor, under atmospheric pressure. The effects of nitrogen (N_2) flow rate as the toluene vapor carrier, amount of formaldehyde-treated walnut shells, concentration of toluene vapor at the inlet and temperature on adsorption process were investigated separately. For the analysis of adsorption kinetics, pseudo-first order and pseudo-second order models were used. Equilibrium isotherm data were analysed by Langmuir and Freundlich isotherm models. Thermodynamic parameters such as Gibbs free energy ($\Delta G°$), enthalpy change ($\Delta H°$) and entropy change ($\Delta S°$) were also calculated using van't Hoff equation to characterize the adsorption process.

2. MATERIALS AND METHODS

In this study, the samples of walnut shells were obtained from the province of Siirt which is located in the South-East of Turkey. Walnut shells were ground in a mortar and sieved to a particle size of -850+500 μm. The obtained samples were stored in closed containers. In order to be used as an adsorbent in the process of toluene vapor adsorption, walnut shells were treated with 1% formaldehyde solution at a ratio of 1:5 (walnut shells: formaldehyde; w/v) at room temperature for 24 h. The walnut shells were then removed by filtration and washed with hot deionized water to remove formaldehyde in the medium. Washed walnut shells at 80°C for 24 hours after drying the adsorption experiments were taken to be used in closed containers. The adsorbate used in this study is toluene at analytical grade (Sigma Aldrich, 99.0%). The experimental setup used in toluene vapor adsorption studies is schematically shown in Figure 1. Toluene vapor adsorption experiments of the formaldehyde-treated walnut shells adsorbent were performed in the fixed bed of a Pyrex-glass reactor with the height of 16 cm and an internal diameter of 0.9 cm. To determine the effects of adsorption conditions, the study was carried out under atmospheric pressure at different N_2 flow rates (50-120 mL min^{-1}) as a toluene vapor carrier, amounts of formaldehyde-treated walnut shells (0.25-1.00 g), concentrations of toluene vapor at the inlet (10.00-15.00 mg L^{-1}) and temperatures (20-50°C). For this purpose, 300 mL of the toluene solution to be subjected to the dynamic adsorption was placed in a 500 mL glass balloon and then placed in the thermostat set to the study temperature. Toluene vapor was introduced into the fixed bed by using N_2 as a carrier gas and it was continuously adsorbed onto formaldehyde-treated walnut shells. The internal temperature of the jacketed adsorbent, in which the adsorption is carried out, and the toluene vapor temperature was kept constant by using the thermostat connected to both the adsorber and the heat exchanger. The concentration of toluene vapor at the inlet of the adsorber was analyzed while the valve-2 line was closed and the valve-1 bypass line was open. When the concentration of toluene vapor at the inlet of the adsorber reached the steady state, about 0.50 g of formaldehyde-treated walnut shells was weighed out and formaldehyde-treated walnut shells ged into the adsorption column and then the experiments were carried out by turning the valve-1 line to closed and the valve-2 line to the open position. The concentrations of toluene vapor at the inlet and outlet (after adsorption) of the adsorber were produced using a PID controlled heated thermostat at 20, 30, 40 and 50°C, respectively. The formaldehyde-treated walnut shells particles were supported by microsieve at the outlet of the adsorber. Then, the carrier gas containing a previously arranged concentration of toluene vapor was passed through the column until the toluene vapor concentration become constant and stable. The concentrations of toluene vapor at the inlet and outlet of the adsorber were measured by a Gas Chromatograph equipped with a Flame Ionization Detector (GC-FID, GC 910, Buck Scientific) and recorded by a computer.

The dynamic adsorption capacity was determined using the following equation [16]:

$$q = \frac{F}{m}\int_0^t (C_{in} - C_{eff})dt \quad (1)$$

The integrated form of Eq. (1), which was used in this study to determine the adsorption capacity of toluene vapor onto formaldehyde-treated walnut shells, can be defined as:

$$q_t = \sum_0^n \left[\frac{F}{m}(C_{in} - C_{eff})\Delta t\right] \quad (2)$$

Where, q_t (mg g^{-1}) is the toluene vapor adsorption capacity, as shown in Eq. (1), which is integrated from t=0 to t (min), m (g) is the amount of adsorbent, F (L min^{-1}) is the gas flow rate, n is the number of samples taken, C_{in} (ppm) and C_{eff} (ppm) are the concentrations of toluene vapor at the inlet and outlet (after adsorption) of the adsorber, respectively. In the adsorption process, q_t=qe is achieved when the equilibrium time (t_e) is reached and refers to the adsorption capacity at equilibrium.

The adsorption efficiency of toluene vapor onto formaldehyde-treated walnut shells is defined as below:

$$Adsorption\ efficiency\ (\%) = \frac{C_{in} - C_e}{C_{in}} \times 100 \quad (3)$$

Where, C_{in} (ppm) and C_e (ppm) are the concentrations of toluene vapor at the inlet and equilibrium, respectively.

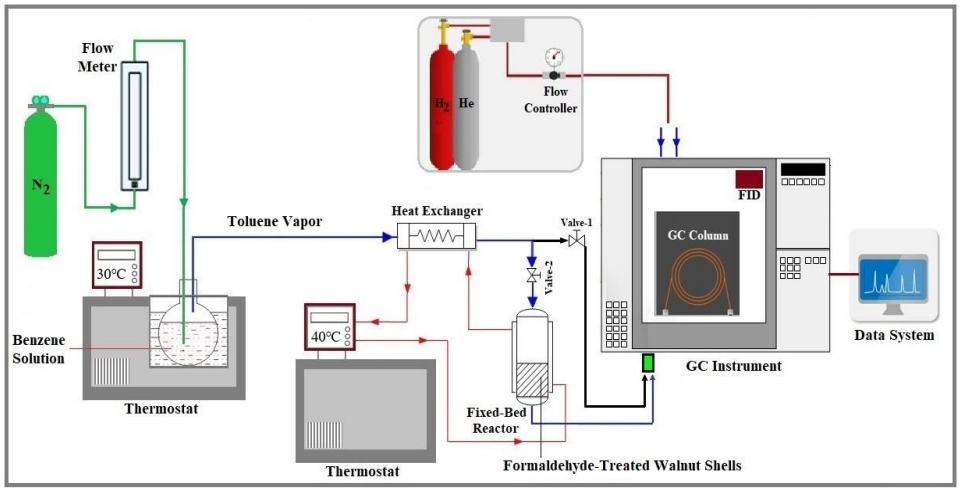

Figure 1. Experimental setup for the adsorption of toluene vapor onto formaldehyde-treated walnut shells

3. RESULTS AND DISCUSSION

In the study, the effects of adsorption conditions such as nitrogen (N_2) flow rate as the toluene vapor carrier, amount of formaldehyde-treated walnut shells, concentration of toluene vapor at the inlet and temperature on the adsorption process were determined, in a continuous system. In addition, adsorption kinetics, isotherms and thermodynamics of adsorption process were investigated at different temperatures.

Effect of Flow Rate on Adsorption Process

To determine the effect of the flow rate on both the adsorption capacity and the adsorption efficiency of toluene vapor onto formaldehyde-treated walnut shells, different flow rates as 50, 75, 100 and 120 mL min^{-1} were investigated, and the results are given in Figure 2. To determine the equilibrium time of the adsorption, the adsorption capacity was investigated depending on the time (0-120 min) (Figure 2a). As shown in Figure 2a, depending on the increase in the flow rate, the adsorption capacity is increased and the maximum adsorption capacity is achieved in a shorter time. However, in Figure 2b, the adsorption capacity at equilibrium is increased with increasing flow rate, while the adsorption efficiency is not changed. This result means that the flow rate in the equation (Eq.2), in which the adsorption capacity is determined, changes the adsorption capacity in proportion to the numerical value it has. In other words, it has been observed that the amount of toluene adsorbed onto formaldehyde-treated walnut shells does not increase at higher flow rates.

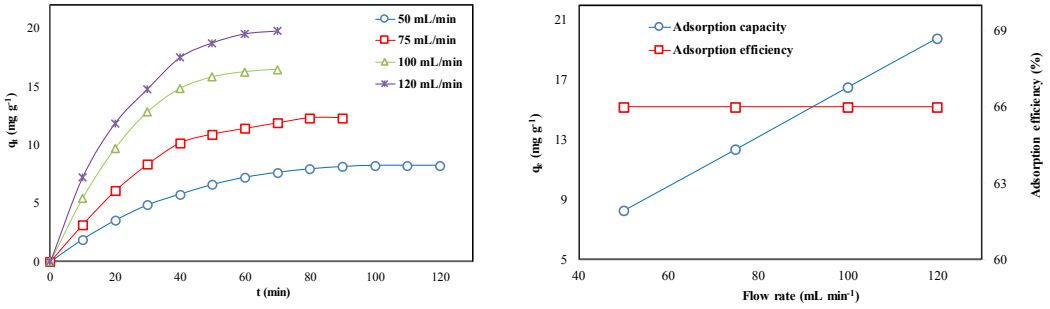

(a) (b)

Figure 2. Effect of flow rate of N_2 as the carrier gas on the adsorption capacity with time (a) and the adsorption capacity at equilibrium and the adsorption efficiency (b) of toluene vapor (conditions: amount of formaldehyde-treated walnut shells 0.50 g, concentration of toluene vapor at the inlet 12.50 mg L^{-1} and temperature 30°C)

Effect of the Amount of Formaldehyde-Treated Walnut Shells on Adsorption Process

The amount of adsorbent is one of the important parameters for the adsorption process. To determine the effect of the formaldehyde-treated walnut shells amount on both the adsorption capacity and the adsorption efficiency of toluene vapor onto formaldehyde-treated walnut shells, different formaldehyde-treated walnut shells amounts as 0.25, 0.50, 0.75 and 1.00 g were investigated, and the results are given in Figure 3. To determine the adsorption equilibrium time, the adsorption capacity was investigated depending on the time (0-90 min) (Figure 3a). Figure 3a shows that an increase in the amount of formaldehyde-treated walnut shells causes a decrease in the adsorption capacity. The possible causes of this result can be expressed as the increase in the amount of formaldehyde-treated walnut shells and the increase in the number of activated sites available and non-saturation of these zones [17], the increase of the activated site ratio of the toluene vapor and adsorbent surface, the absence of toluene ions in the medium [18]. As seen in Figure 3b, it was observed that the adsorption capacity at equilibrium decreased with the increasing amount of formaldehyde-treated walnut shells, the adsorption efficiency increased up to 0.50 g of formaldehyde-treated walnut shells, and did not change with higher amounts of formaldehyde-treated walnut shells. An increase in the amount of

adsorbent increases the number of active sites available for adsorption, thereby increasing the adsorption efficiency [19]. In this work, the minimum amount of adsorbent corresponding to maximum adsorption for formaldehyde-treated walnut shells is 0.50 g.

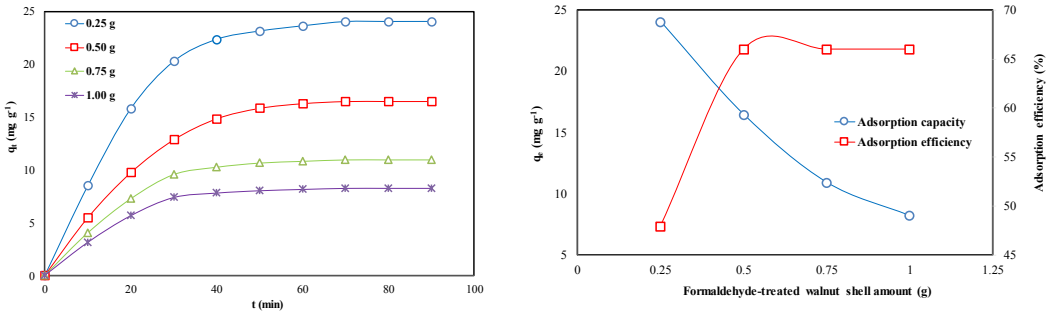

(a) (b)

Figure 3. Effect of formaldehyde-treated walnut shells amount on the adsorption capacity with time (a) and the adsorption capacity at equilibrium and the adsorption efficiency (b) of toluene vapor (conditions: gas flow rate 100 mL min^{-1}, concentration of toluene vapor at the inlet 12.50 mg L^{-1} and temperature 30°C)

Effect of Concentration of Toluene vapor at the inlet on Adsorption Process

To determine the effect of concentration of toluene vapor at the inlet on both the adsorption capacity and the adsorption efficiency of toluene vapor onto formaldehyde-treated walnut shells, different concentrations of toluene vapor at the inlet as 10.00, 12.50, 13.50 and 15.00 mg L^{-1} were investigated, and the results are given in Figure 4. To determine the adsorption equilibrium time, the adsorption capacity was investigated depending on the time (0-100 min) (Figure 4a). As shown in Figure 4a, it was observed that the adsorption capacity increased up to 12.50 ppm and did not change at higher concentrations due to the increase in toluene vapor concentration at the influent. In addition, the increase in the concentration of toluene vapor at the inlet shows that equilibrium adsorption capacity has been reached in a shorter time. These tendencies can be explained with the constant present specific surface area and adsorption area on the formaldehyde-treated walnut shells surface, and with the fact that an increase in the concentration of toluene vapor at influent would naturally result in a shorter exhaustion time. In Figure 4b, the increase in the concentration of toluene vapor at the inlet shows that the adsorption capacity at equilibrium increases up to 12.50 mg L^{-1} and does not change at higher concentrations. However, the adsorption efficiency was observed to decrease at concentrations greater than 12.50 mg L^{-1} (Figure 4b). Possible reasons for these may be the fact that the adsorption capacity, which is a function of the equilibrium concentration, is increased by the increasing concentration of toluene vapor at the inlet [20], or the increase in the number of adsorbate molecules in the vapor that accelerated the adsorption to reach the equilibrium [21]. For all these evaluations, the concentration of toluene vapor at the inlet was taken as 12.50 mg L^{-1} in other adsorption experiments.

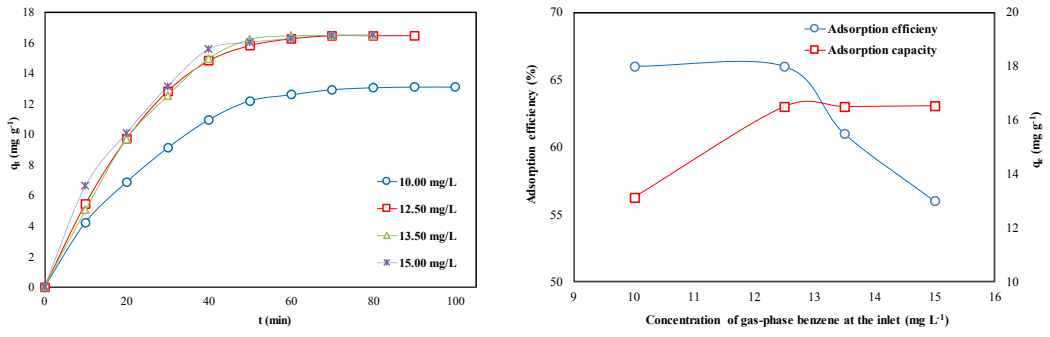

(a) (b)

Figure 4. Effect of concentration of toluene vapor at the inlet on its adsorption capacity with time (a) and the adsorption capacity at equilibrium and the adsorption efficiency (b) of toluene vapor (conditions: amount of formaldehyde-treated walnut shells 0.50 g, gas flow rate 100 mL min^{-1} and temperature 30°C)

Effect of Temperature on Adsorption Process

In the adsorption process, temperature plays an important role in adsorption behavior. To determine the effect of temperature on both the adsorption capacity and the adsorption efficiency of toluene vapor onto formaldehyde-treated walnut shells, different adsorption temperatures as 20, 30, 40 and 50°C were investigated, and the results are given in Figure 5. To determine the adsorption equilibrium time, the adsorption capacity was investigated depending on the time (0-90 min) (Figure 5a). Figure 5a shows that, depending on the increase in adsorption temperature, the adsorption capacity does not change up to 30°C and decreases at higher temperatures. As shown in Figure 5b, both the adsorption capacity at equilibrium and the adsorption efficiency did not change up to 30°C, while decreasing at higher temperatures with the increase in adsorption temperature. Since gas adsorption is an exothermic process, the adsorption capacity decreases

with the increasing temperature. This result shows that physical adsorption is a mechanism that separates the vapor [22].

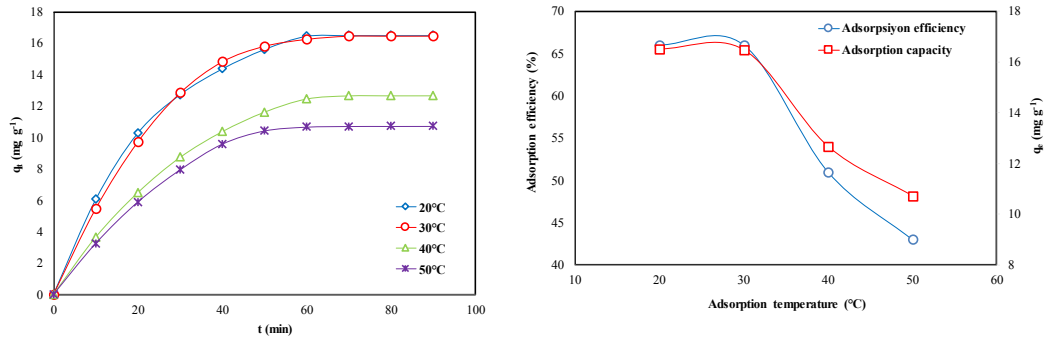

(a) (b)

Figure 5. Effect of adsorption temperature on the adsorption capacity with time (a) and the adsorption capacity at equilibrium and the adsorption efficiency (b) of toluene vapor (conditions: amount of formaldehyde-treated walnut shells 0.50 g, gas flow rate 100 mL min^{-1} and concentration of toluene vapor at the inlet 12.50 mg L^{-1})

Adsorption Kinetics

In order to understand the adsorption process of toluene vapor onto formaldehyde-treated walnut shells, pseudo-first-order and pseudo-second-order kinetics models were applied to experimental data obtained at different temperatures. The pseudo-first-order and pseudo-second-order kinetics models are shown in Figure 6. Figure 6a shows that the pseudo-first-order kinetics model not give beneficient results for adsorption of toluene vapor onto formaldehyde-treated walnut shells, indicating that it is not in good agreement with adsorption data. On the other hand, Figure 6b shows that the pseudo-second-order kinetics model gives beneficient results for adsorption of toluene vapor onto formaldehyde-treated walnut shells and shows a satisfactory agreement with experimental adsorption data.

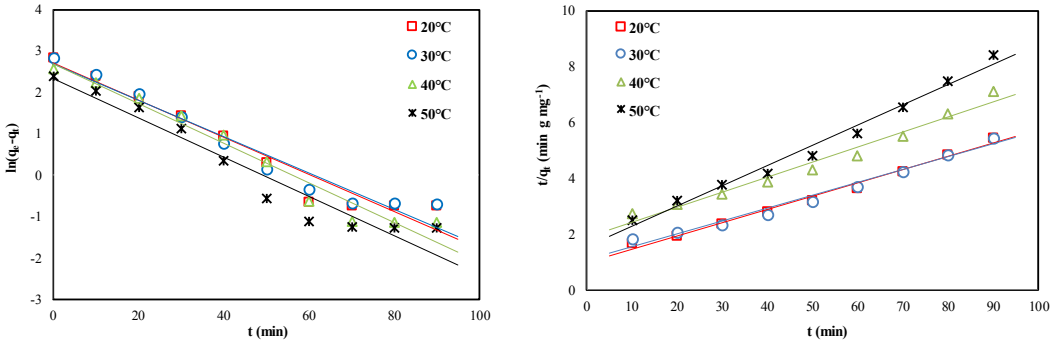

(a) (b)

Figure 6. Pseudo-first-order (a) and pseudo-second-order (b) kinetic models for adsorption of toluene vapor onto formaldehyde-treated walnut shells

Adsorption Isotherms

In order to be able to analyse the adsorption process of toluene vapor onto formaldehyde-treated walnut shells, experimental adsorption equilibrium data obtained at different temperatures were evaluated by applying Langmuir and Freundlich isotherm models. Adsorption tendencies are investigated as the functions of equilibrium concentration. Plots of Langmuir and Freundlich isotherm models are presented in Figure 7. As can be seen from Figure 7a and 7b, it is clear that the plots of the Langmuir isotherm model fit well with the experimental data, while the plots of Freundlich isotherm models do not fit. The compatibility of adsorption equilibrium data with the Langmuir isotherm suggests that the surface of the formaldehyde-treated walnut shells has a homogeneous structure and identical active sites. In addition, this result indicates that the surface energy is homogeneously distributed and that single-plate adsorption occurs [23]. The maximum monolayer adsorption capacity (q_{max}) of formaldehyde-treated walnut shells was calculated to be 19.15 mg g^{-1} for 30°C.

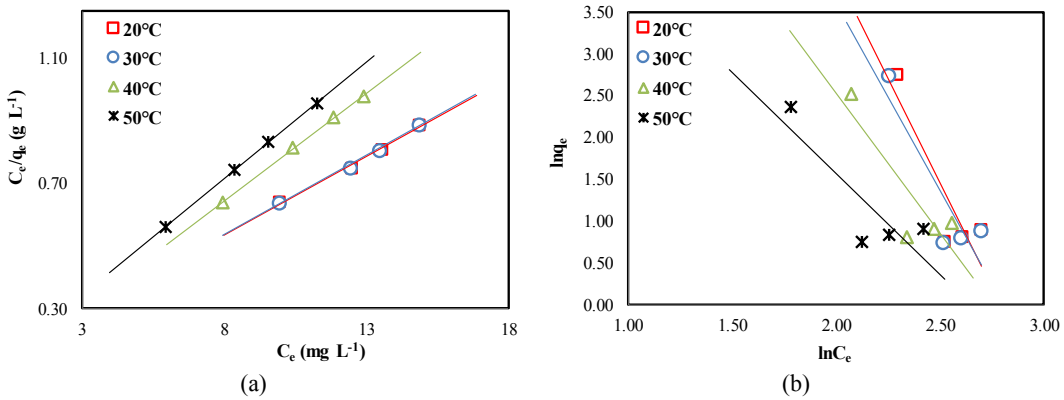

Figure 7. Langmuir (a) and Freundlich (b) isotherm models for adsorption of toluene vapor onto formaldehyde-treated walnut shells

Adsorption Thermodynamics

In an adsorption study, the determination of the adsorption mechanism is rather essential [24]. Adsorption mechanism can be explained by thermodynamic parameters such as Gibbs free energy change (*ΔG°)*, enthalpy change (*ΔH°)* and entropy change (*ΔS°*) [25]. In order to determine the thermodynamic parameters, experiments were carried out at four different temperatures (20, 30, 40 and 50°C). The negative sign of *ΔG°* (-8.67 kJ mol^{-1}) indicates that the adsorption process of toluene vapor onto formaldehyde-treated walnut shells was appropriate and spontaneous [26]. The *ΔG°* values between -20 kJ mol^{-1} and 0 kJ mol^{-1} were reduced to the physical adsorption range [27]. This result shows that physical adsorption was the dominant mechanism for adsorption of toluene vapor onto formaldehyde-treated walnut shells. The *ΔH°* value for toluene vapor was calculated as -16.04 kJ mol^{-1}. The negative value of the calculated *ΔH°* indicates that the adsorption process was exothermic. This means that the energy in the form of heat was released to the environment during the adsorptive process as new bonds were formed. Furthermore, the magnitude of *ΔH°* (<20 kJ mol^{-1}) indicates that physical adsorption was predominant [28]. The negative value of *ΔS°* (-0.024 kJ mol^{-1} K^{-1}). indicates that the entropy of the system decreases. This means that the disorder of the system during the adsorption process and the randomization of the adsorbate at the solid/gas interface were reduced [29]. That is, toluene vapor molecules pass from a random step to a regular step (on the surface of the adsorbent).

4. CONCLUSİONS

In this study, the adsorption kinetics, equilibrium and thermodynamics of toluene vapor onto formaldehyde-treated walnut shells was performed using a laboratory-scale fixed-bed reactor, under atmospheric pressure. Adsorption parameters such as N_2 flow rate as the toluene vapor carrier, amount of formaldehyde-treated walnut shells, concentration of toluene vapor at the inlet, and adsorption temperature play important role on both the adsorption capacity and the adsorption efficiency of toluene vapor onto formaldehyde-treated walnut shells. Experimental results were showed that the adsorption capacity decreases with increasing temperature and amount of formaldehyde-treated walnut shells, while increasing with gas flow rate and the concentration of toluene vapor at the inlet. The results indicated that the adsorption process follows pseudo-second order kinetic model in the most efficient way. It was determined that the data obtained for the adsorption of toluene vapor onto formaldehyde-treated walnut shells were in fitting with the Langmuir isotherm. Thermodynamic parameters, ΔG° = -8.67 kJ mol^{-1}, ΔH°= -16.04 kJ mol^{-1}, ΔS°= -0.024 kJ mol^{-1} K^{-1}, showed that the adsorption process of toluene vapor onto formaldehyde-treated walnut shells was spontaneous exothermic and physical. The maximum monolayer adsorption capacity (q_{max}) of formaldehyde-treated walnut shells was determined to be 19.15 mg g^{-1} for 30°C.

REFERENCES

[1] R. Koppmann, Volatile Organic Compounds in the Atmopshere, Blackwell Publishing Ltd., UK., 2007.
[2] A.K. Ghoshal, S.D. Manjare, Selection of appropriate adsorption technique for recovery of VOCs: an analysis, Journal of Loss Prevention in the Process Industries 15 (2002) 413-421.
[3] F.I. Khan, A. Kr. Ghoshal, Removal of Volatile Organic Compounds from polluted air, Journal of Loss Prevention in the Process Industries 13 (2000) 527-545.
[4] J. Pires, A. Carvalho, M.B. de Carvalho, Adsorption of volatile organic compounds in Y zeolites and pillared clays, Microporous and Mesoporous Materials 43 (2001) 277-287.
[5] N.C. Srivastava, I.W. Eames, A review of adsorbents and adsorbates in solid–vapour adsorption heat pump systems, Applied Thermal Engineering 18 (1998) 707-714.
[6] W.-T. Tsai, A review of environmental hazards and adsorption recovery of cleaning solvent hydrochlorofluorocarbons (HCFCs), Journal of Loss Prevention in the Process Industries 15 (2002) 147-157.
[7] J.N. Cape, D. Fowler, A. Davison, Ecological effects of sulfur dioxide, fluorides, and minor air pollutants: recent trends and research needs, Environment International 29 (2003) 201-211.

[8] Delia M. Pinto, James D. Blande, Silvia R. Souza, Anne-Marja Nerg, J.K. Holopainen, Plant Volatile Organic Compounds (VOCs) in Ozone (O3) Polluted Atmospheres: The Ecological Effects, Journal of Chemical Ecology 36 (2010) 22-34.
[9] M.A. Parra, D. Elustondo, R. Bermejo, J.M. Santamaría, Quantification of indoor and outdoor volatile organic compounds (VOCs) in pubs and cafés in Pamplona, Spain, Atmospheric Environment 42 (2008) 6647-6654.
[10] V.K. Gupta, N. Verma, Removal of volatile organic compounds by cryogenic condensation followed by adsorption, Chemical Engineering Science 57 (2002) 2679-2696.
[11] K.S. Hwang, C. Dae Ki, G. Sung Yong, C. Sung Yong, Adsorption and thermal regeneration of methylene chloride vapor on an activated carbon bed, Chemical Engineering Science 52 (1997) 1111-1123.
[12] D.M. Ruthven, Principles of Adsorption and Adsorption Processes, John Wiley, New York, 1984.
[13] R.W.K. Allen, E. D Archer, J. MacInnes, Adsorption by Particles Injected into a Gas Stream, Chemical Engineering Journal - CHEM ENG J 83 (2001) 165-174.
[14] R.W.K. Allen, E.D. Archer, J.M. MacInnes, Theoretical account of a dry sorption injection experiment, AIChE 47 (2001) 2684-2695.
[15] E.D. Archer, R.W.K. Allen, J.M. MacInnes, Measurements of VOC take-up by adsorbing particles in a gas stream, Filtration & Separation 37 (2000) 32-39.
[16] Z. Zhao, S. Wang, Y. Yang, X. Li, J. Li, Z. Li, Competitive adsorption and selectivity of benzene and water vapor on the microporous metal organic frameworks (HKUST-1), Chemical Engineering Journal 259 (2015) 79-89.
[17] A.F. Hassan, A.M. Abdel-Mohsen, M.M.G. Fouda, Comparative study of calcium alginate, activated carbon, and their composite beads on methylene blue adsorption, Carbohydrate Polymers 102 (2014) 192-198.
[18] Z. Noorimotlagh, R. Darvishi Cheshmeh Soltani, A.R. Khataee, S. Shahriyar, H. Nourmoradi, Adsorption of a textile dye in aqueous phase using mesoporous activated carbon prepared from Iranian milk vetch, Journal of the Taiwan Institute of Chemical Engineers 45 (2014) 1783-1791.
[19] Bazrafshan E., Faridi H., K. M.F., M. A.H., Arsenic removal from aqueous environments using moringa peregrina seed extract as a natural coagulant, Asian Journal of Chemistry 25 (2013) 3557-3561.
[20] M.D.G. de Luna, E.D. Flores, D.A.D. Genuino, C.M. Futalan, M.-W. Wan, Adsorption of Eriochrome Black T (EBT) dye using activated carbon prepared from waste rice hulls—Optimization, isotherm and kinetic studies, Journal of the Taiwan Institute of Chemical Engineers 44 (2013) 646-653.
[21] B.H. Hameed, M.I. El-Khaiary, Equilibrium, kinetics and mechanism of malachite green adsorption on activated carbon prepared from bamboo by K2CO3 activation and subsequent gasification with CO2, Journal of Hazardous Materials 157 (2008) 344-351.
[22] D. Ramirez, S. Qi, M.J. Rood, K.J. Hay, Equilibrium and Heat of Adsorption for Organic Vapors and Activated Carbons, Environmental Science & Technology 39 (2005) 5864-5871.
[23] Y. Guo, Y. Li, T. Zhu, J. Wang, M. Ye, Modeling of dioxin adsorption on activated carbon, Chemical Engineering Journal 283 (2016) 1210-1215.
[24] H.N. Tran, S.-J. You, H.-P. Chao, Thermodynamic parameters of cadmium adsorption onto orange peel calculated from various methods: A comparison study, Journal of Environmental Chemical Engineering 4 (2016) 2671-2682.
[25] P. Ammendola, F. Raganati, R. Chirone, CO2 adsorption on a fine activated carbon in a sound assisted fluidized bed: Thermodynamics and kinetics, Chemical Engineering Journal 322 (2017) 302-313.
[26] J. He, S. Hong, L. Zhang, F. Gan, Y.-S. Ho, Equilibrium and Thermodynamic Parameters of Adsorption of Methylene Blue onto Rectorite, Fresenius Environmental Bulletin 19 (2010) 2651–2656.
[27] D. Duranoğlu, A.W. Trochimczuk, U. Beker, Kinetics and thermodynamics of hexavalent chromium adsorption onto activated carbon derived from acrylonitrile-divinylbenzene copolymer, Chemical Engineering Journal 187 (2012) 193-202.
[28] A.A. Adelodun, J.C. Ngila, D.-G. Kim, Y.M. Jo, Isotherm, Thermodynamic and Kinetic Studies of Selective CO2 Adsorption on Chemically Modified Carbon Surfaces, Aerosol and Air Quality Research (2016) 3312–3329.
[29] A. Gürses, Ç. Doğar, M. Yalçın, M. Açıkyıldız, R. Bayrak, S. Karaca, The adsorption kinetics of the cationic dye, methylene blue, onto clay, Journal of Hazardous Materials 131 (2006) 217-228.

BIOGRAPHY

Sinan KUTLUAY was born in 1988 in Ağrı/Tutak. He graduated from Yildiz Technical University, Faculty of Chemistry-Metallurgy, Department of Chemical Engineering in 2010. Between the years 2010-2012, he completed his master's degree at Yıldız Technical University, Graduate School of Natural Sciences, Department of Chemical Engineering. Between the years 2014-2018, he completed his doctorate's degree at Selçuk University, Graduate School of Natural Sciences, Department of Chemical Engineering. In 2011, he was appointed as research assistant at Siirt University, Department of Chemical Engineering. He is currently working as Assist. Prof. Dr. in the same department. Sinan KUTLUAY is married and has one child.

ICACChE
2nd International Conference on Applications in Chemistry and Chemical Engineering
10 - 14 October 2018 Belgrade

An Optimization Study for Production of PEDOT: PSS Based Conductive Polymeric Films

Didem Aycan[1], Nihal Dolapçı, Özge Gülüzar Karaca, Neslihan Alemdar

Abstract

Conductive polymers have the highest possibility to become promising candidates for energy storage, solar cells, supercapacitors and also bio-applications due to provide remarkable difference such as environmental stability, low cost, high capacitance, and high conductivity when compared with metals. In recent years, especially energy storage has been attracting much interest, since conductivity is the key parameter for the materials used in this application area. Poly (3, 4-ethyleendioxythiophene) (PEDOT) is a well-preferred conductive polymer owing to its attractive combination of properties including long-term mechanical and chemical stability coupled with a multiplicity of synthesis options, high transparency and enabling cost-effective mass production. In this study, the polymeric films were prepared by using different amount of gelatin (Gel), sodium alginate (SA), and hyaluronic acid (HyA) via solvent casting method. Following that, the different amounts of PEDOT:PSS were incorporated into polymeric structure to provide conductivity to polymeric films. PEDOT:PSS-based conductive polymeric films were characterized by FT-IR analyses. The water uptake capacity of the films was determined via swelling tests gravimetrically. The electrical conductivity of PEDOT:PSS-based conductive films was derived from the sheet resistivity determined by the four-point probe technique. According to the obtained results, optimum amount of PEDOT:PSS and polymeric content were determined for the best film formulation. Additionally, it was concluded that the obtained polymeric films which were produced based on optimum conditions would be used in energy storage applications for future works

Keywords: Conductive film, Energy storage, Hyaluronic acid, Gelatin, Sodium alginate, PEDOT:PS

1. INTRODUCTION

Conductive polymers are attractive materials for researchers due to their unique properties including environmental stability, low cost, high capacitance, and high conductivity [1]. The property of electrical conductivity is improved by the addition of conductive particles such as carbon nanotubes [2], graphene-family materials (graphene, graphene oxide (GO), reduced graphene oxide (RGO) etc.) [3]–[5], metallic nanoparticles [6], into the polymeric network or modifications of polymeric structure with inherently conducting polymers including polyaniline (PANI) [7], poly(pyrrole) [8], Poly(3,4-ethylenedioxythiophene) (PEDOT) [9].

PEDOT, can conduct charge like metals and are also flexible like conventional polymers, is commonly preferred for using in many applications such as; optical devices, polymeric light emitting diodes (LEDs), electrochromic windows and displays, chemical and biological sensors, corrosion protective coatings, electrodes of batteries and electromagnetic shielding materials [10]-[13]. However, its applications especially in biotechnology application field is limited because of toxicity and nonbiocompatibility.

Electroconductive polymeric films can be fabricated as biocompatible by using biomolecules. Natural polymers like alginate, collagen, agarose, fibrin, hyaluronic acid (HyA), cellulose and chitosan are generally used for this purpose. These biopolymers have specific properties according to their sources and chemical structure. HyA, fibrin and collagen are obtained from mammalian tissues. Alginate and agarose are marine algal polysaccharides [14],[15]. HyA is used in wound healing and tissue engineering which found in extracellular matrix [16]. Native HyA degrade rapidly in living organisms [17]. Its poor mechanical properties can be enhanced by producing HyA-based polymeric structures. Alginate gels are created easily by means of divalent cations (Ca+2, Mg+2) [18]. However, losing of these ions causes uncontrollable and incalculable dissolution. Covalent crosslinking of alginate enhances mechanical and/or swelling properties

[1] *Corresponding author: Marmara University, Faculty of Engineering, Chemical Engineering Department, 34722, Istanbul, Turkey, didem.aycan@marmara.edu.tr*

[15],[16]. Gelatin (Gel) obtained through controlled hydrolysis of collagen has also desired features such as biodegradability, biocompatibility, film forming ability and solubility at body temperature for biomedical applications [19].

Based on the all brilliant properties, it is visualized that the combination of Gel/SA/HyA and PEDOT could be used as a potential electroconductive and biocompatible material for future applications.

2. MATERIALS AND METHODS

2.1 Materials

Sodium Alginate (SA, medical grade, viscosity 250 cps, 25◦C),gelatin (Gel, medical grade, 280–320 bloom, Type A), hyaluronic acid (HyA, food grade, MW= 8 × 105Da) and 1-Ethyl-(3-3-dimethylaminopropyl) carbodiimide (EDC) were purchased from Heze Better Biochemical Co., Ltd. (China). 3,4-ethylenedioxythiophene (EDOT), sodium polystyrene sulfonate (NaPSS), iron (III) nitrate nonahydrate and ethanol were purchased from Sigma Aldrich. All the chemicals were used as received,

2.2 Synthesis of PEDOT:PSS

Firstly, EDOT (0.8 ml) was added into NaPSS solution (15 ml) and mixed for 30 min. 15.3 g $Fe(NO_3)_3.9H_2O$, which was dissolved in 5 ml distilled water, was added into first solution. The solution obtained after the reaction was centrifuged at 6500 rpm during 10 min. Following that, precipitate were placed into glass petri dishes and dried under vacuum for 24 h.

2.3 Preparation of conductive composite film

Gel/SA/HyA/PEDOT:PSS composite films were prepared by using a solvent casting evaporation method. 3 different formulations were used for film composition. In the first formulation step, Gel, SA and HyA were each dissolved in distilled water (0.5 w/v) until homogenous solutions were obtained. These solutions were mixed in proportion of 45 v. % Gel, 45 v. % SA and 10 v. % HyA. Stock suspension of PEDOT:PSS (1 w. %) was prepared by ultrasonic treatment for 10 min and then it was added to Gel/SA/HyA solution with different concentrations (4 v.%, 6 v.% and 8 v.%). EDC was used as a crosslinker. Its solution was prepared in ethanol (0.5 w.%) and added to polymeric mixture. The final polymeric mixtures were dried in petri dishes at 37 ºC for 3 days. The same procedures were repeated for other 2 formulations but with different amount of Gel, SA, HyA and PEDOT:PSS. While Gel, SA and HyA amounts in the polymeric mixture were kept constant in formulation 2, PEDOT:PSS suspension was added to polymeric mixture with concentrations of 1 v.%, 3 v.% and 5 v.% to investigate the effect of the amount of PEDOT:PSS in the polymeric network. In formulation 3, Gel, SA and HyA amounts in the polymeric mixture were changed as 60 v.% Gel, 30 v.% SA and 10 v.% HyA to observe the effect of the polymeric mixture composition.

2.4 Characterization of Gel/SA/HyA w/out PEDOT:PSS composite films

The chemical structure of Gel/SA/HyA w/out PEDOT:PSS composite films was verified by Fourier transform infrared spectroscopy (FT-IR). FT-IR analysis was carried out with Perkin Elmer Spectrum One FT-IR with attenuated total reflectance (ATR) unit and film samples were scanned in the range of 600 and 4000 cm^{-1} .

2.5 Electrical conductivity test

The electrical conductivity of the composite films was derived from the sheet resistivity determined by the four-point probe technique which is a characterization tool used widely for examining the electrical properties of solids and thin films. In this study, Lucas Labs S-302 Four Point Resistivity Probing Equipment which was connected to a Gamry Instruments power source to supply the constant current and to read the voltage, was used.

Sheet resistivity (ρ) was calculated by using Eq. (1);

$$\rho = \frac{\pi x t x V}{ln2 x I} \quad (1)$$

Where, V (volt) is the potential difference between the two inner probes, I (ampere) is the current through the outer pair of probes, t is the film thickness (cm). Then, the conductivity values of the films were calculated by using Eq. (2) (Ref);

$$\sigma = \frac{1}{\rho} \quad (2)$$

2.6 Swelling tests

The water uptake capacity of the films was determined via swelling test based on measuring the equilibrium water content in the films after immersing it in distilled water for a certain period at a fixed temperature. After 24 h, swollen film samples were taken out and were immediately weighed. Swelling ratios were calculated by using Eq. (3);

$$Swelling\ ratio = \frac{W_s - W_d}{W_d} \times 100 \quad (3)$$

where, W_s and W_d are the weights of the swollen and dry film samples, respectively.

3. RESULTS AND DISCUSSION

3.1 Characterization of Gel/SA/HyA w/out PEDOT:PSS composite films

Fig. 1 shows FT-IR spectrums of Gel/SA/HyA w/out PEDOT:PSS composite films. The FT-IR spectra reveal that characteristic bands of Gel, SA and HyA. The peaks located at 1540 and 3250 cm $^{-1}$ are associated with –OH stretching and N-H bending vibrations of Gel. The peaks appearing at 1030 and 1300 cm $^{-1}$, which are due to C-O-C stretching and ester band for C-H bending of saccharide structure, provides the presence of SA in the composite film structure. The bands at about 3300 and 1600 cm $^{-1}$ represent stretching vibrations of O-H and N-H bonds which come from HyA structure, respectively. The characteristic absorption bands of C=C, C-C and C-S stretching coming from PEDOT:PSS structure at 1550, 1300 and 600 cm $^{-1}$ were overlapped with the peaks of Gel/SA/HyA. Furthermore, the peaks at about 3300 cm $^{-1}$ corresponding –OH stretching decreases due to reaction between hydroxyl groups and SO_3H which is the functional group of PEDOT:PSS. It confirms that PEDOT:PSS was successfully incorporated into Gel/SA/HyA polymeric network.

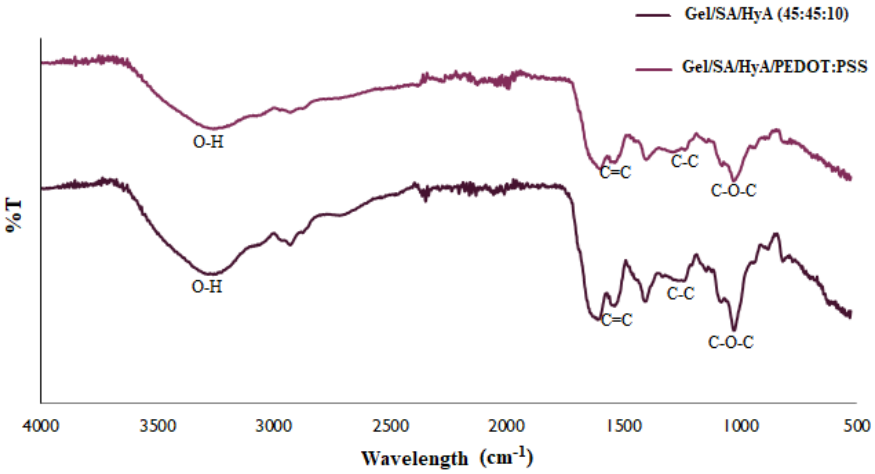

Fig. 1. FT-IR spectra of Gel/SA/HyA w/out PEDOT:PSS

3.2 Electrical conductivity test

The PEDOT:PSS based conductive films were prepared by using 3 different formulations and PEDOT:PSS content. Electrical conductivity measurements obtained by four-probe technique were listed in Table 1 and Fig. 2. In formulation 1, Gel/SA/HyA/ 4 v.% PEDOT:PSS showed highest conductivity. The conductivity of Gel/SA/HyA/ 6 v.% PEDOT:PSS is lower than that of Gel/SA/HyA/ 4 v.% PEDOT:PSS because of agglomeration of high amount of PEDOT:PSS molecules. However, the conductivity value increased with the increasing amount of PEDOT:PSS to 8 v.%. This situation could be explained by the low dispersion of PEDOT:PSS in the polymeric network. As seen, trend of conductivity change with respect of PEDOT:PSS amount is similar for both formulation 2 and formulation 3.

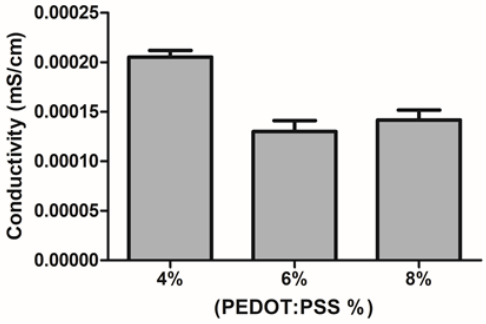

Fig. 2 Effect of PEDOT:PSS amount on the electrical conductivity of Gel/SA/HyA composite films

Table 1. Conductivities of Gel/SA/HyA/PEDOT:PSS composite films

Sample	Film Thickness (cm)	Conductivity ($S.cm^{-1}$) $\sigma = 1/\rho$
Formulation 1- 4 v.% PEDOT:PSS	0,006	$2,05x10^{-7}$
Formulation 1- 6 v.% PEDOT:PSS	0,005	$1,30x10^{-7}$
Formulation 1- 8 v.% PEDOT:PSS	0,007	$1,41x10^{-7}$
Formulation 2- 1 v.% PEDOT:PSS	0,007	$1,19x10^{-7}$
Formulation 2- 3 v.% PEDOT:PSS	0,007	$8,77x10^{-8}$
Formulation 2- 5 v.% PEDOT:PSS	0,007	$1,62x10^{-7}$
Formulation 3- 4 v.% PEDOT:PSS	0,008	$3,63x10^{-7}$
Formulation 3- 6 v.% PEDOT:PSS	0,008	$3,30x10^{-7}$
Formulation 3- 8 v.% PEDOT:PSS	0,008	$3,58x10^{-7}$

3.3 Swelling tests

Swelling tests of composite films w/out PEDOT:PSS were carried out to investigate the effect of PEDOT:PSS amount on the water uptake capacity of composite films. While Gel/SA/HyA v.%4 PEDOT:PSS protected its integrity after 24 h for formulation 1, composite films with 6 and 8 v.% and all film samples of both formulation 2 and 3 could not. This result could be attributed that filling of the voids in the polymeric network with PEDOT:PSS molecules instead of water molecules causes to decrease the crosslinking density. Therefore, effect of PEDOT:PSS amount on swelling capacity was studied by comparing pure and 4 v.% PEDOT:PSS film sample of formulation 1. Also, this result is consistent with the conductivity results of the films. As illustrated in Fig. 3, the swelling capacity of the composite film approximately doubled by incorporating PEDOT:PSS into polymeric network.

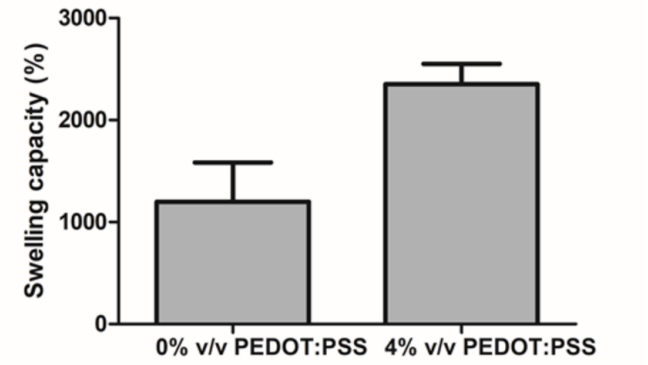

Fig 3. Effect of PEDOT:PSS amount on the swelling ratio of Gel/SA/HyA composite films

4. CONCLUSIONS

The Gel/SA/HyA based electroconductive and biocompatible composite films were fabricated by incorporating of PEDOT:PSS into polymeric network. Three different formulation for film composition was used to optimize parameters. The results of swelling tests indicate that the best composition of the composite films is formulation 1 with the 4 v.% PEDOT:PSS. Additionally, Gel/SA/HyA/4 v.% PEDOT:PSS has the highest conductivity value as $2.05x10^{-7}$ S/cm for formulation 1 in keeping with water uptake capacity results. At the end of the study, it was understood that Gel/SA/HyA/PEDOT:PSS formulation could be used as an electroconductive and biocompatible material in bioelectronics, biosensor, supercapacitor, drug release and battery applications for future works.

REFERENCES

[1] M. A. Enas, "Hydrogel: Preparation, characterization, and applications: A review", *Journal of Advanced Research*, vol. 6(2), pp. 105–121, 2015.

[2] C. Chen, C. Yang, S. Li, and D. Li, “A three-dimensionally chitin nanofiber/carbon nanotube hydrogel network for foldable conductive paper,” *Carbohydrate Polymers*, vol. 134, pp. 309–313, 2015.
[3] T. Tungkavet, N. Seetapan, D. Pattavarakorn, and A. Sirivat, “Graphene/gelatin hydrogel composites with high storage modulus sensitivity for using as electroactive actuator: Effects of surface area and electric field strength,” *Polymer*, vol. 70, pp. 242–251, 2015.
[4] A. Alam, Q. Meng, G. Shi, S. Arabi, J. Ma, N. Zhao, and H. C. Kuan, “Electrically conductive, mechanically robust, pH-sensitive graphene/polymer composite hydrogels,” *Composites Science and Technology*, vol. 127, pp. 119–126, 2014.
[5] G. Sun, B. Li, J. Ran, X. Shen, and H. Tong, “Three-dimensional hierarchical porous carbon/graphene composites derived from graphene oxidechitosan hydrogels for high performance supercapacitors,” *Electrochimica Acta*, vol. 171, pp. 13–22, 2015.
[6] P. Baei, S. Jalili-Firoozinezhad, S. Rajabi-Zeleti, M. Tafazzoli-Shadpour, H. Baharvand, and N. Aghdami, “Electrically conductive gold nanoparticlechitosan thermosensitive hydrogels for cardiac tissue engineering,” *Materials Science and Engineering: C*, vol. 63, pp. 131–141, 2016.
[7] B. S. Kaith, K. Sharma, V. Kumar, S. Kalia, and H. C. Swart, “Fabrication and characterization of gum ghatti-polymethacrylic acid based electrically conductive hydrogels,” *Synthetic Metals*, vol. 187(1), pp. 61–67, 2014.
[8] X. Liang, B. Qu, J. Li, H. Xiao, B. He, and L. Qian, “Preparation of cellulose-based conductive hydrogels with ionic liquid,” *Reactive and Functional Polymers*, vol. 86, pp. 1–6, 2015.
[9] Y. Han, M. Shen, Y. Wu, J. Zhu, B. Ding, H. Tong, and X. Zhang, “Preparation and electrochemical performances of PEDOT/sulfonic acid-functionalized graphene composite hydrogel,” *Synthetic Metals*, vol. 172, pp. 21–27, 2013.
[10] Z. Lizhi, S. Zhiping, Z. Jingyu, T. Jing, Z. Hui, Z. Yunhang, and Z. Caimao, “PEDOT: Cathode Active Material with High Specific Capacity in Novel Electrolyte System,” *J. of Electrochimica Acta*, vol. 53, pp. 8319–8323, 2008.
[11] Y. Wen and J. Xu, “Scientific Importance of Water-Processable PEDOT–PSS and Preparation, Challenge and New Application in Sensors of Its Film Electrode: A Review,” *Journal of Polymer Science*, vol. 55, pp. 1121–1150, 2017.
[12] A. Guiseppi-Elie, “Electroconductive hydrogels: Synthesis, characterization and biomedical applications,” *Biomaterials*, vol. 31(10), pp. 2701–2716, 2010.
[13] R. Balint, N. J. Cassidy, and S. H. Cartmell, “Conductive polymers: Towards a smart biomaterial for tissue engineering,” *Acta Biomaterialia*, vol. 10(6), pp. 2341–2353, 2014.
[14] N. A. Peppas, J. Z. Hilt, A. Khademhosseini, and R. Langer, “Hydrogels in biology and medicine: From molecular principles to bionanotechnology,” *Advanced Materials*, vol. 18(11), pp. 1345–1360, 2006.
[15] K. Y. Lee and D. J. Mooney, “Hydrogels for tissue engineering,” *Chemical Reviews*, vol. 101(7), pp. 1869–1879, 2003.
[16] F. Lee and M. Kurisawa, “Formation and stability of interpenetrating polymer network hydrogels consisting of fibrin and hyaluronic acid for tissue engineering,” *Acta Biomaterialia*, vol. 9(2), pp. 5143–5152, 2013.
[17] M. Al-Sibani, A. Al-Harrasi, and R. H. H. Neubert, “Study of the effect of mixing approach on cross-linking efficiency of hyaluronic acid-based hydrogel cross-linked with 1.4 – butandiol diglycidyl ether,” *European Journal of Pharmaceutical Sciences*, vol. 91, pp. 131–137, 2016.
[18] W. Zhao, X. Jin, Y. Cong, Y. Liu, and J. Fu, “Degradable natural polymer hydrogels for articular cartilage tissue engineering,” *Journal of Chemical Technology and Biotechnology*, vol. 88(3), pp 327–339, 2013.
[19] B. Cohena, A. Shefy-Pelega, and M. Zilbermana, “Novel gelatin/alginate soft tissue adhesives loaded with drugs for pain management: structure and properties,” *Journal of Biomaterials Science*, vol. 25, pp. 224–240, 2014.

BIOGRAPHY

Didem Aycan is currently Ph.D. student in the Department of Chemical Engineering at Marmara University, Istanbul, Turkey. Aycan received her Bachelor Degree from Hacettepe University in Chemical Engineering in 2013 and received her Master Degree from Istanbul Technical University in Chemical Engineering in 2016. During 2013–2016, she worked as a Research Assistant at Istanbul Technical University at Chemical Engineering Department. Her research interests are focused on the synthesis of smart polymers and conductive polymers, their characterizations and its application for drug delivery systems, biosensor and tissue engineering applications and also oil-based film production for coating applications.

Recent Publications

1. Dolapçı N., Karaca Ö.G., Aycan D., Alemdar N. (2018) Production of PEDOT:PSS-Based Conductive Polymeric Film For Future Energy Storage Applications", VII. Polymer Science & Technology Congress With International Participation (POLYMER 2018).

2. Aycan D., Alemdar N. (2018) Fabrication of reduced graphene oxide-based conductive film for controlled drug delivery applications", 8th World Congress on Biopolymers Bioplastics.

3. Aycan D., Alemdar N. (2018) Development of pH-Responsive Chitosan-Based Hydrogel Modified with Bone Ash for Controlled Release of Amoxicillin. Carbohydrate Polymers 184:401-407.

4. Aycan D., Alemdar N. (2017) Production Of pH-Stimuli Responsive Hydrogel for Treatment of Gastric Ulcer. Advanced Polymers via Macromolecular Engineering (APME 2017).

5. Aycan D., Alemdar N. (2017) Fabrication of Bone Ash-Reinforced Smart Hydrogel with Enhanced Mechanical and Thermal Performance. European Polymer Federation Congress (EPF 2017).

6. Alemdar N., Uluturk C., Aycan D., Akyuz D., Koca A., Albayrak F.K. (2017) PANI-Based Hydrogel For Glucose Sensıng. International Conference on Applications in Chemistry and Chemical Engineering (ICACCHE 2017).

7. Aycan D., Alemdar N (2016) Chitosan-Based Hydrogel with A High Water Uptake Capacity for Biomedical Applications. 80th Prague Meetings on Macromolecules, Self-assembly in the world of polymers (8Oth PPM).

8. Aycan D., Erciyes A.T. (2015) An Easy Way to Modify Triglyceride Oils for Oil Based Binder Preparation", Bayreuth Polymer Symposium (BPS 2015).

ICACChE
2nd International Conference on Applications in Chemistry and Chemical Engineering
10 - 14 October 2018 Belgrade

A Country-Based Comparison of Global Warming Potential of National Electricity Generation

Gülşah Yılan[1], Gökçen Çiftçioğlu, Neşet Kadırgan

Abstract

Since the electricity generation activities from fossil fuels are the main contributor to climate change problems, especially for the countries that rely on fossil fuels to supply their electricity demand, impacts associated with the electricity generation activities should be carefully analyzed. As the sustainability concept emerges with the rising environmental awareness, policy-making strategies have changed in a way to consider all related issues like technical, environmental, and socio-economic factors. Among these factors, environmental issues are one of the least studied ones compared to financial and technical aspects. In order to investigate the environmental impacts related with electricity sector in Turkey, a life cycle assessment methodology is applied for the 2014 electricity generation mix. The IPCC 2013 impact assessment method is used for calculating the global warming potential (GWP) of electricity generation activities. As the computation results indicate, fossil fuel technologies are the main responsible for environmental burdens generated. In a global warming potential basis, country-based comparisons are also conducted with electricity mix of various countries. In this study, environmental impacts for 2014 electricity mix is compared with other studies concerning Turkey and also with different countries as follows: the Czech Republic, China, Portugal, India, US, Thailand, and New Zealand. Selected studies apply the same methodology with this paper in terms of functional unit and impact assessment method. The comparison is conducted with environmental impacts of national electricity mix expressed in kg CO_2 equivalents per kWh. The GWP scores for fossil fuel technologies are consistent with Turkey-specific studies available in the literature with respect to their order of magnitude affirming the reliability of the inventory data.

Keywords: country-based comparison, electricity generation, global warming potential, sustainability, Turkey.

1. INTRODUCTİON

Fossil fuel related environmental impacts draw attention to emerging climate change mitigation problems for the last decades. Especially for the countries like Turkey, that supply their energy demand from fossil fuel technologies, environmental burdens should be comprehensively analyzed. There exist a number of impact assessment studies in the literature for Turkey [1 – 3]. Yet, published studies have limited scopes, outdated input data, and significant errors in the assumptions.

This study is an investigation of electricity generation technologies in Turkey with the up-to-date input data for the year 2014 since it is the latest verified year in the calculation process. The aim of this study is to assess the environmental burdens generated in terms of global warming potential (GWP) per kWh electricity for each generation technology. Also the impact assessment results are compared with the previously published studies about Turkey and also with different countries as the Czech Republic [4], China [5], Portugal [6], India [7], US [8], Thailand [9], and New Zealand [10]. The selected studies are screened in a way to apply the same methodology with this paper in terms of functional unit, system boundaries and impact assessment methodology. The comparison is conducted with environmental impacts of national electricity mix expressed in kg CO_2 equivalents per kWh.

Corresponding author: Marmara University, Faculty of Engineering, Department of Chemical Engineering, Goztepe Campus, 34722 Kadıköy, Istanbul, Turkey, gulsah.yilan@marmara.edu.tr

2. MATERIAL AND METHOD

The methodology used in the calculation of environmental impacts is LCA, which is described in the ISO standards [11, 12]. According to the standards, an LCA study consists of four phases, namely, (i) goal and scope definition; (ii) inventory analysis; (iii) impact assessment; (iv) interpretation. In the first phase, goal of the study is defined as well as the scope and functional unit. In the second phase, inventory data of the investigated generation technology is collected and introduced to the computer program. In the third phase, an impact assessment methodology is selected and environmental impact scores are obtained from inventory data. In the last phase, input and output data belonging to the previous steps are evaluated and a final report is proposed.

Goal and Scope Definition

The aim of this study is to investigate the environmental impacts related to electricity generation in Turkey for the year 2014. Functional unit is selected as 1 kWh electricity generated by the investigated technology. The scope of this study is "cradle-to-gate" including extraction, processing and transport of fuels; operation of the power plants along with power plant construction. The environmental impacts are also compared with the previously published country-based studies with the same functional unit, system boundary, and impact assessment methodology.

Inventory Analysis

The schematic of electricity generation technologies in Turkey by the year 2014 are given in Figure 1. Background data is obtained from Ecoinvent v3.01 database [13]. Total electricity generated in 2014 is gathered from Turkish Electricity Transmission Company (TETC) statistics [14]. Lignite and hard coal data is gathered from Turkish Statistical Institute (TSI) [15] and Turkish Coal Enterprises [16]. Natural gas data is gathered from Turkish Petroleum (TP) [17]. Hydropower, wind and solar PV processes are based on the Ecoinvent database due to the lack of country-specific data.

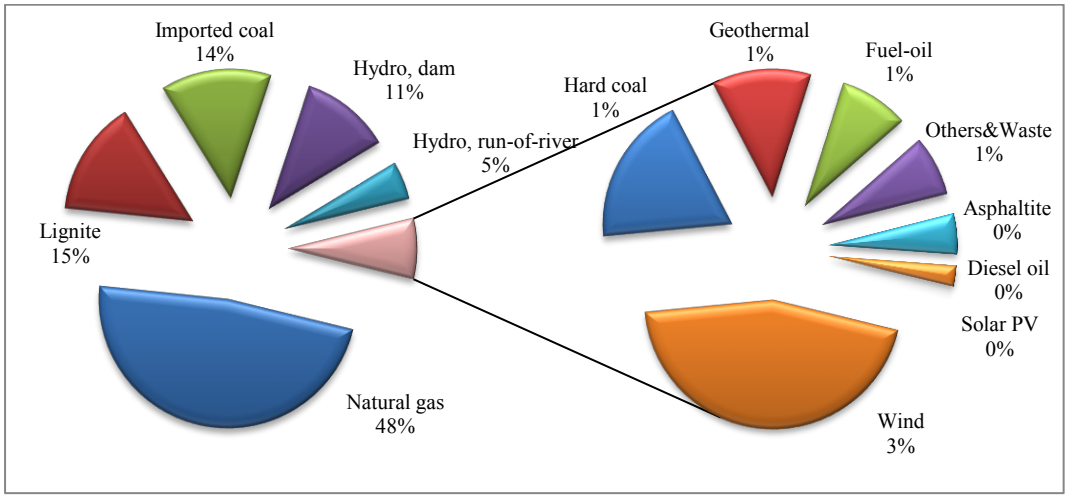

Figure 1. The distribution of electricity generation technologies in 2014, Turkey (TETC)

Impact Assessment

The single issue IPCC 2013 impact assessment method is used for calculating the global warming potential (GWP) of electricity generation activities. GWP score indicates how much a given gas warms the Earth compared to CO_2 over that specific time period. The time period usually referred for GWPs is 100 years.

Interpretation

Final reporting of the assessment results are discussed in the following section in detail.

3. RESULTS AND DISCUSSION

The interpretation phase of an LCA study includes the reporting of the findings gathered from the previous three phases. First, the results of GWP scores of electricity generation technologies in 2014, Turkey are discussed and then a comparison is conducted with the literature studies applying the same methodological basis.

Estimation of Global Warming Potential Scores of Current Generation Technologies

GWP scores indicate how much energy the emissions of 1 ton of a gas absorbs over a given period of time, relative to the emissions of 1 ton of carbon dioxide (CO_2). As the generation technologies are considered individually, the highest environmental burden is calculated for lignite with a score of 1.27 kg CO_2-eq/kWh (*Figure 2*). Hard coal and natural gas technology scores follow the lignite technology. Compared to the fossil

fuel counterparts, alternative renewable energy technologies have dramatically lower scores. The lowest score is calculated for onshore wind technology as $9.32x10^{-5}$ kg CO_2-eq/kWh.

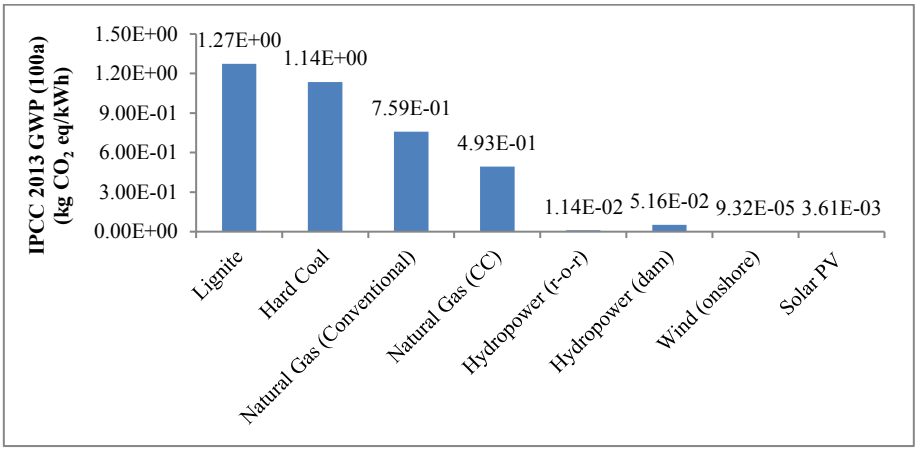

Figure 2. Life cycle impact assessment analysis results for2014 electricity generation mix in Turkey

In addition to the individual scores, the total GWP score of the year 2014 is also calculated to depict the full picture of energy generation. Almost all of the equivalent emissions of CO_2 are resulted from the fossil fuel technologies due to their high carbon content as seen in the *Figure 3*. In order to reduce the GWP scores, countries are aiming to shift from fossil fuel technologies to low-carbon policies; this shift is possible via the utilization of renewable energy technologies.

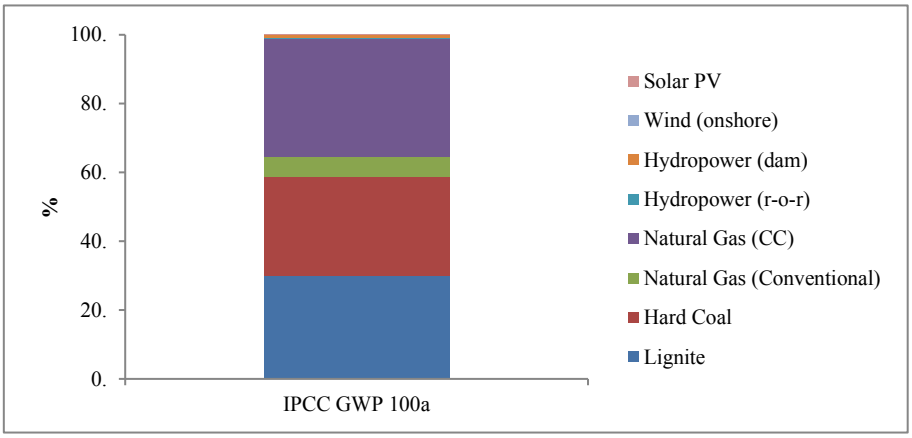

Figure 3. Contribution of generation technologies to the total GWP score in 2014, Turkey

Comparison of Country-Based Global Warming Potential Scores

In order to check the consistency of GWP scores, a comparison is conducted with previously published studies in terms of the same functional unit, system boundary, and impact assessment methodology. The environmental impacts for 2014 electricity mix are compared with other studies concerning Turkey and also with different countries as follows: the Czech Republic, China, Portugal, India, US, Thailand, and New Zealand. The country-based GWP scores of national electricity generation mix of selected countries are expressed in kg CO_2 equivalents per kWh. The GWP scores for fossil fuel technologies are consistent with Turkey-specific studies available in the literature with respect to their order of magnitude affirming the reliability of the inventory data (Figure 4). However, renewable energy technology scores differ from each other in a wide range (Figure 5). This variation may come about as a result of the assumptions made, geographic location characteristics, and power plant characteristics. As the investigation of environmental impacts arising from the renewable technologies proceeds, more consistent comparison studies may be performed.

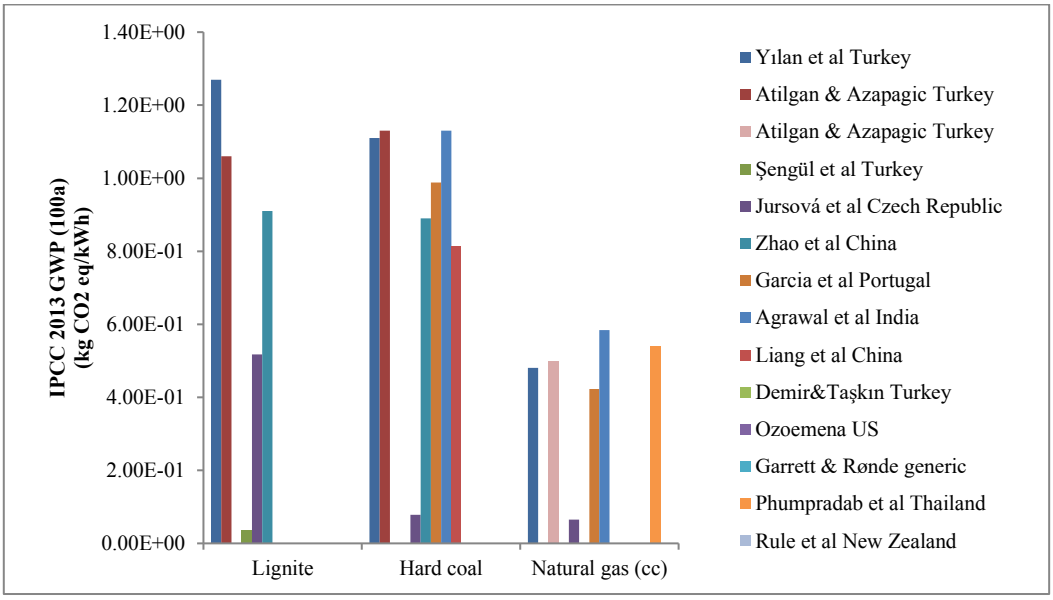

Figure 4.Comparison of GWP scores of fossil fuel technologies with the previous studies

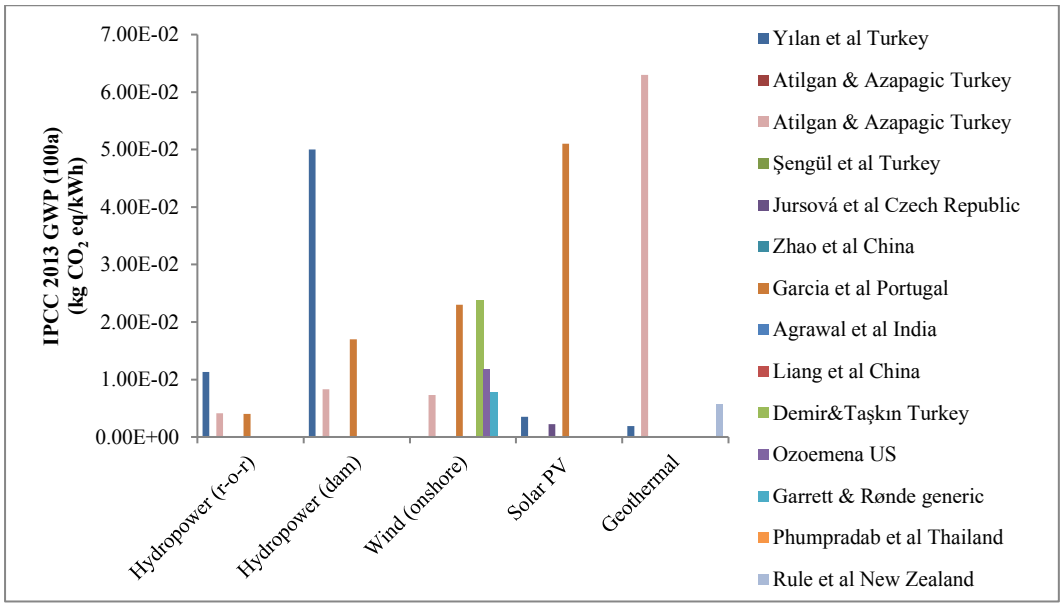

Figure 5. Comparison of GWP scores of alternative technologies with the previous studies

4. CONCLUSION

Environmental problems caused by the electricity generation activities have drawn great attention as the sustainability concept becomes popular among the societies. In order to investigate the environmental impacts associated with electricity sector in Turkey, a life cycle assessment methodology is applied for the 2014 generation mix. The IPCC 2013 impact assessment method is used for calculating the global warming potential scores of commercially-available electricity generation technologies. According to the computation results, fossil fuel technologies are the main responsible for environmental burdens generated. In a global warming potential basis, country-based comparisons are also conducted with electricity mix of various countries in order to check the consistency of calculation methodology. The global warming potential scores for fossil fuel technologies are consistent with Turkey-specific studies available in the literature with respect to their order of magnitude affirming the reliability of the inventory data affirming the reliability of inventory data.

ACKNOWLEDGMENT

This study is financially supported by Marmara University, Scientific Research Projects Committee with the project number FEN-D-080818-0468.

REFERENCES

[1]. Z. Günkaya, et al., "Environmental Performance of Electricity Generation Based on Resources: A Life Cycle Assessment Case Study in Turkey," *Sustainability*, vol. 8 (11), pp. 1097, 2016.

[2]. B. Atilgan and A. Azapagic, “Life cycle environmental impacts of electricity from fossil fuels in Turkey,” *Journal of Cleaner Production*, vol. 106, pp. 555-564, 2015.
[3]. B. Atilgan and A. Azapagic, “Renewable electricity in Turkey: Life cycle environmental impacts,” *Renewable Energy*, vol. 89, pp. 649-657, 2016.
[4]. S. Jursová, et al., “Greenhouse Gas Emission Assessment from Electricity Production in the Czech Republic. Environments,” vol. 5(1), pp. 17, 2018.
[5]. G. Zhao and S. Chen, “Greenhouse gas emissions reduction in China by cleaner coal technology towards 2020,” *Energy Strategy Reviews*, vol. 7, pp. 63-70, 2015.
[6]. R. Garcia, P. Marques, and F. Freire, “Life-cycle assessment of electricity in Portugal,” *Applied Energy*, vol. 134, pp. 563-572, 2014.
[7]. K. K. Agrawal, et al., “A life cycle environmental impact assessment of natural gas combined cycle thermal power plant in Andhra Pradesh, India,” *Environmental Development*, vol. 11, pp. 162-174, 2014.
[8]. M. Ozoemena , W.M. Cheung, and R. Hasan, “Comparative LCA of technology improvement opportunities for a 1.5-MW wind turbine in the context of an onshore wind farm,” *Clean Technologies and Environmental Policy*, vol. 20(1), pp. 173-190, 2018.
[9]. K. Phumpradab, S.H. Gheewala, and M. Sagisaka, “Life cycle assessment of natural gas power plants in Thailand,” *The International Journal of Life Cycle Assessment*, vol. 14(4), pp. 354-363, 2009.
[10]. B.M. Rule, Z.J. Worth, and C.A. Boyle, “Comparison of Life Cycle Carbon Dioxide Emissions and Embodied Energy in Four Renewable Electricity Generation Technologies in New Zealand,” *Environmental Science & Technology*, vol. 43(16), pp. 6406-6413, 2009.
[11]. *Environmental management - Life cycle assessment - Principles and framework*, ISO Std. 14040, 2006.
[12]. *Environmental management - Life cycle assessment - Requirements and guidelines,* ISO Std. 14044, 2006.
[13]. G. Wernet, et al., “The ecoinvent database version 3 (part I): overview and methodology,” *The International Journal of Life Cycle Assessment*, vol. 21(9), pp. 1218-1230, 2016.
[14]. (2014) The TETC website. [Online]. Available: http://www.tuik.gov.tr/PreTablo.do?alt_id=1029
[15]. (2016) The TSI website. [Online]. Available: http://www.tuik.gov.tr/basinOdasi/haberler/2016_26_20160303.pdf
[16]. (2015) The TKI website. [Online]. Available: http://www.tki.gov.tr/depo/file/k%C3%B6m%C3%BCr%20sekt%C3%B6r%20raporu/k%C3%B6m%C3%BCr%20sekt%C3%B6r%20raporu%202016.pdf
[17]. (2015) The TP website. [Online]. Available: www.tpao.gov.tr/tp5/docs/rapor/sektorrapor3105.pdf

BİOGRAPHY

Gülşah Yılan is a research assistant in Marmara University Chemical Engineering Department. She had her BSc in Chemical Engineering, MSc in Bioengineering and PhD in Chemical Engineering, Marmara University. Her interest areas are renewable energy, sustainability, impact assessment, decision analysis.

ICACChE
2nd International Conference on Applications in Chemistry and Chemical Engineering
10 - 14 October 2018 Belgrade

Electricity Sector Investments in Turkey with the Comparison of Environmental Burdens Generated

Gülşah Yılan[1], Gökçen Çiftçioğlu, Neşet Kadırgan

Abstract

Energy generation activities are the main contributor to environmental burdens generated country-wide. In order to suggest environmental-friendly policies for future energy planning studies, a comprehensive analysis is required to depict the actual generation profile. With this aim, an impact assessment analysis of electricity generation activities in Turkey for the year 2014 is conducted via life cycle assessment methodology. The midpoint CML 2001 impact assessment method is used for calculating the environmental burdens of electricity generation. As the computation results indicate, fossil fuel technologies are the main responsible for each category of environmental impacts generated. The results also state that increasing the share of renewable technologies is essential in response to meet the increasing energy demand. However, electricity sector investments do not reflect the best case in terms of environmental issues. According to the investments made in the energy sector since 2014, new investments of the Turkish electricity market still depend on fossil fuel technologies despite its being a country of considerable potential regarding renewable energy sources. The trend of investments does not show a linear change throughout the years not only for the total installed power but also for any type of technologies. The fluctuation in the new investments may result from the socio-eco-political situation of the country, the increase in energy efficiency scores of available technologies, and also the public opinion of related power generation technique. Even the investment trend cannot be received from the short-term statistics, renewable energy shares can be supposed to increase from a broad perspective in order to meet sustainable policy-making goals.

Keywords: electricity generation, energy investment, environmental burdens, Turkey.

1. INTRODUCTİON

In energy decision making process, generally financial and technical aspects are of great importance while environmental factors are ignored. In order to propose a sustainable future scenario, current situation and all possible circumstances should be carefully analyzed. Although electricity generation mix in 2016 is still dominated by fossil fuels with a total share of 67%, shares of renewable energy sources tend to increase during the last decade in Turkey as sustainability concept emerges with increasing awareness about the environment [1].

In the Institute for Energy Economics and Financial Analysis [2] report, authors propose a future scenario for Turkey with diversifying its energy mix by adding larger amounts of renewable - wind and solar- resources to keep away from fossil fuels. Since national consensus clearly favors better energy security and greater diversification in how the country fuels its electricity grid, renewable energy has the potential to provide greater benefits and a better economic alternative for Turkey on its path to becoming a more competitive economy. There are various studies in the literature concerning with the sustainability of electricity generation technologies. Incekara and Ogulata [3] emphasize the need for energy policies in reduction on emissions of greenhouse gases, minimization of the use of power plants that use fossil fuels that have significant impacts on ecosystem, environment and causes of climate change. Also, Balat [4] mentions that the fossil fuel dependency problem of Turkey may be solved via diversification of the electricity generation mix from a sustainable point of view. Reducing the share of fossil fuels in the electricity mix would not only reduce the environmental impacts, but also the costs, injuries and fatalities, while also improving energy security problem [5,6]. The aim of this study is to make a comprehensive analysis of electricity sector in Turkey via a life cycle assessment (LCA) methodology for the year 2014. In addition, investment profile of electricity generation technologies is investigated to depict a throughout perspective of the energy sector trends.

Corresponding author: Marmara University, Faculty of Engineering, Department of Chemical Engineering, Goztepe Campus, 34722 Kadıköy, Istanbul, Turkey, gulsah.yilan@marmara.edu.tr

2. MATERIAL AND METHOD

The methodology used in the calculation of environmental impacts is LCA, which is described in the ISO standards [7,8]. According to the standards, an LCA study consists of four phases, namely, (i) goal and scope definition; (ii) inventory analysis; (iii) impact assessment; (iv) interpretation. In the first phase, goal of the study is defined as well as the scope and functional unit. In the second phase, inventory data of the investigated generation technology is collected and introduced to the computer program. In the third phase, an impact assessment methodology is selected and environmental impact scores are obtained from inventory data. In the last phase, input and output data belonging to the previous steps are evaluated and a final report is proposed.

Goal and Scope Definition

The aim of this study is to investigate the environmental impacts related to electricity generation in Turkey for the year 2014. Functional unit is selected as the total electricity generated by commercially available technologies. The scope of this study is "cradle-to-gate" including extraction, processing and transport of fuels; operation of the power plants along with power plant construction. Also, energy sector investments are investigated for a time period of 2010 – 2017 in order to see the trend of the priorities of the energy policy-making strategies.

Inventory Analysis

The available electricity generation technologies in Turkey by the year 2014 are given in *Table 1*. Background data is obtained from Ecoinvent v3.01 database [9]. Total electricity generated in 2014 is gathered from Turkish Electricity Transmission Company (TETC) statistics [1]. Lignite and hard coal data is gathered from Turkish Statistical Institute (TSI) [10] and Turkish Coal Enterprises (TKI) [11]. Natural gas data is gathered from Turkish Petroleum (TP) [12]. Hydropower, wind and solar PV processes are based on the Ecoinvent database due to the lack of country-specific data. The energy sector investment data is gathered from the online database of Ministry of Energy and Natural Resources (MENR) [13].

Table 1.The electricity generation technologies in 2014, Turkey

Alternative	**Resource/Fuel**	**Characteristics**
Lignite	Domestic lignite	Steam turbine based pulverized coal plants
Hard coal	Imported and domestic coal	Steam turbine based pulverized coal plants
Natural gas (Conventional)	Natural gas	Conventional natural gas turbine plants
Natural gas (CC)	Natural gas	Combined cycle gas turbine plants
Hydro (dam)	Water flow	Reservoir (dam) plants
Hydro (r-o-r)	Water flow	Run-of-river (r-o-r) plants
Wind (onshore)	Wind	Onshore wind farms
Solar PV	Solar radiation	Photovoltaic solar panels

Impact Assessment

The multiple issue CML 2001 impact assessment method is used for calculating the environmental burdens of electricity generation activities. The midpoint indicators used in this study are abiotic depletion, acidification, eutrophication, global warming, ozone layer depletion, human toxicity, fresh water aquatic toxicity, marine aquatic toxicity, terrestrial ecotoxicity, photochemical oxidation.

Interpretation

Final reporting of the assessment results are discussed in the following section in detail.

3. RESULTS AND DISCUSSION

The interpretation phase of an LCA study includes the reporting of the findings gathered from the previous three phases. First, the results of CML 2001 methodology are discussed and then electricity sector investments are investigated for a time scale of 2010 – 2017.

Estimation of Environmental Burdens of Electricity Generation Technologies

In order to draw a general perspective of environmental burdens resulting from the electricity generation activities, ten different indicator scores are expressed as contribution percentages. Contribution analysis allows depicting the individual shares of each generation technology for a specific indicator regardless of its dimension across the other indicators. As clearly seen in the *Figure 6*, fossil fuel technologies constitute a

great share of each indicator score. Especially lignite and hard coal technologies create more than 75% of the indicator scores of acidification, eutrophication, human toxicity, fresh water, aquatic and terrestrial ecotoxicity, as well as photochemical oxidation mainly due to their high carbon content. Natural gas technology has moderate burdens for the remaining indicator scores except for ozone layer depletion. Since ozone layer depletion score is strictly based on the long-distance transfer of fuels, pipeline transport of imported natural gas makes a considerable contribution. On the other hand, renewable technology scores have minor contributions to the total scores due to their small generation shares. But even if their share is larger, the environmental burdens they generate are quite lower compared to the fossil fuel counterparts. The results clearly show the necessity of employing renewable energy alternatives instead of conventional fossil fuel technologies.

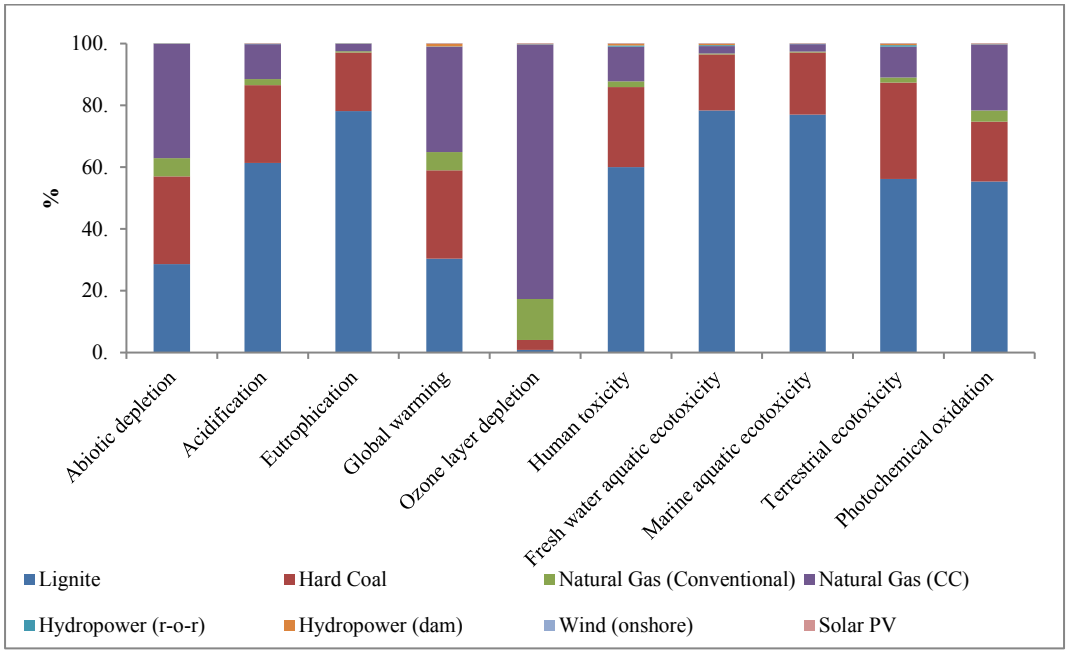

Figure 6. Contribution analysis results for 2014 electricity generation mix in Turkey

Electricity sector investments in Turkey

Although the life cycle analysis shows the environmental burdens of fossil fuel related technologies, energy sector investments do not follow the findings driven by only environmental concerns. As well as environmental issues; financial, technical, and social issues are considered comprehensively in policy-making strategies. Despite being a country of significant potential for renewable energy sources, Turkey electricity sector mainly depends on the fossil fuels. As seen in the *Figure 7*, except for the year 2015, new investments are based on the fossil technologies, too. The trend of new investments does not show a linear change throughout the years not only for the total installed power but also for any type of technologies. The fluctuation in the new investments may result from the socio-eco-political situation of the country, the increase in energy efficiency scores of available technologies, and also the public opinion of related power generation technique. Even the investment trend cannot be received from the short-term statistics, renewable energy shares can be supposed to increase from a broad perspective.

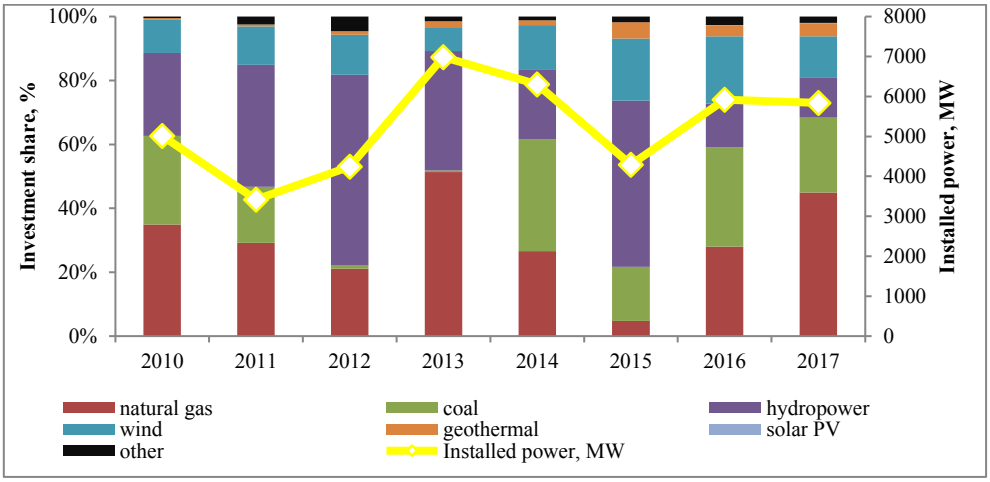

Figure 7. Life cycle impact assessment analysis results for2014 electricity generation mix in Turkey

4. CONCLUSION

The current electricity generation profile of Turkey is analysed comprehensively for the first time with up-to-date country-specific data. LCA methodology is applied for the year 2014 considering generation technology alternatives with different midpoint indicators. LCA results indicate that, fossil fuel technologies are the main reasons of environmental impacts related to electricity generation activities. In order to decrease the environmental burdens, fossil fuel technologies should be substituted with renewable energy technologies for future scenarios. Yet, new investments of the Turkish electricity market still depend on fossil fuel technologies despite its being a country of considerable potential regarding renewable energy sources. The trend of investments does not show a linear change throughout the years not only for the total installed power but also for any type of technologies. Even the investment trend cannot be received from the short-term statistics, renewable energy shares can be supposed to increase from a broad perspective in order to meet sustainable policy-making goals.

REFERENCES

(2014) The TETC website. [Online]. Available: http://www.tuik.gov.tr/PreTablo.do?alt_id=1029

(2016). The IEEFA report. Turkey at a Crossroads: Invest in the Old Energy Economy or the New?. [Online]. Available: http://ieefa.org/wp-content/uploads/2016/09/Turkey-Crossroads-Invest-in-the-Old-Energy-Economy-or-the-New_June-2016-v2.pdf

C. O. Incekara and S. N. Ogulata. "Turkey's energy planning considering global environmental concerns," *Ecological Engineering*, vol. 102, pp. 589-595, 2017.

M. Balat, "Security of energy supply in Turkey: Challenges and solutions," *Energy Conversion and Management*, vol. 51(10), pp. 1998-2011, 2010

B. Atilgan and A. Azapagic, "Energy challenges for Turkey: Identifying sustainable options for future electricity generation up to 2050," *Sustainable Production and Consumption*, vol. 12, pp. 234-254, 2017.

M. Ozcan, "The role of renewables in increasing Turkey's self-sufficiency in electrical energy," *Renewable and Sustainable Energy Reviews*, vol. 82, pp. 2629-2639, 2018.

Environmental management - Life cycle assessment - Principles and framework, ISO Std. 14040, 2006.

Environmental management - Life cycle assessment - Requirements and guidelines, ISO Std. 14044, 2006.

G. Wernet, et al., "The ecoinvent database version 3 (part I): overview and methodology," *The International Journal of Life Cycle Assessment*, vol. 21(9), pp. 1218-1230, 2016.

(2016) The TSI website. [Online]. Available: http://www.tuik.gov.tr/basinOdasi/haberler/2016_26_ 20160303.pdf

(2015) The TKI website. [Online]. Available: http://www.tki.gov.tr/depo/file/k%C3%B6m%C3 %BCr%20sekt%C3%B6r%20raporu/k%C3%B6m%C3%BCr%20sekt%C3%B6r%20raporu%202016.pdf

(2015) The TP website. [Online]. Available: www.tpao.gov.tr/tp5/docs/rapor/sektorrapor3105.pdf

(2018) The MENR website. [Online]. Available: http://www.eigm.gov.tr/tr-TR/Sayfalar/Enerji-Yatirimlari

BİOGRAPHY

Gülşah Yılan is a research assistant in Marmara University Chemical Engineering Department. She had her BSc in Chemical Engineering, MSc in Bioengineering and PhD in Chemical Engineering, Marmara University. Her interest areas are renewable energy, sustainability, impact assessment, decision analysis.

ICACChE
2nd International Conference on Applications in Chemistry and Chemical Engineering
10 - 14 October 2018 Belgrade

Electrochemical oxidation of hydrazine at the metal nanoparticles and polymer film modified electrodes

Müge Hatip, Süleyman Koçak[1], Zekerya Dursun

Abstract

The polymerization of phenol phthalein (PP) has been studied on a glassy carbon electrode (GCE) modified with multi-walled carbon nanotubes (MWCNT) and the surface have been coated with Au nanoparticles by electrochemical reduction technique. The AuNPs/MWCNT/poly(PP)/GC electrode is fabricated and the electrochemical behavior of hydrazine on this modified electrode surface was tested. The AuNPs/MWCNT/poly(PP)/GC electrode has been used as a sensing platform for the detection of hydrazine in Britton Robinson buffer (pH 10.0). A shift in the overpotential to more negative direction and an enhancement in the peak current indicate that the AuNPs/MWCNT/poly(PP)/GC electrode presents an efficient electrocatalytic activity toward oxidation of hydrazine. The nanocomposite modified electrode can be expected to enhance the mass transfer rate and will reduce the over potential for hydrazine electro-oxidation. The electrochemical performance of the modified electrode is investigated using cyclic voltammetry and amperometric technique. Modifying electrodes have been characterized by scanning electron microscopy (SEM).

Keywords: Gold nanoparticles, hydrazine, multi-walled carbon nanotube, phenol phthalein

1. INTRODUCTİON

Conducting polymers have received much attention due to their high surface area, high stability and low resistance. Polymer thin films improve their use as supporting material for the development of new electrocatalytic materials. Because of the high electric conductivity of some polymers, it is possible to shuttle the electrons through polymer chains between the electrode and dispersed metal nanoparticles [1].

Hydrazine is also an ideal fuel for a direct fuel cell system with high hydrogen content (12.5 wt%) and have a very negative potential for electro-oxidation. The oxidation of hydrazine does not induce poisoning effects (CO) on the electrode surface [2]. Hydrazine has been studied as a corrosion inhibitor, rocket, emulsifier, antioxidant, reducer, starting material for pesticides, explosives and manufacture of fuel cells etc. Moreover, hydrazine is an efficient and nontoxic alternative fuel [3]. For the hydrazine determination, were reported several techniques such as spectrophotometric, colorimetric, choromatografic and electrochemical techniques. Voltammetric techniques offer an opportunity for portable, rapid, sensitive and economical methodologies. However, direct electrochemical oxidation of hydrazine at ordinary solid electrodes is a slow electrode process requiring a large overpotential [4]. By modifying the electrodes, the electron transfer rate of hydrazine can be increased and the excess potential can be reduced.

Cyclic voltammetry (CV) is a simple, rapid and powerful method commonly employed to investigate the reduction and oxidation processes of molecular species [5]. CV technique is based on varying the applied potential at a working electrode in both forward and reverse directions while monitoring the current [6].

Metal nanoparticles among the nanomaterials have played an important role in applications such as optics, electronics, magnetics, catalysis and biology because of various unusual chemical and physical properties compared with those of metal atoms or bulk metal [7]. Metal nanoparticles generally exhibit small sizes in a narrow size distribution and well defined regular shapes. They provide very fast kinetics and enhanced sorption capacity due to their high surface to volume ratio [8].

Corresponding author: Manisa Celal Bayar University, Science and Art Faculty, Department of Chemistry, Manisa, Turkey. dr.suleymankocak@gmail.com(s.kocak)

In this study, composite electrodes were prepared by modifying with conductive polymers-carbon nanotube-metal nanoparticle (AuNPs/MWCNT/poly(PP)/GCE) which can increase selectivity and sensitivity and the electrocatalytic oxidation of hydrazine was investigated. Optimum conditions were determined. The electrochemical performance of the modified electrode was investigated using cyclic voltammetry. Modifying electrodes were characterized by scanning electron microscopy technique (SEM).

2. EXPERIMENTAL

Materials and Methods

Voltammetric measurements were carried out by Autolab PGSTAT101 voltammetric analyzer. A three electrode system consisted of the GCE as the working electrode, a platinum wire as the auxiliary electrode and Ag/AgCl (std. KCl) electrode was used as the reference electrode. Cyclic voltammetry was used during the electroanalytical studies.

Hydrazine (N_2H_4) and phenol phthalein were obtained from Sigma Aldrich. All other reagents used were of analytical grade. The solutions were prepared with ultrapure water from a Millipore water system. Britton Robinson buffer (BRB) solution was prepared from a mixture of H_3BO_3, H_3PO_4 and CH_3COOH and the pH was set at 10.0 by addition of necessary amount of NaOH solution.

Under optimal conditions, electrochemical polymerization of phenol phthalein was carried out in 1.0 mM phenol phthalein solution by cyclic voltammetry. The polymerization voltammogram was obtained by repetitive 15 potential cycles from -1.2 V ile +1.8 V in 0.1 M $NaNO_3$ solution media at a scan rate of 200 mVs^{-1} (Figure 1a).

A 10 µL of MWCNT suspension was injected on poly(PP)/GCE surface. The solvent (DMF) of the suspension on the poly(PP)/GCE surface was evaporated at infrared lamp.

The gold nanoparticle was electrochemically deposited on the MWCNT/poly(PP)/GCE by cyclic voltammetry scanning between -0.9 and 0.6 V in $HAuCl_4$ with a scan rate of 100 mV/s for 15 cycles (Figure 1b).

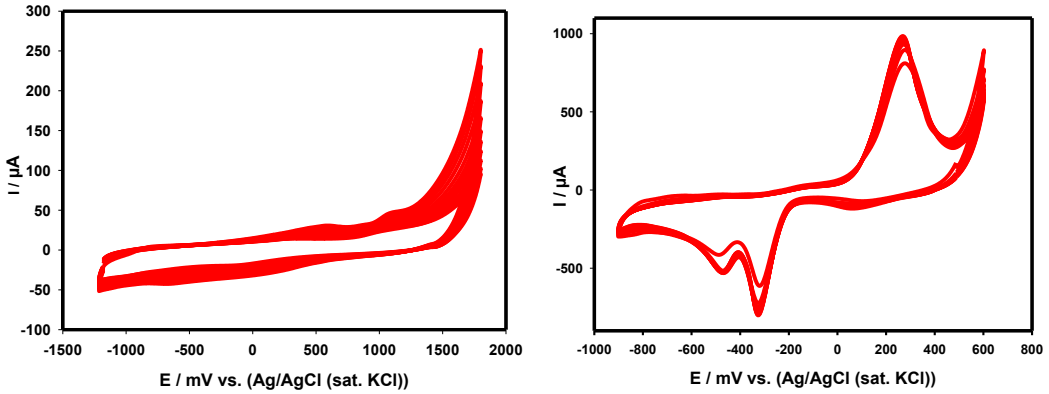

Figure 1. Cyclic voltammogram during electropolymerization of phenol phthalein on GC electrode (scan rate: 200 mV/s) (a), Au nanoparticle deposition on MWCNT/poly(PP)/GCE, at 100 mV/s for 15 cycles in 1 mM $HAuCl_4$ solution (b).

3. RESULTS AND DISCUSSION

The hydrazine oxidation behavior was studied by using cyclic voltammetry on the GCE, MWCNT/GCE, poly(PP)/GCE, MWCNT/poly(PP)/GCE and poly(PP)/MWCNT/GC electrodes (Figure 2). At the bare GCE electrode, the oxidation potential of hydrazine is +0.47 V, +0.31 V when the phenol phthalein monomer is coated, +0.29 V when the MWCNT/poly(PP) is coated. In the peak potential and current, the best electrocatalytic effect was observed on the MWCNT/poly(PP)/GC electrode surface. The best catalytic activity in terms of peak potential was obtained with MWCNT/poly(PP)/GC electrode with a 0.18 V potential shift to negative as compared to the bare GCE.

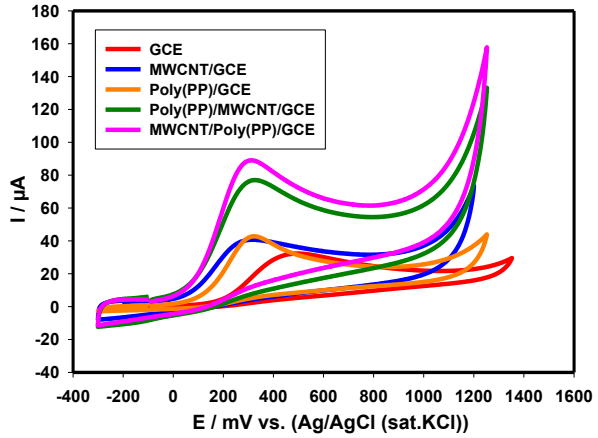

Figure 2. Cyclic voltammograms for the oxidation of hydrazine in bare GCE and modified electrodes in pH 10.0 BRB.

Poly(PP)/GCE and poly(PP)/MWCNT/GC modified electrode surfaces have been characterized by SEM analyses as given in Figure 3. In the SEM images, the morphology of the poly(PP) on GC electrode showed in Figure 3a almost homogeneously distributed porous polymer surface. SEM image of acid-treated MWCNT (Fig. 3b) showed the distribution of tubular like carbon nanotubes on the GCE surface with a smooth and rather uniform pattern. MWCNT are also homogeneously distributed on the poly(PP) surface.

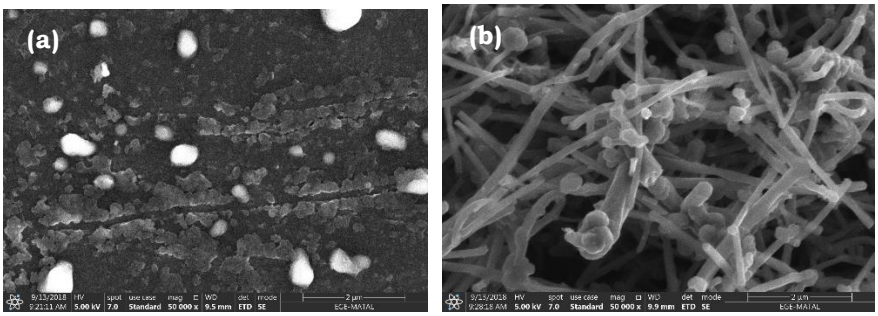

Figure 3. SEM analysis for poly(PP)/GCE (a) and poly(PP)/MWCNT/GCE (b)

The amperogram indicated that the currents of hydrazine oxidation are stabilized and stay constant after 500 s. The oxidation currents reached steady-state quickly after constant potentials were applied and displayed no sign of decrease within the test period (Figure 4).

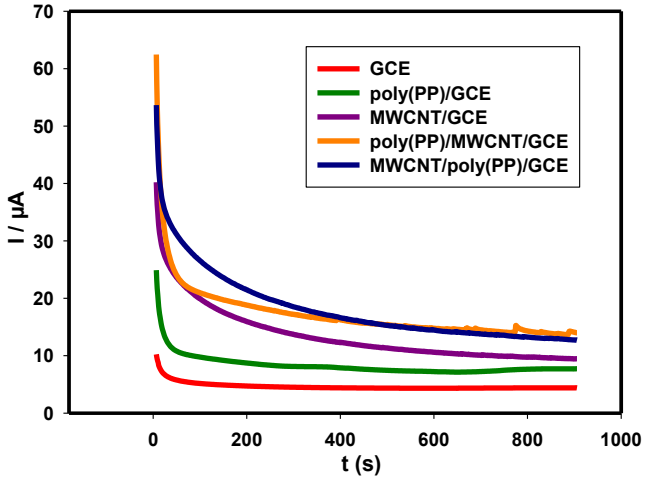

Figure 4. Chronoamperometry measurement of bare and modified electrode at constant potential (0.29 V) and 900 duration time

The electrochemical impedance spectroscopy (EIS) data were fitted with an R(C(RctW)) equivalent circuit. A large semicircle was obtained as a high electron transfer resistance (1270 ohm) in the poly(PP)/GC

electrode compared to the other electrodes. The Rct for the bare GCE was 189 ohm, which was higher than the Rct values obtained for MWCNT/GCE (77.0 ohm). The smaller Rct value confirmed the good conductivity observed for MWCNT/poly(PP)/GCE (64.9 ohm) (Figure 5). The polymerization of the phenol ftale to the glass carbon surface is clearly understood from the increase the resistance of electron transfer on the electrode surface.

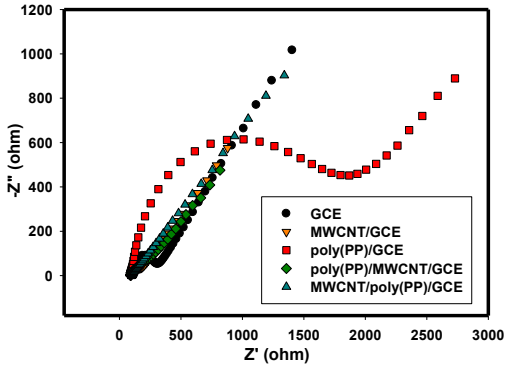

Figure 5.Nyquist plots for bare GCE, MWCNT/GCE, poly(PP)/GCE, poly(PP)/MWCNT/GCE and MWCNT/poly(PP)/GCE in 5mM $K_3[Fe(CN)_6]/K_4[Fe(CN)_6]$ (1:1) containing 0.1 M KCl with frequency of 0.01 Hz – 50,000 Hz.

In order to obtain the best electro-polymerization of phenol phthalein, the different solutions media were studied. The maximum peak was observed for 0.1 M $NaNO_3$ that it was chosen for further studies (Figure 6a). The $NaNO_3$ concentration was varied in a range of 0.01–0.3 M. The best result was obtained in 0.1 M $NaNO_3$ (Figure 6b). The electro-polymerization scan rates of phenol phthalein in 0.1 M $NaNO_3$ were studied by varying potential scan rate (25-200 mV/s). The best electro-polymerization scan rate of phenol phthalein was choosen as 200 mV/s (Figure 6c). The oxidation reaction of the prepared hydrazin was studied at pH 2.0-12.0 BRB solution. The best results were obtained in pH 10.0 and further experiments were carried out at pH 10.0 BRB (Figure 6d).

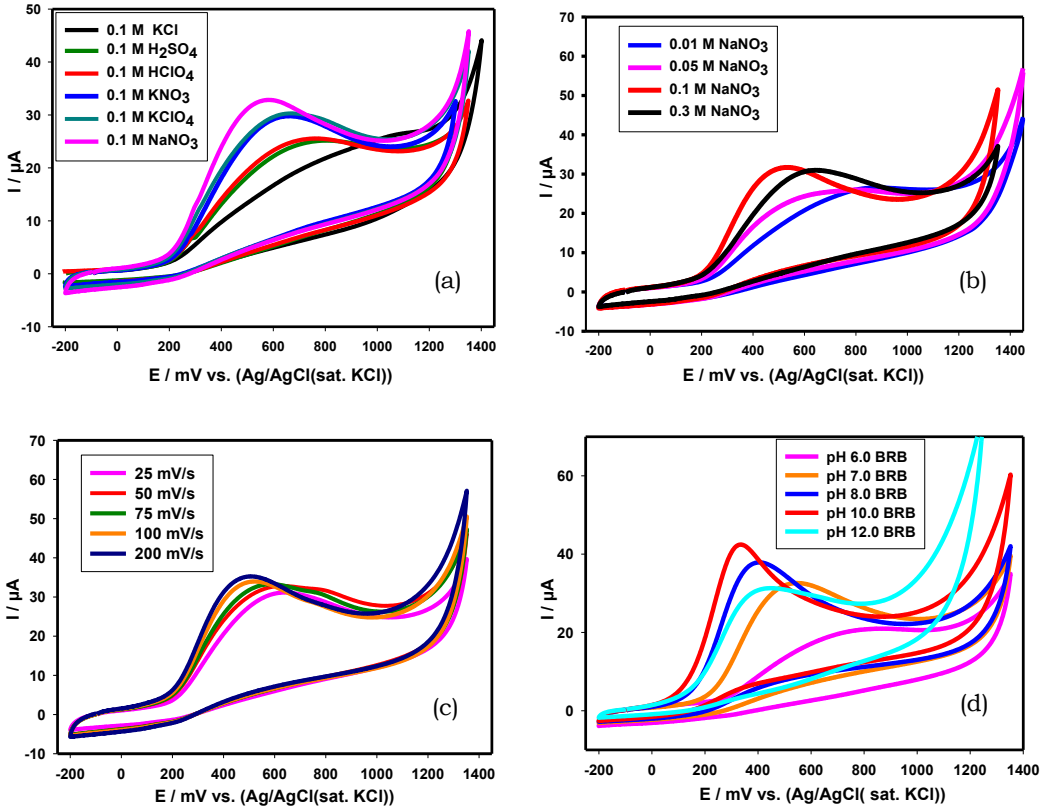

Figure 6. Effect of the different solutions media for the electropolymerization of phenol phthalein (a), Effect of $NaNO_3$ concentration (b), Effect of the electropolymerization scan rate of phenol phthalein (c), Effect of pH for 1 mM hydrazine (d)

MWCNT/poly(PP)/GC modified electrode was prepared by electrodeposition various metal nanoparticles such as Au, Pt, Cu, Ni, Co and the effect of modified electrodes on hydrazine oxidation was studied. It was observed that these modified electrodes were increased hydrazine oxidation peak current. It was observed that AuNPs/MWCNT/poly(PP)/GCE and PtNPs/MWCNT/poly(PP)/GC electrode surfaces shifted hydrazine oxidation peak potentials to negative compared to other modified electrodes. Pt nanoparticle modified electrode surface shifted hydrazine oxidation peak potential to more negative (-0.53 V) while Au nanoparticle modified electrode surface indicated the highest peak current for hydrazine oxidation (177 µA) (Figure 7).

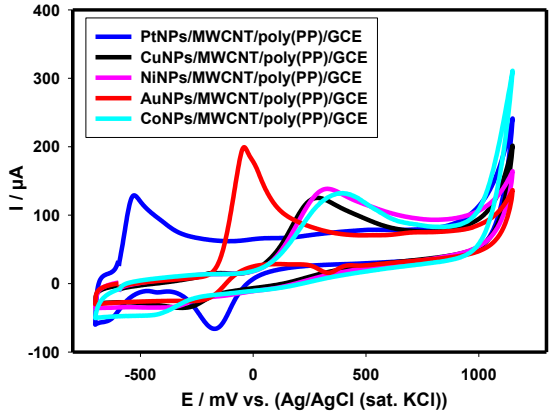

Figure 7. Effect of different metal nanoparticles modification on hydrazine oxidation on MWCNT/poly(PP)/GCE surface

4. CONCLUSION

This study indicates the electro-catalytic oxidation of hydrazine on metal nanoparticle, carbon nanotube and thin polymers film modified electrode. Modification of GC electrode was performed with electrodeposition of phenol phthalein monomer. Platinum and gold nanostructures resulted in a significant increase in the hydrazine peak current and shifted negatively direction at peak potential. Consequently, PtNPs/MWCNT/poly(PP)/GC and AuNPs/MWCNT/poly(PP)/GC electrodes developed can find many applications in energy conversion and sensor systems, respectively.

ACKNOWLEDGEMENTS

This work was supported by Scientific Research Project Office of Manisa Celal Bayar University. Project Number: 2018-097. One of the authors (M. Hatip) would like to acknowledge TÜBİTAK for scholarship (BİDEB 2211).

REFERENCES

E. Antolini and E. R. Gonzalez, "Polymer support for low-temperature fuel cell catalysts", *Appl. Catal. A*, vol.365, pp.1-19, 2009.

S. Koçak, B. Aslışen, and Ç. C. Koçak, "Determination of Hydrazine at a Platinum Nanoparticle and Poly Bromocresol Purple Modified Carbon Nanotube Electrode", *Anal. Lett.*, vol. 49(7), pp. 990-1003, 2016.

S. Koçak, A. Altın and Ç.C. Koçak, "Electrochemical Determination of Hydrazine at Gold and Platinum Nanoparticles Modified Poly L Serine Glassy Carbon Electrodes", *Anal. Lett.,* vol.49(7), pp.1015-1031, 2016.

S.K. Kim,, Y.N. Jeong,, M.S. Ahmed,, J.-M. You,, H.C. Choi and S. Jeon, "Electrocatalytic determination of hydrazine by a glassy carbon electrode modified with PEDOP/MWCNTs-Pd nanoparticles", *Sensor. Actuat. B,* vol.153, pp.246-251, 2011.

S.P. Kounaves, *Voltammetric techniques in Handbook of Instrumental Techniques for Analytical Chemistry*, Settle, F.A., Chapter 37, Prentice Hall PTR, 1997.

J. Wang, *Analytical Electrochemistry*, 3rd ed., Wiley, VCH, 2006.

S.K. Ghosh and T. Pal, "Interparticle Coupling Effect on the surface plasmon resonance of gold nanoparticles: from theory to applications", *Chem. Rev*., vol.107, pp.4797, 2007.

S. Sarkar, E. Guibal,, F. Quignard and A. K. S. Gupta, "Polymer supported metals and metal oxide nanoparticles: synthesis, characterization and applications", *J. Nanopart. Res*., vol.14, pp.715, 2012.

Biography:

Süleyman Koçak received his PhD in analytical chemistry from Ege University, Turkey in 2009. He is now an associate professor at Manisa Celal Bayar University, Department of Chemistry. His current interests include electroanalytical chemistry, voltammetric techniques, sensors, fuel cell, metal oxides, nanoparticles and heavy metal analysis.

ICACChE
2nd International Conference on Applications in Chemistry and Chemical Engineering
10 - 14 October 2018 Belgrade

Optimization of Electrochemical Processes for the Treatment of Raw Woollen Yarn Dye Wastewater

Kubra Ulucan-Altuntas[1], Fatih Ilhan, Can Dogan, Ugur Kurt

Abstract

The textile industry is an important source of pollution due to its intensive water consumption and the toxic content of dye and, this wastewater deteriorate the quality of water when they received to surface waters. In this study, electrochemical treatment methods, which are less costly than many treatment methods, have been investigated for raw woollen yarn dye wastewater. Four iron electrodes connected parallel for electrocoagulation process. As optimization method, response surface methodology was applied by having current density (20 -100 A/m2), reaction time (5-25 minutes) and initial pH (pH 4-pH 8) as independent conditions. The highest Colour and COD removal were obtained as 94% and 38.6%, respectively. High colour removal rate can be achieved in as little as 18,3 minutes. Electrocoagulation can reduce the time required for colour treatment. In order to obtain these results, it is necessary to apply a current density of 85,4 A/m2 to the wastewater which has been set to an initial pH of 5 and 15 minutes. Although the colour removal is high, COD removal does not meet discharge standards. In order to enhance COD removal rate, electrofenton process was also applied. Electrofenton process increased COD removal rate to 77%, where the colour removal rate stayed almost the same as 96,5%.

Keywords: Electrocoagulation, Electrofenton, Parallel Electrodes, Iron electrodes, COD, Colour

1. INTRODUCTION

Industrial activities take an important place among the pollution sources. The textile industry is one of the sectors that need to be considered in order to prevent industrial pollution and to protect water resources. The fact that the textile industry has an important position in the export and employment of developing countries makes the subject even more sensitive.

One of the products used in textile industry is woollen products, which are subjected to processes such as washing and carbonization before painting. A good cleaning can be achieved without damaging the wool fibre if the basic conditions are provided in the washing bath. After washing, carbonization process should be applied properly because it affects the dyeing properties of the woollen product. Generally, there is only one application and in this application, it is applied by absorbing the acid solution by the wool product. Before dyeing the woollen material, dyestuff selection is made according to the material form to be dyeing (fabric, yarn, tops fiber). Acidic dyes are one of the most applied dyes and their applications can be varied according to enterprises. Even their molecular structure varies, typical applications can be summarize as follows. All acidic dyestuff groups are prepared in paste form with cold water before wool dyeing. At a later stage, the water temperature is increased to 100ºC and dissolved. The temperature of the dye bath water is increased to 100ºC in 30-45 minutes and the dyeing process is expected to be at this temperature for 45-90 minutes depending on the colour intensity.

Different conventional treatment methods are used in the treatment of these acidic wastewater from dye baths. Baban et.al. has studied with wool dyeing and finishing wastewater, after application of biological treatment, they investigated ozone efficiency. They found 98-99% colour can be removed by combination of biological treatment and ozonation [1]. Different advanced treatment methods are used in the treatment of textile industry wastewater [1-6]. Since the dyeing process of each industrial products is different from each other, the suitability of the treatment methods has to be investigated for each dye bath wastewaters.

[1]Corresponding author: Yildiz Technical University, Environmental Engineering Department, 34220 Istanbul, Turkey. kulucan@yildiz.edu.tr

In this study, the suitability of electrochemical methods for the treatment of acidic wastewater of the woollen yarn dye was investigated and the system was optimized by using response surface methodology. With the use of the information obtained by optimization, the effectiveness of the electrofenton process has been demonstrated in order to increase COD removal.

2. MATERIAL AND METHOD

The waste water used in the experimental studies was obtained from the wool yarn dyeing shop. After the wool yarn dyeing, the dyeing bath wastewater and the bath washing water are collected in the balancing pond without being combined with the domestic wastewater.

Table 2. Properties of the acrylic yarn dye wastewaters

COD mg/L	TOC mg/L	Colour				pH	Conductivity µs/cm
		λ_{436}	λ_{525}	λ_{620}	Abs		
1.140	470	0,095	0,082	0,127	0,314	4,37	1.860

Experimental studies were carried out with 250 ml sample volume in plexiglas reactors with size of 6.5 cm x 6.5 cm x 18 cm. Fe and Al electrodes were used in dimensions of 5 cm x 18 cm. In electrocoagulation studies, 4 electrodes with a total active anode area of 101 cm^2 were placed in parallel with 15 mm intervals. In contrast to the electrocoagulation treatment reactor, two electrodes were used as 1 anode and 1 cathode in electrofenton experiments and the electrode intervals were determined as 6 cm.

Response surface methodology has been used to optimize the experimental data in which the following second-degree polynomial regression model has been used.

$$y = a_0 + \sum a_i x_i + \sum a_{ij} x_i x_j + \sum a_{ii} x_i^2$$

where; y is the response variables, a_o is the constant, a_i, a_{ii} and a_{ij} are the linear coefficients and x_i, x_j are the independent variables. Variables have been coded by the following equation.

$$\alpha = \frac{x_i - x_0}{\Delta x}$$

where; $\propto$ gives the code value of the independent variables, x_i is the real value, x_o is the real value in the medium point and Δx gives the change in x_i variable.

A five-level three-factor CCD was applied and current Density (x_1), initial pH (x_2) and reaction time (x_3) are the selected as independent variables. $\propto$ is selected as ±2. Codded factors can be seen in Table 2.

Table 3. Study matrix for the electrocoagulation

Independent Variables	Factor	Levels				
	X_i	α = -2	-1	0	+1	α = +2
Current Density (A/m²)	X_1	20	40	60	80	100
Initial pH	X_2	4	5	6	7	8
Reaction time (min)	X_3	5	10	15	20	25

3. RESULTS AND DISCUSSION

Considering the pH value (pH = 4,37) of the wollen yarn dye wastewater, in order to observe the effect of pH, the pH range has been determined as pH 4 and pH 8. The conductivity value of wastewater was measured as 1.860 µs/cm. With increase of pH, conductivity values have been reached to 2.500-2.600 µs / cm, which is sufficient for a current density of 150 A/m^2 without electrolyte addition, but it was found not sufficient for 200 A/m^2 current density. Therefore, the preliminary study was conducted at a current density of 60-150 A/m^2at pH6 with 15 min reaction time. The obtained results are given in Table 3. Since there is no significant increase in COD and Colour removal efficiency, the current density range to be used is defined as 20-100 A/m^2 in Table 2. With the light of the data obtained in preliminary study, CCD was conducted as in Table 4 and Table 5 for aluminium and iron electrodes, respectively.

Table 4. Results of the preliminary study conducted for the electrocoagulation process

Current Density (A/m²)	Al Electrodes		Fe Electrodes	
	COD removal (%)	Colour Removal (%)	COD removal (%)	Colour Removal (%)
60	25,28	83,75	30,35	95,22
80	26,36	85,60	35,83	94,95
100	28,84	84,85	36,59	97,13
150	31,47	86,35	38,12	96,41

Table 5. RSM results conducted with aluminium electrodes

No	Current Density (A/m^2)	Influent pH	Reaction Time (min)	COD Removal (%)	Colour Removal (%)	TOC Removal (%)	Energy Consumption (kWh/m^3)	Dried Sludge (mg)
	x_1	x_2	x_3	y_1	y_2	y_3	y_4	y_5
1	-1	-1	-1	20,32	79,85	19,33	1,28	613
2	1	-1	-1	25,72	82,16	25,35	4,7	718
3	-1	1	-1	20,03	76,65	21,12	1,2	779
4	1	1	-1	25,12	81,56	25,09	4,21	527
5	-1	-1	1	24,02	80,23	22,89	2,57	813
6	1	-1	1	33,54	83,06	29,89	9,4	1049
7	-1	1	1	24,18	77,86	25,85	2,41	548
8	1	1	1	29,69	82,63	29,12	8,42	1467
9	0	0	0	25,61	82,9	24,13	3,9	688
10	0	0	0	25,42	83,13	23,85	3,9	706
11	0	0	0	25,83	83,24	24,34	3,9	707
12	0	0	0	25,14	83,63	23,66	3,9	705
13	-2	0	0	17,74	76,73	17,72	0,61	449
14	2	0	0	31,69	83,51	29,65	10,2	1229
15	0	-2	0	27,79	80,95	25,76	4,27	622
16	0	2	0	25,05	77,11	27,02	3,28	718
17	0	0	-2	20,66	80,12	20,26	1,3	285
18	0	0	2	33,83	82,56	30,15	6,51	1067
19	0	0	0	25,37	83,85	23,88	3,9	784
20	0	0	0	25,11	83,51	24,75	3,9	713

Table 6. RSM results conducted with iron electrodes

No	Current Density (A/m^2)	Influent pH	Reaction Time (min)	COD Removal (%)	Colour Removal (%)	TOC Removal (%)	Energy Consumption (kWh/m^3)	Dried Sludge (mg)
	x_1	x_2	x_3	y_1	y_2	y_3	y_4	y_5
1	-1	-1	-1	25,15	87,91	21,96	1,18	470
2	1	-1	-1	31,72	92,32	25,89	4,21	690
3	-1	1	-1	27,91	90,74	23,41	1,12	500
4	1	1	-1	36,86	92,36	30,13	4	844
5	-1	-1	1	31,25	89,32	24,65	2,35	848
6	1	-1	1	36,92	93,68	30,14	8,42	1830
7	-1	1	1	33,76	92,77	27,17	2,24	977
8	1	1	1	38,15	94,47	31,14	7,99	1740
9	0	0	0	32,04	93,83	26,15	3,54	1079
10	0	0	0	32,44	93,95	25,98	3,54	1129
11	0	0	0	31,84	92,98	25,69	3,54	1142
12	0	0	0	31,55	93,65	25,72	3,54	1134
13	-2	0	0	24,52	88,12	20,23	0,28	473
14	2	0	0	40,35	94,55	32,94	7,58	1756
15	0	-2	0	27,53	88,52	25,56	3,72	982
16	0	2	0	33,12	94,32	27,89	3,42	1192
17	0	0	-2	28,44	89,05	23,22	1,18	325
18	0	0	2	38,22	92,62	31,2	5,9	1573
19	0	0	0	30,91	93,19	26,35	3,54	988
20	0	0	0	32,31	93,12	26,56	3,54	995

The ANOVA results for COD, Colour, TOC removal efficiencies, energy consumption and dried sludge production of both aluminium and iron electrodes are given in Table 6. Relevance and regression coefficients of each design are high, which shows the applied CCD is suitable.

Table 7. ANOVA results attained for electrocoagulation

Electrode	Depended Variables	Coded	R^2	Relevance
Al	COD Removal	y_1	0,990	2,07 E-07
	Colour Removal	y_2	0,992	9,87 E-08
	TOC Removal	y_3	0,994	1,60 E-08
	Energy Consumption	y_4	0,999	1,28 E-14
	Dried Sludge	y_5	0,925	3,54 E-03
Fe	COD Removal	y_1	0,989	4,79 E-07
	Colour Removal	y_2	0,989	4,36 E-07
	TOC Removal	y_3	0,982	4,68 E-06
	Energy Consumption	y_4	0,994	1,37 E-09
	Dried Sludge	y_5	0,989	3,50 E-07

The equations obtained with efficient parameters are given in Table 7. Efficient parameters are selected when confidence range is higher P>0,05. From the equations obtained for COD and Colour removal by aluminium electrode, it can be said that all independent parameters are effective. In addition, the effective parameters for both COD and Colour removal are the same for both aluminium and iron electrodes. Independent parameters can be ordered in their effectiveness on COD as current density, reaction time and pH, respectively. However, it can be ordered for Colour removal as current density, pH and reaction time, respectively. The effective parameters can also be seen in Figure 1 and Figure 2 for COD and Colour removal.

Table 8. Equations attained with Aluminum and Iron electrodes

Electrode	Depended Variables	Equation
Al	COD Removal	$y_1 = 25{,}30 + 3{,}339x_1 - 0{,}629x_2 + 2{,}911x_3 - 0{,}40\ x_3^2$
	Colour Removal	$y_2 = 83{,}29 + 1{,}774x_1 - 0{,}893x_2 + 0{,}528x_3 + 0{,}568x_1.x_2 - 0{,}857x_1^2 - 1{,}129x_2^2 - 0{,}552x_3^2$
	TOC Removal	$y_3 = 24{,}1 + 2{,}758x_1 + 0{,}39x_2 - 0{,}723x_3 + 0{,}57x_2^2 + 0{,}274\ x_3^2$
	Energy Consumption	$y_4 = 3{,}905 + 2{,}403x_1 - 0{,}23x_2 + 1{,}364x_3 - 0{,}154x_1.x_2 + 0{,}801x_1.x_3 + 0{,}379x_1^2$
	Dried Sludge	$y_3 = 733{,}30 + 160{,}5x_1 + 175{,}25x_3 + 162{,}75\ x_1.x_3$
Fe	COD Removal	$y_1 = 31{,}98 + 3{,}578x_1 + 1{,}426x_2 + 2{,}375x_3 - 0{,}437\ x_3^2$
	Colour Removal	$y_2 = 93{,}44 + 1{,}56x_1 + 1{,}169x_2 + 0{,}878x_3 - 0{,}681x_1.x_2 - 0{,}535\ x_1^2 - 0{,}514x_2^2 - 0{,}66x_3^2$
	TOC Removal	$y_3 = 26{,}1 + 2{,}845x_1 + 0{,}867x_2 + 1{,}729x_3$
	Energy Consumption	$y_4 = 3{,}593 + 2{,}021x_1 + 1{,}246x_3 + 0{,}738x_1.x_3$
	Dried Sludge	$y_3 = 1065{,}159 + 304{,}688x_1 + 336{,}688x_3 + 147{,}625\ x_1.x_3$

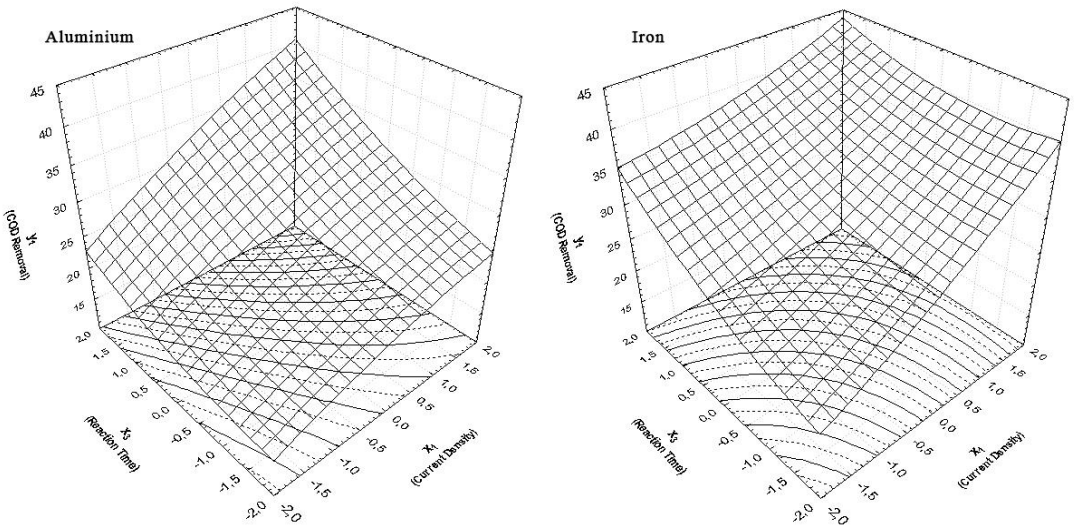

Figure 8. Effect of Current Density and Reaction Time on COD removal

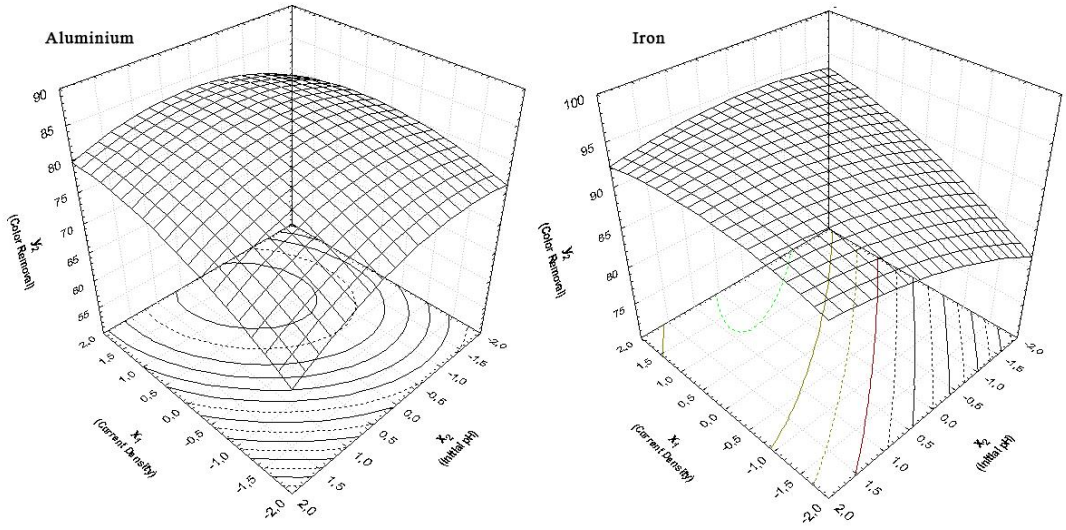

Figure 9. Effect of Current Density and Initial pH on Colour Removal

In the electrocoagulation treatment of woollen yarn wastewater it can be said from the coefficients that most effective parameter is the current density. While initial pH effected COD and Colour removal negatively for aluminium electrodes, it effected positively for iron electrodes (Figure 1 and Figure 2).

As it could be seen in Figure 1; approximately 44% COD removal could be achieved with iron electrodes while 40% could be achieved with the aluminum electrodes. This also can be observed in Figure 2 for colour removal, while colour removal by aluminium is 83%, it is higher than 90% by iron electrodes.

When the TOC removals for both electrodes are compared (Table 7), it can be said that initial pH and reaction time are more effective in electrocoagulation by aluminium than iron electrodes. The effect can be seen in Figure 3. TOC removal for both electrodes are similar.

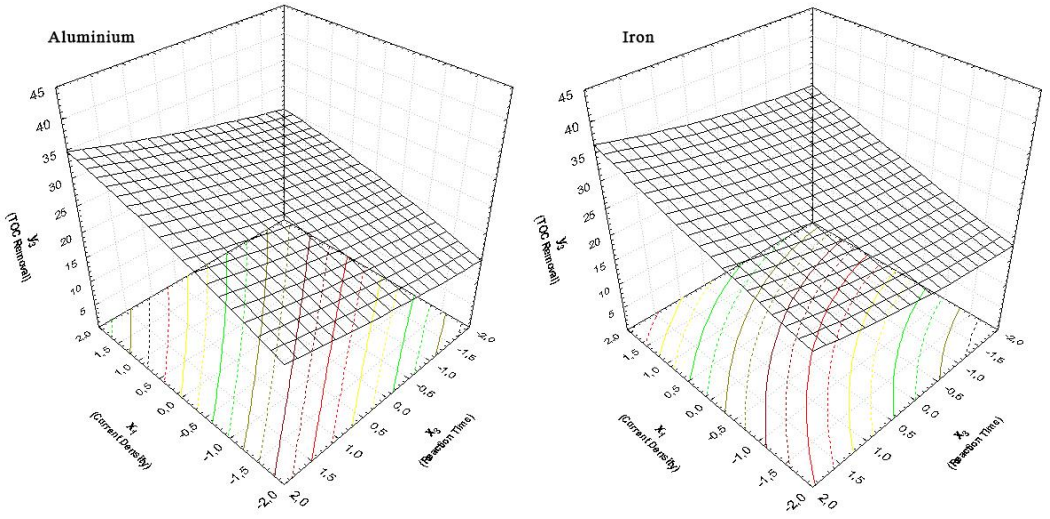

Figure 10. Effect of Current Density and Reaction Time on TOC Removal

As predicted, the most effective parameter in energy consumption is current density and, energy consumption was increased with the increment in current density for both electrodes (Table 7). It is also found that initial pH was not an effective parameter for energy consumption with the treatment by iron electrodes, while it is effective with aluminium electrodes. Furthermore, the initial pH was found not to be effective parameter for the amount of produced dried sludge and, the effect of current density and reaction time is almost equal.

The intercepts for all CCD systems shows that iron electrodes are more effective in electrocoagulation treatment of woollen yarn wastewater than aluminium electrodes. This also can be gathered from surface plots in Figure 1 and Figure 2. Furthermore, from the intercepts for dried sludge amount, it can be said that iron electrodes produced more sludge than aluminium electrodes. It is generally specified that iron electrodes are as effective as aluminum electrodes in the removal of COD from wastewaters. This is due to the fact that the iron oxidation capacity increases the efficiency of COD removal [7].

Optimum conditions have been calculated via MathCad by the equations attained for the iron electrodes given in Table 7. The results can be seen in Table 8, and according to table 38,6 % COD, 94% Colour and 28 % TOC removal could be achieved according to these optimized values. When optimum conditions applied in electrocoagulation process, 39,4% COD, 95,1% colour, 28,9% TOC removal was obtained which are in the 95% confidence interval. Required energy is calculated as 5,54 kWH/m^3 textile wastewater. Energy

consumption in Turkey was 0,08 US $/kWH for industry, the cost of electrocoagulation process by iron electrodes will be 0,44 US $/$m^3$ textile wastewater. When dried sludge is calculated with optimum values, 1760 mg sludge will be produced.

Table 9. Optimization of the electrocoagulation process

Independed Factors	Coded Levels	Real Values
Current Density (A/m^2)	1.27	85,4 A/m^2
Initial pH	-1	pH 5
Reaction Time (min)	0,665	18,3 min

While colour removal could be achieved in high ratio with the electrocoagulation process, COD and TOC removals have remained less than 40%. The electrofenton process has been applied within the direction of the study data attained as a result of the optimization of the electrocoagulation process. In this study, initial pH was adjusted as 3, H_2O_2 concentration of 1200 mg/L and reaction time of 30 minutes was chosen.

Table 10. Removal Efficiencies with Electrofenton process

Current Density, A/m^2	COD Removal Rate,%	Color Removal Rate, %	TOC Removal Rate, %
50	67,1	85,4	48,0
100	74,9	95,5	55,1
150	73,9	95,2	53,2
200	77,0	96,5	65,5

As seen in Table 9; even 50 A/m^2 of current density is applied, which is less than the optimum current density in electrocoagulation process, the COD removal rate was increased from 38,6% to 67,1%. COD, Colour and TOC removals was increased as 74,9 %, 95,5 % and 55,5 % when a current density of 100 A/m^2 is applied, thus the discharge limits will be provided. Removal rates were achieved in higher ratio when compared to the electrocoagulation.

CONCLUSION

Treatment of woollen yarn dye wastewaters by electrochemical processes was compared. In electrocoagulation process, the most effective parameter on removal of COD, Colour and TOC was determined as current density for both electrodes. 4 iron electrodes placed parallel was found to be more effective than aluminium electrodes. Energy consumption is studied and required energy is calculated as 5,54 kWH/m^3 textile wastewater which is cost 0,08 US $/$m^3$ textile wastewater. By electrocoagulation process, maximum 44% of COD removal can be achieved. Thus, electrofenton process is investigated and even in less current density, removal rate was increased to 67,1%. In addition, in electrofenton process 100 A/m^2 of current density was determined as suitable to reach discharge limits. Electrofenton process can be applicable for woollen yarn dye wastewaters as a treatment process that provides high removal rate in less space compared to conventional treatment systems.

REFERENCES

Sundrarajan M., Vishnu G. ve Joseph K., (2007), “Ozonation of light-shaded exhausted reactive dye bath for reuse”, Dyes and pigments, 75:273-278

Baban A., Yediler A., Lienert D., Kemerdere N. ve Kettrup A., (2003), “Ozonation of high strength segragated effluents from a wollen textile dyeing and finishing plant”, Dye and pigments, 58:93-98

Ulucan-Altuntas K., İlhan F., "Enhancing Biodegradability Of The Textile Wastewater By Ozonation Process: Optimization With Response Surface Methodology", Ozone-Science & Engineering, pp.1-1, 2018

Dilek F.B., Sahinkaya E., Uzal N. ve Yetis U., (2008), “Biological treatment and nanofiltration of denim textile wastewater for reuse”, Journals of hazardous materials, 153:1142-1148

Avlonitis S.A., Poulios I., Sotiriou D., Pappas M. ve Moutesidis K., (2008), “Simulated cotton dye effluents treatment and reuse by nanofiltration”, Desalination, 221:259-267

Korbahti, BK; Artut, K, Gecgel, C, Ozer, A., (2011), ” Electrochemical decolorization of textile dyes and removal of metal ions from textile dye and metal ion binary mixtures” Chemical Engineering Journal, 173(3) 677-688.

Diaz C.B., Hernandez I.L., Morales G.R., Bilyeu B., Urena-Nunez F., (2009), “Influence of the anodic material on electrocoagulation performance”, Chemical Enginering Journal, 148:97-105

ICACChE
2nd International Conference on Applications in Chemistry and Chemical Engineering
10 - 14 October 2018 Belgrade

Termal Yöntem ile İndirgenmiş Grafen Oksit Sentezi ve Karakterizasyonu

Osman Eksik[1]

Özet

Grafen yapı olarak grafitin tek bir tabakasını oluşturmakta ve karbon atomlarının sp^2 melezleşmesi yaptığı iki boyutlu planar yapıdır. Elektronik iletkenliği, ısıl ve mekanik dayanıklığı, yüzey alanı oldukça yüksek bir malzemedir. Yapılan çalışmada, pul grafitten az katmanlı indirgenmiş grafen oksit üretimine odaklanıldı. Ayrıca grafen oksit (GO) ve indirgenmiş grafen oksidin (RGO) üretimi ve karakterizasyon yöntemleri araştırıldı. Öncelikle grafit, büyük ölçekli üretime elverişli yöntemlerden olan Staudenmaier yöntemiyle grafen oksit (GO) yapısına dönüştürülmüştür. Elde edilen grafen oksit numuneleri termal yöntemle indirgendi. Grafen oksit ve indirgenmiş grafen numuneleri FT-IR, SEM, XRD, XPS, BET ve Raman spektroskopisiyle karakterize edilmiştir. FT-IR spektroskopisi sonuçları, oksijen içeren fonksiyonel grupların (OH, C=O, C-OH) sentezlenmiş grafen oksitin yapısına girdiğini kanıtlamaktadır. XRD analizi sonucunda tabakalar arası mesafelere bakıldığında ise grafit için 0,32 nm, grafen oksit için ise 0,85 nm değerlerine ulaşılmaktadır. Bu sonuçlar oksitleme işleminin başarıyla gerçekleştiğini göstermektedir. XPS spektrumu grafen oksit ve indirgenmiş grafen oksidin kimyasal yapısındaki atomik C:O oranlarının sırasıyla yaklaşık 1,88 ve 11,17 olduğunu göstermektedir. SEM görüntülerinden saydam ve kırışık indirgenmiş grafen oksit (RGO) yapıları tespit edilmiştir. RGO örnekleri raman spektroskopisinde yeni sp^2 yapıların oluştuğu ve düzenli yapı miktarının arttığını görülmüştür. İndirgenmiş grafen oksit numunelerinin BET analizi sonucunda yüzey alanının 1g başına yaklaşık 600 m^2g^{-1} olduğu tespit edilmiştir. Bu durum sentezlenen RGO'ların az tabakalı yapıda olduklarını göstermektedir.

Anahtar kelimeler: Grafen, İndirgenmiş Grafen Oksit, Termal İndirgeme.

1. Giriş

Grafen karbon allotropu olup, karbon atomlarının tek düzlemde hekzagonal yapıda dizilmesiyle oluşan iki boyutlu bir yapıya sahiptir. Kendine özgü elektriksel ve yapısal özelliklere sahip iki boyutlu yeni bir malzeme olan grafen son yıllarda oldukça ilgi çekmiştir. Grafenin bu yapısı ona olağanüstü özellikler kazandırmaktadır. Grafen kütle oranına göre oldukça geniş spesifik yüzey alanına (teorik olarak, 2630 m^2g^{-1}), oldukça yüksek termal iletkenliğe (~5000 $Wm^{-1}K^{-1}$, bakırdan 10 kat daha yüksek) ve optik geçirgenliğe (~ %97.7) sahiptir. Grafenin başka bir ilginç özelliği de esnek ve çok dayanıklı olmasıdır. Sp^2 hibridizasyonu adı verilen bir bağ şekli yüzünden, belli yönlerdeki kuvvetlere karşı elmas kadar dayanıklıdır ve yüksek young modülüne (~1100 Gpa) sahiptir. Grafenin bu olağanüstü özelliklerinden dolayı farklı kullanım alanlarında uygulama yapılmasına olanak sağlamaktadır. Termal ve elektrik iletkenliğinde, nanokompozitleri güçlendirmede, saydam iletken filmlerde, ultra ince karbon filmlerde, elektronik devrelerde, sensörlerde (kimyasal ve biyosensörler), ilaç ve gen salınım araçlarında, ağır metalleri ayrıştırmada, nanoelektronikte, ekranlar için saydam ve esnek elektrotlarda, enerji depolama cihazları gibi karbon tabanlı malzemelerde grafen uygulama alanları bulmaktadır [1-6]. Aynı zamanda hızla ilerleyen teknolojik gelişmeler ile grafenin yakın gelecekte robot yapımı, güneş hücreleri, telekomünikasyon, biyokimya, tıp gibi birçok alanda karşımıza çıkacağını göstermektedir. Grafenin farklı yöntemlerle elde edilmelerine bağlı olarak, özellikleri ve kullanım alanları değişiklik göstermektedir.

Günümüzde devam eden grafen ile ilgili yoğun bilimsel araştırmalar grafenin günlük hayattaki uygulama alanlarını ve üretim metotlarını geliştirmek için yapılmaktadır [7,8]. Bununla birlikte grafenin düşük maliyette ve yüksek miktarlarda üretiminde halen zorluklar yaşanmaktadır. Yüksek miktarlarda grafen üretiminin yolunu açacak olan metot grafitin oksitlenmesidir. Bu çalışmada, grafitin oksidasyonu için ucuza satılan doğal grafit tozu başlangıç malzemesi olarak kullanılmış ve Staudenmaier metodu kullanılarak grafen oksitlenmiştir. Elde edilen grafen oksitin termal yöntemle indirgenmesiyle birkaç tabakalı grafen üretimi gerçekleştirilmiştir.

1.1. Grafen Oksit Üretimi

Grafen elde etmek için en umut verici yöntemlerden birisi grafitin oksidasyonudur. Grafen oksit sentezindeki ilk örnek 1859 yılında Brodie'nin grafitin yapısını keşfetmesidir. Gerçekleştirdiği reaksiyonlardan birisi, derişik nitrik asit (HNO_3) içindeki grafit bulamacına potasyum klorat ($KClO_3$) ilavesi şeklindedir [9]. Brodie grafitin toplam ağırlığında artışla oluşan malzemenin karbon, hidrojen ve oksijenden oluştuğunu belirlemiştir.

[1]*Corresponding author: İstanbul Teknik Üniversitesi, Kimya Mühendisliği Bölümü, İstanbul, eksikos@itu.edu.tr*

Başarılı bir oksitleyici muamelesiyle, dört reaksiyon sonrasında limit değere ulaşan bir oksijen içeriği artışı ile olduğunu ortaya koymuştur. Brodie bu malzemenin saf veya normal su içerisinde dağıtılabildiğini fakat asidik ortamda dağıtılamadığını belirlemiştir. Bu durum, onu malzemeyi "grafit asit" olarak tanımlamaya sevk etmiştir.

Brodie"nin grafitin oksitlenebilirliğini keşfinin ardından Staudenmaier 1898 yılında potasyum klorat"ı ($KClO_3$), dumanlı nitrik asit (HNO_3) ve derişik H_2SO_4 karışımına Brodie"nin yaptığı gibi tek seferde ilave etmek yerine yavaşça ekleyerek geliştirmiştir [10]. Daha sonra Hofmann, Staudenmaier ve Brodie"nin yönteminde kullanılan dumanlı nitrik asitin yerine derişik nitrik asit (HNO_3) kullanarak grafen oksit sentezini gerçekleştirmiştir [10]. Staudenmaier"den yaklaşık 60 yıl sonra Hummers grafitin potasyum permanganat ($KMnO_4$) ve derişik sülfürik asit (H_2SO_4) karışımıyla reaksiyonuna dayanan ve benzer oksitlenme seviyelerine ulaşan bir yöntem geliştirmiştir [10]. Brodie, Staudenmaier ve Hofmann yaklaşımlarında genellikle $KClO_3$, derişik HNO3 ve H_2SO_4 kullanılmıştır. Nitrik asit yaygın kullanılan bir oksitleyicidir ve karbon nano tüpleri de içeren aromatik karbon yüzeyleri ile kuvvetli etkileşimleri bilinmektedir. Tepkime, karboksiller, laktonlar ve ketonlar gibi çeşitli oksijen içeren türlerin oluşumu ile sonuçlanmaktadır. Nitrik asit ile oksitleme NO_2 ve/veya N_2O_4 gazlarının salınımı ile sonuçlanır [10]. Aynı zamanda, $KClO_3$ da kuvvetli bir oksitleyicidir. Hummers yöntemi potasyum permanganat ($KMnO_4$) ve sülfürik asit (H_2SO_4) bileşimini kullanır. Permanganat kuvvetli bir oksitleyicidir ve bu özelliğiyle aktif grafen oksit (GO) yüzeyinde farklı oksijen gruplarını (karboksil, hidroksil ve epoksi vb.) içererek, GO yapısını hidrofilik hale getirir [11].

1.2. Grafen Oksit İndirgeme Yöntemleri

Grafen oksitin termal ve kimyasal yöntemlerle indirgenmesiyle tek ve çok tabakalı grafen üretimi gerçekleştirilebilmektedir. Grafen oksitin indirgenmesi için termal ve kimyasal birçok yaklaşım öne sürülmüştür. Grafen sentezinde kullanılan termal indirgeme yöntemleri; ısıl tavlama, mikrodalga ve foto indirgemedir [12]. Grafen üretiminde kullanılan diğer bir yöntem ise kimyasal indirgemedir. Kimyasal indirgeme yöntemi ise başlıca; kimyasal ayırıcı indirgeme, foto katalitik ve elektrokimyasal indirgemeden meydana gelmektedir [13].

Isıl tavlama yöntemi, grafen tabakaları arasındaki CO ve CO_2 gazlarının grafit oksidin hızlı ısıtılması esnasında oluşup ani genleşmesi süreçlerinin içermektedir. Bu işlem 1050°C"da gerçekleştirilmekte ve bu sıcaklıkta yığın halindeki grafen oksit katmanları birbirinden ayrılarak grafen tabakalarını oluşturmaktadır [12]. Diğer bir termal indirgeme işleminde ise mikrodalga [14] ve foto ışınlamayla [15] grafen sentezi gerçekleştirilmektedir.

2. Materyal ve Metot

2.1. Staudenmaier Metodu ile Grafen Ooksit Sentezi

Grafen oksidin sentezlenmesi için uygulanan yöntemlerden birisi olan Staudenmaier yönteminde öncelikle kuvvetli oksitleyici olarak kullanılan dumanlı nitrik asit (HNO_3 %98, 45 mL) ve sülfürik asit (H_2SO_4 , %95-98, 90 mL) mekanik karıştırıcı vasıtası ile karıştırılmış, karışımın sıcaklığı buz banyosu kullanılarak 5°C' e düşürülmüştür. Sentez süreci sıcaklık kontrollü gerçekleştirilmiş olup, sıcaklık artış eğilimine girdiğinde buz ilavesi yapılarak tüm sentez süresince sıcaklığın 5°C civarında kalması sağlanmıştır. Daha sonra 5 g grafit, hazırlanan karışıma yavaşça ilave edilmiştir. Bu aşamadan sonra 55 g $KClO_3$, buz banyosunda karışmakta olan karışımın üzerine yavaşça eklenmiştir. Bu işlem, karışma kesintiye uğratılmaksızın 12 saat süre ile gerçekleştirilmiştir. 12 saat sonunda, karışım 4 gün boyunca sıcaklığı 50°C'yi geçmeyecek şekilde karıştırılmaya devam edilmiştir. Bu işlem sonunda grafitin oksitlenme süreci tamamlanmış ve grafen oksit elde edilmiştir. Elde edilen grafen oksit yapısının saflaştırılması amacıyla sırasıyla %5"lik HCl çözeltisi ve aseton ile yıkama işlemi yapılmıştır. Saflaştırılan numune etüvde 105°C'de içerisinde nem kalmayacak şekilde 24 saat boyunca kurutulmuştur.

2.2. Termal İndirgeme ile Grafen Sentezi

Grafen oksitin termal indirgenmesiyle tek ve çok tabakalı grafen üretimi gerçekleştirilebilmektedir. Termal indirgeme metodunda, grafen oksit numunesi, argon gazı akışı altında 1050°C"deki boru fırın sistemine kısa süreli yerleştirilmiş (45 san.) ve termal şok ile indirgenerek grafen elde edilmiştir. Termal indirgeme sırasında grafen oksidin yapısındaki oksijen içeren fonksiyonel gruplar (epoksi, hidroksil ve karboksil vb.) yapıdan uzaklaşmaktadır. Tabakalar arasında oluşan CO ve CO_2 gazları yüksek basınç oluşturarak genleşmek suretiyle termal eksfoliasyona uğramaktadır. Bu işlemler Grafik 1'de şematik olarak gösterilmiştir.

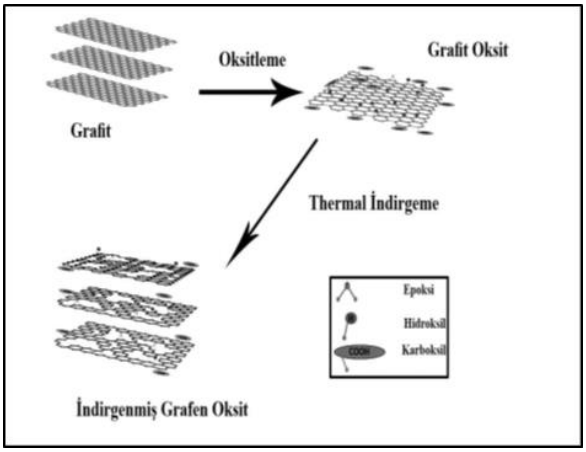

Grafik 1. Grafen oksidin termal yöntem ile indirgenmesi.

3. Bulgular ve Tartışma

3.1. Grafit, Grafen Oktit ve İndirgenmiş Grafenin TGA Analizleri

Grafik 2'de TGA analizi ile grafit, grafen oksit (GO) ve indirgnenmiş grafen oksite (RGO) ait termal özellikler incelenmiştir.

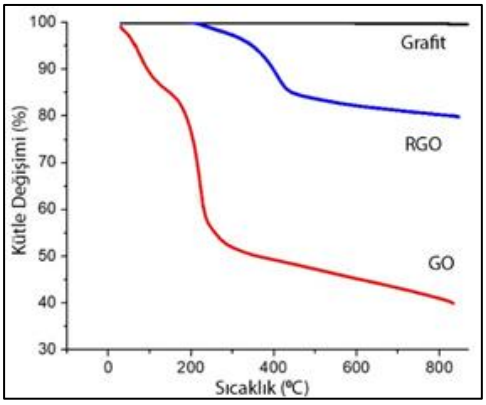

Grafik 2. Grafit, GO ve RGO'nun TGA sonuçları.

Grafitin termal özellikleri incelendiğinde, grafitte sıcaklık değişimine bağlı bir ağırlık değişimi görülmemiştir (Grafik 2). Buna karşılık Staudenmaier yöntemiyle elde edilen GO'da üç aşamalı degredasyonun olduğu gözlemlenmiştir. İlk evre, 50-150 °C aralığında GO'ya adsorbe olmuş suyun kütle kaybı ile yapıdan uzaklaşmasıdır. İkinci evre, 150 °C ile 400 °C arasındadır. Buradaki kütle kaybı, GO yapısındaki oksijen içeren hidroksil, epoksi ve karboksil gibi grupların grafien oksit yapısından uzaklaşması olarak açıklanabilir. Üçüncü evre ise 400 °C ile 800 °C arasıdır. Bu aralıktaki kütle kaybı ise GO içerisindeki kararlı olmayan karbon yapılarının pirolizinden kaynaklanmaktadır. Termal indirgeme yöntemi kullanılarak elde edilen RGO, ağırlığının %25' ini kabetmiştir. Bunun sebebi RGO'nun yapısında kalan oksijen içeren grupların yapıdan uzaklaşmasıdır ve bu değerler literatür ile uyuşmaktadır [16,17].

3.2. Grafiti Grafen Oktitin XRD Analizleri

Grafik 3'de grafit ve grafen oksitin (GO) XRD analizleri görülmektedir.

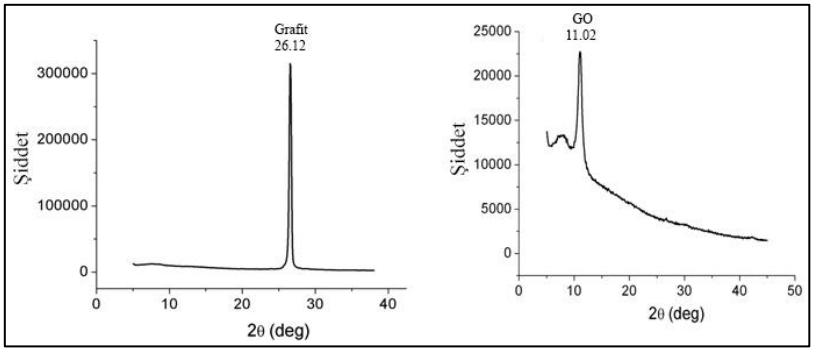

Grafik 3. Grafit ve Grafen Oksit numunelerinin"in XRD spektrumları.

Grafik 3'de grafit için 2θ=26.12°'de grafite ait bir pik gözükmektedir. Grafen oksite ait pik değeri ise 2θ=11.02° olarak gözükmektedir. Literatürden bakılan değerler doğrultusunda bu pikler sırasıyla grafit için 26.48°, grafen oksit için ise 10.90° olarak bilinmektedir [18]. Elde edilen verilerle literatür verileri kıyaslandığında oksitleme işleminin başarıya ulaştığı görülmektedir. Tabakalar arası mesafelere bakıldığında ise grafit için 0.32 nm, grafen oksit için ise 0.85 nm değerlerine ulaşılmaktadır. Oksitleme işlemi sonucunda grafen oksit tabakaları arası mesafenin artması, oksitleme işleminin başarıyla gerçekleştiğini göstermektedir.

3.3. Grafit, Grafen Oktit ve İndirgenmiş Grafenin FT-IR Analizleri

Grafit tozundan GO sentezlendiğinde görülmesi gereken FT-IR frekansları, alınan FT-IR spektrumlarında gözlemlenmiştir (Grafik 4).

GO'nun FT-IR spektrumunda önemli olan karboksilik asit gruplarının, hidroksil gruplarının ve epoksi gruplarının gözlemlenmiş olmasıdır. Grafik 4'de görüldüğü üzere, OH gerilme titreşimi 3377 cm^{-1}, C=O gerilme titreşimi 1731 cm^{-1}, C=C gerilme titreşimi 1620 cm^{-1}, C-OH gerilme titreşimi 1226 cm^{-1} ve C-O gerilme titreşimi 1056 cm^{-1} olarak ölçülmüştür. Literatür araştırması sonucunda, OH gerilme titreşimi 3391 cm^{-1}, C=O gerilme titreşimi 1721 cm^{-1}, C=C gerilme titreşimi 1620-1680 cm^{-1}, C-OH gerilme titreşimi 1226 cm^{-1} ve C-O gerilme titreşimi 1046 cm^{-1} olarak bulunduğu tespit edilmiştir [19]. Grafit numunesi bu titreşimlerden hiç birine sahip değildir. GO'daki tüm bu gerilmeler grafen oksidin başarıyla oluştuğunu ortaya koymaktadır.

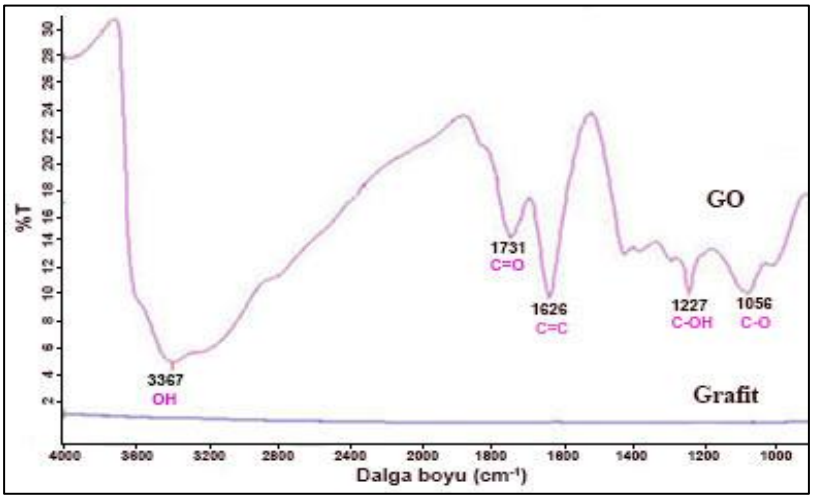

Grafik 4. Grafit ve GO'ya ait FTIR spektrumu.

Çalışılan şartlarda ayrıca ısıl ındirgemenin etkisi incelenmiştir. Grafik 5'de görülebileceği gibi indirgeyici olarak termal yöntem kullanıldığında grafen okside ait karakteristik piklerin kaybolduğu görülmektedir

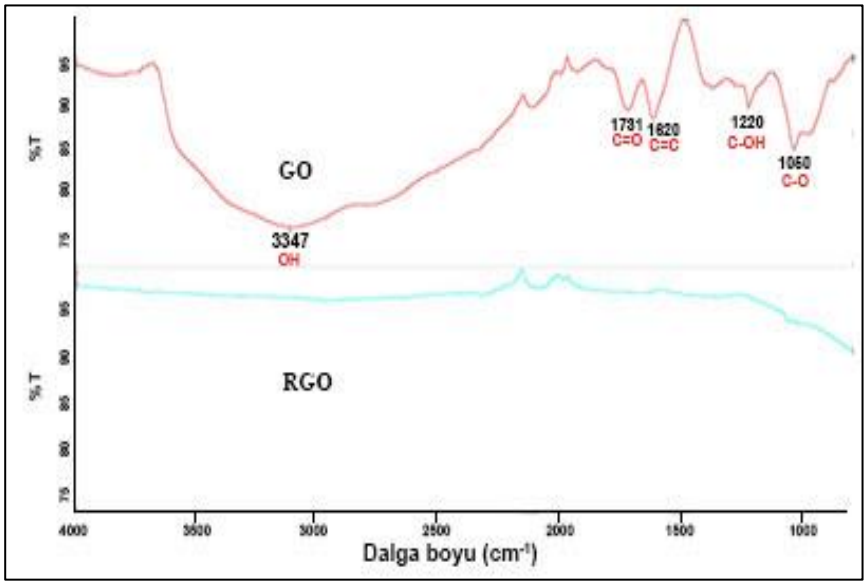

Grafik 5. GO ve RGO'ya ait FTIR spektrumu.

3.4. Grafen Oksit ve İndirgenmiş Grafen Oktitin XPS Analizleri

GO ve RGO'nun yapılan XPS analizleri sonuçları ile tespit edilen karbon, oksijen elementler miktarı ile karbon/oksijen oranı sonucu, Tablo 1'de verilmiştir.

Tablo 1. Grafen oksit ile thermal yöntemle indirgenmiş olan grafenin C/O oranları.

Element	GO	Isıl İndirgeme RGO
% C	65.27	91.78
% O	35.73	8.22
C/O	1.88	11.17

GO'nun yapısında %35 oksijenin varlığı, GO yapısı içerisinde fonksiyonel grupların oluştuğunu göstermektedir. GO'nun termal indirgemesi ile elde edilen RGO'daki oksijenin varlığı ise %8.22 ye kadar düşmüştür. . Bu sonuçlara bakıldığında termal yöntem ile indirgeme sonucunda oksijenli fonksiyonel grupların yapıdan uzaklaştığı anlaşılmaktadır. GO ve RGO'nun C/O oranı sırasıyla 1,88 ve 11,17 olarak bulunmuştur. Bu sonuçlar literatür ile uyumlu sonuç vermiştir [19, 20].

3.5. Termal İndirgeme Metoduyla Sentezlenmiş Grafenin Raman Analizi

RGO'nun yapısal özellikleri Raman spektroskopisi ile analiz edilmiştir. Grafik 6'da termal yöntem ile elde edilen RGO'nun yapısındaki değişimi gösteren Raman spektroskopisindeki D (sp^3) bandı, aromatik yapıdaki düzensizlikleri, amorf yapıları ve oksidasyon sonucunda oluşan alifatik yapıları ifade ederken, G (sp^2) bandı düzenli/aromatik yapıları göstermektedir. Raman deseninde 2D bandı graphene ait karakteristik piki göstermektedir. Raman spektrumunda beklendiği gibi D piki 1350 cm^{-1}'de, G piki 1585 cm^{-1} 'de ve 2D piki, 2685 cm^{-1}'de görülmektedir. D pikinin şiddeti (I_D) düzensiz yapıların derecesini, G pikinin şiddeti (I_G) düzenli yapıların şiddet değerini vermektedir. Literatürde belirtildiği gibi karbon esaslı materyallerin I_D/I_G oranı 0,95-1,22 aralığında olması beklenmektedir [20, 21]. Çalışmamız da ise RGO yapısının I_D/I_G oranı 0,97 bulunmuştur. Dolayısıyla, Raman spektroskopisi, sentezlenen RGO'da sp2 yapıların oluştuğu ve düzenli yapı miktarının arttığı tespit edilmiştir.

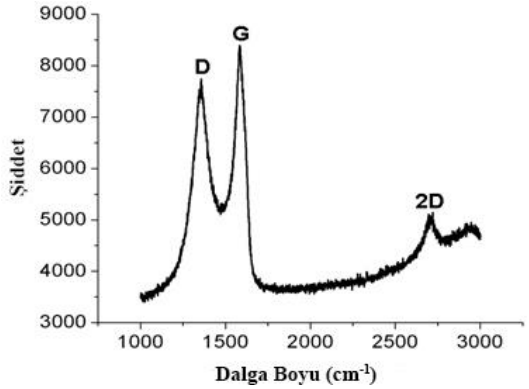

Grafik 6. Thermal metod ile elde edilen graphene ait Raman deseni.

3.6. Grafit, Grafen Oksit ve İndirgenmiş Grafenin SEM Analizleri

SEM cihazı ile 200nm (30.00kx) yakınlaştırılarak grafit, GO ve RGO yapılarının görüntüleri elde edilmiştir (Grafik 7).

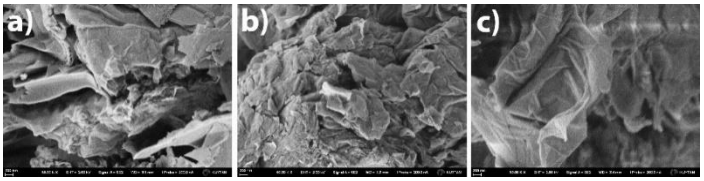

Grafik 7. Saf grafit tozu (a), grafen oksit (b) indirgenmiş grafen oksit (c).

Grafik 7'de görüldüğü üzere, grafitin (a) oksitleme işleminden sonra, grafit tabakalarının arası açılmıştır (b). Bu görüntüler, oksitleme işleminin başarılı bir şekilde gerçekleştiğini göstermektedir. Termal olarak

indirgenmiş grafenin SEM görüntüleri (c), şeffaf, kırışmış grafen yapılarının elde edildiğini göstermektedir.

3.7. BET Sonuçlarının Değerlendirilmesi

Brunauer, Emmet ve Teller (BET) methoduyla 77 K'deki sıvı azot ortamında, azot (N_2) gazı adsorpsiyonu tekniğine dayalı olarak yüzey alanı ve gözeneklilik ölçümü yapılmıştır. Isıl indirgeme metoduyla sentezlenmiş grafenlerin (RGO) BET analizi sonuçları Tablo 2'deki gibidir.

Tablo 2. Isıl indirgeme metoduyla sentezlenmiş grafene (RGO) ait BET analiz sonuçları

	BET yüzey alanı (m^2/g)	**Hacim (cc/g)**	**Gözenek çapı (4V/S, Nanometer)**
RGO	600	1.176	9.02

Termal metod yoluyla üretilen grafen çalışmasına ait numunenin BET analizi sonucunda grafenin yüzey alanı 600 (m^2/g) çıkmıştır. Bunun sebebi, Staudenmaier-GO'nun termal inirgeme yapılarak grafen eldesi sırasında oksijenli grupların daha etkin ayrılarak daha gözenekli yapı oluşturması ve yüzey alanının yüksek olmasını sağlamıştır.

4. Sonuç ve Öneriler

Bu araştırmada, pul grafitten az katmanlı indirgenmiş grafen oksit üretimine odaklanıldı. Ayrıca grafen oksit (GO) ve indirgenmiş grafen oksidin (RGO) üretimi ve karakterizasyon yöntemleri araştırıldı. Öncelikle grafit, büyük ölçekli üretime elverişli yöntemlerden olan Staudenmaier yöntemiyle grafen oksit yapısına dönüştürülmüştür. Elde edilen grafen oksit numuneleri termal yöntemle indirgendi. Grafen oksit ve indirgenmiş grafen numuneleri FT-IR, SEM, XRD, XPS, BET ve Raman spektroskopisiyle karakterize edilmiştir. FT-IR spektroskopisi sonuçları, oksijen içeren fonksiyonel grupların (OH, C=O, C-OH) sentezlenmiş grafen oksit bünyesindeki varlığına işaret etmektedir. XRD analizi sonucunda tabakalar arası mesafelere bakıldığında ise grafit için 0.32 nm, grafen oksit için ise 0.85 nm değerlerine ulaşılmaktadır. Bu sonuçlar oksitleme işleminin başarıyla gerçekleştiğini göstermektedir. XPS spektrumu GO ve indirgenmiş grafen oksidin kimyasal yapısındaki atomik C:O oranlarının sırasıyla yaklaşık 1.88 ve 11.47 olduğunu göstermektedir. RGO örnekleri raman spektroskopisinde yeni sp^2 yapıların oluştuğu ve düzenli yapı miktarının arttığını görülmüştür.SEM görüntülerinden saydam ve kırışık RGO yapıları tespit edilmiştir. İndirgenmiş grafen oksit numunelerinin BET analizi sonucunda yüzey alanının 1g. başına yaklaşık 600 m^2 olduğu tespit edilmiştir. Bu durum sentezlenen RGO'larin az tabakalı yapıda olduğunu göstermektedir.

Referanslar

[1] Geim, A.K., Novoselov, K.S., The rise of graphene, Nature, 6(3), pp. 183-191, 2007.
[2] Slonczewski J.C., Weiss P. R., Band Structure of Graphite, Physical Review, 109 (2), pp. 272-279, 1958.
[3] Allen, M.J., Tung, W.J., Kaner, R.B., Honeycomb Carbon: A Review of Graphene, Chemical Review, 110 (1), pp. 132-145, 2010.
[4] Balandin A.A., Ghosh S., Bao W., Calizo I., Teweldebrhan D., Miao F.,Lau C.N.,2008. Superior Thermal Conductivity of Single-Layer Graphene, Nano Letters, 8 (3), 902-907.
[5] Lee, C., Wei, X.W., Kysar, J., Hone, J., Measurement of elastic properties and intrinsic strength of monolayer graphene, Science, pp. 321, 385, 2008.
[6] Singh, V., Joung , D., Zhai, L., Das, S., Khondaker, S.I., Seal, S., 2012. Graphene based materials: Past, present and future, Progress in Materials Science, 56, pp. 1178–1271, 2012.
[7] Novoselov1, K.S., Fal'ko, V.I., Colombo, L., Gellert, P.R., Schwab, M.G., Kim, K., A roadmap for graphene, Nature, 490, pp. 192-200, 2012.
[8] Das1, T.K., Prusty, S., Recent advances in applications of graphene, International Journal of Chemical Sciences and Applications, 4(1), pp. 39-55, 2013.
[9] Brodie B.C., On the Atomic Weight of Graphite, Philosophical Transactions of the Royal Society of London, 149, ppç 249-259, 1859.
[10] Dreyer, D.R., Park, S., Bielawski, C.W., Ruof, R.S., The chemistry of graphene oxide, Chem. Soc. Review, 39, 228–240, 2009.
[11] Park S. and Ruoff R. S., Chemical methods for the production of graphenes, Nature Nanotechnology, 4 (4), 271-224, 2009.
[12] McAllister M. J., 2007. Single sheet functionalized graphene by oxidation and thermal expansion of graphite, Chemistry of Materials, 19, 4396-4404.
[13] Chua, C. K., & Pumera, M., Chemical reduction of graphene oxide: a synthetic chemistry viewpoint. Chemical Society Reviews, 43 (1), pp. 291- 312, 2014.
[14] Zhu Y., Murali S., Stoller M.D., Velamakanni A., Piner R.D., Ruoff R.S., Microwave assisted exfoliation and reduction of graphite oxide for ultracapacitors, Carbon, 48 (7), pp. 2118-2122, 2010.
[15] Cote L. J., Cruz-Silva R.,Huang J., Flash reduction and patterning of graphite oxide and its polymer composite, Journal of the American Chemical Society, 131(31), pp. 11027-11032, 2009.
[16] Loryuenyong V., Totepvimarn K., Eimburanapravat P., Boonchompoo W., and Buasri A., Preparation

and characterization of reduced graphene oxide sheets via water-based exfoliation and reduction methods, Hindawi-Advances In Materials Science and Engineering, Vol. 2013:5 pages, 2013.
[17] Chen J., Yao B., Li C., Shi G., "An improved hummers method for eco-friendly synthesis of graphene oxide", Carbon, 64, pp. 225–229, 2013.
[18] Fatima T. J., Jee W.L., Woo W.L., Facile and safe graphene preparation on solution based platform, Journal of Industrial and Engineering Chemistry, 20 pp. 2883–2887, 2014.
[19] Wufeng C., Lifeng Y., Prakriti R. B., Preparation of graphene by the rapid and mild thermal reduction of graphene oxide induced by microwaves, Carbon 48 pp. 1146 – 1152, 2010.
[20] Ferrari A.C., Raman spectroscopy of graphene and graphite: disorder, electron-phonon coupling, doping and nonadiabatic effects, Solid State Communications, 143(1), pp. 47-57, 2007.
[21] Chen W., Yan L., and Bangal P.R., Chemical reduction of graphene oxide to graphene by sulfur containing compounds, The Journal of Physical Chemistry C, 114(47), pp. 19885-19890, 2010.

ICACChE
2nd International Conference on Applications in Chemistry and Chemical Engineering
10 - 14 October 2018 Belgrade

Toxicity and Antibacterial Activity of Ciprofloxacine in Conventionally Treated Urban Wastewater Before and after Oxidative Treatment

L. Boudriche[1], I. Michael-Kordatou[2], S. Michael[2], P. Karaolia[2], A. Boudjemaa[1], D. Fatta-Kassinos[2]

Abstract

This study evaluates the feasibility of UV-C-driven advanced oxidation process in degrading ciprofloxacin (CIP) in urban wastewater effluents, using H_2O_2 as oxidant at various concentrations for the process optimization.
The results revealed that a complete degradation of CIP was achieved within 15 min of treatment under the optimum concentration of H_2O_2 which it was found to be 10 mg L^{-1}. Also CIP decay exhibited a pseudo-first-order kinetics pattern under the different experimental conditions applied.
The phytotoxicity and ecotoxicity of the treated samples was investigated against one plant species (Sinapis alba) and a crustacean (D. magna), respectively. At the end of the process the phytotoxic effect was eliminated. In addition, this study demonstrated the ability of the UV-C process to reduce the toxicity towards D. magna since the immobilization of the organisms was significantly reduced comparatively to the untreated wastewater. The antibacterial activity of the treated samples was investigated and a total inactivation of CIP-resistant Escherichia coli within 2 min of treatment was recorded.

Keywords: antibiotics; ciprofloxacin; UV-C/H_2O_2; toxicity; antibiotic resistance.

1. INTRODUCTİON

Ciprofloxacin (CIP), poorly biodegradable, consists of a recalcitrant quinolone structure and a piperazine moiety is a second generation fluoroquinolone. The antibiotic is one of the most prescribed antibiotics worldwide for the treatment of urinary and respiratory tract infections [1,2]. Some studies demonstrated that CIP can be extremely genotoxic [3] and can also exhibit acute toxic effect towards algal species and various aquatic organisms [4,5]. Moreover, bacterial strains harbouring resistance to CIP have been detected in various environmental compartments. Many studies on the degradation of CIP in distilled water have been conducted, including heterogeneous photocatalysis [6] ultrasound irradiation [7] ozonation [8] electron ionizing energy [9] photooxidation with UV irradiation [10] but only very few studies have been performed in real wastewater effluents and at a concentration of CIP close to real environmental levels (50 μM). Despite all of the research studies that have been conducted, no studies were performed to evaluate the efficiency of the UV-C/H_2O_2 process in removing toxicity of treated wastewater, as well as CIP-resistant bacteria. Thus, the aim of this study was to assess the efficiency of a UV-C-driven chemical oxidation process in the presence of H_2O_2, to degrade CIP at environmentally relevant concentration level in urban wastewater effluents. The treatment efficiency through the evaluation of phyto- and eco-toxicity effects, towards Sinapis alba and Daphnia magna, respectively, was explored. Also, the study investigated the removal of E. coli harbouring resistance to CIP during UV-C irradiation. According to the authors' knowledge, this work is the first one revealing comprehensive data regarding the oxidation of CIP by UV-C/H_2O_2 process, the assessment of the process in removing phyto- and exo-toxicity, and finally antibiotic-resistant bacteria.

[1]*Corresponding author: Centre de Recherche Scientifique et Technique en Analyses Physico-Chimiques, BP 384 Bou-Ismail, RP 42004 Tipaza, Algeria, boud_lil@yahoo.fr.*

[2]*Department of Civil and Environmental Engineering and Nireas-International Water Research Centre, School of Engineering, University of Cyprus, P.O. Box 20537, 1678 Nicosia, Cyprus.*

2. MATERIALS AND METHODS

All experiments were run in a photochemical apparatus consisting of an immersion well, batch type bench-scale cylindrical reaction vessel with a total capacity of 600 mL. The aqueous solution was irradiated with 9 W low-pressure mercury monochromatic lamp (254 nm).

The oxidation experiments were performed using secondary treated wastewater (taken after the secondary clarifier). All wastewater samples were grab samples and they were conserved in amber glass bottles (1 L each) after filtration through 0.45 μm.

CIP concentration evolution was monitored using an ACQUITY TQD UPLC-MS/MS system.

Toxicity Assessment

The phytotoxicity of the treated samples was evaluated towards *Sinapis alba* using the Phytotestkit microbiotest (MicroBioTests Inc.), which measures the direct effect of chemical compounds on plants.

The ecotoxicity of the treated samples were evaluated towards the crustacean *Daphnia magna* using the Daphtoxkit magna toxicity test. Ecotoxicity was expressed as the percentage of the immobilized organisms after an exposure time of 24 h and 48 h, for each sample.

Enumeration of total cultivable and CIP-resistant E. coli

The prevalence of total cultivable and CIP-resistant *E. coli* prior to and after the UV-C oxidation treatment was evaluated. *E. coli* were enumerated on TBX agar or on this medium supplemented with CIP. The antibiotic concentration in the culture medium (1 mg L^{-1}) was chosen based on its environmental relevance and its minimum inhibitory concentration (MIC) to *E. coli*. The treated samples were passed through cellulose ester membranes using a membrane filtration apparatus to ensure a reliable count in each sampling time. Then, the membranes were placed onto the culture media and incubated for 24 h at 44 °C. The prevalence of CIP-resistant *E. coli* was calculated by directly comparing the CFU mL^{-1}counts on the antibiotic plate supplemented culture medium with the corresponding counts without antibiotic.

$$\text{Resistance (\%)} = \frac{CFU\ ml^{-1}\ medium\ with\ CIP}{CFU\ ml^{-1}\ medium\ without\ CIP} \text{ x } 100 \quad (1)$$

3. RESULTS AND DISCUSSION

Phytotoxicity

Seed Germination İnhibition (GI)

From Fig. 1 (a), it is evident that the wastewater samples spiked with 100 μg L^{-1} of CIP (WW), exhibited no inhibition effect on the germination of *S.alba*, indicating that the presence of this antibiotic in wastewater did not have any adverse effect on the germination. Similar results were obtained with the same plant species when adding ofloxacin and trimethoprim in secondary treated wastewater at 100 μg L^{-1} [11].

The treated samples collected after15 min and 60 min of treatment caused low inhibition on the germination of *S. alba* (3.33%) possibly due to the formation of new oxidation products which apparently were toxic to these seeds. However, at the end of treatment (180 min), no seed germination inhibition was observed, indicating that the toxic intermediates were eliminated (or further transformed to less toxic compounds) at the end of the process.

Root growth inhibition (RI)

The phytotoxicity effect against root growth was higher compared to that observed on seed germination, indicating that the roots were more sensitive (Fig. 1 (b)). In the case of untreated wastewater, a favourable effect on root growth was observed (negative inhibition values), which can be possibly assigned to the presence of nutrients in the wastewater samples. Similar negative values were obtained when investigating the efficiency of a sulfate radical-based oxidation process under UV-C irradiation in degrading erythromycin [12].

RI increased at 15, 30 and 60 min of treatment yielding 2.8%, 7% and 18.1% of inhibition, respectively, implying thus the formation of new oxidation products that are more toxic than the original wastewater matrix. From that time onwards, RI decreased at 90 and 120 min (2.56% and 0.13%, respectively), indicating the removal or transformation of the toxic oxidation products. At

the end of the treatment (120 min), the value of RI was lower than that observed for the untreated wastewater sample (6.89%), meaning that the oxidation process reduced significantly the phytotoxicity of the matrix. Michael-Kordatou [12] investigated the phytotoxicity of erythromycin-spiked wastewater effluents subjected UV-C/sodium persulfate treatment. The maximum inhibition of root growth of *S.alba* reached 54%, within 30 min of treatment, and beyond this time RI was significantly decreased up to 5%.

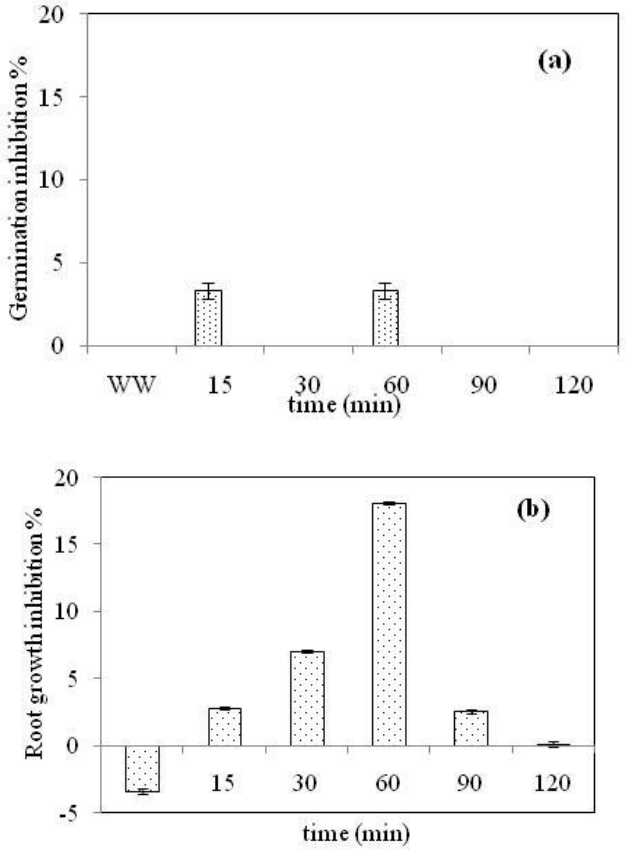

Figure 1. (a) Seed germination inhibition (GI), (b) Root growth inhibition (RI) during the UV-C oxidation treatment. Experimental conditions: $[CIP]_0$=100 μg L^{-1}, $[H_2O_2]_0$=10 mg L^{-1}, pH=7.8.

Ecotoxicity assessment

In further experiments, toxicity tests were performed by exposing *D. magna* to the treated samples collected at different times of treatment. The ecotoxicity profile was expressed as % immobilization of *D. magna* after 24 and 48 h of exposure (Fig. 2).

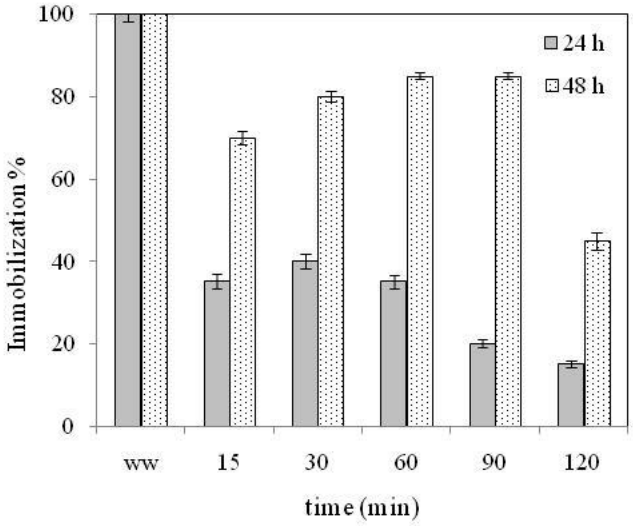

Figure 2. Immobilization of *D. magna* during UV-C/H_2O_2. Experimental conditions: $[CIP]_0$=100 μg L^{-1}, $[H_2O_2]_0$=10 mg L^{-1}, pH=7.8.

The untreated CIP-spiked wastewater resulted in a complete immobilization (100%) of *D. magna* after 24 h exposure time, indicating the toxic effects of dE_fOM originally present in the matrix. From that time onwards, the immobilization decreased and reached 15% after 24 h exposure time. When increasing exposure time to 48 h, the toxic effect towards daphnids was found to be higher and the immobilization reached its maximum value (85%) at 60 and 90 min of treatment. After increasing the treatment time to 120 min, a sharp decrease in the immobilization by 55% occurred compared to the untreated wastewater.

Similar observations were obtained by Rozas [13] during the UV/H_2O_2 treatment (UV dose=1200 mJ cm^{-2}; [H_2O_2]=10 mg L^{-1}) of a mixture of microcontaminants (i.e. diclofenac, triclosan, atrazine, carbamazepine). The immobilization of *D. Magna* was found to be 20 and 42% after 24 and 48h, respectively. In another study, the increase of the toxic effect towards *D. magna* induced by the early degradation of diclofenac (10 mg L^{-1}) using UV-A/TiO_2 treatment was reported [14]. It was found that the toxicity rapidly increases within the first 15 min of treatment before gradually decreasing up to 60 min. The toxicity effect to *D. magna*, induced by the oxidation products derived from antibiotics oxidation, has already been explored in previous studies using other AOPs [11,15].

Considering the low concentration of the spiked antibiotic (i.e. 100 μg/L), it can be assumed that *D. magna* was not affected by the presence of CIP photo-oxidation products but the observed toxicity can be assigned to the oxidation of the various organic constituents prevailing in the dE_fOM of the wastewater samples. Of course, additional runs (in the absence/presence of CIP in the reaction solution) accompanied with statistical validation should be carried out, in order to exclude (or not) the contribution of the TPs resulted from the oxidation of the parent compound.

Removal of total and CIP-resistant *Escherichia coli* during UV-C/H_2O_2

E. coli typically detected in UWTPs effluents [16], was selected as model microorganism due to its wide use as indicator of faecal contamination and antibiotic resistance in wastewater [17]. Therefore, theability of the UV-C/H_2O_2 treatment to remove total cultivable *E. coli* and CIP-resistant *E. coli* against irradiation time was investigated (Fig. 3). A complete inactivation of *E. coli* occurred within 1 min of UV-C treatment. The total cultivable (medium without CIP) and CIP-resistant *E. coli* (medium with CIP) decreased rapidly, with time irradiation, nevertheless the removal of *E. coli* in the culture medium enriched with CIP, was lower compared to that observed in the medium without CIP.

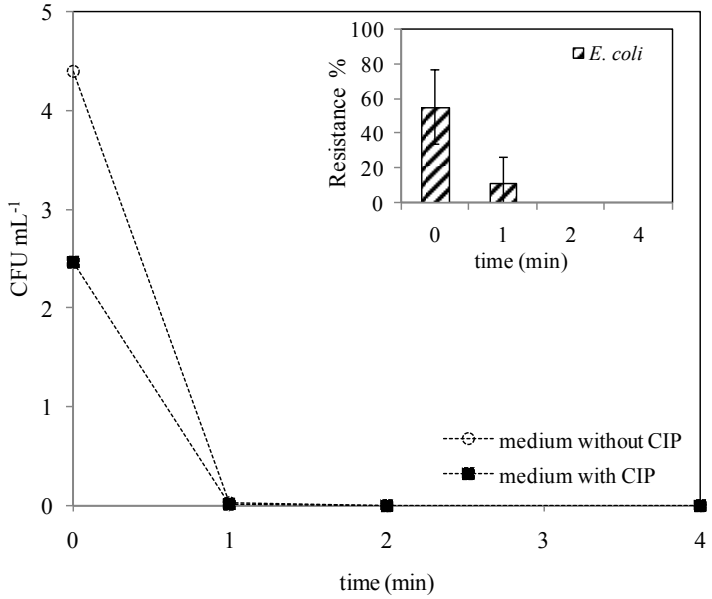

Figure 3. Total cultivable and CIP-resistant *E. coli* during UV-C (expressed as CFU mL^{-1}). Inset graph illustrates the resistance percentage profile during the treatment. Experimental conditions: $[CIP]_0$ = 100 μg L^{-1}, $[H_2O_2]_0$= 10 mg L^{-1}, pH = 7.8.

The resistance percentage (inset of Fig.3), decreased significantly from 55% to 15% after 1 min of UV-C treatment, and it was eliminated within 2 min of treatment. The total and fast disinfection

can be mainly attributed to the combination of three effects. The UV-C irradiation (254 nm) can contribute to the inactivation of microorganisms, through the damage caused to intracellular chromophores due to radiation absorption [17, 18]. In addition, the reactive oxygen species (ROS) generated during oxidation, like $HO^{\bullet}$, can inhibit a wide range of microorganisms.

To date there have been few and conflicting reports regarding the efficiency of UV-based processes in removing ARB from wastewater. For example, Michael-Kordatou [12] showed that under the optimum experimental conditions, the UV-C oxidation process resulted in total inactivation of erythromycin-resistant *E. coli* within 90 min.

4. CONCLUSION

A complete reduction in the inhibition percentage was achieved for seed germination and root growth, at the end of the treatment. Furthermore, the root growth of *S. alba* were shown to be more sensitive to the oxidation products formed during the treatment compared to seed germination.

The toxicity to *D. magna,* was decreased at the end of treatment, comparatively to the untreated wastewater. Further studies are needed however, to reveal the dE_fOM-associated compounds' nature and characteristics that are responsible for their potential toxic effects.

Finally, this study showed the ability of the UV-C process in inactivating both total *E. coli* and those carrying resistance to CIP.

REFERENCES

[1] H.A. Okeri and I.M. Arhewoh, Analytical profile of the fluoroquinolone antibacterials. I. Ofloxacin. *Afr J Biotechnol*7: 670-680 (2008).

[2] I. Hayder, I.A. Qazi, M.A. Awan, M.A. Khan, A. Turabi, Degradation and inactivation of ciprofloxacin by photocatalysis using TiO_2 nanoparticles. *J App Pharm*04: 487-497 (2012).

[3] A. Hartmann, A.C. Alder AC, T. Koller T and R.M. Widmer RM, Identification of fluoroquinolone antibiotics as the main source of umuCgenotoxicity in native hospital wastewater. *Environ ToxicolChem*17: 377-382(1998).

[4] B. Halling - Sørensen, H.C. Lützhøft, F. Anderson, A. Ingerslev, Environmental risk assessment of antibiotics: comparison of mecillinam, trimethoprim and ciprofloxacin. *J AntimicrobChemother*46: 53-58 (2000).

[5] S.M. Richards, C.J.Wilson, D.J. Johnson, D.M. Castle, M. Lam, S.A. Mabury, P.K. Sibley and K.R. Solomon, Effects of Pharmaceutical Mixtures in Aquatic Microcosms. *Environ Toxic Chem*23: 1035-1042 (2004).

[6] A. Hassani, A. Khataee and S. Karaca, Photocatalytic degradation of ciprofloxacin by synthesized TiO_2 nanoparticles on montmorillonite: Effect of operation parameters and artificial neural network modelling. *J MolCatal A-Chem*409: 149–161 (2015).

[7] R.S. Sutar and V.K. Rathod, Ultrasound assisted Laccase catalyzed degradation of Ciprofloxacin hydrochloride. *J IndEngChem*31: 276-282 (2015).

[8] H.M. Jalali, Kinetic study of antibiotic ciprofloxacin ozonation by MWCNT/MnO_2 using Monte Carlo simulation. *Mat SciEng*59: 924-929 (2016).

[9] J.Y. Cho, B.Y. Chung, K.B. Lee, G.H. Lee and S.A. Hwang, Decomposition reaction of the veterinary antibiotic ciprofloxacin using electron ionizing energy. *Chemosphere*117: 158-163 (2014).

[10] H.S. Ou, J.S. Ye, S. Ma, C.H. Wei, N.Y. Gao and J.Z. He, Degradation of ciprofloxacin by UV and UV/H_2O_2 via multiple-wavelength ultraviolet light-emitting diodes: Effectiveness, intermediates and antibacterial activity, Chemical Engineering Journal (2016), doi: http://dx.doi.org/10.1016/j.cej.2016.01.006.

[11] I. Michael, E. Hapeshi, C. Michael, A.R. Varela, S. Kyriakou, C. Manaia and D. Fatta-Kassinos, Effectiveness of solar Fenton process on abatement of antibiotics at a pilot plant scale: degradation kinetics, ecotoxicity assessment and removal of antibiotic resistant enterococci. *Water Res* 46: 5621-5634 (2012).

[12] I. Michael-Kordatou, M. Iacovou, Z. Frontistis, E. Hapeshi, D.D. Dionysiou and D. Fatta-kassinos, Erythromycin oxidation and ERY-resistant Escherichia coli inactivation in urban wastewater by sulphate radical-based oxidation process under UV-C irradiation. Water Res 85:346–358 (2015).

[13] O. Rozas, C. Vidal, C. Baeza, W.F. Jardim, A. Rossner and H.D. Mansilla, Organic Micropollutants (OMPs) in Natural Waters: Oxidation by UV/H_2O_2 Treatment and Toxicity Assessment, Water Research (2016), doi: 10.1016/j.watres.2016.03.069.

[14] A. Achilleos, E. Hapeshi, N.P. Xekoukoulotakis, D. Mantzavinos and D. Fatta-Kassinos, Factors affecting diclofenac decomposition in water by UV-A/TiO_2 photocatalysis.*ChemEng J*161: 53-59 (2010).

[15] G. Lofrano, G. Libralato, R. Adinolfi, A. Siciliano, P. Iannece, M. Guida, M. Giugni, A.V. Ghirardini AV and M. Carotenuto M, Photocatalytic degradation of the antibiotic chloramphenicol and effluent toxicity effects. *Ecotox Environ Safe*123: 65-71 (2016).

[16] L. Rizzo, A. Della Sala, A. Fiorentino and G. Li Puma, Disinfection of urban wastewater by solar driven and UV lampe TiO_2 photocatalysis: Effect on a multi drug resistant Escherichia coli strain. *Water Res*53: 145-152 (2014).

[17] M. Radman and M. Errera, Enhanced efficiency of excision repair of non-replicated UV-damaged E. coli DNA. *Mutation Res* 9: 553-560 (1970).

[18] A.C. Miranda, L. Lepretti, Rizzo, I. Caputo, V. Vaiano, O. Sacco, WS. Lopes and D. Sannino, Surface water disinfection by chlorination and advanced oxidation processes: Inactivation of an antibiotic resistant *E. coli* strain and cytotoxicity evaluation. *Sci Total Environ* 554-555: 1-6 (2016)

ICACChE
2nd International Conference on Applications in Chemistry and Chemical Engineering
10 - 14 October 2018 Belgrade

Influence of pH and Radicals Ions on the Removal of Sulfaquinoxaline from Aqueous Media Using UV/$Na_2S_2O_8$

L. Boudriche[1,2], Z. Safaei[3], D. Ramasamy[3], M. Sillanpää[3], A. Boudjemaa[1]

Abstract

This study evaluates the feasibility of UV-C driven advanced oxidation process induced by sulfate radicals in degrading sulfaquinoxaline (SQ-Na) sodium in water.
The results show that SQ-Na was decomposed at 90% within 300 min of irradiation under the optimum concentration (200 mg/L) of sodium persulfate (SPS). The SQ-Na decay exhibited a pseudo-first-order kinetics when the initial sulfate radical anion concentration varied from 0 to 240 mg/L.
The decomposition of SQ-Na via UV/sodium persulfate process was strongly favorable under acidic conditions but was slowed down at inherent pH (6.8) and almost inhibited under alkaline conditions (pH 9).
This study revealed that UV/SPS system is a good alternative to eliminating veterinary drugs residues, such as SQ-Na, before they are released into natural waters.
Keywords: Sulfaquinoxaline sodium, UV-C, degradation, pH effect, ions efficiency.

1. INTRODUCTION

Sulfonamides are one of the oldest and more consumed groups of veterinary drugs, having been used since many years. As these compounds are not completely metabolized, both the unmetabolized antibiotics and their metabolites are released to the environment at high proportion, either directly in aquacultures and by grazing animals or indirectly during the applications of manure or slurry [1,2]. It is therefore important to focus on eliminating residues of veterinary drugs in wastewater before they are released into natural waters or for agricultural purposes.
In the recent years, a great scientific interest is being placed on the sulfate radical based-advanced oxidation processes (AOPs) due to their high efficiency in degrading a wide range of recalcitrant microcontaminants in aqueous matrices, including pharmaceuticals [3-5]. Persulfate radicals can be produced by the activation of persulfate, peroxymonosulfate, potassium persulfate and ammonium persulfate anion [6] by various methods, such as heat [7], ultrasonic [8] and UV [9].
Within this context, the current study investigated the efficiency of UV-C-activated persulfate process in degrading sulfaquinoxaline sodium (SQ-Na), which consists of a sulfa group and a quinoxaline group, often used as a drug to prevent coccidiosis in poultry, swine, and sheep by inhibiting the synthesis of nucleic acids and proteins in microorganisms [10, 11]. Therefore, in this work, special attention was paid to the optimization of the process with regard to various operating parameters such as oxidant dose, presence or absence of UV-C irradiation, antibiotic initial concentration, solution pH and radicals nature.
It should be noted that the degradation of sulfaquinoxaline sodium was carried out during the UV/H_2O_2 [12], but no studies have been conducted in the presence of sulfate radicals.

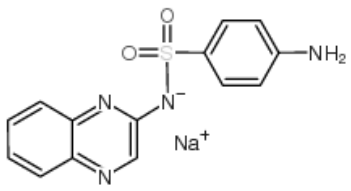

Figure 1. Chemical structural formula of sulfaquinoxaline sodium.

[1]*Corresponding author: Centre de Recherche Scientifique et Technique en Analyses Physico-Chimiques, BP 384 Bou-Ismail, RP 42004 Tipaza, Algeria. e-mail : boud_lil@yahoo.fr*
[(2)]*Laboratoire E.P.C.M.A.E., Faculté de Chimie, USTHB, BP 32 El Alia, Bab Ezzouar,16111 Alger, Algeria.*
[(3)]*Laboratory of Green Chemistry, Lappeenranta University of Technology, Sammonkatu 12, FI-50130 Mikkeli, Finland.*

2. MATERIALS AND METHODS

2.1. Chemicals

Sulfaquinoxaline sodium salt (SQ-Na) ($C_{14}H_{11}N_4NaO_2S$, molecular weight 322.32 g/mol, purity > 92.5 %, Sigma-Aldrich).
Sodium persulfate (SPS) ($Na_2S_2O_8$, > 98%, Sigma-Aldrich), Anhydrous sodium sulfite (Na_2SO_3, 98.7 %, VWR Chemicals), hydrogen peroxide (H_2O_2, 30% w/w, Merck).
NaOH (99 %, Merck) and HNO_3 (65%, VWR Chemicals) aqueous solutions were used to adjust the pH. Stock solutions were prepared in Ultrapure Water System (arium® mini –Sartorius, German).

2.2. Experimental Procedures

Experiments to investigate the UV/SPS degradation of SQ-Na were carried out at room temperature in a photochemical apparatus in batch mode. A volume of 0.7 L of the antibiotics aqueous solution (10 mg/L) is put into 1 L glass reactor at fixed agitation speed (400 rpm) for a period of 300 min. The appropriate amount of SPS was added to achieve the desired oxidant concentration and subsequently the solution was irradiated with 5 W low-pressure mercury monochromatic lamp (UVC-Lamp G8T5, λ=254 nm). All the assembly was put in a cabinet in order to avoid external light penetration during the experiment.
For all experiments, samples were withdrawn using a syringe at pre-determined time intervals, were then filtered through 0.2 µm (PES, Agilent) syringe-driven filter and transferred in vials previously filled with the appropriate volume of reagents to quench further reactions before measurements (methanol and anhydrous sodium sulfite for the HPLC and total organic carbon analysis, respectively).
Experiments were triplicate; the results of the analysis are presented as the mean with a standard deviation less than 5%.

2.3. Analytical Method

The analyses were performed on a HPLC Shimadzu chromatographic apparatus (Shimadzu Corporation, Kyoto, Japan) equipped with solvent delivery systems. The system control, data acquisition, and data evaluation were performed by Shimadzu "Lab-Solution" software (Shimadzu Corporation, Kyoto, Japan). The isocratic mobile phase was prepared by on-line mixing in HPLC gradient grade organic solvents. The mobile phase consisted of acetonitrile and potassium phosphate monobasic buffer (32.5: 67.5, v/v), pH 2.5, at a flow rate of 1 $ml.min^{-1}$. The column temperature was set as 35 ºC, and the injected volumes were 50µl. Three parallel injections were performed for each sample, and photometric UV detection at 254 and 208 nm were applied. The peak profile data were acquired at the frequency of 100 Hz.

3. RESULTS AND DISCUSSION

3. 1. UV/$SO_4^{\cdot-}$ Advanced Oxidation/Degradation Kinetics

In order to determine the optimum oxidant concentration, the degradation of SQ-Na during the UV-C/$SO_4^{\cdot-}$ process was investigated under various sodium persulfate (SPS) concentrations (ranging from 20 to 240 mg/L) while the initial concentration of SQ-Na was maintained constant ($[SQ\text{-}Na]_0$ =10 mg/L) in each experimental run. The results (Fig. 2) demonstrated that under UV-C irradiation alone (in the absence of SPS) there was no effect on the SQ-Na until 300 min of irradiation, which may be due to the high molar absorption coefficient of SQ-Na at 254 nm [12].
Then, the degradation occurs when only 80 mg/L of SPS was added in the photolytic experiments. The rate was rapidly increased from 63% to 90% by increasing the concentration of SPS from 80 to 200 mg/L, respectively, within 300 min of irradiation. At 240 mg/L SPS concentration, the SQ-Na degradation rate remained constant (90%).

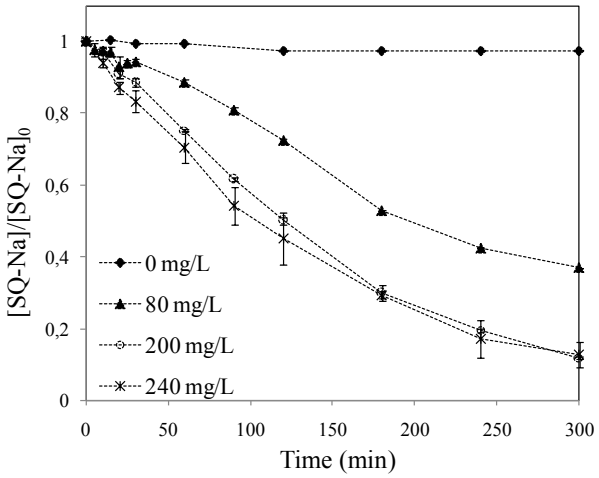

Figure. 2. Effect of SPS concentration on the degradation of SQ-Na under UV-C irradiation. Experimental conditions: [SQ-Na]$_0$=10 mg/L; pH=6.8.

Similar results on the high performance of UV irradiation in presence or absence of sulfate radicals have been reported, as in the degradation of chloramphenicol [4], erythromycin [3] and sulfamethoxazole [6].

A linear relationship between Ln([SQ-Na]/[SQ-Na]$_0$) against UV irradiation time was obtained, related to pseudo first-order kinetics, knowing that [SQ-Na]$_0$ and [SQ-Na] refer to the concentrations of the antibiotic at times 0 and t (min), respectively.

$$-\mathrm{Ln}\frac{[SQ-Na]}{[SQ-Na]0} = kt \qquad (1)$$

The removal rate of dissolved organic carbon (DOC) was determined. This parameter brings information about the mineralization rate of the treated samples. After 300 min of irradiation and under the various SPS concentrations, DOC does not change significantly, indicating the formation of recalcitrant organic compounds derived from the oxidation of SQ-Na in water, despite 90 % degradation of SQ-Na was achieved. Similar results were reported by Liao et al. [12] on the same antibiotic under UV/H_2O_2 oxidation, where the DOC decreased only by 10% even the antibiotic was completely degraded.

As shown in Fig. 3, the rate degradation became slow and significantly decreases from 100 % to 25 %, at 60 min of reaction, as the initial SQ-Na concentration increase from 1 mg/L to 10 mg/L. The degradation followed a pseudo-first-order kinetics pattern ($R^2 \geq 0.988$). The rate constant k_{app} declined and followed the order k_{app} (1mg/L) >k_{app} (5 mg/L) >k_{app} (10 mg/L). The decrease could be attributed to the competition of SQ-Na with SPS radicals, which makes the system more efficient when the SQ-Na is less predominant, compared to the SPS radicals.

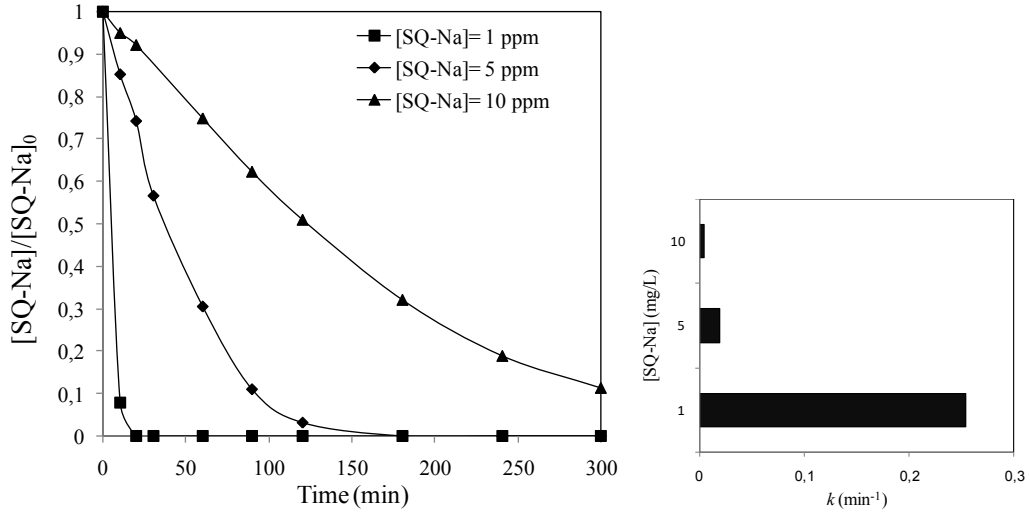

Figure 3. Effect of initial SQ-Na concentration on the degradation of SQ-Na under UV-C irradiation. The right figure indicates the rate constants (k_{app}) at different SQ-Na concentration. Experimental conditions: [SPS]$_0$=200 mg/L; pH=6.8,

3. 2. pH effect

pH plays an important role in the degradation efficiency of antibiotics by AOPs based sulfate radicals [13]. The decomposition of SQ-Na during the UV/SPS process, at optimal oxidant concentration and at three pH values (3, 6.8 and 9) was investigated in this study, knowing that the pH around 6.8, is the inherent pH of the synthetic solutions of SQ-Na.

In addition to these three pHs, a SQ-Na degradation monitoring test; at pH = 3, without UV and without oxidant was also studied, to evaluate the effect of acidity on the degradation of the antibiotic.

Fig. 4, shows that under UV/SPS, the degradation rate of SQ-Na increased from 28 % to 100 % with decreasing pH from 9 to 3 within 300 min of reaction. This means that the amount of radicals and the composition of active species during UV-C irradiation-closely depend on the pH of the medium.

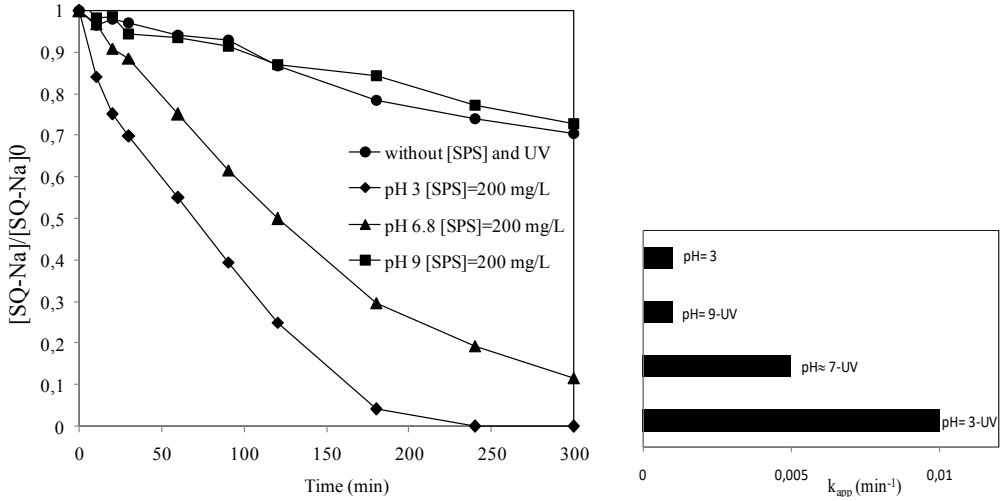

Figure 4. SQ-Na degradation during UV-C activated persulfate oxidation under various pH conditions. The right figure shows the effect of pH on the degradation rate constant, k_{app}.
Experimental conditions: $[SQ\text{-}Na]_0$= 10 mg/L; $[SPS]_0$=200 mg/L.

Several studies have shown that pH plays an important role in the degradation of antibiotics under UV based sulfate radicals**.** Some authors [4,14] have demonstrated that during the activation of persulfate, sulphate radicals become predominant and play a determining role in the elimination of the antibiotic at pH <7. Under acidic conditions, other sulfate radicals can be formed from acid-catalysis, which favor the degradation process.

When pH is between 7 and 10.5, the hydroxyl and sulfate radicals coexist at the same time in the solution, and can therefore interact with each other inducing the inhibition of the substrate decomposition.

Note that the influence of pH on the degradation of SQ-Na during UV/SPS irradiation is a complex issue since it concerns not only the generation of SO_4^{2-} and $HO^{\cdot}$, but also the ionization state of the chemicals (pKa) during the process[6].

The monitoring of SQ-Na degradation in an acidic medium without UV irradiation (Fig.4.) proves that the acid medium alone does not allow degradation of the antibiotic. Only, the combination of UV radiation with acidic conditions makes the process efficient.

4. CONCLUSİON

UV/SPS system was used to remove SQ-Na antibiotic from water. Several parameters were studied and assessed for a better efficiency of the treatment process. The experimental results revealed that the degradation rate increased with increasing oxidant dosage. The SQ-Na degradation fitted the pseudo-first-order kinetics and optimum oxidant concentration was found at 200 mg/L. However, a very low SQ-Na mineralization was obtained.

The maximum SQ-Na degradation occurred at acidic conditions, whereas at pH 9 the contribution of both $SO_4^{-\cdot}$ and $OH^{\cdot}$ radicals was very slow.

$SO_4^{-\cdot}$ was found to be the predominant radical species formed in the UV-C/SPS system yielding 69 % degradation of SQ-Na, whereas the contribution of $HO^{\cdot}$ was estimated to be much lower (8 %).

An evaluation of the toxic effect of transformation products (TPs) derived from SQ-Na degradation under UV/SPS will be investigated using a battery of tests based bioassays.

REFERENCES

[1] M. Jesú García-Galán, M. Silvia Díaz-Cruz, D. Barceló, Identification and determination of metabolites and degradation products of sulfonamide antibiotics, Trends Anal. Chem. 27 (2008) 1008–1022.

[2] K. Kümmerer, Antibiotics in the aquatic environment – A review – Part I, Chemosphere. 75 (2009) 417–434.

[3] I. Michael-Kordatou, M. Iacovou, Z. Frontistis, E. Hapeshi, D.D. Dionysiou, D. Fatta-Kassinos, Erythromycin oxidation and ERY-resistant Escherichia coli inactivation in urban wastewater by sulfate radical-based oxidation process under UV-C irradiation, Water Res. 85 (2015) 346–358.

[4] C. Tan, D. Fu, N. Gao, Q. Qin, Y. Xu, H. Xiang, Kinetic degradation of chloramphenicol in water by UV/persulfate system, J. Photochem. Photobiol. A Chem. 332 (2017) 406–412.

[5] H. Guo, T. Ke, N. Gao, Y. Liu, X. Cheng, Enhanced degradation of aqueous norfloxacin and enrofloxacin by UV-activated persulfate: Kinetics, pathways and deactivation, Chem. Eng. J. 316 (2017) 471–480.

[6] X. Ao, W. Liu, Degradation of sulfamethoxazole by medium pressure UV and oxidants: Peroxymonosulfate, persulfate, and hydrogen peroxide, Chem. Eng. J. 313 (2017) 629–637.

[7] R.O.J. R. L. Johnson, P. G. Tratnyek, persulfate persistence under thermal activation conditions, Environ. Sci. Technol. 42 (2008) 9350–9356.

[8] H. Hori, Y. Nagano, M. Murayama, K. Koike, S. Kutsuna, Efficient decomposition of perfluoroether carboxylic acids in water with a combination of persulfate oxidant and ultrasonic irradiation, J. Fluor. Chem. 141 (2012) 5–10.

[9] M. Mahdi-Ahmed, S. Chiron, Ciprofloxacin oxidation by UV-C activated peroxymonosulfate in wastewater, J. Hazard. Mater. 265 (2014) 41–46.

[10] W.C. Campbell, W.C. Campbell, History of the Discovery of Sulfaquinoxaline as a Coccidiostat, 94 (2008) 934–945.

[11] R. Barcellos, L. Meneghini, M. Pizzolato, C. Ruaro, M.D. Silvia, D. Barcelo, Structural Elucidation of Sulfaquinoxaline Metabolism Products and Their Occurrence in Biological Samples Using High-Resolution Orbitrap Mass Spectrometry, (2014).

[12] Q.N. Liao, F. Ji, J.C. Li, X. Zhan, Z.H. Hu, Decomposition and mineralization of sulfaquinoxaline sodium during UV/H2O2oxidation processes, Chem. Eng. J. 284 (2016) 494–502.

[13] C. Cui, L. Jin, L. jiang, Q. Han, K. Lin, S. Lu, D. Zhang, G. Cao, Removal of trace level amounts of twelve sulfonamides from drinking water by UV-activated peroxymonosulfate, Sci. Total Environ. 572 (2016) 244–251.

[14] R. Zhang, Y. Yang, C.H. Huang, L. Zhao, P. Sun, Kinetics and modeling of sulfonamide antibiotic degradation in wastewater and human urine by UV/H_2O_2 and UV/PDS, Water Res. 103 (2016) 283–292.

[16] X. He, A.A. de la Cruz, K.E. O'Shea, D.D. Dionysiou, Kinetics and mechanisms of cylindrospermopsin destruction by sulfate radical-based advanced oxidation processes, Water Res. 63 (2014) 168–178.

[17] Z. Zhang, Q. Yang, J. Wang, Degradation of trimethoprim by gamma irradiation in the presence of persulfate, Radiat. Phys. Chem. 127 (2016) 85–91.

[18] F. Wang, W. Wang, S. Yuan, W. Wang, Z.H. Hu, Comparison of UV/H_2O_2 and UV/PS processes for the degradation of thiamphenicol in aqueous solution, J. Photochem. Photobiol. A Chem. 348 (2017) 79–8

ICACChE
2nd International Conference on Applications in Chemistry and Chemical Engineering
10 - 14 October 2018 Belgrade

Effect of Co-B-Ag Catalyst Sodium Borohydride Hydrolysis

***Mehmet Sait İzgi*[1]**

Abstract

One of the chemical compounds with high energy density, which removes the problem of the storage of hydrogen from the clean energy sources, is sodium borohydride. The basic parameter that determines the hydrolysis of sodium borohydride, hydrogen production efficiency and reaction course is the catalyst. Energy sources are undoubtedly one of the greatest challenges facing humanity due to increasing concerns over a series of worldwide energy and environmental problems. In the past decades, research around nano scale interface technologies related to photovoltaic, batteries and fuel cells has brought fascinating breakthroughs in energy conversion and storage. In particular, hydrogen has become one of the most promising future energy resources due to concerns about global warming and the depletion of fossil fuels. Metal hydrides like sodium borohydride ($NaBH_4$) have attracted much attention worldwide as a source of high purity hydrogen for portable and stationary applications.

In this study, Co-B-Ag catalyst was studied for hydrogen generation from the hydrolysis of the sodium borohydride solution. Then, the optimal metal ratio, the amount of catalyst, the concentration of different, and the catalytic activity at different temperatures were examined for sodium borohydride hydrolysis. The kinetic model of first order and according to the values obtained the activation energy was determined as 20.301 kJ/mol.

Keywords: Sodium Borohydride, Co-B-Ag, Catalyst, Hydrogen Energy

1. GİRİŞ

Hayatımızda önemli bir yeri olan enerji gelişmiş ülkelerde olduğu gibi gelişmekte olan ülkelerin de en önemli ihtiyacı haline gelmiş, bununla birlikte enerji üretimi ve tüketimi ülkelerin gelişmişlik düzeylerini belirleyen bir ölçüt olarak ortaya çıkmıştır. Dünya nüfusu artışı ve teknolojik gelişmelere paralel olarak enerji ihtiyacı hızlı bir şekilde artmaktadır. Mevcut enerji sistemi, başta fosil kaynaklı yakıtlar olmak üzere tükenebilir özellikteki kaynaklardan sağlanmaktadır. Bu kaynakların tükenir olması ve çevre üzerindeki olumsuz etkileri ülkelerin; ucuz, çevreyle dost ve yenilenebilir özellikteki enerji kaynaklarına olan ihtiyaçlarını günden güne arttırmaktadır. Hidrojen teknolojisi de; enerji taşıyıcı sistemlerin yerini alabilecek; yenilenebilir bir enerji kaynağı olarak geleceğin enerji sistemleri için potansiyel teşkil etmektedir. Hidrojeni yenilenebilir kaynaklardan üretmek ve yüksek verimli yakıt hücrelerinde veya motorlarda kullanmak, küresel ısınmayı ve çevre kirliliğini önemli ölçüde azaltacaktır.

[1]*Corresponding author: Siirt University, Faculty of Engineering, Department of Chemical Engineering, saitizgi@hotmail.com*

İçten yanmalı motor teknolojisi veya türbin teknolojisinin yanı sıra çok daha verimli yakıt hücreleri de hidrojenden güç elde etmek için kullanılır. Şimdiden yakıt hücresi teknolojisi verimi %65 gibi büyük oranlara sahiptir [1]. Hidrojenin kullanılmaya başlanmasıyla birlikte kimyasal enerjinin elektrik enerjisine direkt çevirilmesi, yakıt hücrelerinin geliştirilmesini netice vermiştir. Zaman içerisinde, hidrojenin depolama ve üretim proseslerinin de geliştirilmeye başlanmıştır.

$NaBH_4$, en dengeli alkali metal bor hidrürlerden biri olup, nemli havada çok yavaş reaksiyon verirken kuru havada kararlı bir yapı göstermektedir. Suyla reaksiyonu ile yapısındaki hidrojen serbest kalmaktadır. Suyun sıcaklığı, oda sıcaklığında veya altında ise hidrojenin serbest kalması yavaştır [2]. $NaBH_4$'ün sudaki kararlılığı sıcaklığa ve pH'a bağlı olarak değişir. Sıcaklığın artması ve pH'ın azalması aşağıda verilen Eşitlik 1'e göre hidroliz reaksiyonunu hızlandırmaktadır.

$$NaBH_4 + 2\,H_2O \rightarrow NaBO_2 + 4\,H_2 \qquad (1)$$

$NaBH_4$ 12-13 pH aralığındaki depolama koşullarında bozunma gözlenmez. Belirtilen pH aralıklarında sodyum bor hidrür kararlıdır. Kararlı olan sodyum bor hidrürün hidrolizinde sadece katalizör etkin olarak rol almaktadır. Bu sayede katalizörün katalitik etkisi ölçülebilmekte karakteristik özellikleri yorumlanabilmektedir. Yüksek sıcaklılarda bile kararlı bir yapıya sahip olan sodyum borhidrür, yapısındaki hidrojenin katalizör varlığında hidroliz edilerek ayrılıyor olması, hidrolizde kullanılan katalizörün önemini arttırmaktadır.

Sodyum bor hidrürün hidrolizi sonucu elde edilen hidrojende katalizörler önemli rol oynamaktadır, Co-Cu-B katalizörü [3], Ru katalizörü[4] (Liu vd., 2008; Krishan vd., 2005), Co-B katalizörü [5], gibi katalizörler sodyum bor hidrürün hidrolizinde kullanılan katalizörlerdendir. Ancak bunlardan bazılarının pahalı olması sebebiyle bunların arasında en iyi katalitik aktiviteye ve düşük maliyete sahip olan Co-B katalizörleri daha çok dikkat çekmektedir. Bunun için bizim sentezleyeceğimiz katalizörlerin Co bazlı olması oldukça önem arz etmektedir. Bunun yanında bu katalizörleri sentezledikten sonra katalizörün aktifliğini arttırmak adına son yıllarda kullanılmaya başlanılan mikrodalga ve plazma sistemiyle de katalizörlerin katalitik etkisi artırılarak sodyum bor hidrür hidrolizinin gerçekleştirilmesi amaçlanmıştır .

2. MATERYAL VE YÖNTEM

Öncelikle indirgenmede kullanıma uygun bir erlen belirlenir. Bu erlene yukarıdaki kimyasallar eklenir. Ayrıca manyetik karıştırıcı katılarak 50 mL saf su eklenir. Oluşturulan karışım oda sıcaklığında 300 RPM de bir saat karıştırılır. Bir saatlik karıştırmanın sonunda karışımın sıcaklığı 4-5 ^oC olacak şekilde soğutulmak üzere, karışım buz banyosuna alınır. Bu esnada $NaBH_4$'ün %2.5'luk 50 mL çözeltisi hazırlanır. 5 ^oC' ye soğutulmuş karışıma %2.5'luk $NaBH_4$, ve %1 lik NaOH çözeltisi eşliğinde N_2 ortamında damlatılarak katalizör indirgenir. Katalizör sentezinin indirgenmesine ilişkin görsel Şekil 1'de verilmiştir. İndirgenmenin ardından karışım süzülür. Süzülen karışım alkolle yıkanarak su molekülleri ortamdan uzaklaştırılır. Daha sonra elde edilen katalizör etüvde yine N_2 ortamında 70 ^oC de 6-8 saat kurutulur.

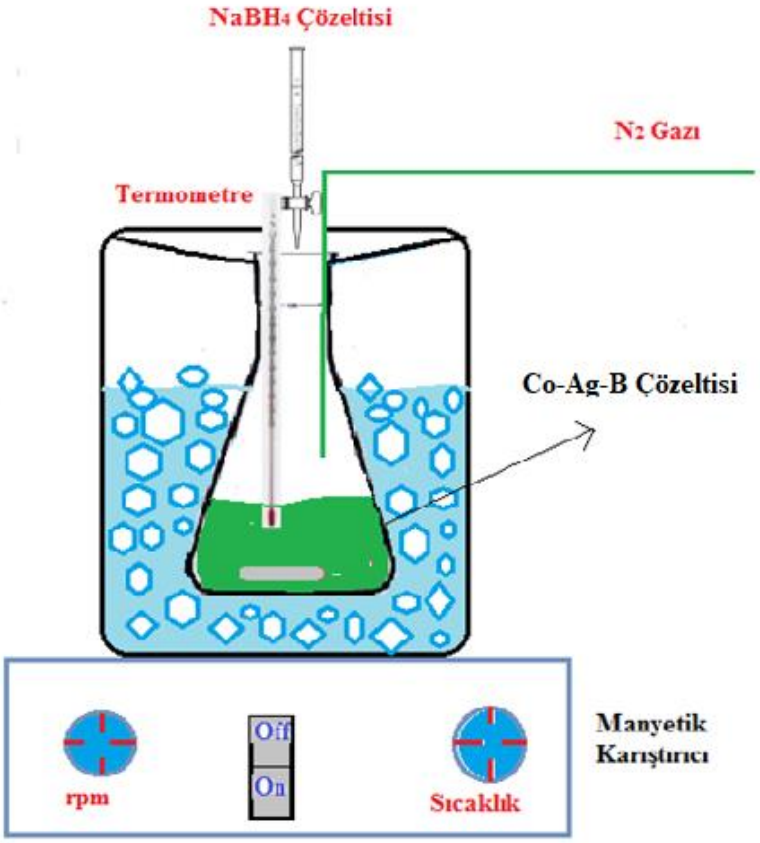

Şekil 1. Co-Ag-B, katalizörlerinin sentezlenmesinde kullanılan düzenek

Sodyum bor hidrürün katalizör varlığında, hidrolizine ilişkin deneysel çalışmalarda kullanılan sistem; bir gaz büreti, kapaklı bir erlen ve bir termostatlı çalkalayıcıdan meydana gelmektedir. Belirli bir miktar ve konsantrasyona sahip sodyum borhidrür çözeltisi kapaklı erlene konularak, daha önceden hazırlanmış olan katalizörler çalışma kapsamında belirlenen kütle oranlarında eklenerek hidroliz olayı gerçekleştirildi. Sentezlenen katalizörlerin miktarına, NaOH konsantrasyonu, farklı katalizör miktarı, farklı $NaBH_4$ Konsantrasyonu ve farklı sıcaklıklarda $NaBH_4$' ün hidroliziyle elde edilen hidrojen gazı, hazırlanan su tuzağı kullanılarak hidrojen gaz büretinde toplatıldı. Bürette toplanan hidrojen gazının hacim değerleri, belirli zamanlarda okunarak grafiksel olarak katalizörün etkinliği belirlendi. Elde edilen bu grafiklere göre tepkimelere ilişkin aktivasyon enerjisi, tepkime derecesi gibi reaksiyon kinetiğine ilişkin veriler oluşturuldu.

3. SONUÇLAR

Deneysel çalışmalarda belirtildiği şekilde sentezlenen Co-Ag-B katalizörünün sodyum bor hidrür hidrolizinde kullanmadan önce stabiliteyi sağlamak amacıyla sodyum hidroksit etkisinin ayrıca incelenmesi ve hidroliz için optimum şartların belirlenmesi için 30 ^oC'de %2.0 sodyum bor hidrür çözeltiye farklı konsantrasyonlarda sodyum hidroksit konularak çözündürülmüş ve buna

mütakiben 25 mg Co-Ag-B katalizörü ilave edilerek zamana bağlı olarak elde edilen hidrojen değişimleri Şekil 2'de verilmiştir. Şekil 2'de hidrojen üretim hızı grafiğinde açıkça görüleceği gibi % (1-7,5) NaOH varlığında hidrolizin 15 dakikada tamamlandığını ve %5 NaOH varlığında dönüşümün daha hızlı olduğu görülmektedir. Bu nedenle Ni-B katalizörü varlığında optimum NaOH konsantrasyonu bundan sonraki çalışmalarda %5 olarak alınacaktır.

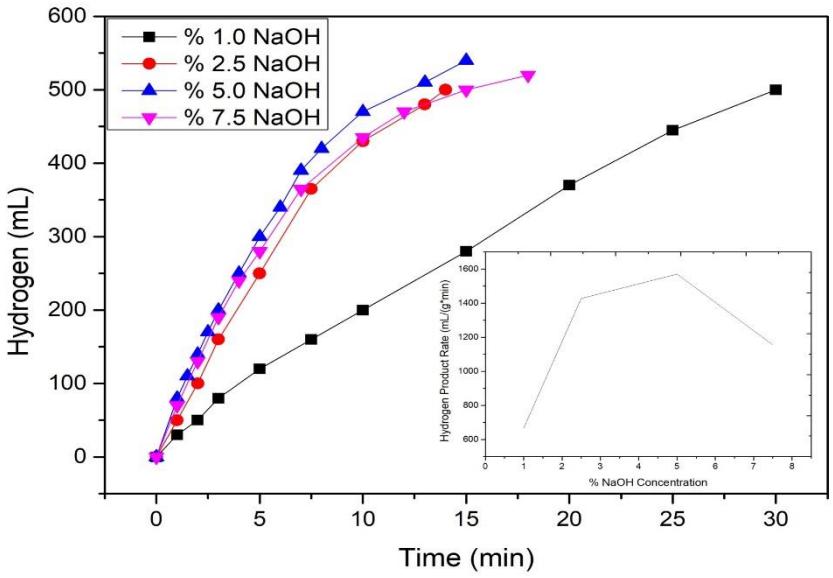

Şekil 2. Farklı NaOH konsantrasyonlardaki $NaBH_4$ hidrolizine etkisi (30 °C, %2 $NaBH_4$, 25 mg katalizör, 10 mL çözelti)

Hidrojen üretim hızını etkileyen önemli parametrelerden biriside optimum çözelti içindeki katalizör miktarının belirlenmesidir. Buna bağlı olarak farklı katalizör miktarlarının 30 °C'de %2 $NaBH_4$ içeren çözeltinin hidrolizinde kullanıldığında açığa çıkan H_2 hacimlerinin zamanla değişimi Şekil 3'te verilmiştir. Şekilde görüleceği gibi katalizör miktarı arttıkça hidroliz süresi kısalmakta 15 mg katalizör varlığında aynı şartlar altında hidroliz reaksiyonu 30 dakikada biterken 50 mg katalizör varlığında ise 8 dakikada bitmektedir.

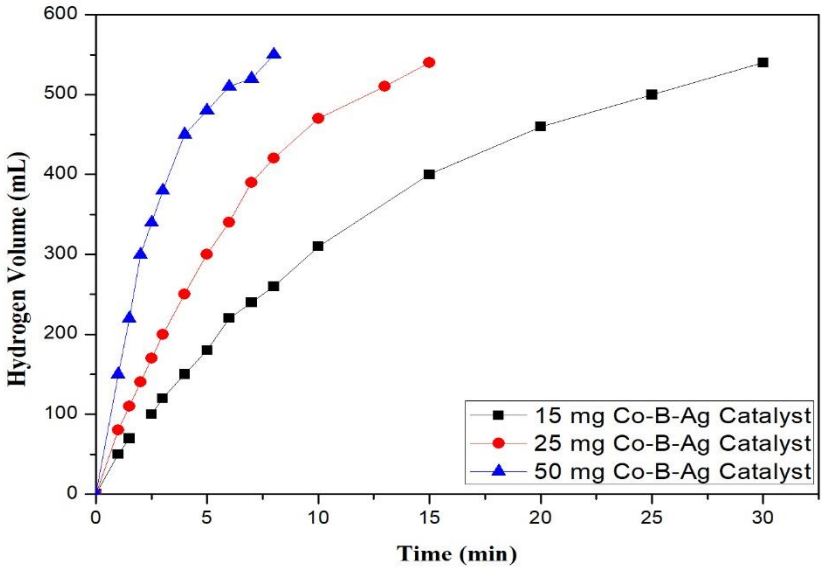

Şekil 3. Farklı katalizör miktarlarının $NaBH_4$ hidrolizine etkisi

Ancak burada 50 mg katalizör varlığında hidroliz süresini daha kısa sürede bitirmesine karşılık 25 mg katalizör varlığında hidrojen üretim hızının daha etkin olduğu görülmektedir.

Aynı şekilde $NaBH_4$ hidrolizinde diğer bir parametre ise sodyum borhidrürün konsantrasyonu olup, kullanılan $NaBH_4$ konsantrasyonu arttıkça aktivitesinin artması ya da aktivitesini koruması yakıt pilleri üretiminde kullanılacak hidrojen için önem arz etmektedir. Farklı $NaBH_4$ konsantrasyonları varlığında Co-Ag-B katalizörü varlığında gerçekleştirilen hidroliz reaksiyonunda elde edilen hidrojen hacimlerinin zamanla değişimi Şekil 4. te verilmiştir. Şekilden görüleceği üzere NaBH4'ün konsantrasyonu arttıkça hidrojen üretim hızının arttığı görülmektedir.

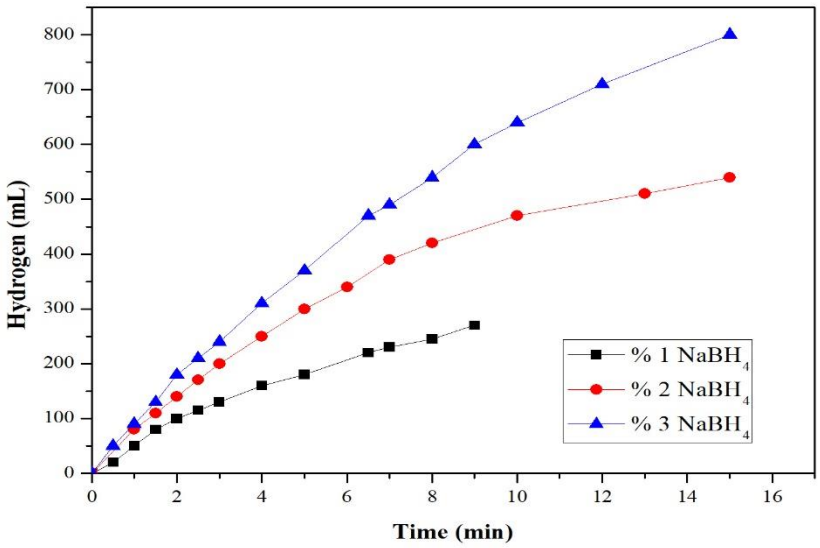

Şekil 4: Farklı $NaBH_4$ konsantrasyonlarının, $NaBH_4$ hidrolizine etkisi

Katalizör çalışmalarında diğer önemli parametre ise sıcaklık değişimi ile katalizörlerin katalitik etkilerinin ve dolayısıyla hidrojen üretim hızlarının değişiminin kinetiksel incelemesi olup Şekil 5'te farklı sıcaklıklard $NaBH_4$ hidrolizinden elde edilen H_2 hacimlerinin zamanla değişimi verilmiştir.

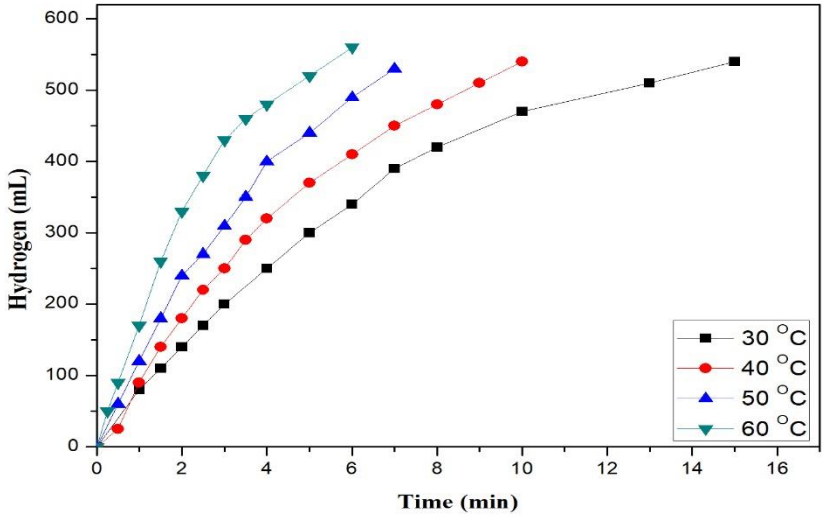

Şekil 5: Farklı sıcaklıkların, $NaBH_4$ hidrolizine etkisi

Şekilde de görüleceği gibi sıcaklığın artmasıyla birlikte hidrojen üretim hızları artmakta ve hidroliz reaksiyonu daha kısa sürede tamamlanmaktadır.

Sodyum bor hidrürün hidroliz eşitliğini ifade eden Eşitlik (1)'de geçen suyun konsantrasyonu değişimi ihmal edilerek Ni-B-Ag katalizörü varlığındaki hidrojen üretim değerlerinden yararlanılarak elde edilen değerlere karşı t grafiği çizildiğinde Şekil 5'te görüldüğü gibi tepkimenin 1. dereceden olduğu anlaşılmaktadır. Saf su ortamında sentezlenen Ni-B-Ag katalizörünün farklı sıcaklıklarda elde edilen hidrojen hacimlerinin zamanla değişimi değerlerinden yararlanılarak hız sabitlerinin, reaksiyon hız derecesinin ve aktivasyon enerjisini bulmak amacıyla 1. derecede reaksiyon hız eşitliği kullanılmıştır. 1. derecede kinetik eşitliği uygulanırken sodyum borhidrürün hidroliz eşitliğini, yukarıda gösterilen Eşitlik 1.de geçen suyun konsantrasyonu değişimi ihmal edilerek aşağıdaki şekilde yapılmıştır.

Bu çalışmada 1. derece kinetik modeli uygulanarak saf su ortamında sentezlenen Ni-B-Ag katalizörünün davranışının $NaBH_4$ hidrolizi üzerine etkisi integrasyon metodu uygulanarak reaksiyon derecesi belirlendi.

$$r_{NaBH4} = \frac{dC_{NaBH4}}{dt} = kC_{NaBH4} \qquad (2)$$

Eşitliği integre edilirse

$$\ln\left(\frac{C_{NaBH4\ (t=0)}}{C_{NaBH4\ (t=t)}}\right) = kt \qquad (3)$$

Şeklinde integral hız denklemi elde edilir. Buradan 30 ºC, 40 ºC, 50 ºC ve 60 ºC'ye ait kinetik değerlendirme yapılmıştır. Eşitlik 3'e göre t'ye karşı ln $\frac{C_{NaBH4\ (t=0)}}{C_{NaBH4\ (t=t)}}$ grafiğe çizilirse Şekil 6 grafiği elde edilir. Şekil 6'da görüldüğü gibi farklı sıcaklıklarda elde edilen konsantrasyon zaman değişimlerinin doğrusal olduğu görülmektedir. Bu da bize bulduğumuz 1. derece değerlerinin ve reaksiyon hız sabitlerinin ne kadar uygun olduğunu göstermektedir.

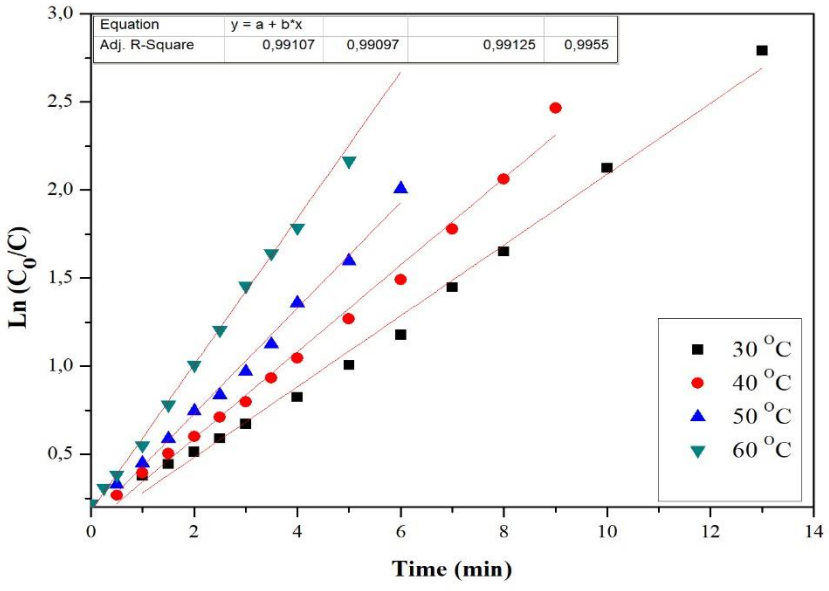

Şekil 6. Co-B-Ag katalizörünün farklı sıcaklıklardaki 1. dereceye dayalı reaksiyon kinetiği

Farklı sıcaklıklarda elde edilen reaksiyon hız sabitleri kullanılarak hidroliz reaksiyonuna ait aktivasyon enerjisini bulmak amacıyla yukarıda verilen Eşitlikleri kullanarak Arhenius eşitliği belirlenmiştir.

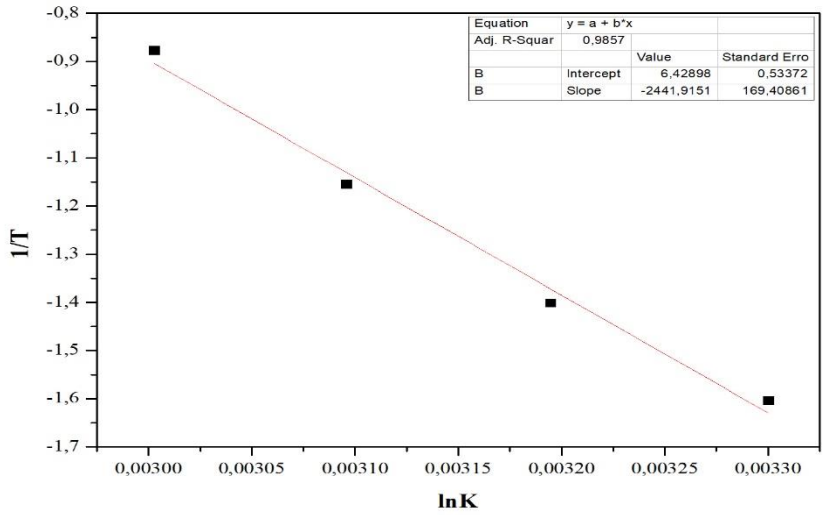

Şekil 7. Etanollü ortamda sentezlenen Ni-B katalizörünün n. dereceye göre Arhenius eşitliği

Eşitlik 2'ye göre lnk değerlerine karşın 1/T grafiği çizildiğinde Şekil 7'de elde edilen doğrunun eğiminden aktivasyon enerjisi bulunur. Kayımında ise Arhenius sabiti olan (A) bulunur. Elde edilen doğru denklemi Şekil 7'de verilmiş olup bu değerlere göre aktivasyon enerjisi 20,301 kJ/mol olarak belirlenmiştir.

KAYNAKLAR

[1] Bakır G, 2013. Füzyon-Fisyon Hibrid Reaktöründe Nükleer Hidrojen Üretimi. Yüksek Lisans Tezi, Erciyes Üniversitesi Fen Bilimleri Enstitüsü, Kayseri.

[2] İnger E, Tırıs M, Özdemir Z, Yaşar İ, Bahar T, San FG, 2007. Sodyum borhidrür üretimi ve doğrudan sodyum borhidrürlü yakıt pili üretimi ve entegrasyonu, Ulusal Bor Araştırma Enstitüsü & TÜBİTAK Marmara Araştırma Merkezi Enerji Enstitüsü Raporu, s: 17-21.

[3] İzgi MS, Şahin Ö, Saka C, 2016. Hydrogen production from $NaBH_4$ using Co–Cu–B catalysts prepared in methanol: Effect of plasma treatment. International Journal of Hydrogen Energy, 41: 1600-1608.

[4] Amendola SC, Sharp-Goldman SL, Janjua MS, Kelly MT, Petillo PJ, Binder M, 2000b. An Ultrasafe hydrogen generator: aquous, alkaline borohydride solutions and Ru catalyst. Journal of Power Sources, 85: 186–189.

[5] Jeong SU, Cho EA, Nam SW, Oh IH, Jung UH, Kim SH, 2007. Effect of preparation method on Co-B catalytic activity for hydrogen generation from alkali $NaBH_4$. International Journal of Hydrogen Energy, 32: 1749-1754.

ICACChE
2nd International Conference on Applications in Chemistry and Chemical Engineering
10 - 14 October 2018 Belgrade

Hydrogen Production from Hydrolysis of Sodium Borohydride in the Presence of Ni-B-Ag Catalyst

Mehmet Sait İzgi[1], Ömer Şahin

Abstract

One of the chemical compounds with high energy density, which removes the problem of the storage of hydrogen from the clean energy sources, is sodium borohydride. The basic parameter that determines the hydrolysis of sodium borohydride, hydrogen production efficiency and reaction course is the catalyst. Energy sources are undoubtedly one of the greatest challenges facing humanity due to increasing concerns over a series of worldwide energy and environmental problems. In the past decades, research around nano scale interface technologies related to photovoltaic, batteries and fuel cells has brought fascinating breakthroughs in energy conversion and storage. In particular, hydrogen has become one of the most promising future energy resources due to concerns about global warming and the depletion of fossil fuels. Metal hydrides like sodium borohydride ($NaBH_4$) have attracted much attention worldwide as a source of high purity hydrogen for portable and stationary applications.

In this study, Co-B-Ag catalyst was studied for hydrogen generation from the hydrolysis of the sodium borohydride solution. Then, the optimal metal ratio, the amount of catalyst, the concentration of different, and the catalytic activity at different temperatures were examined for sodium borohydride hydrolysis. The kinetic model of first order and according to the values obtained the activation energy was determined as 20.301 kJ/mol.

Keywords: Sodium Borohydride, Co-B-Ag, Catalyst, Hydrogen Energy

1. GİRİŞ

Hayatımızda önemli bir yeri olan enerji gelişmiş ülkelerde olduğu gibi gelişmekte olan ülkelerin de en önemli ihtiyacı haline gelmiş, bununla birlikte enerji üretimi ve tüketimi ülkelerin gelişmişlik düzeylerini belirleyen bir ölçüt olarak ortaya çıkmıştır. Dünya nüfusu artışı ve teknolojik gelişmelere paralel olarak enerji ihtiyacı hızlı bir şekilde artmaktadır. Mevcut enerji sistemi, başta fosil kaynaklı yakıtlar olmak üzere tükenebilir özellikteki kaynaklardan sağlanmaktadır. Bu kaynakların tükenir olması ve çevre üzerindeki olumsuz etkileri ülkelerin; ucuz, çevreyle dost ve yenilenebilir özellikteki enerji kaynaklarına olan ihtiyaçlarını günden güne arttırmaktadır.

[1]*Corresponding author: Siirt University, Faculty of Engineering, Department of Chemical Engineering, saitizgi@hotmail.com*

Hidrojen teknolojisi de; enerji taşıyıcı sistemlerin yerini alabilecek; yenilenebilir bir enerji kaynağı olarak geleceğin enerji sistemleri için potansiyel teşkil etmektedir. Hidrojeni yenilenebilir kaynaklardan üretmek ve yüksek verimli yakıt hücrelerinde veya motorlarda kullanmak, küresel ısınmayı ve çevre kirliliğini önemli ölçüde azaltacaktır. İçten yanmalı motor teknolojisi veya türbin teknolojisinin yanı sıra çok daha verimli yakıt hücreleri de hidrojenden güç elde etmek için kullanılır. Şimdiden yakıt hücresi teknolojisi verimi %65 gibi büyük oranlara sahiptir [1]. Hidrojenin kullanılmaya başlanmasıyla birlikte kimyasal enerjinin elektrik enerjisine direkt çevirilmesi, yakıt hücrelerinin geliştirilmesini netice vermiştir. Zaman içerisinde, hidrojenin depolama ve üretim proseslerinin de geliştirilmeye başlanmıştır.

$NaBH_4$, en dengeli alkali metal bor hidrürlerden biri olup, nemli havada çok yavaş reaksiyon verirken kuru havada kararlı bir yapı göstermektedir. Suyla reaksiyonu ile yapısındaki hidrojen serbest kalmaktadır. Suyun sıcaklığı, oda sıcaklığında veya altında ise hidrojenin serbest kalması yavaştır [2]. $NaBH_4$'ün sudaki kararlılığı sıcaklığa ve pH'a bağlı olarak değişir. Sıcaklığın artması ve pH'ın azalması aşağıda verilen Eşitlik 1'e göre hidroliz reaksiyonunu hızlandırmaktadır.

$$NaBH_4 + 2\,H_2O \rightarrow NaBO_2 + 4\,H_2 \qquad (1)$$

$NaBH_4$ 12-13 pH aralığındaki depolama koşullarında bozunma gözlenmez. Belirtilen pH aralıklarında sodyum bor hidrür kararlıdır. Kararlı olan sodyum bor hidrürün hidrolizinde sadece katalizör etkin olarak rol almaktadır. Bu sayede katalizörün katalitik etkisi ölçülebilmekte karakteristik özellikleri yorumlanabilmektedir. Yüksek sıcaklılarda bile kararlı bir yapıya sahip olan sodyum borhidrür, yapısındaki hidrojenin katalizör varlığında hidroliz edilerek ayrılıyor olması, hidrolizde kullanılan katalizörün önemini arttırmaktadır.

Sodyum bor hidrürün hidrolizi sonucu elde edilen hidrojende katalizörler önemli rol oynamaktadır, Co-Cu-B katalizörü [3], Ru katalizörü[4] (Liu vd., 2008; Krishan vd., 2005), Co-B katalizörü [5], gibi katalizörler sodyum bor hidrürün hidrolizinde kullanılan katalizörlerdendir. Ancak bunlardan bazılarının pahalı olması sebebiyle bunların arasında en iyi katalitik aktiviteye ve düşük maliyete sahip olan Co-B katalizörleri daha çok dikkat çekmektedir. Bunun için bizim sentezleyeceğimiz katalizörlerin Co bazlı olması oldukça önem arz etmektedir. Bunun yanında bu katalizörleri sentezledikten sonra katalizörün aktifliğini arttırmak adına son yıllarda kullanılmaya başlanılan mikrodalga ve plazma sistemiyle de katalizörlerin katalitik etkisi artırılarak sodyum bor hidrür hidrolizinin gerçekleştirilmesi amaçlanmıştır .

2. MATERYAL VE YÖNTEM

Öncelikle indirgenmede kullanıma uygun bir erlen belirlenir. Bu erlene yukarıdaki kimyasallar eklenir. Ayrıca manyetik karıştırıcı katılarak 50 mL saf su eklenir. Oluşturulan karışım oda sıcaklığında 300 RPM de bir saat karıştırılır. Bir saatlik karıştırmanın sonunda karışımın sıcaklığı 4-5 ^oC olacak şekilde soğutulmak üzere, karışım buz banyosuna alınır. Bu esnada $NaBH_4$'ün %2.5'luk 50 mL çözeltisi hazırlanır. 5 ^oC' ye soğutulmuş karışıma %2.5'luk $NaBH_4$, ve %1 lik

NaOH çözeltisi eşliğinde N_2 ortamında damlatılarak katalizör indirgenir. Katalizör sentezinin indirgenmesine ilişkin görsel Şekil 1'de verilmiştir. İndirgenmenin ardından karışım süzülür. Süzülen karışım alkolle yıkanarak su molekülleri ortamdan uzaklaştırılır. Daha sonra elde edilen katalizör etüvde yine N_2 ortamında 70 ^oC de 6-8 saat kurutulur.

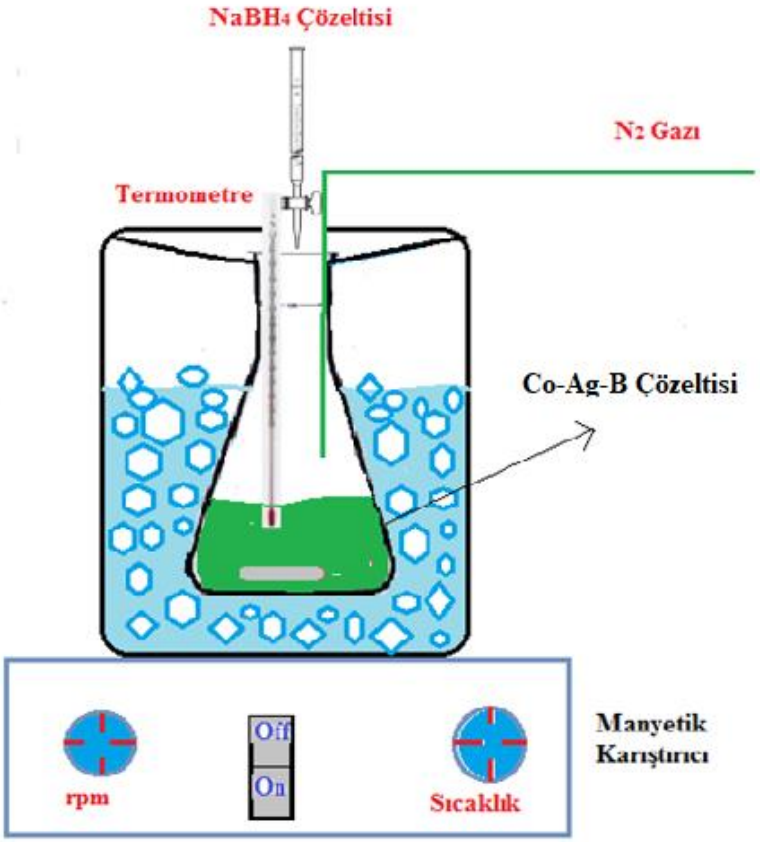

Şekil 1. Co-Ag-B, katalizörlerinin sentezlenmesinde kullanılan düzenek

Sodyum bor hidrürün katalizör varlığında, hidrolizine ilişkin deneysel çalışmalarda kullanılan sistem; bir gaz büreti, kapaklı bir erlen ve bir termostatlı çalkalayıcıdan meydana gelmektedir. Belirli bir miktar ve konsantrasyona sahip sodyum borhidrür çözeltisi kapaklı erlene konularak, daha önceden hazırlanmış olan katalizörler çalışma kapsamında belirlenen kütle oranlarında eklenerek hidroliz olayı gerçekleştirildi. Sentezlenen katalizörlerin miktarına, NaOH konsantrasyonu, farklı katalizör miktarı, farklı $NaBH_4$ Konsantrasyonu ve farklı sıcaklıklarda $NaBH_4$' ün hidroliziyle elde edilen hidrojen gazı, hazırlanan su tuzağı kullanılarak hidrojen gaz büretinde toplatıldı. Bürette toplanan hidrojen gazının hacim değerleri, belirli zamanlarda okunarak grafiksel olarak katalizörün etkinliği belirlendi. Elde edilen bu grafiklere göre tepkimelere ilişkin aktivasyon enerjisi, tepkime derecesi gibi reaksiyon kinetiğine ilişkin veriler oluşturuldu.

SONUÇLAR

Deneysel çalışmalarda belirtildiği şekilde sentezlenen Co-Ag-B katalizörünün sodyum bor hidrür hidrolizinde kullanmadan önce stabiliteyi sağlamak amacıyla sodyum hidroksit etkisinin ayrıca incelenmesi ve hidroliz için optimum şartların belirlenmesi için 30 ºC'de %2.0 sodyum bor hidrür çözeltiye farklı konsantrasyonlarda sodyum hidroksit konularak çözündürülmüş ve buna mütakiben 25 mg Co-Ag-B katalizörü ilave edilerek zamana bağlı olarak elde edilen hidrojen değişimleri Şekil 2'de verilmiştir. Şekil 2'de hidrojen üretim hızı grafiğinde açıkça görüleceği gibi % (1-7,5) NaOH varlığında hidrolizin 15 dakikada tamamlandığını ve %5 NaOH varlığında dönüşümün daha hızlı olduğu görülmektedir. Bu nedenle Ni-B katalizörü varlığında optimum NaOH konsantrasyonu bundan sonraki çalışmalarda %5 olarak alınacaktır.

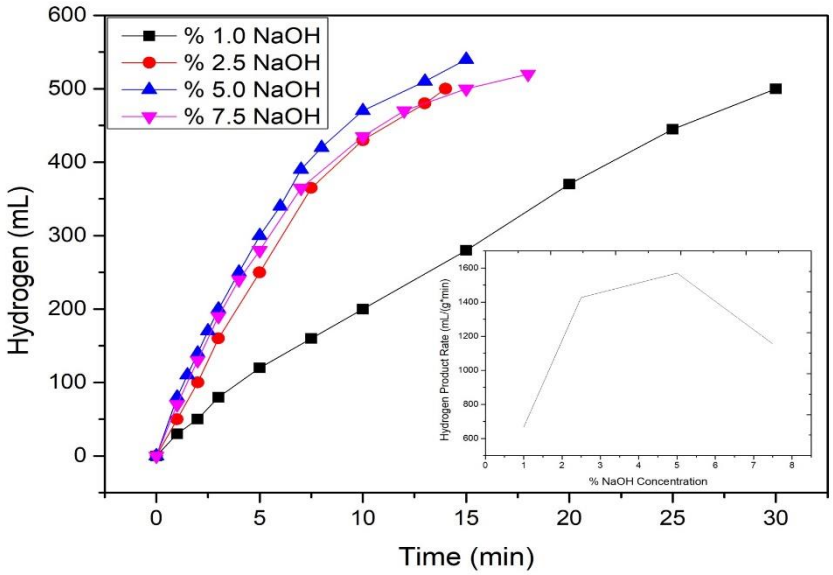

Şekil 2. Farklı NaOH konsantrasyonlardaki $NaBH_4$ hidrolizine etkisi (30 ºC, %2 $NaBH_4$, 25 mg katalizör, 10 mL çözelti)

Hidrojen üretim hızını etkileyen önemli parametrelerden biriside optimum çözelti içindeki katalizör miktarının belirlenmesidir. Buna bağlı olarak farklı katalizör miktarlarının 30 ºC'de %2 $NaBH_4$ içeren çözeltinin hidrolizinde kullanıldığında açığa çıkan H_2 hacimlerinin zamanla değişimi Şekil 3'te verilmiştir. Şekilde görüleceği gibi katalizör miktarı arttıkça hidroliz süresi kısalmakta 15 mg katalizör varlığında aynı şartlar altında hidroliz reaksiyonu 30 dakikada biterken 50 mg katalizör varlığında ise 8 dakikada bitmektedir.

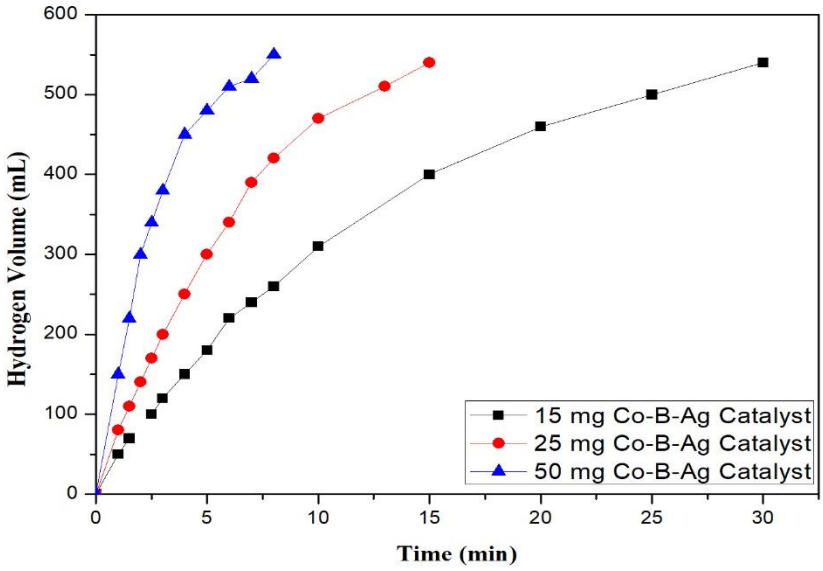

Şekil 3. Farklı katalizör miktarlarının $NaBH_4$ hidrolizine etkisi

Ancak burada 50 mg katalizör varlığında hidroliz süresini daha kısa sürede bitirmesine karşılık 25 mg katalizör varlığında hidrojen üretim hızının daha etkin olduğu görülmektedir.

Aynı şekilde $NaBH_4$ hidrolizinde diğer bir parametre ise sodyum borhidrürün konsantrasyonu olup, kullanılan $NaBH_4$ konsantrasyonu arttıkça aktivitesinin artması ya da aktivitesini koruması yakıt pilleri üretiminde kullanılacak hidrojen için önem arz etmektedir. Farklı $NaBH_4$ konsantrasyonları varlığında Co-Ag-B katalizörü varlığında gerçekleştirilen hidroliz reaksiyonunda elde edilen hidrojen hacimlerinin zamanla değişimi Şekil 4. te verilmiştir. Şekilden görüleceği üzere NaBH4'ün konsantrasyonu arttıkça hidrojen üretim hızının arttığı görülmektedir.

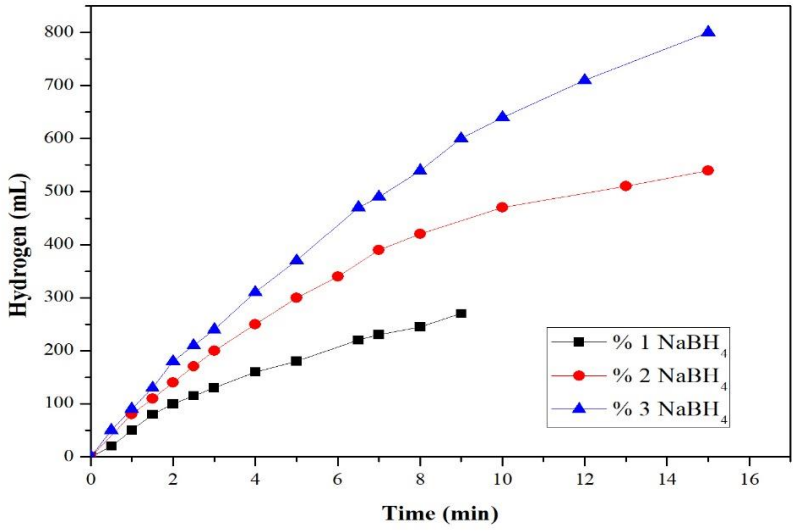

Şekil 4: Farklı $NaBH_4$ konsantrasyonlarının, $NaBH_4$ hidrolizine etkisi

Katalizör çalışmalarında diğer önemli parametre ise sıcaklık değişimi ile katalizörlerin katalitik etkilerinin ve dolayısıyla hidrojen üretim hızlarının değişiminin kinetiksel incelemesi olup Şekil 5'te farklı sıcaklıklard $NaBH_4$ hidrolizinden elde edilen H_2 hacimlerinin zamanla değişimi verilmiştir.

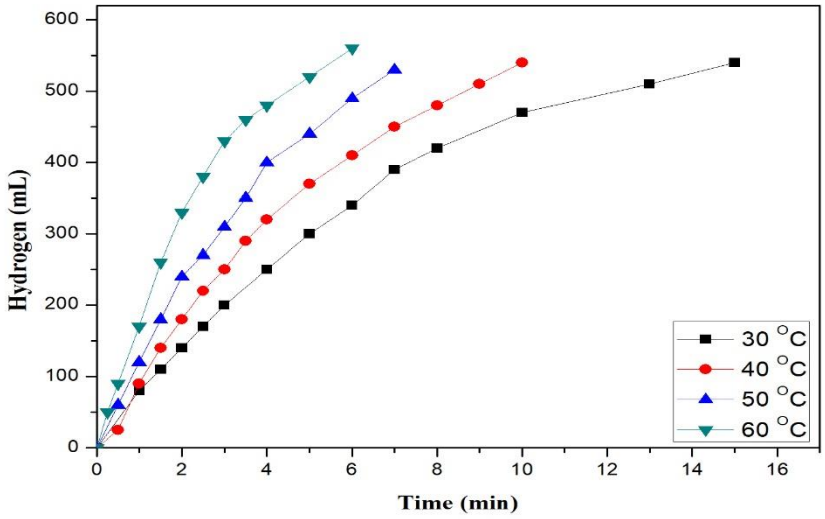

Şekil 5: Farklı sıcaklıkların, $NaBH_4$ hidrolizine etkisi

Şekilde de görüleceği gibi sıcaklığın artmasıyla birlikte hidrojen üretim hızları artmakta ve hidroliz reaksiyonu daha kısa sürede tamamlanmaktadır.

Sodyum bor hidrürün hidroliz eşitliğini ifade eden Eşitlik (1)'de geçen suyun konsantrasyonu değişimi ihmal edilerek Ni-B-Ag katalizörü varlığındaki hidrojen üretim değerlerinden yararlanılarak elde edilen değerlere karşı t grafiği çizildiğinde Şekil 5'te görüldüğü gibi tepkimenin 1. dereceden olduğu anlaşılmaktadır. Saf su ortamında sentezlenen Ni-B-Ag katalizörünün farklı sıcaklıklarda elde edilen hidrojen hacimlerinin zamanla değişimi değerlerinden yararlanılarak hız sabitlerinin, reaksiyon hız derecesinin ve aktivasyon enerjisini bulmak amacıyla 1. derecede reaksiyon hız eşitliği kullanılmıştır. 1. derecede kinetik eşitliği uygulanırken sodyum borhidrürün hidroliz eşitliğini, yukarıda gösterilen Eşitlik 1.de geçen suyun konsantrasyonu değişimi ihmal edilerek aşağıdaki şekilde yapılmıştır.

Bu çalışmada 1. derece kinetik modeli uygulanarak saf su ortamında sentezlenen Ni-B-Ag katalizörünün davranışının $NaBH_4$ hidrolizi üzerine etkisi integrasyon metodu uygulanarak reaksiyon derecesi belirlendi.

$$r_{NaBH4} = \frac{dC_{NaBH4}}{dt} = kC_{NaBH4} \qquad (2)$$

Eşitliği integre edilirse

$$\ln\left(\frac{C_{NaBH4\ (t=0)}}{C_{NaBH4\ (t=t)}}\right) = kt \qquad (3)$$

Şeklinde integral hız denklemi elde edilir. Buradan 30 ºC, 40 ºC, 50 ºC ve 60 ºC'ye ait kinetik değerlendirme yapılmıştır. Eşitlik 3'e göre t'ye karşı ln $\frac{C_{NaBH4\ (t=0)}}{C_{NaBH4\ (t=t)}}$ grafiğe çizilirse Şekil 6 grafiği elde edilir. Şekil 6'da görüldüğü gibi farklı sıcaklıklarda elde edilen konsantrasyon zaman değişimlerinin doğrusal olduğu görülmektedir. Bu da bize bulduğumuz 1. derece değerlerinin ve reaksiyon hız sabitlerinin ne kadar uygun olduğunu göstermektedir.

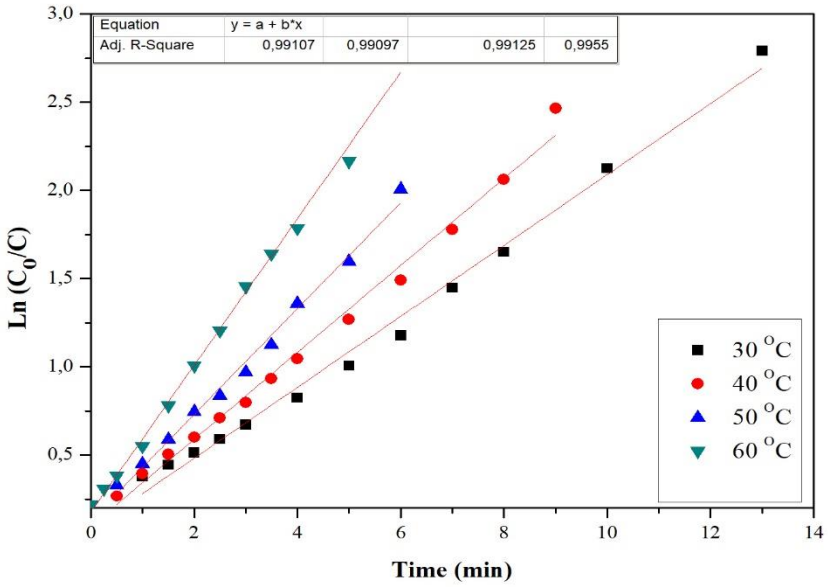

Şekil 6. Co-B-Ag katalizörünün farklı sıcaklıklardaki 1. dereceye dayalı reaksiyon kinetiği

Farklı sıcaklıklarda elde edilen reaksiyon hız sabitleri kullanılarak hidroliz reaksiyonuna ait aktivasyon enerjisini bulmak amacıyla yukarıda verilen Eşitlikleri kullanarak Arhenius eşitliği belirlenmiştir.

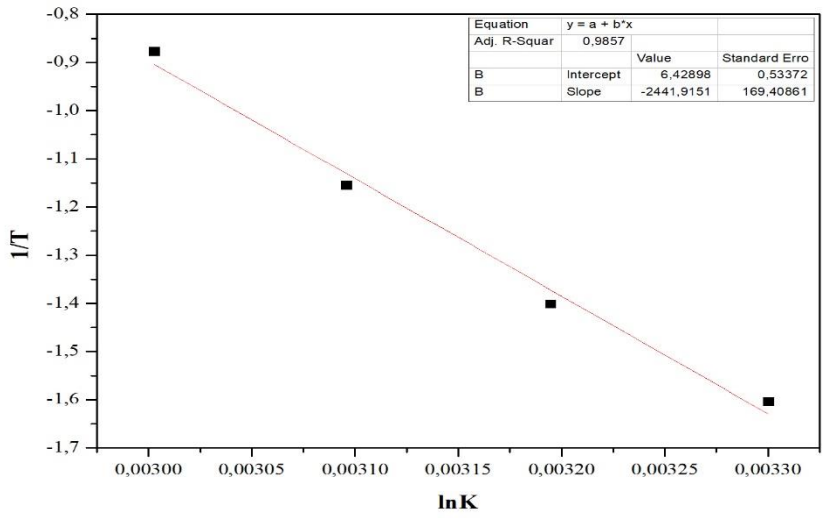

Şekil 7. Etanollü ortamda sentezlenen Ni-B katalizörünün n. dereceye göre Arhenius eşitliği

Eşitlik 2'ye göre lnk değerlerine karşın 1/T grafiği çizildiğinde Şekil 7'de elde edilen doğrunun eğiminden aktivasyon enerjisi bulunur. Kayımında ise Arhenius sabiti olan (A) bulunur. Elde edilen doğru denklemi Şekil 7'de verilmiş olup bu değerlere göre aktivasyon enerjisi 20,301 kJ/mol olarak belirlenmiştir.

KAYNAKLAR

[1] Bakır G, 2013. Füzyon-Fisyon Hibrid Reaktöründe Nükleer Hidrojen Üretimi. Yüksek Lisans Tezi, Erciyes Üniversitesi Fen Bilimleri Enstitüsü, Kayseri.

[2] İnger E, Tırıs M, Özdemir Z, Yaşar İ, Bahar T, San FG, 2007. Sodyum borhidrür üretimi ve doğrudan sodyum borhidrürlü yakıt pili üretimi ve entegrasyonu, Ulusal Bor Araştırma Enstitüsü & TÜBİTAK Marmara Araştırma Merkezi Enerji Enstitüsü Raporu, s: 17-21.

[3] İzgi MS, Şahin Ö, Saka C, 2016. Hydrogen production from $NaBH_4$ using Co–Cu–B catalysts prepared in methanol: Effect of plasma treatment. International Journal of Hydrogen Energy, 41: 1600-1608.

[4] Amendola SC, Sharp-Goldman SL, Janjua MS, Kelly MT, Petillo PJ, Binder M, 2000b. An Ultrasafe hydrogen generator: aquous, alkaline borohydride solutions and Ru catalyst. Journal of Power Sources, 85: 186–189.

[5] Jeong SU, Cho EA, Nam SW, Oh IH, Jung UH, Kim SH, 2007. Effect of preparation method on Co-B catalytic activity for hydrogen generation from alkali $NaBH_4$. International Journal of Hydrogen Energy, 32: 1749-1754.

ICACChE
2nd International Conference on Applications in Chemistry and Chemical Engineering
10 - 14 October 2018 Belgrade

Effect of Microwave Irritated Ni-B-P Catalyst on the Hydrolysis of Potassium Borohydride

M. Salih Keskin[1], M. Salih Ağırtaş, Ömer Şahin, Mehmet Sait İZGİ

Abstract

Hydrogen can be produced using a wide variety of techniques without the emission of pollutants and greenhouse gases, and as technology improves, production costs are targeted to reach levels comparable to other sources. Nowadays, hydrogen is produced by catalytic conversion from natural gas or hydrolysis of water. However, these methods are not fast enough and flexible for portable PEM fuel cells. This work, Ni-B-P catalysts were synthesized from $Ni(NO_3)_2.\ 9H_2O$ and $NaHPO_4$ compounds by using KBH_4 as chemical reducing agent at temperature range of 3–8°C. The microwave irradiation method utilized depends on different gas medium (N_2, Ar, CO_2), microwave power (0–1,000 W), and microwave applying time (0–20 min) to increase the catalytic activity of Ni-B-P catalysis used in the hydrolysis of KBH_4. It was found that the Ni-B-P catalyst with best catalytic activity for KBH_4 hydrolysis was produced under microwave conditions of N_2 gases for 10 min treatment time and 300 W applying power. Hydrolysis of KBH_4 is completed in 15 min by using Ni-B-P catalysis treatment optimum irradiation microwave conditions and it is completed in 18 min in the case of non-microwave treatment of Ni- B-P.

Keywords: Hydrolysis, KBH_4, Catalyst, Microwave

1. GİRİŞ

Hidrojen enerjisi enerji bakımından öneme sahip, doğada en çok bulunan elementtir, renksiz, kokusuz, zehirsiz gaz halinde bir elementtir. Bir proton ve bir elektrondan oluşan hidrojen periyodik cetvelde en üstte yer almakta ve doğada genellikle iki atomlu(H_2) halde bulunmaktadır. Doğada bol miktarda bulunan, yüksek verime sahip ve çevre dostu bir enerji taşıyıcıdır. Yanması ile çok yüksek verim elde edilir ve yanması sonucunda çevreye sadece su buharı salınır. Molekül ağırlığı 1,008 olup, bilinen en hafif elementtir [1]. Bununla birlikte, Hidrojen diğer yeni enerji kaynaklarından daha avantajlı olması nedeniyle geleceğe yönelik yeni bir enerji kaynağı olarak ümit vermektedir. Borhidrürler ($NaBH_4$, KBH_4) geleceğin enerjisi olarak düşünülen hidrojenin üretimi ve depolanması için kullanılan, birçok açıdan avantajları olan bir maddedir. Ancak potasyum bor hidrürle alakalı çok az çalışma mevcuttur [2]. KBH_4'den hidrojen eldesi sadece seçilen katalizörler varlığında kontrollü bir şekilde gerçekleşir ve reaksiyon ürünleri çevreye zararlı değildir.

[1]*Corresponding author: Siirt University, Faculty of Education,*
[2]*Yüzüncü Yıl University, Science of Faculty, Department of Chemical*
[3]*Siirt University, Faculty of Engineering, Department of Chemical Engineering*

Fakat potasyum bor hidrür sodyum bor hidrüre nazaran hidroskobik özelliği daha iyi ve hidroliz için gerekli olan ısı daha az olacağı için reaktör dizaynında önemli bir yere sahiptir [3]. Aynı zamanda potasyum bor hidrürün katalizör varlığındaki davranışı hala tam olarak bilinmemektedir. KBH_4'ün su içerisindeki çözünürlüğü yüksektir, ancak sulu çözeltilerde oldukça hızlı bir şekilde bozunur. Ortamın pH'ı arttıkça bozunma hızı azalmakta ve sıcaklık arttıkça da bozunma hızı artmaktadır [4].

$$KBH_4 + 2\,H_2O \rightarrow 4\,H_2 + NaBO_2 + Q\ (300\ kj) \qquad (1.1)$$

Reaksiyonuna göre hidroliz olmakta ve reaksiyon kinetiksel olarak sıfırıncı dereceden olduğu için hidrojen üretim hızı katalizör tarafında kontrol edilmektedir. Genellikle Pt [5], Ru [4]), Rh gibi pahalı katalizörler borhidrülerin hidrolizinde kullanılmaktadır. Ancak son zamanlarda ikili ve üçlü ucuz metal katalizörler kulanılarak sodyum bor hidrürün hidrolizinde kullanılmışlardır. Bunlar Co-B, Ni-B, Co-B-P, Co-B-Cr, Co-Cu-B, Co-Ni-B, Co-Mo-B, Co-W-B gibi katalizörler kullanılmaktadır. Ancak potasyum borhidrür ile alakalı pek fazla çalışmaya rastlanılmadığından dolayı; bu çalışma potasyum borhidrürün hidrolizi için özgün bir çalışma olacaktır. Dahası temiz bir teknoloji olan yakıt pilleri için de ön plana çıkmaktadır. Bor hidrürlerin çoğu su ile çok hızlı reaksiyona girmektedir. Diğer hidrürlerle kıyaslandığında KBH_4'den hidrojen gazı üretiminin bazı avantajları vardır. KBH_4 çözeltileri yanıcı değildir bu nedenle reaksiyonlar daha güvenli ve verimlidir ayrıca çözeltiler aylarca kararlılığını koruyarak bozunmadan saklanabilir. H_2 oluşumu sadece seçilen katalizörün varlığında gerçekleşir ve oluşum hızları kolayca kontrol edilebilir. Hacimsel ve gravimetrik H_2 depolama verimi yüksektir ve en önemlisi reaksiyon ürünleri geri dönüştürülebilir.

Kuvvetli indirgenme özelliğine sahip bir bor bileşiği olan potasyum borhidrür bir katalizör varlığında su ile tepkimeye girerek hidrojen gazı üretme özelliğine sahiptir. Potasyum bor hidrürde hidrojen depolamanın en önemli üstünlüğü depolanan hidrojenin oda sıcaklığında geri alınabilmesi ve geri alımı katalizör yardımı ile kolaylıkla kontrol edilebilmesidir. Potasyum bor hidrür ün hidrojen amaçlı kullanımında en önemli sorun, oluşan metaboratın tekrar KBH_4 e dönüştürülmesidir. Hidrojen depolamada sodyum bor hidrür kullanmanın diğer bir avantajı, hidrojenin patlayıcılık riskinin azaltılmasıdır. Potasyum bor hidrür, belli koşullarda yanmayan, ancak istendiğinde hidrojeni açığa çıkartan bir özelliğe sahiptir.

2. MATERYAL VE YÖNTEM

Deneysel çalışmalarda kullanılan sistemin açık şeması Şekil 1' de verilmiştir. Sistem, kapaklı bir erlen, bir gaz büreti ve bir adet termostatlı çalkalayıcıdan oluşmaktadır. Kapaklı erlene konan belirli miktar ve konsantrasyona sahip sodyum bor hidrür çözeltisine, daha önceden hazırlanmış olan katalizörler eklenerek hidroliz olayı gerçekleştirildi. Potasyum borhidrür hidrolizine katalizör miktarı, potasyum hidroksit konsantrasyonu, mikrodalga ortamında farklı gazların etkisi, farklı

sürelerin etkisi ve farklı güçlerin etkileri ayrıı ayrı incelendi ve bu parametreler uygulanırken açığa çıkan hidrojen gazı su tuzağı kullanılarak gaz büretinde toplatıldı. Reaksiyonun yürüyüşü su dolu büretteki suyun hidrojen gazıyla yer değiştirmesi sonucunda hacim değerleri zamanla okunarak, takip edildi.

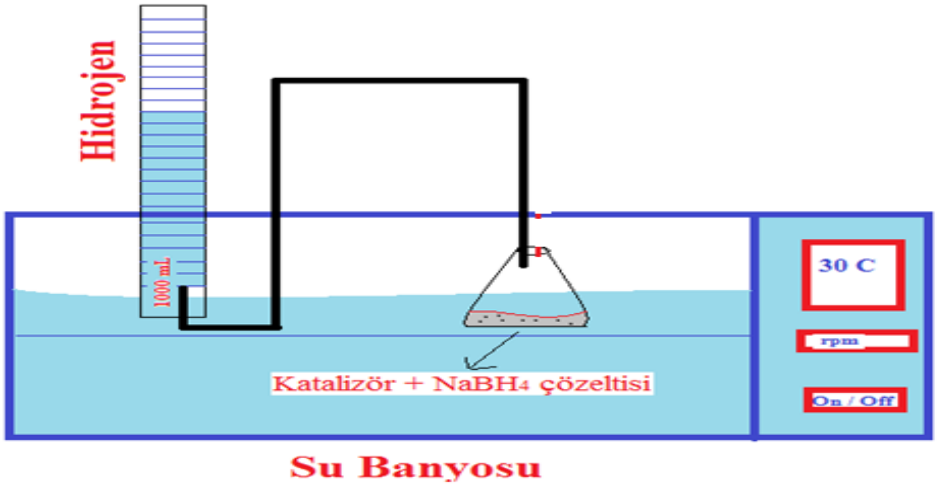

Şekil 1. Deney sisteminin açık şeması

3. SONUÇLAR

Bu çalışma kapsamında saf su ortamında Ni-B-P katalizörü sentezlendi. Bu katalizörümüzün potasyum borhidrür hidrolizle hidrojen üretimine yönelik sırasıyla; KOH etkisi, farklı katalizör miktarlarının etkisi farklı sıcaklık etkisi gibi özelliklerin değişimi, her seferinde sabit tutulan değerlere karşılık bir değişken değiştirilerek katalizörün davranışları, etkinliği ve buna bağlı olarakta kinetiği çıkarılarak reaksiyon derecesi ve aktivasyon enerjisi hesaplanmıştır..

Öncelikle farklı KOH başlangıç konsantrasyonlarında (%0-10) sodyum bor hidrürün hidrolizi incelendiğinde, % 2,5 KOH konsantrasyonuyla yapılan hidrolizde tepkimenin daha erken sonuçlandığı tespit edilmiştir. Ni-B-P katalizörü ile yapılacak bundan sonraki hidroliz çalışmalarında sodyum borhidrür çözeltisinin başlangıç KOH konsantrasyonu % 2.5 olacak şekilde ölçümlere devam edilecektir.

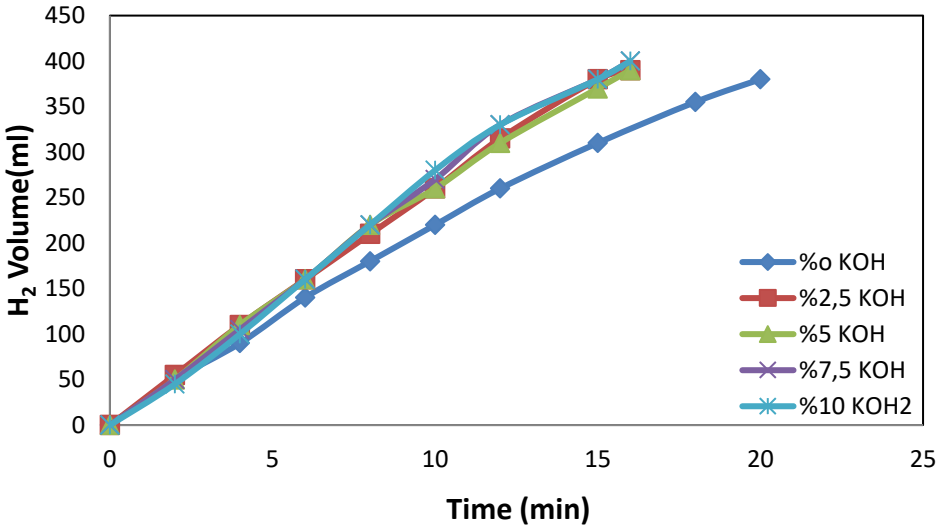

Şekil 2. Ni-B-P katalizörü varlığındaNaBH$_4$'ün hidrolizinde KOH etkisi

Daha sonra belirlenen mikrodalga ortamında farklı gazlar varlığında 50 mg Ni-B-P katalizörü 500 W, 10 dakika maruz bırakıldıktan sonra 30 ^oC de potasyum bor hidrürün hidrolizi incelendi. Şekil 3'te açıkça görülmediğinden dolayı hidrojen üretim hızlarının zamana bağlı grafiği çizilmiştir.

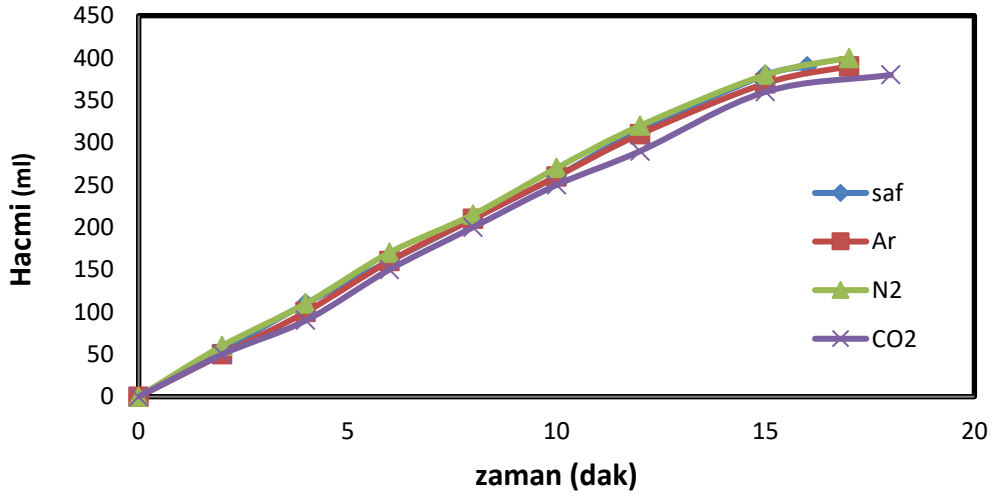

Şekil 3. Ni-B-P katalizörünün mikrodalga varlığındaki farklı gazların etkisi.

Şekil 4'ten görüleceği üzere azot gazı varlığında hidrojen üretiminin hızının daha etkin olduğu görülmektedir.

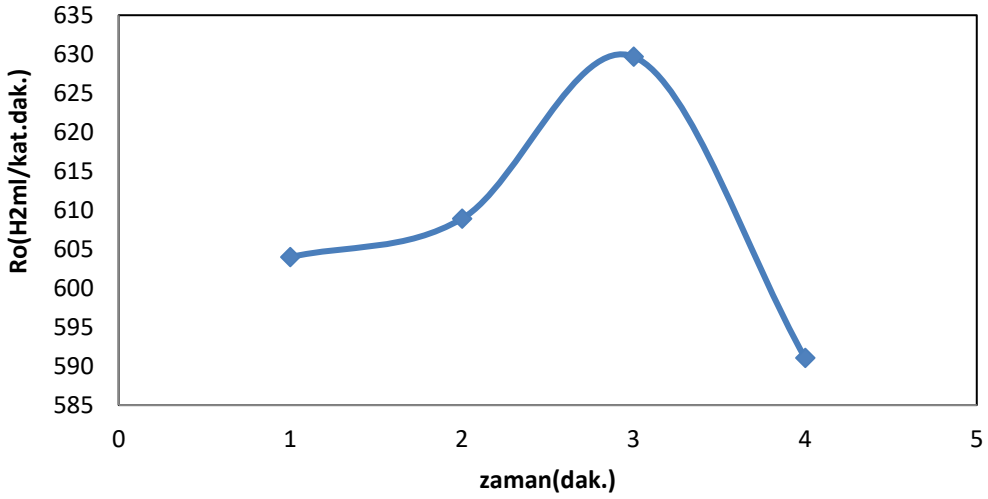

Şekil 4. Ni-B-P katalizörünün mikrodalga varlığındaki farklı gazların hidrojen üretimine etkisi.

Bir sonraki adımda ise potasyum bor hidrürün Ni-B-P katalizörüne mikrodalgada azot gazı varlığında farklı güçleri incelendi. Şekil 5-6 dan görüleceği üzere 300 Watt gücünün Ni-B-P katalizörü varlığında potasyum bor hidrür hidrolizi üzerinde etkin olduğu görüldü.

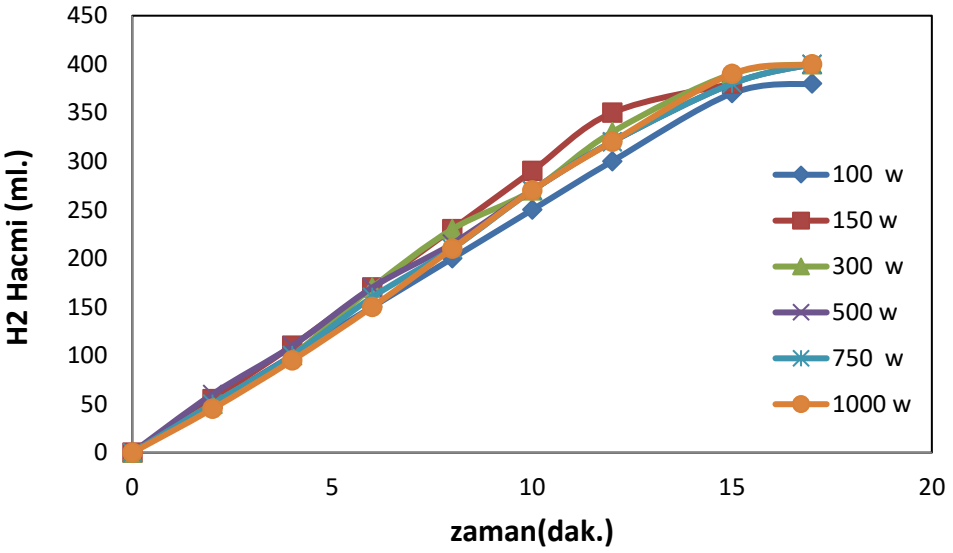

Şekil 5. Ni-B-P katalizörünün mikrodalga varlığındaki farklı gazların etkisi.

Farklı sıcaklıklarda elde edilen reaksiyon hız sabitleri kullanılarak hidroliz reaksiyonuna ait aktivasyon enerjisini bulmak amacıyla yukarıda verilen Eşitlikleri kullanarak Arhenius eşitliği belirlenmiştir.

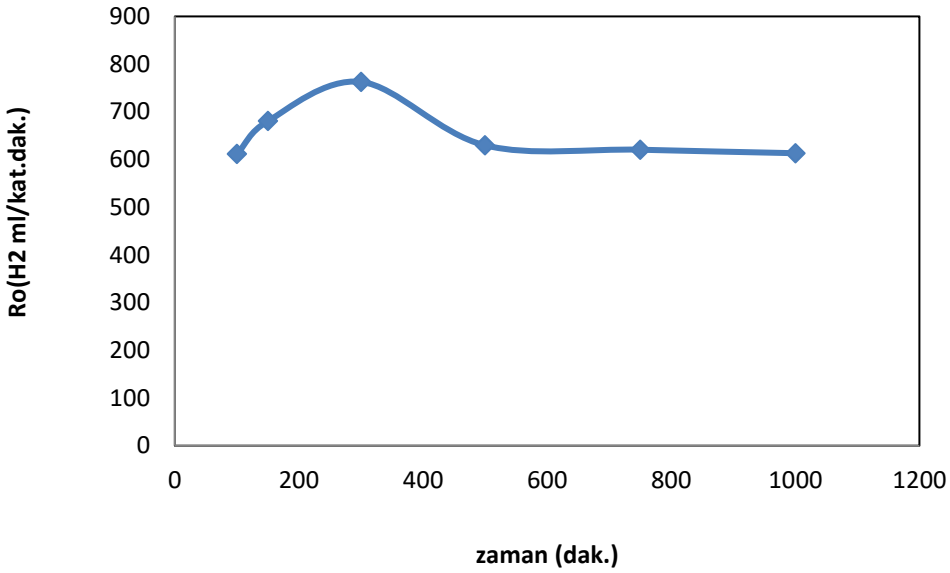

Şekil 6. Ni-B-P katalizörünün mikrodalga varlığındaki farklı güçlerin hidrojen üretimine etkisi

Ni-B-P katalizörünün mikrodalga ortamında 300 Watt ve azot gazının belirlenmesinden sonra mikrodalga ortamında en etkin sürenin belirlenmesi için 5-15 dakika arasında mikrodalgaya maruz bırakıldı.

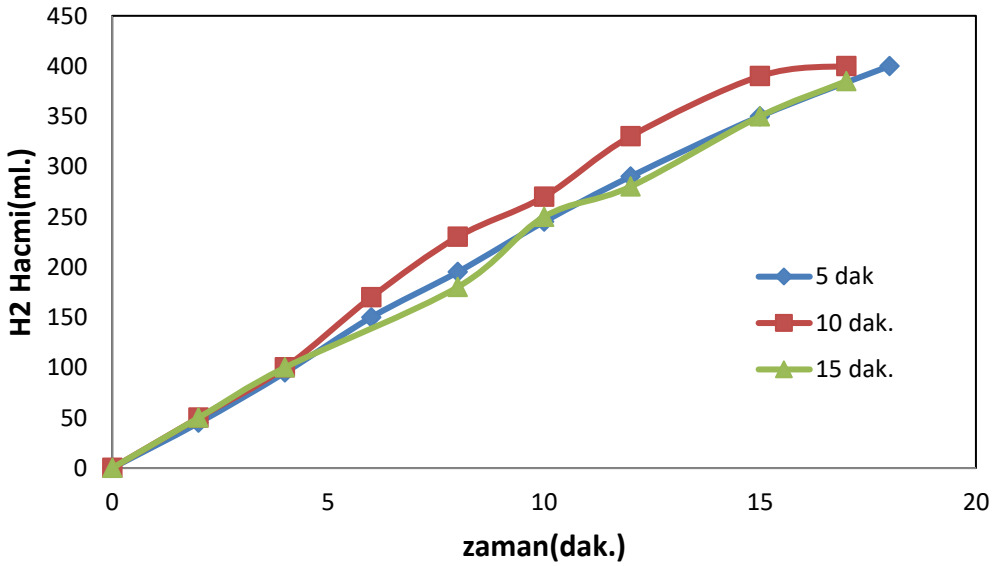

Şekil 7. Ni-B-P katalizörünün mikrodalga varlığındaki farklı sürelerin etkisi.

Şekilden görüleceği gibi 10 dakika mikrodalga süresinin katalizörün katalitik aktivitesini artırdığı, daha yüksek sürelerde ise katalizörün aktivitesini negatif yönde etkilediği görülmüştür.

KAYNAKLAR

[1] Johnston, B., Mayo, M.C. ve Khare, A., 2005. Hydrogen: the energy source for the 21st. Technovation, 25, (569-585).

[2] Kojima Y, Haga T, 2003. Recycling Process of Sodium Metaborate to Sodium Borohydride. International Journal of Hydrogen Energy, 28: 989-993.

[3] Amendola SC, Kelly MT, Wu Y, 2003. Process of Synthesizing Borohydride Compounds. United State Patent No: 6, 524-542.

[4] Liu BH, Li Q, 2008. A highly Active Co-B Catalyst for Hydrogen Generation from Sodium Borohydride Hydrolysis. Int. J. Hydrogen Energy, 33: 7385–7391.

[5] Biniwale RB, Rayalu S, Devotta S, Ichikawa M, 2008. Chemical hydrides a Solution to High Capacity Hydrogen Storage and Supply. Int J Hydrogen Energy. 33: 360–365.

[6] Lee J, Kong KY, Jung CR, Cho E, Yoon SP, Han J, Lee TG, Nam SW, 2007. A structured Co–B catalyst for hydrogen extraction from $NaBH_4$ solution. Catalayst Today 120: 305–310.

[7] Amendola SC, Shap SL, Janjua MS, Spencer NC, Kelly MT, Petillo PJ, Blinder M, 2000. A safe, portable, hydrogen gas generator using aqueous borohydride solution and Ru catalyst Int. Journal of Hydrogen Energy. 25: 969–975.

[8] Özkar S, Zahmakiran M, 2005. Hydrogen Generation from Hydrolysis of Sodium Borohydride Using Ru (0) Nanoclusters as Catalyst. J. Alloys. Compd. 404–406: 728–731.

[9] Park JH, Shakkthivel P, Kim HJ, Han MK, Jang JH, Kim YR, Kim HS, Shue YG, 2008. Investigation of metal alloy catalyst for hydrogen release from sodium borohydride for polymer electrolyte membrane fuel cell application Int. J. Hydrogen. Energy. 33:1845-1852.

[10] Patel N, Patton B, Zanchetta C, Fernades R, Guella G, Kale A, 2008. Pd-C powder and thin film catalysts for hydrogen production by hydrolysis of sodium borohydride. Int. J. Hydrogen Energy, 33: 287–292.

[11] Yin SF, Zhang QH, Xu BQ, Zhu WX, Au CT, 2004. Investigation on the catalysis of COx-free hydrogen generation from ammonia, J.Cat. 224: 384-396.

[12] Kojima Y, Suzuki K, Fukumoto K, Sasaki M, Yamamoto T, Kawai Y, 2002. Hydrogen generation using sodium borohydride solution and metal catalyst coated on metal oxide Int. J. Hydrogen Energy, 27: 1029–1034.

[13] Dong H, Yang H, Ai X, Cha C, 2003. Hydrogen production from catalytic hydrolysis of sodium borohydride solution using nickel boride catalyst Int. J. Hydrogen Energy, 28: 1095–1100.

[14] Jeong SU, Cho EA, Nam SW, Oh IH, Jung UH, Kim SH. 2007. Effect of preparation method on Co–B catalytic activity for hydrogen generation from alkali NaBH4 solution. Int. J. Hydrogen Energy, 32: 1749–54.

[15] Wu C, Wu F, Bai Y, Yi BL, Zhang HM, 2005. Cobalt boride catalysts for hydrogen generation from alkaline NaBH4 solution. Mater. Letter, 59: 1748–1751.

[16] Xu D, Dai P, Liu X, Cao C, Guo Q, 2008. Carbon-supported cobalt catalyst for hydrogen generation from alkaline sodium borohydride solution. J. Power Sources, 182: 616–620.

[17] Şahin Ö, Kaya M, Izgi, MS Saka C, 2015. Effect of Microwave Irradiation on a Co-B based Catalyst for hydrogen generation by hydrolysis of $NaBH_4$ solution. Energy Sour. Part A: Recovery, Utilization, and Environmental Effects, 37: 462-467

[18] Suresh BK, Vernekar AA, Jagirdar BR, 2009. Co-Co2B, Ni-Ni_3B and Co-Ni-B Nanocomposites Catalyzed Ammonia Borane Methanolysis for Hydrogen Generation.

ICACChE
2nd International Conference on Applications in Chemistry and Chemical Engineering
10 - 14 October 2018 Belgrade

The Design of Organohybrid Structures

Rodlovkaya E.N.[1], Vasnev V.A., Izmailov B.A.

Abstract

One of the most urgent problems in the informational nanotechnology is the development of photochromic recording media for three-dimensional optical memory with a high information capacity. Usually these light-sensitive materials are developed using thermally irreversible photochromic compounds, particularly 1,2-diarylethenes, in polymer binders [1]. Unfortunately, the information capacity (resolution) of these recording media is limited by diffusion and low content (up to 5 mass %) of photochromic compounds in a polymer matrix.

This report represents synthesis and spectral-kinetic study of photochromic three-dimensional silicone polymers (coatings) based on 1,2-dihetarylethenes with N-hydroxyethyl and N-allyl groups, polysiloxanes and polysilazanes. The polymers obtained contain photochromic moieties linked to the polymer chain by covalent bonds that allow achieving of photochromic units with a high concentration (up to 40%).

Keywords: Photochromic compounds. 1,2-diarylethenes, polymer matrix

1. INTRODUCTION

Thiophene-containing polymers, primarily polythiophene and its derivatives, have attracted the attention of researchers owing to their wide range of properties, such as conductance, luminescence, and electroluminescence [1–3]. These properties predetermine their possible application as organic conductors and semiconductors [1–4], light-emitting diodes [1, 5], sensors [1, 4], etc. However, the infusibility and insolubility of polythiophenes make them difficult to process and restrict their practical applications. The processability of thiophene-containing polymers may be improved via incorporation of hinge bridge fragments into their chains. However, simultaneously with improving processability of rigid-chain polymers, the incorporation of hinge bridge fragments into the structure of rigid-chain polymers may lead to the breakage of their conjugation chains and deterioration of their electrophysical properties. Therefore, from our point of view, the most promising method includes the incorporation of bridge fragments that will not break the conjugation chain or that will restore it through polymer-analogous transformations in the processing.

Previously, we synthesized new arylene-bis(2-ami-nothiophene-3-carbonitrile)s (1) and (2) [7] via the Gewald reaction. In our opinion, these compounds are promising as monomers for the synthesis of thiophene-containing polymers characterized by improved processibility and the ability to form poly-conjugated structures. At the same time, the presence of nitrile groups in thiophene fragments is interesting from both the synthesis of polymers with new photoelectric properties and the feasibility of their subsequent chemical transformations point of views. In this study, we investigated the synthesis of polythiophenes with main-chain acrylamide groups via the interaction of compounds (1) and (2) with arylenedicarboxylic acid dichlorides (3a), (3b), (4a), and (4b).

[1] *Corresponding author: A.N. Nesmeyanov Institute of Organoelement Compounds Russian Academy of Sciences, ul. Vavilova 28, Moscow, 119991, Russia. Corresponding author e-mail: rodlovskaya@mail.ru*

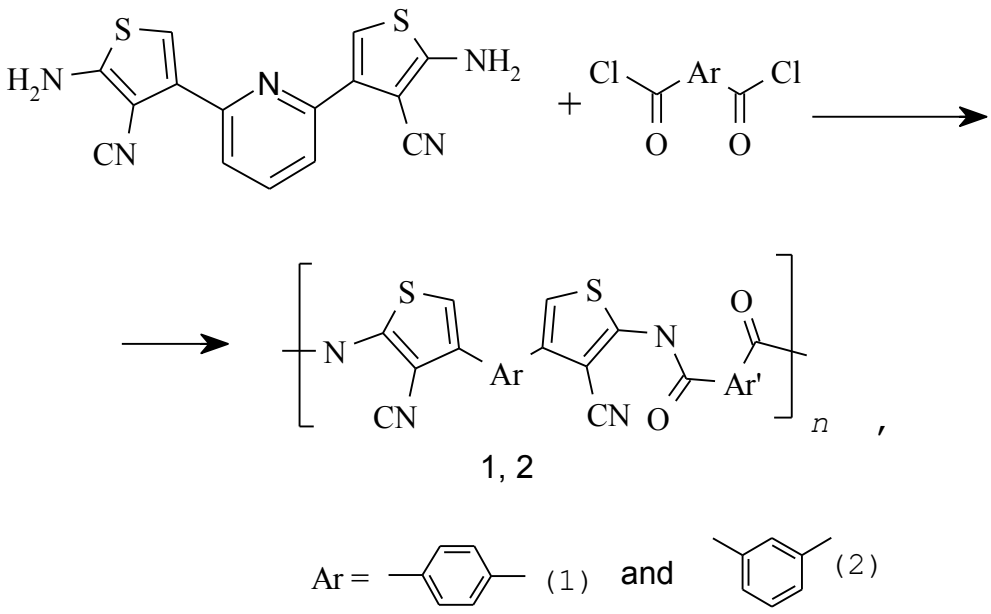

Fig. 1. Scheme of synthesis of polythienothiophenes 1, 2

Samples of organic light-emitting devices were fabricated through the use of a combined technique of centrifugation and thermal evaporation in vacuum and had the following structure: Substrate/ITO/PEDOT/Polythiophene(1, 2)(~30 nm)/QD/TAZ(30 nm)/Al(100 nm) (see Fig. 2).

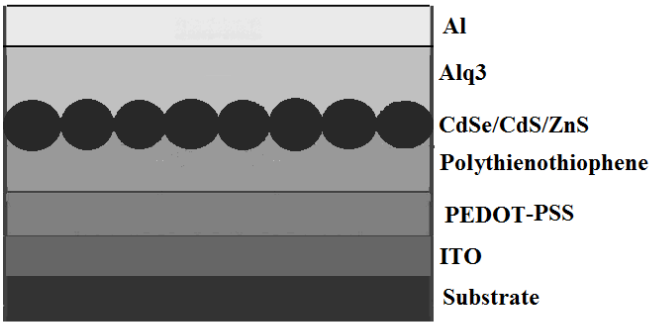

Fig. 2. Scheme of a light-emitting diode with a polythienothiophene hole injection layer and QDs as the active layer.

Layers of PEDOT (poly(3,4)-ethylenedioxythiophene, Aldrich), new polythiophenes, and QDs were produced by centrifugation from solutions in water, dimethylformamide, and toluene, respectively. The solvents of polythiophenes and QDs have strongly different polarities, which makes impossible their direct mixing and formation of a composite. Nevertheless, these layers are strongly mixed when successively deposited, especially if the QD layer is deposited immediately after the deposition of polythiophene, before its complete drying. The electron conducting layer of TAZ (3-(4-biphenyl-5-tert-butylphenyl-1,2,4-triazole, Lumtec Corp.) and the aluminum cathode were deposited by thermal evaporation in vacuum at a residual pressure in the chamber not exceeding 10–5 mbar.

The EL spectra of the samples, shown in Fig. 3, coincide with the photoluminescence spectra of QDs in toluene. Good coincidence of both the emission peaks (I, 635 nm; II, 638 nm: III, 641 nm) and the shapes of the spectra indicates that we do observe the emission from QD-LEDs. The shift of the emission peaks of the

diodes, independently of the applied voltage, may be due to the different degrees of conjugation of the polymers and QDs for different samples.

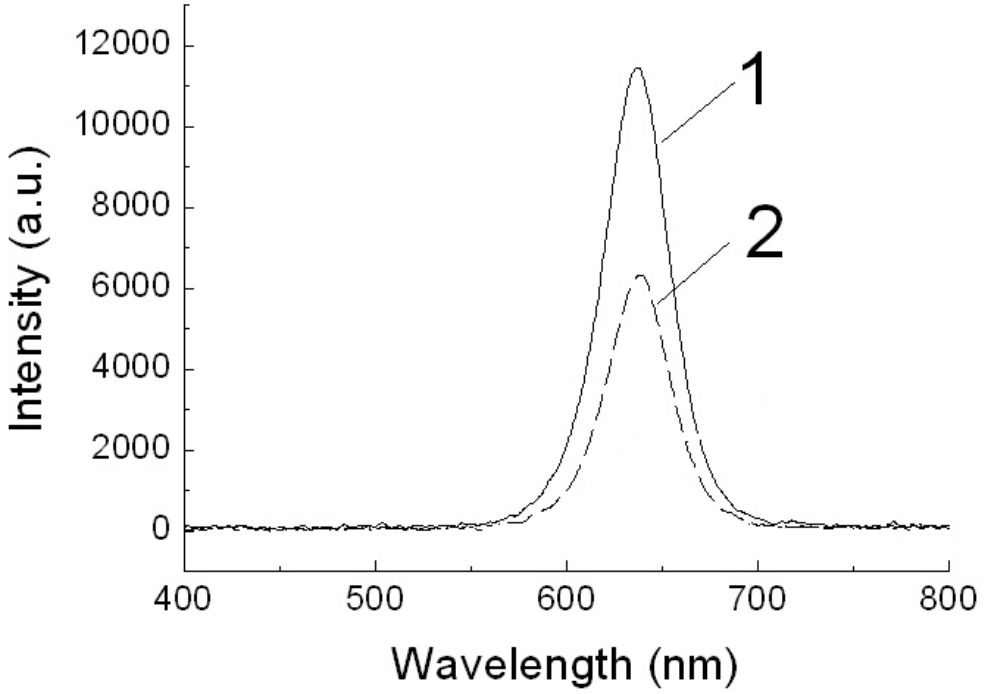

Fig. 3. Emission spectra of LEDs with QDs and polythiophenes as holeconducting layers: (1) (solid line) polythiophene (dashed line) polythiophene 2.

Thus, it was showed that polymeric conducting materials based on aminobithienyls can be effectively used to develop hybrid organo-inorganic structures based on cadmium chalcogenides. The results obtained give reason to believe that optimization of the properties of the polymeric modifier would give effective hybrid active layers for electroluminescent devices, which would combine the high technological convenience of polymeric materials and the good photophysical properties of inorganic emitters for QD-OLEDs.

ACKNOWLEDGMENT

This study was supported by the Russian Foundation for Basic Research (project nos. 18-03-00892).

REFERENCES

P. Reiss, E. Couderc, J. De Girolamo, A. Pron, Nanoscale 3, 446 (2011).
U. Mehmood, A. Al-Ahmed, I. A. Hussein, Renewable and Sustainable Energy Rev., 57, 550 (2016).
M. Jaymand, M. Hatamzadeh, Y. Omidi, Prog. Polymer Sci., 47, 26 (2015).
E. N. Rodlovskaya, N. G. Frolova, E. D. Savin, V. I. Nedel'kin, Polymer Sci., Ser. A 46, 593 (2004).
Y. F. Loginova, S. V. Dezhurov, V. V. Zherdeva, N. I. Kazachkina, M. S. Wakstein, and A. P. Savitsky, Biochem. Bioph. Res. Co., 419(1), 54 (2012).

ICACChE
2nd International Conference on Applications in Chemistry and Chemical Engineering
10 - 14 October 2018 Belgrade

Investigation of Linear Growth Rates of Potassium Pentaborate tetrahydrate in Stationary Medium of Single Crystal System

Halil Demir[1], Ömer Şahin[1], Mustafa Kaya[1]

Abstract

Although boron minerals are composed of more than 150 compounds containing boron oxide (B_2O_3) which contain different proportions of boron in nature. Boron minerals are found naturally in the form of hydrate compounds with Na, K, Mg and Ca elements. Some of the commercial boron compounds produced by crystallization are not investigated as well as sodium compounds. Potassium 1:5 borates (potassium pentaborate tetrahydrate, $KB_5O_8.4H_2O$) are obtained by maintaining a molar ratio of B_2O_3 / K_2O of the reaction of boric acid and KOH in aqueous medium at 5. The production equation of potassium pentaborate tetrahydrate can be given as follows:

$5H_3BO_3$ + KOH → $KB_5O_8.4H_2O$ + $4H_2O$

In this study, the linear growth rates of potassium pentaborate tetrahydrate in the stagnant medium of single crystal system were investigated due to temperature and supersaturation. It was determined by experimental studies that a single crystal of potassium pentaborate tetrahydrate was scattered at the linear growth rate. In the presence of Ca impurity, linear growth rates due to different supersaturation were investigated and it was determined that scattering continued at growth rates.

Keywords: potassium pentaborate tetrahydrate, growth rate, supersaturation, single crystal

1. INTRODUCTION

Although boron minerals are composed of more than 150 compounds containing borax (B2O3) which contain different proportions of boron in nature, boron minerals are found naturally in the form of hydrate compounds with Na, Mg and Ca elements. Nowadays, these natural compounds do not have much material income, although they are worthy. For this reason, the production of special boron products such as boric acid, sodium perborate tetrahydrate and monohydrate such as ammonium borate, potassium borate, lithium borate, boron carbide, boron nitride, boroxide, and boron acid with high added value by using these natural compounds and determination of industrial production conditions. It is very important for our country which has around 70% of its deposits. Commercially available boron minerals; tincal, colemanite, ulexite, probesite, boracite, pendermite, hydroboracite and kernite.

The reaction of potassium pentaborate tetrahydrate, can be obtained by using boric acid and KOH in aqueous medium by maintaining a mole ratio of B_2O_3/K_2O [1, 2, 3]. In some studies K_2CO_3 have been used instead of KOH [4]. The production equation of potassium pentaborate tetrahydrate can be given as follows.

$5H_3BO_3 + KOH \rightarrow 4\ KB_5O_8.4H_2O + 4H_2O$

On the other hand, the calcination of potassium pentaborate tetrahydrate in the fluidized bed has been investigated depending on the calcination temperature, flow rate and particle size [5].

In addition, the use of potassium pentaborate tetrahydrate, which is increasing in use, has been determined by this study and the production conditions have been determined. At the rate of growth, the scattering event is expressed as the growth of the crystals having the same size at the beginning of the experiment, ie at different rates of growth under the same experimental conditions (temperature, supersaturation, solution).

[1] *Corresponding author: Siirt University, Faculty of Engineering, Department of Chemical Engineering, Siirt, Turkey. halildemir@siirt.edu.tr*

This scatterin can easily be observed in measurements made in single crystal cells. In order to eliminate the effects of these deviations a large number of particle size-dependent growth models were developed in between 1970 and 1980 years [6]. In later studies, the physical causes of these deviations were emphasized and kinetic models were rearranged.

Fabian [11], in their dissolution experiments with K2SO4, identified a scattering phenomenon just as in growth. The presence of scattering in the dissolution zone was also determined experimentally by Şahin [12, 13] for boric acid and sodium perbororate tetrahydrate. In these studies, the scattering at the growth and dissolution rates suggested that the static load on the crystal surface was the cause and proved experimentally. This phenomenon also shows that dissolution is affected by the specific characteristics of the surface. Two basic models have been developed for the evaluation of such properties in the crystallization design phase.

Scattering at growth rates does not only occur in small and imperfect crystals, but also to large-sized and large-sized crystals of the same size.

The first view on the causes of scattering at growth rates was done by Janse and De Jong [14]. Janse and De Jong suggested that scattering at growth rates was not due to the velocity of the solution in the environment in which the crystals grew, but because of the reaction on the crystal surface. Later, in the studies conducted by many researchers on this subject; [15] showed that the cause of scattering in growth should be related to surface reaction. The oldest theory to explain these scatterings is the BCF theory developed by Burton, Cabrera and Frank [17]. This theory shows that there may be different growth rates depending on the distribution of dislocation points on the crystal surface.

Botsaris [20], in his work, showed that the growth of different surfaces of the same crystals at different rates was due to the impurities in the crystallization environment and the adsorption of impurities.

Potassium pentaborate tetrahydrate

Potassium pentaborate tetrahydrate, $KB_5O8.4H_2O$ has a formula weight of 293.20 the crystal structure is orthorhombic prism, heat capacity at 296.6 K is 329.0 J / (mole K) and solubility) is lower than sodium pentaborate. The heat capacity measurements of the solid state were carried out over a wide temperature range [24]. Potassium pentaborate tetrahydrate is stable under normal conditions. The dehydration temperature was calculated to be 110.8 K J / mol between 106-134 ^oC [25]. The thermal stability of potassium pentaborate tetrahydrate is highly dependent on the partial vapor pressure of the water in the environment.

1.3. Factors affecting the kinetics of crystallization

While crystallisation processes are carried out, there may be many factors affecting the crystallization in the crystallization environment. But the most effective of these are temperature and impurity.

1.3.1. Effect of temperature

When examining the effect of temperature on a chemical reaction or physical change, it is first necessary to find activation energy. The relation between the reaction rate constant and temperature in any reaction equation by Arrhenius,

$$\frac{d\ln k}{dt} = \frac{E}{RT^2} \tag{2.10}$$

It is expressed as. If this equation is integrated,

$$k = Ae^{-\frac{E}{RT}} \tag{2.11}$$

takes shape. Ln of Equation 2.8 can be taken and linearized as follows.

$$\ln k = \ln A - \frac{E}{RT} \tag{2.12}$$

If the 1 / T graph is plotted against lnk, the slope E is obtained.

We can examine the effects of growth and habit change on three main topics.

1.3.2. Effect of impurities

The solvent used in the solution medium and the matter to be crystallized can be considered as impurity. Impurities sometimes affect crystallization when not desired, and sometimes they are added to the medium in order to direct the crystallization process and change the quality of the product. The impurities used for

aqueous solutions can be subdivided into free acids and bases, inorganic or organic impurities or different solvents.

2. MATERIAL AND METHOD

2.1 Stationary Media Single Crystal Studies

In the experiments performed with single crystal in a stagnant medium single crystal system was used. The system used in experimental studies is given in Figure 2.1. As can be seen in the figure, the system consists mainly of microscope and the connected camera, image analyzer, computer and monitor. The experiments were carried out with jacketed cell flexiglass and the temperature was adjusted by a cooled thermostat. The cell temperature was recorded every five minutes by means of the thermocouple in the cell.

The crystals used in the experiments were chosen under a microscope prior to the experiments to be of almost the same quality. The selected crystals were placed in the center of the cell to which the solution was placed beforehand and the experiment was placed in the center of the cell to be carried, the top of the cell was immediately covered with a watch glass and thus contacted with air. The experiments were carried out for 40 minutes.

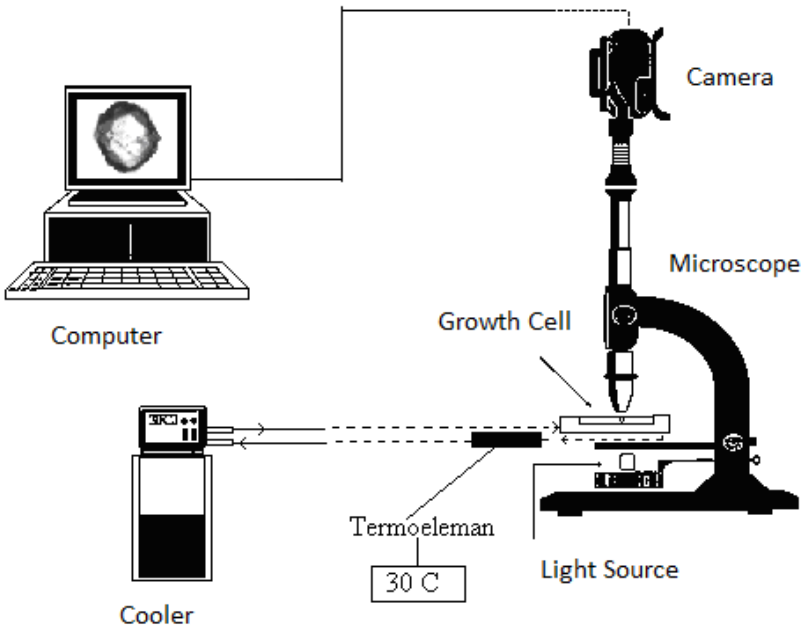

Figure2.1. Steady Medium Single Crystal Measurement System

Since the crystal particles used in this method have different shape factors, the projective area provided by the image analyzer cannot be used directly. For this reason, the equivalent diameter of the sphere with equivalent projection area is shifted from the projective area.

$$A_p = \frac{\Pi}{4} L_i^2 \qquad (2.1)$$

The average linear growth rate is calculated according to the Expression of 2.2. Here

$$G = \frac{\Delta L}{\Delta t} = \frac{L_i - L_o}{\Delta t} \qquad (2.2)$$

Lo, the diameter of the particle at t = 0

Li, shows the diameter of the particle at time t = t.

On the other hand, growth is between linear growth rate and supersaturation.

$$G = k_g \Delta C^g \qquad (2.3)$$

k_g is growth velocity constant in this relation, g gives the degree of growth velocity, and ΔC gives the amount of supersaturation.

3. RESULTS AND DISCUSSION

3.1. Steady Meduma Single Crystal Studies

3.1.1. Studies in Pure Environment

In the first step of the experimental studies performed on the stagnant medium single crystal system, the variation of the equivalent diameters of the different crystals taken in the pure medium of potassium pentaborate tetrahydrate is given in Figure 3.1 and Figure 3.2. In Figure 3.1 we can say that the crystal measured in the equivalent diameter at a certain time intervals for 40 minutes increases in diameter, but in Figure 3.2, the crystal diameter decreases.

As shown in Figure 3.1 and Figure 3.2, the linear variation of the equivalent particle diameter over time indicates that the dL / dt values are constant so that the linear growth and dissolution rates of the potassium pentaborate tetrahydrate are not dependent on the particle size.

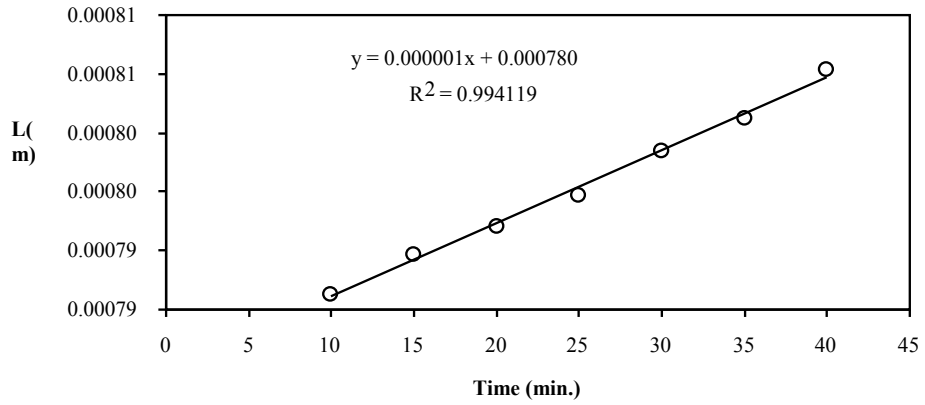

Figure 3.1. Variation of equivalent particle size with time in 0.524 g salt/100 g sat. Solution medium

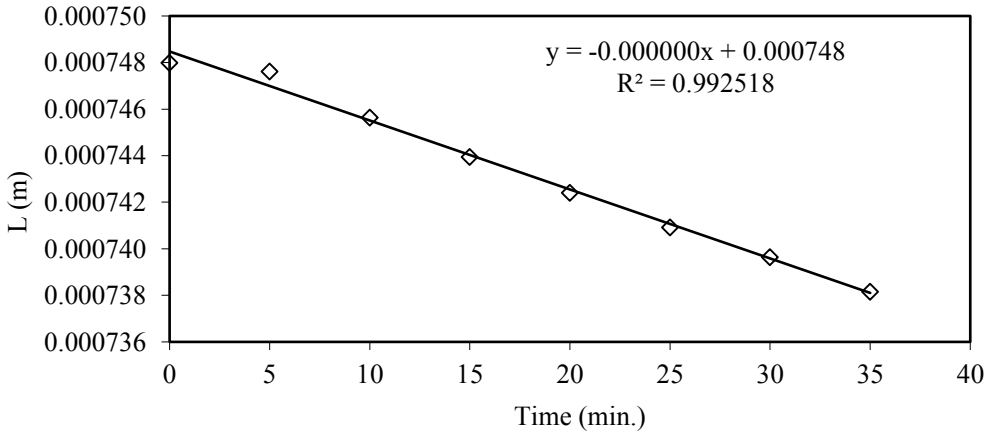

Figure 3.2. The variation of equivalent particle size with time in 0.500 g of salt / 100 g unsaturated solution medium

In the next section of the study, 20 crystals of potassium pentaborate tetrahydrate were taken and grown in different supersaturation environments for about 40 minutes in the saturated solution at about 30 ° C. The linear growth rate change with temperature is given in Figure 3.3. The reason for giving this shape is to show that the saturation temperature of the solution cannot be found by crystal growth or dissolution.

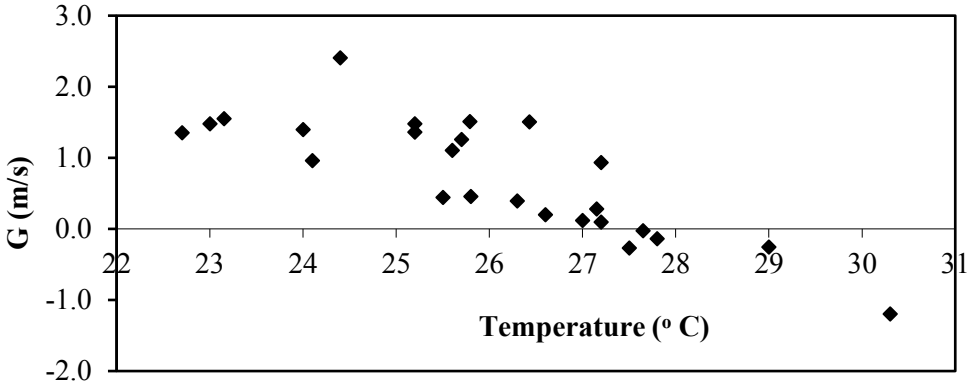

Figure 3. Variation of linear growth rates of potassium pentaborate tetrahydrate with temperature.

As can be seen in the figure, the linear growth rates of potassium pentaborate tetrahydrate are dispersed. The change of linear growth rate and temperature can't be expressed with any equation. Because there is scattering at growth rates.

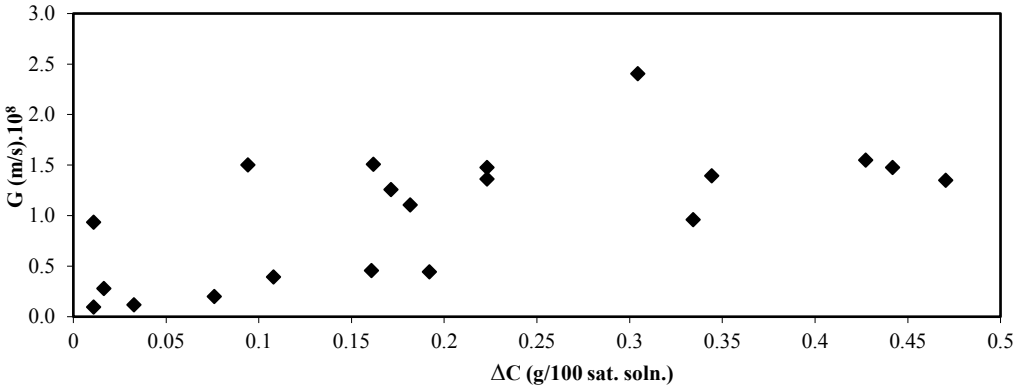

Figure 3. 4. The change of linear growth rates of potassium pentaborate tetrahydrate with supersaturation

By using temperatures given in figure 3, solubility of potassium pentaborate tetrahdrate and saturation temperature of saturated solution depending on supersaturation used figure 3.4 is obtained

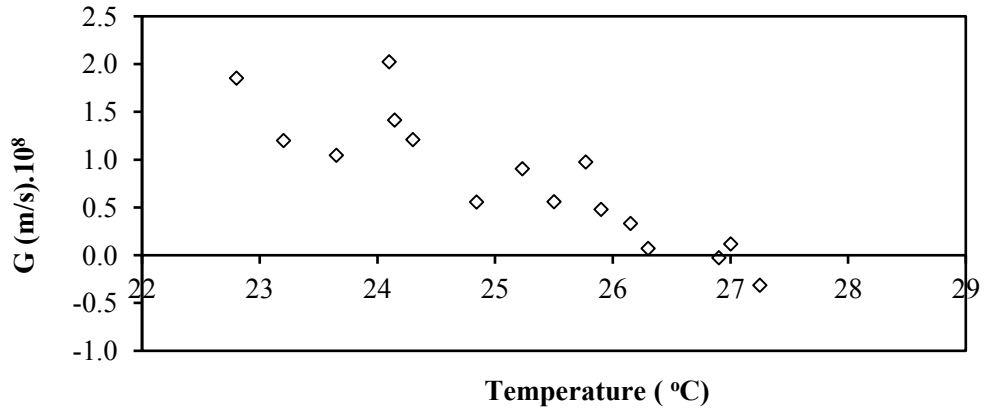

Figure 3.5. Change of linear growth rates of potassium pentaborate tetrahydrate crystals in the presence of 50 ppm Ca (II) with temperature

One of the most common compound in aqueous media is calcium. Therefore, the water used in the solution medium is found in trace amounts even if the water is cleaned as desired. Investigation of the calcium activity in the environment with crystallization is important. In this part of the study, it is aimed to investigate how the calcium impurity affects the crystal appearance and linear growth rates.

In Figure 3.5 and Figure 3.6 the linear growth rates change with temperature in the presence of calcium impurity in different concentrations in the solution medium

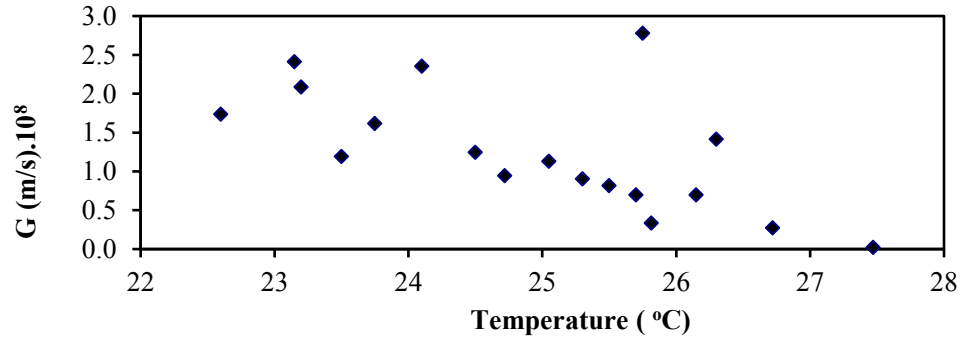

Figure 3.6. Change of linear growth rates of potassium pentaborate tetrahydrate crystals in the presence of 100 ppm Ca (II) with temperature

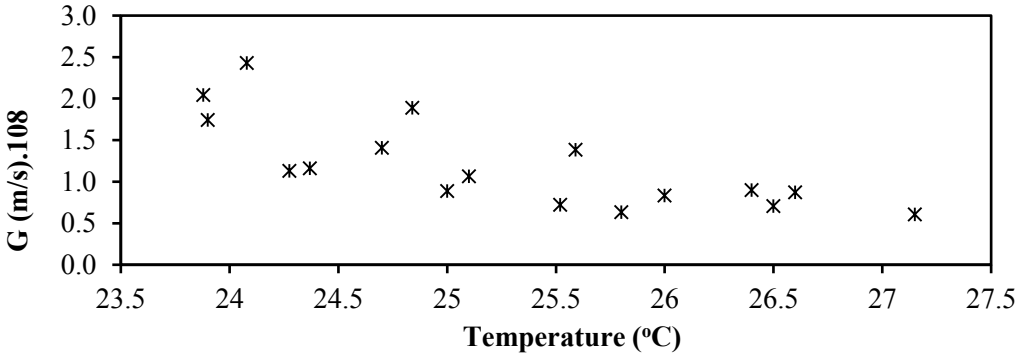

Figure 3.7. Change of linear growth rates of potassium pentaborate tetrahydrate crystals in the presence of 250 ppm Ca (II) with temperature

The variation of linear growth rates in the presence of calcium impurities in different concentrations of potassium pentaborate tetrahydrate crystals is given in Figure 3.7 and 3.8. As can be seen from the figures, as Ca (II) impurity increases, scattering at the growth rates of potassium pentaborate tetrahydrate crystals continues just like in pure medium.

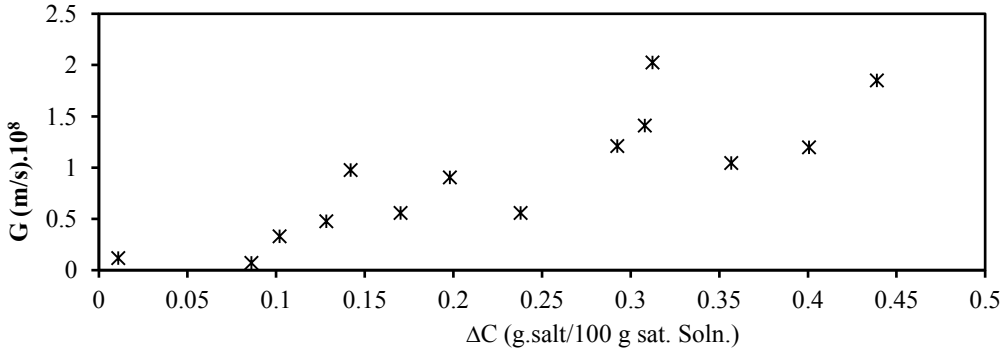

Figure 3.8. The change of linear growth rates of potassium pentaborate tetrahydrate crystals with supersaturation in the presence of 50 ppm calcium,

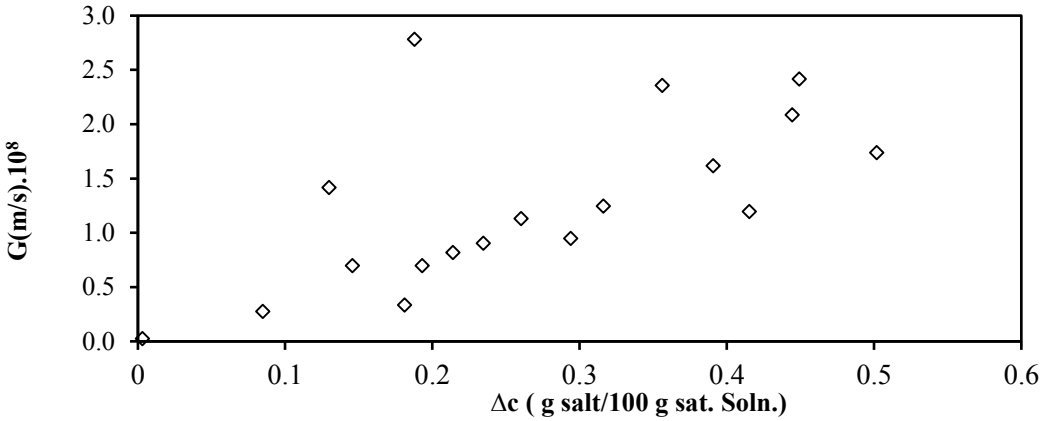

Figure 10. The change of linear growth rates of potassium pentaborate tetrahydrate crystals with supersaturation in the presence of 250 ppm calcium

The variation of linear growth rates in the presence of calcium impurities in different concentrations of potassium pentaborate tetrahydrate crystals is given in Figure 7-8. As can be seen from the figures, as Ca (II) impurity increases, scattering at the growth rates of potassium pentaborate tetrahydrate crystals continues just like in pure medium. As can be seen in the figures, the increase in the presence of Ca (II) impurity in the solution medium reduces the saturation temperature of the solution. For example, for pure medium 30,5 ^{o}C , in the presence of 250 ppm Ca(II) 27,5 ^{o}C.

In this study, it was determined that a single crystal of potassium pentaborate tetrahydrate was scattered at the linear growth rates. In the presence of Ca impurity, linear growth rates depending on different supersaturation were investigated and it was determined that scattering continued at growth rates. In the first part it was determined that the growth and dissolution rates of Potassium Pentaborat Tetrahydrate do not depend on the particle size. In the second part the linear growth rates depending on different supersaturation in both pure environment and in the presence of impurities were investigated. For all cases, the same crystals of the same particle size were found to be scattered at the same growth rates. For this reason, it is not possible to say clearly the effects of pure environment and impurities on the crystal surface because of scattering.

This work was Supported by TUBITAK with the project number 108M043

REFERENCES

[1] U.S. pat. 2, 776,186 F.H. May (to American potash and chemical Corp.) (1957).
[2] Gale William A, "Method of preparing potassium pentaborate, US. Patent 2094881,Oct (1937).
[3] Alfred Newman, " Manufacture of potassium borate, U.S. pat.1961073, May, (1934).
[4] S.A. Rajasekar, K. Thamizhorason, A.J.A. Pragasam, J.P. Julius and P Sagayaraj, Journal of Crystal growth 247 199-206, (2003).
[5] Gang yong, z.li, V. Zhong "Dehydration of tetrahydrate potassium tetraborate in fluidizied bed", Chemical Engineering and processing 44 1216-1220, (2005).
[6] Rousseau, R.W., Woo, R., Effects of Operating variables on potassium alum crystal size distribution, AIChE Symposium Series,76,193, pp.29, (1980).
[7] Bunn, C.W., Concentration gradients and the rate growth of crystals, *Discussions Faraday Society*, 5, pp.132-144, (1949).
[8] Wrıght, P.G., Whıte, E.T., Size-distribution studies in sugar crystallization, Proc. Queensland soc. sugar cane Technology, 36 th conf., pp:299-309, (1969).
[9] Natalına, L.N., Trevius, E.B., Variations in the growth rates of potassium dihydrojen phosphate crystals, *Sov. Phys.cryst.(Engl. Transl.),* 19 (3) 389, (1974).
[10] Ulrıch, J., Growth rate dispersion- a review, *Cryst. Res. Technology*, 24(3), pp. 249-257, (1989).
[11] Fabıan, J., Ulrich, J., Dissolution a two step process- presentation of experimental evidence, 12 th symposium on Industrial crystallization, ed. by Z.H. Rojkowski, Warsow, Poland, (1993).
[12] Sahın, Ö., Bulutcu, A.N, "Effect of surface charge distribution on the crystal growth of sodium perborate tetrahydrate" *Journal of Crystal Growth* 24, 471-480, (2002).
[13] Sahın, Ö., Bulutcu, A.N., The effect of surface potential on the growth and 169 dissolution rate dispersion of boric acid, *Cryst. Res. Technol*. 38, No.1, 56-62, (2003).
[14] Janse, A.H., De Jong, E.H., *Growth and growth dispersion*, Industrial crystalization 78, E.J. de Jong, S.J. Jancýc(ed.), North-Holland Publishig Company, pp.135-140. (1979).

[15] Janse, A.H., De Jong, E.H., *Growth and growth dispersion*, Industrial crystalization 78, E.J. de Jong, S.J. Jancýc(ed.), North-Holland Publishig Company, pp.135-140. (1979).
[17] Tavara, N.S., Garsıde, J., *The characterization of growth dispertion, Industrial Crystallization* 81, ed. by Jancic, S.J., De Jong, E.J., Amsterdam, Pp:21-27, (1982).
[16] Bennema, P., *Industrial crystallization* , ed. by J.W. Mullin, New York, Pp: 91-112, (1986).
[18] Budz, J., Jones, A.G., Mullin, J.W., *Ind. Eng. Chem. Res*. 26, 820, (1987).
[19] Ulrıch, J., Kruse, M.; *Cryst. Res. Technol*. 24, 181, (1989).
[20] Botsarıs, G.B.; *Effect of Impurities in Crystallization Processes*, In Industrial Crystallization'81, ed. By Jancic, S.J.; De Jontg, E.J., North-Holland Amsterdam, Pp:123-135. (1982).
[21] Fabıan, J., Ulrich, J., Dissolution a two step process- presentation of experimental evidence, 12 th symposium on Industrial crystallization, ed. by Z.H. Rojkowski, Warsow, Poland, (1993).
[22] Sahın, Ö., Bulutcu, A.N, "Effect of surface charge distribution on the crystal growth of sodium perborate tetrahydrate" *Journal of Crystal Growth* 24, 471-480, (2002).
[23] Sahın, Ö., Bulutcu, A.N., The effect of surface potential on the growth and dissolution rate dispersion of boric acid, *Cryst. Res. Technol*. 38, No.1, 56-62, (2003).
[24] Furukawa, G.T., Reilly, M.L., and Piccirelli, J.H., J. Res. Nat. Bur. Stand. 68A, 381, (1964).
[25] Haladjıan, J., and Carpenı, G., Bull. Soc. Chim. Fr., 1629. (1960).
[26] Heller. G., and Boschke, F.L., Topics in Current Chemistry, Vol. 131, Springer- Verlag, Berlin, Heidelberg, 39p, (1986).
[27] Ashmore, J.P., and Petch, H.G., Can. J. Phys. Vol. 48, p.1091. (1970).
[28] U.S. pat. 2, 776,186 F.H. May (to American potash and chemical Corp.) (1957).
[29] Gale William A, "Method of preparing potassium pentaborate, US. Patent 2094881,Oct (1937).
[30] Alfred Newman, " Manufacture of potassium borate, U.S. pat.1961073, May, (1934).
[31] S.A. Rajasekar, K. Thamizhorason, A.J.A. Pragasam, J.P. Julius and P Sagayaraj, Journal of Crystal growth 247 199-206, (2003).
[32] Kagishita Kazuhiro, Konishi Shouzaborou, US. Patent No: 20060172900 "Lubricating oil additive and lubricating oil composition", Aug (2006).
[33] Yagishita Kazuhiro, Igarashi Jinichi, Korzumi Takeo, US patent No: 20040242434, Lubricating oil composition for internal combustion engine", Dec (2004).
[34] Yagishita Kazuhiro, Matsuyama Yoho, Kurosama Osamu, "Lubricating oil composition", European patent Application, pat no: Ep995789 Apr (2000).
[35] Sano Takashi, Komatsubara Hitashi, Wade Hisayuki, Kurosama Osamu, Itou Masaaki, matsui Shigeki, Takhashi Masato, Konishi shozaburo, "Lubricant base oil, lubricant composition for internal combustion engine and lubricant composition for driving force transmitting device" European patent Application, EP1845151, Oct (2007).
[36] Komatsubara Hitashi, "Boron containing lubricant oil composition "United Kingdom Patent Application GB2362389, Nov (2001). 173
[37] Toyosumi Masahiko, Ninomiya Kenji, "Resin composition and layered product", EP1152031, Nov (2001).
[38] Aston Mark, "method of stabilizing clay or Shok"; WO03052023, June (2003).
[39] Christiansen Walter, H. Corley larry S., US PatentOffice, , US 200401477111, Jul (2004).
[40] Chatterji J., Heatman James F., Gray Dennis W. Waugh Bryan K. "set retarder composition, cement composition and associated method" USA patent, , US 0060081155, Apr (2006)
[41] Smith Norman R. "Liquid deterjent composition, USA patent Office, jun 1965, US3192166.
[42] Wolk Jonathan J., Wolak Walter A., USA Patent Office, , US20070218692. Sep. (2007).
[43] Alton Robert H., USA Patent Office, US2336227, Dec (1943).
[44] Galleguillar Ramiro, PAnitch maximo M., jadan Anjana K., European Patent Application, EP676196 "Antispirant deodorant compositions" Oct (1995).
[45] Sangwal, K.,. Effect of impurities on crystal growth processes, *Prog.* Crystal Growth and Charact., 32, 3-43, (1996)
[46] Nývlt, J. and Ulrich, J., Admixtures in Crystallization, 1st ed., VCH Publisher, New York, (1995).
[47] Konarı, T., Borik asit büyüme kinetiğine elektriksel alan ve safsızlıkların etkisi, *Yüksek Lisans Tezi,* Đ.T.Ü. Fen Bilimleri Enstitüsü, Đstanbul, (1991).
[48] Veintemillas-Verdaguer, S., Chemical aspects of the effect of impurities in crystal growth, *Prog. Crystal Growth and Charact.,* 32, 75-109, (1996).
[49] Veintemillas-Verdaguer, S., Chemical aspects of the effect of impurities in crystal growth, *Prog. Crystal Growth and Charact.,* 32, 75-109, (1996).

ICACChE
2nd International Conference on Applications in Chemistry and Chemical Engineering
10 - 14 October 2018 Belgrade

Recent Advances in Photocatalytic Treatment by Metal Doped Graphene Nanoparticles

***Kubra Ulucan-Altuntas*[1]**

Abstract

Graphene has unique properties due to its two-dimensional nanostructure properties. It is an important material that draws attention recently, because it has an excellent mobility of charge carriers, superior chemical stability and high specific surface area. Graphene oxide, a derivative of graphene, has many oxygen functional groups on the surface and has similar advantages of graphene. Graphene and graphene oxide are nano materials used in many different industries and in particular for adsorption of pollutants due to its many advantages such as high pore volume and surface area. Over the past decade researchers have been developing a variety of materials such as graphene oxide-based composites, graphene oxide-carbon nanotubes, and metallic nanoparticle production. Metal-doped graphene nanoparticles as photocatalysts have begun to attract attention as novel materials for water treatment and environmental remediation applications. These graphene-based composites are doped with various metals, making them more effective in many areas. These nanoparticles synthesized by doping of various metals can be produced with low cost, and researchers gain great attention in applying as photocatalyst in the removal of pollutants. This review summarizes the recent advances in pollutant removal of graphene based nanoparticles, which have recently been investigated as an innovative nanomaterial.

Keywords: Graphene, Graphene oxide, Nanoparticle, Photocatalysts

2. INTRODUCTION

Catalysis is carried out by substances containing salts, complexes or transition metals. The investigation of alternatives to noble and expensive metals has led to the discovery of catalytic activity of metals mostly found in nature, such as Fe, Ni, Cu or Al, as well as the development of the concept of carbocatalysis. Carbocatalysis is the process in which predominantly carbon-containing substances are used as catalysts. Carbocatalysis became more important with the use of graphene (G) widely. In the early period, the discovery of fullerenes as carbon allotropes was followed by the development of carbon nanotubes (CNT). However, the high costs of the CNTs have made it difficult to produce the required amount of treatment. The use of activated carbon in combination with various metal nanoparticles (NP) such as Au, Ag, Pt, Ti has been recently studied. These metal NPs and their combination with carbonaceous materials have been found to be effective catalysts in the applications under visible light and are particularly suitable for improving especially the optical properties of carbonaceous materials such as graphene, activated carbon and carbon nanotubes.

Graphene is a thin two-dimensional (2D) layer of carbon atoms in a highly crystalline and electronic honeycomb crystal lattice (Fig.1). Graphene as a promising new material, has properties, such as good electronic properties, have high strength and are lightweight, and are considered to be the strongest in mechanical strength.

[1]*Corresponding author: Yildiz Technical University, Environmental Engineering Department, 34220 Istanbul, Turkey. kulucan@yildiz.edu.tr*

Graphene as a promising new material, has properties, such as good electronic properties, have high strength and are lightweight, and are considered to be the strongest in mechanical strength. The electronic transmission property of the graphene layer provides the doping of various metal NPs. The graphene layers doped with metal nanoparticles attracted attention with their innovative catalytic properties and, have great potential in many areas such as water treatment and energy storage.

The specific surface area, exceptional optical transmittance, and electron-conductance properties of the graphene and its derivatives have been used in photocatalytic applications operating under both UV and visible light. Nanoparticles such as Pf, Ag, TiO2 and ZnO are used to improve photocatalyst efficiency.

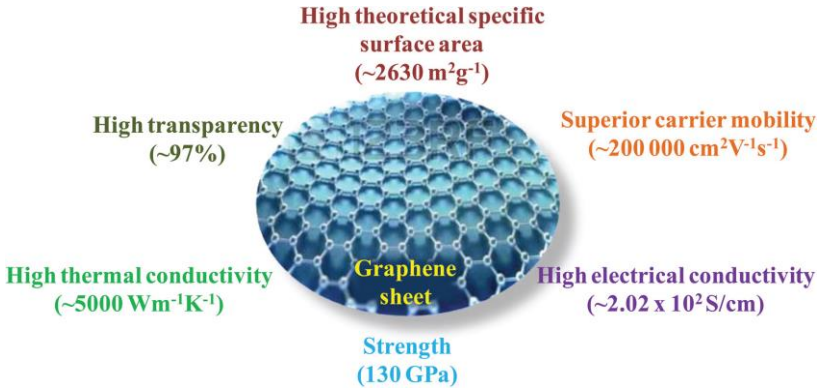

Figure 1. Properities of graphene [1]

This review aims to summarize the current state of graphene-based nanocomposites, a new photocatalyst for degradation of especially non-biodegradable pollutants, and its use in photocatalytic treatment. In addition, future perspectives are discussed at the end of the study.

3. GRAPHENE AND GRAPHENE OXIDE SYNTHESIS METHOD

To date, various methods have been developed for graphene preparation, such as micromechanical exfoliation, epitaxial growth, chemical and electrochemical reduction. In general, these techniques can be separated into to two techniques: the bottom up and top down methods. In bottom-up methods, graphene is synthesized from atoms or molecules by chemical reactions (epitaxial growth). Nevertheless, these methods are not widespread due to their complexity, small amount of production and high cost. The most commonly used method is the method called Hummer method which is based on the chemical reduction of GO. In this method the graphic oxide obtained by the oxidation of natural graphite with strong oxidants ($KMnO_4$, HNO_3 etc.) is exfoliated (Figure 2). Resulting solution is washed in order to remove metal impurities. This exfoliated GO has oxygen-containing groups such as carboxylic, hydroxyl and epoxide functional groups. Oxygen functions in the GO provide reactive sites for nucleation and growth of nanoparticles by interactions with cations. This leads to the rapid growth of various graphene-based composites.

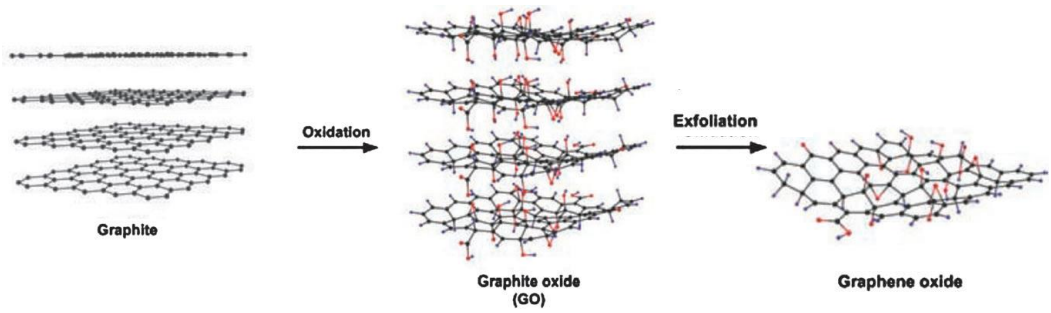

Figure 2. Synthesizing graphene oxide by Hummers' Method [2]

In order to enhance the photocatalytic activity of G and GO, graphene based composite have been synthesized with a variety of metals such as TiO_2, ZnO, SnO_2, Cu_2O, Fe_2O_3, NiO and MnO_2. The most commonly used method for synthesizing graphene based metal composites is in-situ growth strategy. In this method, the metal salt is generally mixed with GO and then the GO-metal composition is formed by reducing the GO. By

adding Ti^{3+}solution to the GO solution, they are deposited at low temperature TiO_2 nanoparticles (Figure 3.a). For example, in the synthesis of Zn-O graphene composites, Zn^{+2} ions adsorbs in graphene oxide layers and converted to ZnO nanoparticles with the addition of NaOH and $NaBH_4$. The nanocomposite is obtained after drying with air at 150°C. Example of TEM Analysis belong to metal doped graphene oxide can be seen on Figure 3.

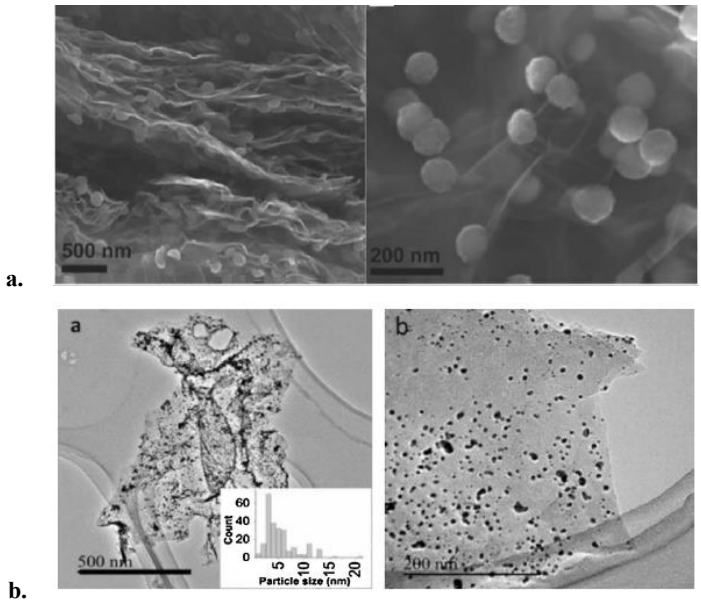

Figure 3. TEM Analysis of a) TiO_2-GO[2] and b) Pd-GO [3]

4. PHOTOCATALICTIC APPLICATIONS ON WATER TREATMENT

Dopping graphene and graphene oxide with metal nanomaterials improves the important properties of graphene and graphene oxide. Adsorption capacity and photocatalytic properties are improved. Also, graphene enlarges the absorption range of the metal from the visible light region. Especially after the water treatment systems, graphene and graphene oxide provides a support material for nanoparticles and avoiding and additional expensive methods for the separation of nanoparticles. In addition, long life-time, easy recycling, extended light absorption range are the other properties of metal doped graphene oxide and graphene.

The photocatalytic degradation mechanism can be shown as in Figure 4. Accordingly, by photocatalytic reduction of oxygen and oxidation of water, reactive oxygen species (ROS) occur under visible light [1]. The resulting ROS species are effective in pollutant degradation. In addition, Fermi energy, which is formed as a result of combining two different materials, metal and graphene, increases the photocatalytic effect by promoting photogenerated electrons and holes[1, 4, 5].

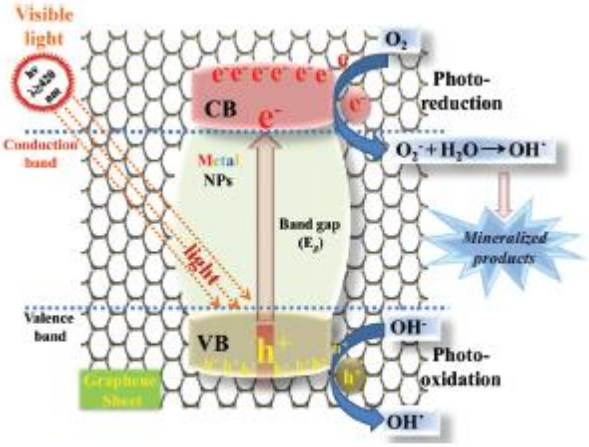

Figure 4. Removal mechanism of Metal doped graphene oxide [1]

Particularly, great numbers of studies are being made to produce solutions against particularly difficult pollutants. Within these technologies, the most researched techniques are catalytic applications. Graphene is named as the rising star in the literature, due to the exceptional feature of graphene. The use of semiconductor photocatalysts with graphene results in improved photocatalytic activity. In this sense, some studies on degradation of organic compounds have been studied in Table 1.

This metal doped graphene oxide has been investigated both for its high adsorption capacity and for the removal of organic matter with its improved light absorption potential. Studies performed under both UV and visible light are shown in Table 1. Both dye and Bisphenol-a are observed to be highly eliminated under visible light.

Table 1. Photocatalytic degradation by metal doped graphene oxides

Composite photocatalyst	**Target Compound**	**Irradiation source**	**Photocatalytic activity**	**Ref**
CdS-Graphene	Methylene Blue	400 W lamp ($\lambda > 500$ nm)	94.5% and 5 h	[5]
TiO_2–GO	Methylene blue	UV light	99% and 15 min	[6]
TiO_2–G	Methylene blue	Sunlight	75%	[7]
TiO_2–x/rGO	Bisphenol a	Visible light irradiation	1 mg/L Bisphenol a - 96% - and 60 min	[8]
RGO/TiO_2/ZnO	Bisphenol a	λ 350-550 nm	99.9% and 3 h	[9]
TiO_2-GO	Butane	Visible light ($\lambda > 420$ nm)	75% and 40 h	[10]
Au- TiO_2–G	Acid blue 92	($\lambda > 574$ nm)	72% and 120 min	[11]
Au–Pd–GO	2-Chlorophenol	Sunlight	100% and 180 min	[12]
Pd–Pt–G	Basic indigo carmine	Visible light ($\lambda > 420$ nm)	70% and 50 min	[13]
Pt–GO/ TiO_2	Methylene blue	LED lamp (8 W, $\lambda > 420$ nm)	93% and 150 min	[14]
Pt/graphene	Rhodamine B	8 W, halogen lamp	70% and 180 min	[15]
AgBr-rGO	Bisphenol a	Visible light	87% and 30 min	[16]
Ag/AgBr/GO	Methylene blue	Visible light	85%	[17]
Ag–Au–GO	4-Nitrophenol	Visible light	100% and 360 s	[18]
Au–G	Methylene blue	Visible light	65% and 7 h	[19]
$Bi_2Fe_4O_9$ /Graphene	Bisphenol a	Visible light	76% and 3 h	[20]

5. FUTURE ASPECTS

In the synthesis of metal dopped graphene and graphene oxide, it should be focused on the investigation of green and environmentally friendly synthesis approaches. In addition, in order for real industrial applications to be possible, many cases still need to be addressed. In particular, high-quality and large-scale production is still difficult.

They have great potential for use as a photocatalyst in environmental applications. Studies have generally been studied in the removal of organic dyes. The effects of the removal of many pollutant materials and the potential removal mechanism are among the issues to be investigated.

Synthesis of metal dopped graphene oxide with excellent photocatalytic activity using green production methods and easy techniques can be a promising area for environmental improvement applications. Therefore, they will be able to solve various wastewater treatment and environmental problems as well as energy problems.

REFERENCES

[1] M.E. Khan, M.M. Khan, M.H. Cho, Recent progress of metal-graphene nanostructures in photocatalysis, Nanoscale, 10 (2018) 9427-9440.
[2] Q. Xiang, J. Yu, M. Jaroniec, Graphene-based semiconductor photocatalysts, Chemical Society reviews, 41 (2012) 782-796.

[3] J. Albero, H. Garcia, Doped graphenes in catalysis, Journal of Molecular Catalysis A: Chemical, 408 (2015) 296-309.
[4] B. Gupta, A.A. Melvin, TiO 2 /RGO composites: Its achievement and factors involved in hydrogen production, Renewable and Sustainable Energy Reviews, 76 (2017) 1384-1392.
[5] M.E. Khan, M.M. Khan, M.H. Cho, CdS-graphene Nanocomposite for Efficient Visible-light-driven Photocatalytic and Photoelectrochemical Applications, J Colloid Interf Sci, 482 (2016) 221-232.
[6] J.C. Liu, H.W. Bai, Y.J. Wang, Z.Y. Liu, X.W. Zhang, D.D. Sun, Self-Assembling TiO2 Nanorods on Large Graphene Oxide Sheets at a Two-Phase Interface and Their Anti-Recombination in Photocatalytic Applications, Adv Funct Mater, 20 (2010) 4175-4181.
[7] K.F. Zhou, Y.H. Zhu, X.L. Yang, X. Jiang, C.Z. Li, Preparation of graphene-TiO2 composites with enhanced photocatalytic activity, New J Chem, 35 (2011) 353-359.
[8] L. Xu, L. Yang, E.M.J. Johansson, Y. Wang, P. Jin, Photocatalytic activity and mechanism of bisphenol a removal over TiO2−x/rGO nanocomposite driven by visible light, Chemical Engineering Journal, 350 (2018) 1043-1055.
[9] E. Bilgin Simsek, B. Kilic, M. Asgin, A. Akan, Graphene oxide based heterojunction TiO 2 –ZnO catalysts with outstanding photocatalytic performance for bisphenol-A, ibuprofen and flurbiprofen, J Ind Eng Chem, 59 (2018) 115-126.
[10] V. Stengl, S. Bakardjieva, T.M. Grygar, J. Bludska, M. Kormunda, TiO2-graphene oxide nanocomposite as advanced photocatalytic materials, Chemistry Central journal, 7 (2013) 41.
[11] S. Ghasemi, S.J. Hashemian, A.A. Alamolhoda, I. Gocheva, S.R. Setayesh, Plasmon enhanced photocatalytic activity of Au@TiO2-graphene nanocomposite under visible light for degradation of pollutants, Mater Res Bull, 87 (2017) 40-47.
[12] G. Darabdhara, P.K. Boruah, P. Borthakur, N. Hussain, M.R. Das, T. Ahamad, S.M. Alshehri, V. Malgras, K.C.W. Wu, Y. Yamauchi, Reduced graphene oxide nanosheets decorated with Au-Pd bimetallic alloy nanoparticles towards efficient photocatalytic degradation of phenolic compounds in water, Nanoscale, 8 (2016) 8276-8287.
[13] B.Z. Kurt, Z. Durmus, A. Durmus, Preparation and characterization of platinum (Pt) and palladium (Pd) nanoparticle decorated graphene sheets and their utilization for the elimination of basic fuchsin and indigo carmine dyes, Solid State Sci, 51 (2016) 51-58.
[14] S. Ye, W.C. Oh, Novel Synthesis and Characterization of Pt-graphene/TiO2 Composite Designed for High Photonic Effect and Photocatalytic Activity under Visible Light, J Korean Ceram Soc, 54 (2017) 28-32.
[15] K. Ullah, S. Ye, L. Zhu, Z.D. Meng, S. Sarkar, W.C. Oh, Microwave assisted synthesis of a noble metal-graphene hybrid photocatalyst for high efficient decomposition of organic dyes under visible light, Mater Sci Eng B-Adv, 180 (2014) 20-26.
[16] F.Y. Chen, W.J. An, L. Liu, Y.H. Liang, W.Q. Cui, Highly efficient removal of bisphenol A by a three-dimensional graphene hydrogel-AgBr@rGO exhibiting adsorption/photocatalysis synergy, Applied Catalysis B-Environmental, 217 (2017) 65-80.
[17] M.S. Zhu, P.L. Chen, M.H. Liu, Graphene Oxide Enwrapped Ag/AgX (X = Br, Cl) Nanocomposite as a Highly Efficient Visible-Light Plasmonic Photocatalyst, Acs Nano, 5 (2011) 4529-4536.
[18] K. Hareesh, R.P. Joshi, D.V. Sunitha, V.N. Bhoraskar, S.D. Dhole, Anchoring of Ag-Au alloy nanoparticles on reduced graphene oxide sheets for the reduction of 4-nitrophenol, Appl Surf Sci, 389 (2016) 1050-1055.
[19] M.E. Khan, M.M. Khan, M.H. Cho, Fabrication of WO3 nanorods on graphene nanosheets for improved visible light-induced photocapacitive and photocatalytic performance, Rsc Adv, 6 (2016) 20824-20833.
[20] Z.T. Hu, J.C. Liu, X.L. Yan, W.D. Oh, T.T. Lim, Low-temperature synthesis of graphene/Bi2Fe4O9 composite for synergistic adsorption-photocatalytic degradation of hydrophobic pollutant under solar irradiation, Chemical Engineering Journal, 262 (2015) 1022-1032.

ICACChE
2nd International Conference on Applications in Chemistry and Chemical Engineering
10 - 14 October 2018 Belgrade

Effect of Fatty Ester-Maleic Anhydride Copolymer Di-Esters on the Crystallization Behavior of Waxy Crude Oil

Marwa R. Elkatory[1], Emad A. Soliman[1], Ahmed I. Hashem[2], Mohamed A. Hassaan[3], Rehab M. Ali[4]

Abstract

Deposition of large aggregated crystals of wax onto the wall of pipelines and tankers at and below the cloud point or wax appearance temperature (WAT) leads to gelation and hence decline the oil flow which is a complex and very costly problem for the petroleum industry. Therefore, the pour point depressants (PPD) are considered a critical processing aid to improve the flow of waxy crude oil. Therefore, maleinzation of fatty acid esters was utilized in this study to synthesize inexpensive and efficient flow improvers. Where fatty acid ester and maleic anhydride were copolymerized in the presence of a free radical generating initiator. The resultant copolymers were then esterified with fatty alcohol ($C_{19}H_{36}O_3$). The copolymers and its esterified form were structurally characterized by FTIR, NMR spectral analysis and scanning electron microscopy. Moreover, the potential interactions between PPD and waxes were investigated by using differential scanning calorimetry (DSC), X-ray diffraction (XRD) and light microscope. The obtained polymeric PPD at a dose of 3000 ppm was able to reduce the pour point of the petroleum waxy crude oil up to 6 ˚C.

Keywords: Pour point depressant; Flow improvers; Copolymerization; Fatty acids, Crystallization of wax; Waxy crude oil.

1. INTRODUCTION

Increasing flowability of waxy crude oil during transferring from reservoirs to pipeline undersea by several ways to mitigate wax deposition and gelation (1) in situ upgrading (2) friction reduction (3) viscosity reduction, the latest solution carry out by several treatments strategist such as; thermal treatment, mechanical treatment, microbial treatments, chemical treatments. Many researches focus on chemical treatment reflected availability and economically to solve this problem and prevent solid wax from crystallization under low pour point temperature. Addition of PPDs is one of the most important methods to eliminate wax precipitation [1], [2].

The PPDs, also known as flow improvers, is often used to lower the gel point/pour point and viscosity of the waxy crude oil to facilitate the crude oil flow through pipeline during transportation [3]. The PPD improves the low-temperature flow properties of waxy crude oils by affecting and changing the morphology and structure of the wax crystals.

[1] *Polymer Materials Research Department, Advanced Technology and New Materials Research Institute, SRTA-City, New Borg El-Arab City 21934, Alexandria, Egypt*
[2] *Chemistry Department, Faculty of Science, Ain Shams University, Cairo, Egypt.*
[3] *National Institute of Oceanography and Fisheries, Marine Pollution Lab, Alexandria, Egypt*
[4] *Corresponding author: Rehab M. Ali, Fabrication Technology Research Department, Advanced Technology and New Materials Research Institute (ATNMRI), City for Scientific Research and Technological Applications, Egypt. Rehabmohamedali1983@gmail.com*

The modification of wax crystallization may help to depress the crude oil's pour point, viscosity and yield stress appreciably, which facilitate the transportation of waxy crude oils [4]-[6]. There are many factors that play an important role in the efficiency of flow improvers and pour point depressants: (1) the number of pendant alkyl branched chains and the length and distance between them are the important factors, (2) the additives solubility, which is generally polymers, in petroleum crude oil, (3) the monomer to monomer ratio should be taken into consideration for additive copolymer, (4) crystalline and amorphous parts of additive are very important in determining its efficiency, (5) physical and chemical stability of additive, (6) prepared polymers are prone to variable molecular weights, (7) monomer mixtures may vary dependent on source and (8) The distributed polymer systems are effectively related to the polydisperse carbon number distributions found in real paraffinic waxy petroleum oil [3].
Soni et al. demonstrated the effect of the structure of maleic anhydride polymers as wax inhibitors on the pour point and viscosity of the paraffinic crude oil. They showed that the more similar the polymer structure (backbone and pendant groups) to the wax components, the better its performance [3], [7]. The PPDs are classified into comb polymers, miscellaneous branched polymers with long alkyl groups, ethylene polymers, and copolymers. These classes of polymers have slightly different characteristics of inhibiting the wax but they similarly function to aggregate and modify the crystal structure. It is important to keep in mind that PPDs are formulated into products with active polymers contained in a solvent. The amount of polymer that can dissolve in a solution is still dependent on the thermodynamic phase behavior of the polymer solution such as the temperature and pressure effects. On the other side, the PPDs with polar crude fractions are often, adsorbing on wax crystal interfaces, modulating crystal–crystal interactions and crystal morphology, and thereby imparting a reduction in pour point values. In the present work, comb-shaped copolymers were produced to evaluate their performance as pour point depressants for Egyptian waxy crude oil. The evaluation was carried out on the Egyptian waxy crude oil via DSC, XRD and photomicrography analysis to study the yield value and wax crystals modification, respectively.

2. MATERIALS AND METHODS

2.1. Materials

Maleic anhydride, oleic acid, octadecanol, p-toluene sulphonic acid, and toluene were obtained as analytical reagents from Aldrich Chemicals and used as received. Benzoyl peroxide was supplied from Acros Organics and was used as an initiator after its recrystallization.

2.2. The additive preparation

2.2.1. *Esterification of the fatty acid;*

Oleic acid esterification was carried out using an excess of the fatty alcohol of molecular formula $C_{18}H_{38}O$ (octadecanol) with a molar ratio R = 18 and concentrated sulfuric acid as a catalyst. The product was neutralized using $NaHCO_3$ solution.

2.2.2. *Copolymerization*

The pre-prepared n-alkyl esters were copolymerized with maleic anhydride in toluene using benzoyl peroxide as initiator (1 % w/w) at 90°C for 20 h with constant stirring. After the completion of the reaction, the copolymer was precipitated in the petroleum ether 40-60 [8].

2.2.3. *Esterification of copolymers*

The obtained copolymers were esterified with octadecanol. The esterification process was carried out at 145-150°C for 15 h after which the temperature was slowly raised to 160-165°C towards the end of the reaction by removing xylene by distillation [3].

2.3. Additive characterization

2.3.1. Infrared spectroscopic analysis

The structure of the prepared poly (n-alkyl oleate-*co*-succinic anhydride) (PAOCOSA) and its esterified form, (EPAOCOSA), was confirmed by using (FTIR Shimadzu 8400S spectrometer, Japan) to compare it and ensure the completion of the esterification process.

2.3.2. Proton nuclear magnetic resonance (^1H NMR) spectroscopic analysis

Proton nuclear magnetic resonance spectra of PAOCOSA and EPAOCOSA were obtained using (JEOL 500 MH NMR spectrometer, Japan) at 500.2 MHz. The samples were dissolved in deuterated chloroform $CDCl_3$ and analyzed by a 5 mm ^{13}C–^1H dual probe head at 25°C. The spectra were accumulated into 32 K data points and processed using exponential multiplication with 2 Hz line broadening into 128K spectra. For the resulting spectra, 25000–35000 scans were accumulated. All spectra were accumulated under identical conditions using power gated Waltz decoupling with 25-degree measurement pulse and 1s pre-pulse delay [9].

2.4. Additive evaluation

2.4.1. Pour point measurements

Solutions of the synthesized PAOCOSA in xylene containing 10% active material were prepared with different concentrations. The solutions were injected into the crude oil at 60°C [10], then subjected to pour point test according to the American Society for Testing and Materials (ASTM) D97.

2.4.2. Crystallization behavior

The effect of the produced PAOCOSA co-polymer on the crystallization behavior was determined using the following tests:

a- Differential Scanning Calorimetry (DSC)

DSC studies were performed in aluminum sealed pans using (TAQ200 Universal Analysis Instrument) V4.3A. About 1 mg of the sample was cooled from 30 to -80 °C under a nitrogen atmosphere.

b- X-ray diffraction

A graphite monochromator selected CuKα radiation. The sample was placed in the sample holder with a scanning rate of 4 °C/min over a 2θ range from 4 to 70°. Data were collected on each sample using a step size of 0.02°.

c- Photomicrography

The morphological features of the paraffin wax crystals present in the untreated and crude oil sample that is treated with the synthesized additives at 3000 ppm concentrations have been recorded using (Olympus BH2-UMA microscope attached with Canon photometric high resolution automatic digital camera). The light source was a helium lamp. The temperature of the tested crude oil samples was controlled on the microscope slide by an attached cooling thermostat. A drop of crude oil was placed on the slide, and the sample was observed under a cooling rate of 10 ºC/min. The microscope was adjusted until a clear observation can be conducted. The cooling process was discontinued after the observation. The adapted magnification was 100× [8], [9].

3. RESULTS AND DISCUSSION

The comb-like PAOCOSA production was carried out according to the following three steps of scheme 1

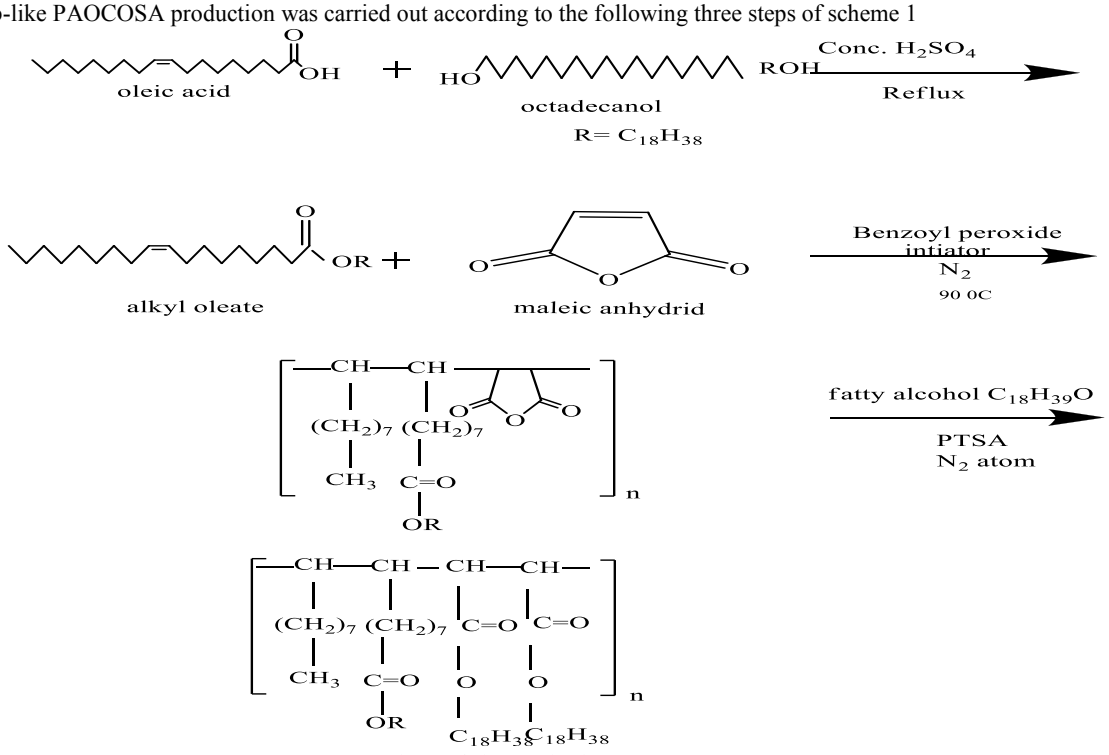

Figure 1. Scheme of oleic acid polymerization

The produced copolymer was used as an additive for a waxy crude oil of the physical properties summarized in Table 1.

Table 1. Physical characteristics of Alamin crude oil

Physical parameters	Method	Values
Pour point (ºC)	ASTMD- 97	24
Density (g/cm^3)	ASTMD-1298	0.8180
API gravity (º)	ASTMD-1298	41.38
Wax content (%)	UOP46	12.40
Asphaltene (%)	ASTMD- 6560	1.32

3.1. Additive Characterization

3.1.1. Infrared spectral analysis

The IR spectrum of the prepared PAOCOSA and EPAOCOSA is presented in Figure 1. The spectrum showed mutual absorption bands at about 665, 1258, 1427, and 1696 cm^{-1}, which may be attributed to (CH_2) n, C–O, CH_2, and C=O vibrational modes, respectively. In case of PAOCOSA, absorption bands at 2891.39 cm^{-1} and this may be related to stretching vibration of C-H bonds of the paraffinic methylene groups. Furthermore, in the case of EPAOCOSA analysis, the adsorption intensity for such bands can indicate the formation of the n-alkyl oleate-co-di-ester. Moreover, absorption bands of CH symmetric and CH asymmetric stretch appeared at 2862.8, and 3028.34 cm^{-1} respectively [9], [11], [12].

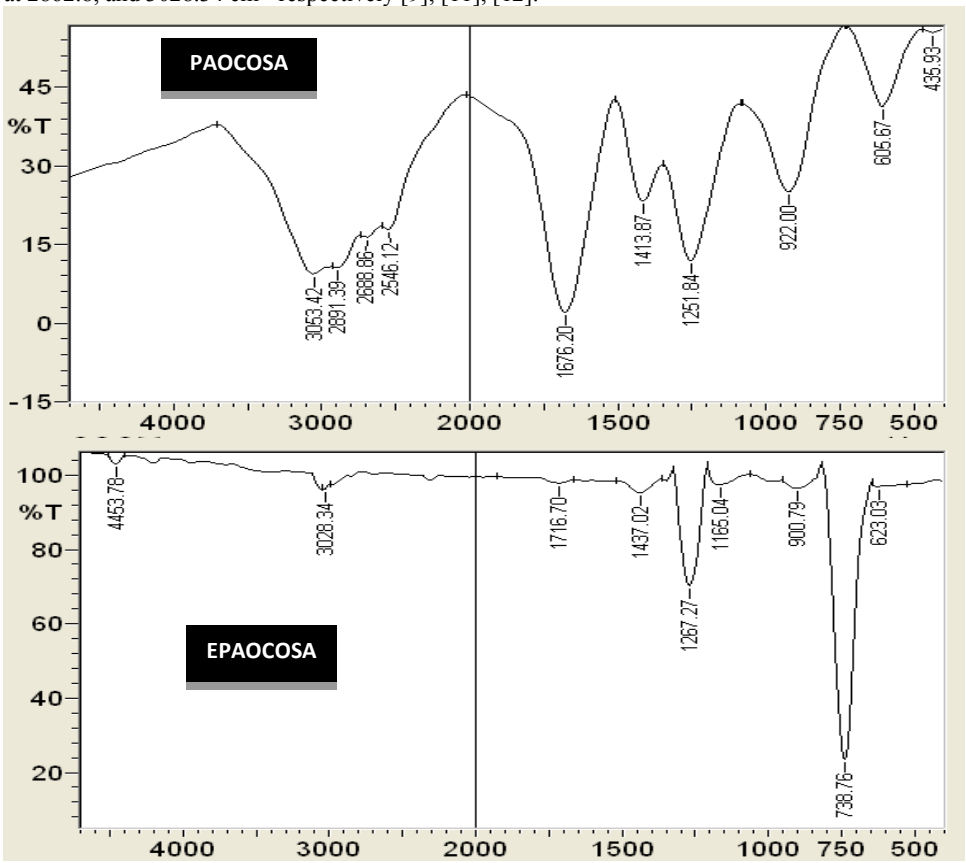

Figure.1. IR Spectrum of PAOCOSA and EPAOCOSA

3.1.2. Proton Nuclear Magnetic Resonance Spectroscopic Analysis

Representative ^{1}H NMR patterns of PAOCOSA and EPAOCOSA are shown in Figure 2. The PAOCOSA peaks assignments were as follows: δ at 1.2, 1.23, 2.47, 4.0 and 6.24 ppm is for CH_3, CH_3–CH_2–$(CH_2)_5$–, –CH_2–$(CH_2)_5$–CH_2–, –CH_2–CH_2– $(CH_2)_n$–and–$(CH_2)_5$–CH_2–(C=O)– protons respectively. However, the pattern of EPAOCOSA exhibited signals at 2.5, 3.336 and 3.37 ppm which are related to –CH– from maleic

anhydride that proves co-polymerizing maleic anhydride with fatty esters. Whereas, δ at 1.20 and 1.35 ppm ascribed to pendant methylene groups of octadecyl moiety.

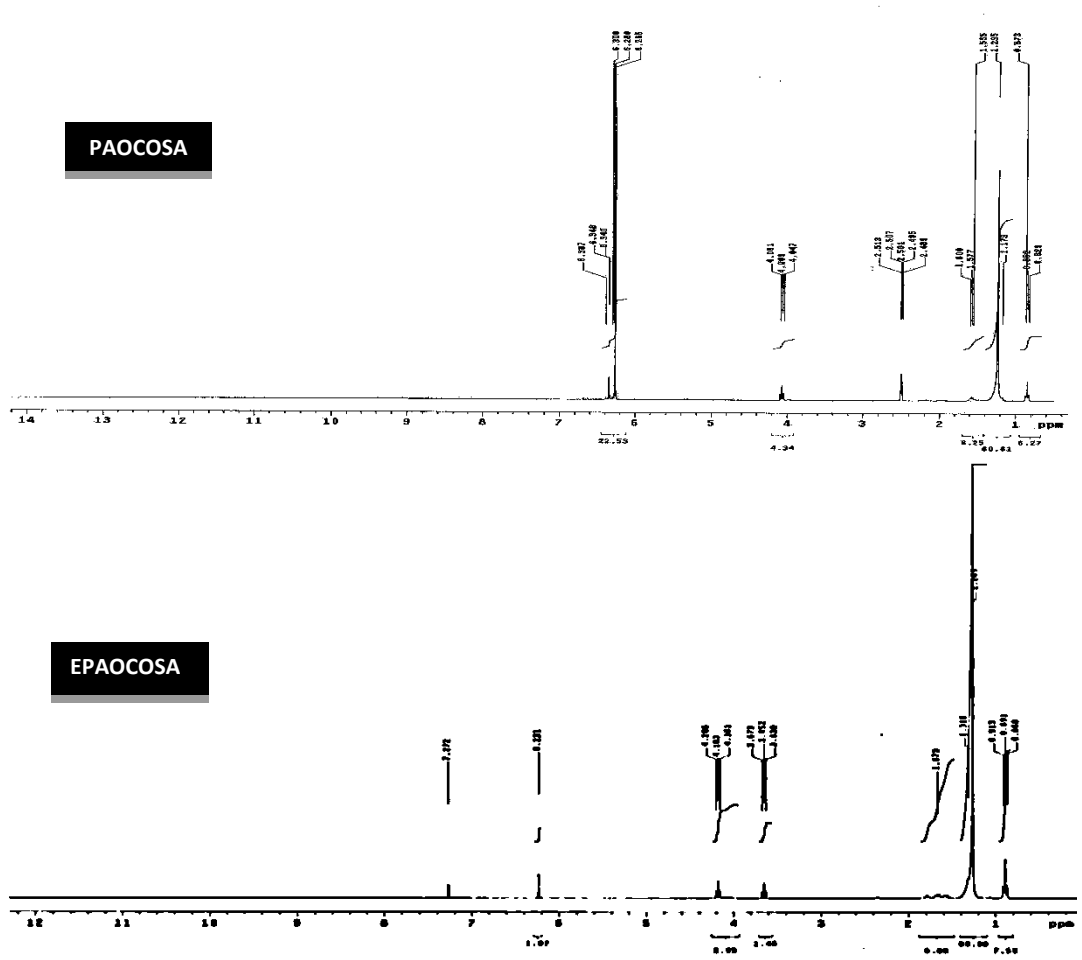

Figure 2. H[1]NMR Spectrum of PAOCOSA and EPAOCOSA

3.2. Evaluation Of The Additive

3.2.1. pour point

As indicated in Table 2, polymeric additive based on EPAOCOSA has long carbons chain (n = 18) and has high potency to reduce pour point of crude oil from 24°C to 6 °C, i.e. pour point depression was 18°C. The pour point values decreased gradually with increasing the concentration of this additive up to 3000 ppm. This can be explained on the basis of tethering such polymeric additive with the paraffin wax and hence hinder the formation of their crystals. However, there is no depression in pour point at higher concentration of EPAOCOSA. This can be attributed to the sideways growth of wax crystals that becomes so much more complicated [5].

Table 2: Effect of concentration of polymeric additives on the pour point of the crude oil.

Additive	Pour point (˚C) of crude oil by using different additive concentration (ppm)						Pour point depression (˚C)
	Blank	500	1000	2000	3000	5000	
EPAOCOSA	24	24	21	18	6	6	18

3.2.2. Crystallization Behavior

a. Thermal analysis (DSC)

DSC analysis of untreated and treated paraffin crystals was shown in Table 3. It was indicated that treating the paraffin by EPAOCOSA additive at a concentration of 3000 ppm leads to shifting the DSC thermogram of wax to lower temperatures where the melting point and the peak temperature of paraffin mixtures decreased when they were treated with PPD. The area of the peak displays a declining tendency, which means that crystallizing processes have occurred when the mixture was continually cooling.

Table 3. Data analysis of DSC

Sample	Onset (ºC)	Peak (ºC)	Endset (ºC)	ΔH (J g-1)
Wax untreated	47.28	40.09	36.18	-6.69
Wax + EPAOCOSA	8.29	2.65	-0.56	-2.55

b. X-ray diffractometry (XRD)

Figure 3 represented the X-ray diffractograms of untreated paraffin wax and treated with EPAOCOSA. These patterns show that the peaks due to crystalline structure appeared at 2θ ≈21.0068 and 23.37 for both of untreated wax and its counterpart treated by EPAOCOSA. Moreover, XRD patterns show that the degree of crystallinity of the untreated wax is higher than that for the paraffin wax treated by EPAOCOSA at a dose of 3000 ppm.

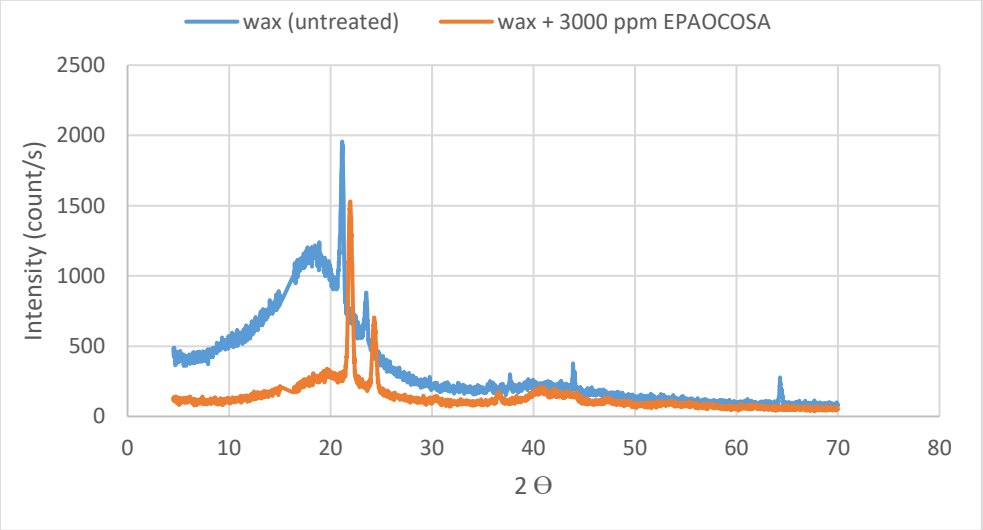

Figure 3. X-ray diffractograms of untreated paraffin wax from crude oil and its corresponding treated by 3000 ppm EPAOCOSA.

c. Light microscopy

The light microscope was used to study the wax crystal morphologies without and with an incorporation of the EPAOCOSA additive, which is significantly correlated with the cold flowability of the crude oils and to confirm the other laboratory tests. Photographs of paraffin crystals from waxy heavy crude oil either untreated or that treated with polymeric additives EPAOCOSA at dosage 3000 ppm is shown in Figure 4. In the case of the untreated wax, in some places the crystals seemed to grow simultaneously from a nucleation site tend to pile upon each other, resulting in agglomeration of crystals. The agglomeration of individual crystals was even more severe, providing sparse large agglomerated crystals. It is found that the morphology of paraffin crystals is obviously changed by adding polymeric PPDs; EPAOCOSA. The change of paraffin crystals to smaller particles, and thus agglomerates of paraffin crystals are disappeared. Thereby, the dissipated energy was reduced and the flowability of the oil was improved. The sizes of paraffin crystals in crude oil were reduced and were not connected to each other and the distribution of paraffin crystals was improved.

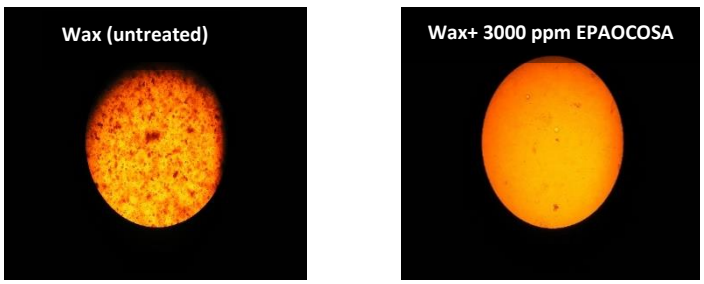

Figure 4. Micrograph of untreated paraffin wax and paraffin wax treated by 3000 ppm EPAOCOSA at room temperature.

4. CONCLUSION

In this study, comb-like copolymer esters were successfully synthesized by esterification of pure fatty acid of oleic acid with the fatty alcohol to form the alkyl ester which is then copolymerized with maleic anhydride, the produced copolymer esterified to form branched copolymer esters. Potential feasibility of these copolymer esters as pour point depressants was investigated by studying its impact on the crystallization of paraffin wax and cold flowability of petroleum waxy crude oil. Findings of DSC, XRD, and light microscope exhibited that EPAOCOSA reduces the paraffin crystallization temperature and enthalpies that lead to inhibit the formation of a layer structure of paraffin wax and intensify the growth of microscopic paraffin crystals. The maximum pour point depression of the crude oil (ΔPP) was 18°C that achieved by using 3000 ppm of EPAOCOSA. This depression was associated with decreasing the paraffin crystal size and suppressing the formation of crystal platelets.

REFERENCE

[1] A. M. Atta, R. A. El-Ghazawy, F. A. Morsy, M. S. A. Ali, and A. Elmorsy, "Synthesis and characterization of polymeric additives and their effect on flow properties of waxy Egyptians crude oil", *Global Journal of Science Frontier Research Chemistry*, vol. 13, pp. 21–27, 2013.

[2] O. P. Akinyemi, J. D. Udonne , V. E. Efeovbokhan, and A. A. Ayoola, "A study on the use of plant seed oils, triethanolamine and xylene as flow improvers of Nigerian waxy crude oil", *Journal of Applied Research and Technology,* vol. 14, pp. 195–205, 2016.

[3] H. P. Soni, and D. P. K. Bharambe, "Performance-based designing of wax crystal growth inhibitors", *Energy Fuels*, vol. 22, pp. 3930–3938, 2008.

[4] D. Chanda, A. Sarmah, A. Borthakur, K. V. Rao, B. Subrahmanyam, and H. C. Das, "Combined effect of asphaltenes and flow improvers on the rheological behaviour of Indian waxy crude oil", *Fuel,* vol. 77, pp. 1163–1167, 1998.

[5] A. L. C. Machado, E. F. Lucas, and l. G. Gonza, "Poly (ethylene-co-vinyl acetate) (EVA) as wax inhibitor of a Brazilian crude oil: oil viscosity, pour point and phase behavior of organic solutions", *J. Pet. Sci. Eng.,* vol. 32, pp. 159–165, 2001.

[6] K. G. Paso, and H. S. Fogler, "Bulk stabilization in wax deposition systems", *Energy Fuels,* vol. 18, pp. 1005–1013, 2004.

[7] H. P. Soni, B. Kiran, K. S. Agrawal, A. Nagar, and D. P. Bharambe, "Designing maleic anhydride-a-olifin copolymeric combs as wax crystal growth nucleators", *Fuel Process Technol,* vol. 91, pp. 997–1004, 2010.

[8] A. M. Al-Sabagh, S. H. El-Hamouly, T. T. Khidr, R. a. El-Ghazawy, and Sh. a. Higazy, "Preparation the Esters of Oleic Acid-Maleic Anhydride Copolymer and Their Evaluation as Flow Improvers for Waxy Crude Oil", *Journal of Dispersion Science and Technology,* vol. 34, pp. 1585–96, 2013.

[9] E. A. Soliman, M. R. Elkatory, A. I. Hashem, and H. S. Ibrahim, "Synthesis and Performance of Maleic Anhydride Copolymers with Alkyl Linoleate or Tetra-Esters as Pour Point Depressants for Waxy Crude Oil", *Fuel,* vol. 211, pp. 535–547, 2018.

[10] A. M. Al-Sabagh, M. W. Sabaa, G. R. Saad, T. T. Khidr, and T. M. Khalil, "Synthesis of Polymeric Additives Based on Itaconic Acid and Their Evaluation as Pour Point Depressants for Lube Oil in Relation to Rheological Flow Properties", *Egyptian Journal of Petroleum,* vol. 21, pp. 19–30, 2012.

[11] D. A. Kamel, H. A. Farag, N. K. Amin, A. A. Zatout, and R. M. Ali, "Smart utilization of jatropha (Jatropha curcas Linnaeus) seeds for biodiesel production: Optimization and mechanism", *Industrial Crops & Products,* vol. 111, pp. 407–413, 2018.

[12] R. M. Ali, H. A. Hamad, M. M. Hussein, and G. F. Malash, "Potential of using green adsorbent of heavy metal removal fromaqueous solutions: Adsorption kinetics, isotherm, thermodynamic, mechanism and economic analysis", *Ecological Engineering,* vol. 91, pp. 317–332, 2016.

ICACChE
2nd International Conference on Applications in Chemistry and Chemical Engineering
10 - 14 October 2018 Belgrade

Krom (Cr) Katkılı CdZnS Nanoparçacıkların Sentezi ve Karakterizasyonu

Arzu Ekinci[1], Sabit Horoz[2], Ömer Şahin[3]

[1]*Siirt Üniversitesi Sağlık Yüksek Okulu, 56100 Siirt, aekinci@siirt.edu.tr*
[2]*Siirt Üniversitesi Müh. Mim. Fakültesi Elektrik ve Elektronik Bölümü, 56100 Siirt, sabithoroz@siirt.edu.tr*
[3]*Siirt Üniversitesi Müh. Mim. Fakültesi, Kimya Mühendisliği Bölümü, Siirt University, 56100 Siirt, omersahin@siirt.edu.tr*

Özet

II-VI grup bileşiklerine dayanan hetero-yapıların, uzun optik fotovoltaik cihaz uygulamaları için, yüksek optik absorpsiyon katsayıları nedeniyle, uygun materyaller oldukları uzun süredir bilinmektedir. Grup II-VI bileşikleri, hetero-bileşimli fotovoltaik cihazların imalatı için malzeme olarak kullanılabilen tüm alaşım bileşimi aralığı ve yüksek emme katsayıları üzerinde doğrudan bir temel bant aralığı ataması ile üçlü ve dörtlü alaşımlar oluşturabilir.

Kadmiyum çinko sülfür (CdZnS) ince filmler, heterojunction güneş hücrelerinde ve foto iletken cihazlarda geniş bant aralığı (2.4 -3.7 eV) pencere malzemesi olarak yaygın şekilde kullanılmaktadır. CdS filmlerinin etkili olduğu kanıtlanmış olan güneş pili sistemlerinde, CdS'nin daha yüksek bandgap üçlü CdZnS ile değiştirilmesi, pencere emilim kayıplarında bir azalmaya yol açmıştır ve solar hücrede kısa devre akımında bir artışa neden olmuştur. Bununla birlikte, CdZnS filmlerinin direnci, çinko bileşimi ile hızla artar. Kompozisyonun özdirencin bağımlılığının CdZnS katı çözelti sisteminin temel bir özelliği olduğu ve hazırlama yöntemiyle kayda değer bir şekilde değiştirilmediği açıktır. CdZnS filmlerin bu yüksek direnci, çoğu heterojunction cihazda bir pencere malzemesi olarak kullanımını sınırlandırmıştır.

Bu çalışmada, oda sıcaklığında saf CdZnS ve krom (Cr) katkılı CdZnS nanopartikülleri kimyasal çökeltme ile sentezlenecektir. Bir X-ışını kırınım cihazı kullanılarak sentezlenmiş nanopartiküllerin yapısal özellikleri incelenecektir. Ayrıca, Cr katkılı CdZnS nanopartiküllerin büyüklüğü, elde edilen XRD verileri kullanılarak hesaplanacaktır. Katkılı CdZnS nanopartiküllerin enerji bandı aralığı UV-Vis spektroskopisi kullanılarak belirlenecektir. Böylece Cr katkısının CdZnS'nin yapısal ve optik özelliklerini nasıl etkilediği incelenecek ve elde edilen veriler yorumlanacaktır.

Anahtar Kelimeler: Nanopartiküller, II-VI bileşikleri, sentez, karakterizasyon, doping

Abstract

Hetero-structures based on II-VI group compounds have long been known to be suitable materials for thin-film photovoltaic device applications because of their high optical absorption coefficients. Group II-VI compounds can form ternary and quaternary alloys with a direct fundamental band gap assignment over the entire alloy composition range and high absorption coefficients, which can be used as materials for fabricating hetero-junction photovoltaic devices. Cadmium zinc sulfide (CdZnS) thin films have been widely used as a wide band-gap (2.4 -3.7 eV) window material in heterojunction solar cells and in photoconductive devices. In solar cell systems, where CdS films have been demonstrated to be effective, the replacement of CdS with the higher bandgap ternary CdZnS has led to a decrease in window absorption losses and has resulted in an increase in the short circuit current in the solar cell. However, the resistivity of CdZnS films increases rapidly with the composition of zinc. It is evident that the composition dependence of resistivity is a basic property of the CdZnS solid–solution system and is not appreciably altered by the method of preparation. This high resistivity of CdZnS films limited their utilization as a window material in most heterojunction devices.

In this study, pure CdZnS and chromium (Cr) doped CdZnS nanoparticles at room temperature will be synthesized by chemical precipitation. The structural properties of synthesized nanoparticles using an X-ray diffraction device will be investigated. Furthermore, the size of Cr doped CdZnS nanoparticles will be calculated using the obtained XRD data. The energy band gap of the doped CdZnS nanoparticles will be determined using UV-Vis spectroscopy. Thus, how the Cr dopant affects the structural and optical properties of CdZnS will be examined and the resulting data interpreted.

Keywords: Nanoparticles, II-VI compounds, synthesis, characterization, doping

[1]*Corresponding author: Siirt Üniversitesi Sağlık Yüksek Okulu, 56100 Siirt, aekinci@siirt.edu.tr*
[2]*Siirt Üniversitesi Müh. Mim. Fakültesi Elektrik ve Elektronik Bölümü, 56100 Siirt, sabithoroz@siirt.edu.tr*
[3]*Siirt Üniversitesi Müh. Mim. Fakültesi, Kimya Mühendisliği Bölümü, Siirt University, 56100 Siirt, omersahin@siirt.edu.tr*

1. GİRİŞ

Son yirmi yıldır, II-VI yarıiletken ince filmler, güneş pili ve diğer opto-elektronik cihazların imalatında geniş kullanımları nedeniyle araştırma alanlarında büyük ilgi görmüştür. Özellikle, güneş pillerinin üretiminde etkin kullanım için kadmiyum sülfide (CdS) çok ilgi gösterilmiştir [1,2]. Düşük bant aralığı nedeniyle CdS, pencere katmanı güneş spektrumunun mavi bölümünü emer ve bu da güneş hücrelerinin akım yoğunluğunun azalmasına neden olur [3,4].

Bir güneş pili cihazının yüksek performansı için uygun bir pencere materyalinin kullanılması gerekir. CdZnS CdS'den daha büyük bir bant boşluğuna, CdS ve ZnS arasındaki özelliklere ve CdS ile karşılaştırıldığında 2,4-3,7 eV'luk geniş bir enerji bandı aralığına sahip olduğundan, CdS yerine CdZnSnanopartiküllerin pencere katmanıolarak kullanılması, kuaterner solar emici tabaka ile ilişkili olan kafes uyumsuzluk problemlerinin yanı sıra pencere emme kayıplarını önlemek için uygundur [5,6].

Bununla birlikte, bir pencere tabakası olarak CdZnS ince filmin kullanılması, aynı zamanda, kafes parametrelerini değiştiren bileşik içindeki çinko konsantrasyonundaki değişime bağlı olarak merak edici bir ilgi sunmaktadır. Dahası, daha yüksek bir çinko konsantrasyonu, levha direncini arttırmaya yardımcı olan yüksek dirençli bir malzemeye yol açar [7].CdZnS nanopartiküller kimyasal banyo çökeltme [8], vakumlu buharlaştırma (CBD), kimyasal sprey piroliz [9] ve ardışık iyonik katman emme ve reaksiyon (SILAR) gibi çeşitli yöntemlerle ince filmlerin hazırlanmasına odaklanmıştır.

Metal katkılamanın alaşım bileşenlerinde kusurları azaltması nedeniyle krom (Cr) katkılı CdZnS nanopartiküller ve CdZnS nanopartiküllerin üretimi için kimyasal çökertme tekniğinin uygulanması ilk kez bu çalışmada mevcuttur. Sentezlenen saf CdZnSnanopartikülleri ve Cr katkılı CdZnS nanopartiküllereait yapısal ve optik özellikler sırasıyla x- ray kırınımı (XRD) ve optik absorpsiyon ölçümleri yapılarak incelendi.

2. MATERYAL VE METOT

CdZnS nanopartiküllerve Cr katkılı CdZnSnanopartiküller oda sıcaklığında kimyasal çökertme tekniği ile sentezlendi. Kadmiyum klorür ($CdCl_2$), Çinko klorür ($ZnCl_2$), Sodyum sülfür (Na_2S) ve krom hegzahidrat(Cr) sırasıyla Cd, Zn, S ve Cr iyon kaynağı olarak kullanıldı.

Bu çalışmada, Kimyasal çökertme yöntemi ile,1,61 gr kadmiyum klorür ($CdCl_2$), 0,62 gr sodyum sülfür ve %1 çinko klorür ($ZnCl_2$)'den meydana gelmiştir ve 100 mL damıtılmış su içeren bir beherde karıştırılarak çözündürüldü. Homojen bir karışım elde etmek için karıştırma işlemi yaklaşık 1 saat sürdürüldü ve daha sonra süzme işlemi ve kurutma işlemi yapıldı. Cr katkılı CdZnS ince filmi de aynı yöntemle yukarıda belirtilen çözeltiye %1 Cr eklenmesi ile hazırlandı. [5].

Filmlerin yapısal ve optik özellikleri detaylı olarak incelenmiştir. Filmleri yapısal özellikleri; X-ışını kırınım ölçümleri 2θ = 20–60°C aralığında Cu Kα radiation, kaynağına sahip bir cihaz kullanılarak elde edildi. Optik soğurma ölçümleri için UV-Vis- spektroskopisi kullanıldı.

3.ANALİZLERİN YORUMU

3.1.Yapısal Özellikler

Saf ve krom (Cr) katkılı CdZnS nanopartiküllerinin XRD modelleri Şekil 1'de gösterilmiştir. Kırınım noktalarının sırasıyla, (111), (220), (311) kafes düzlemleriyle açıkça indekslenir ve buda sentezlenen nanoparçacıkların kübik yapıya sahip olduğunu gösterir [10].

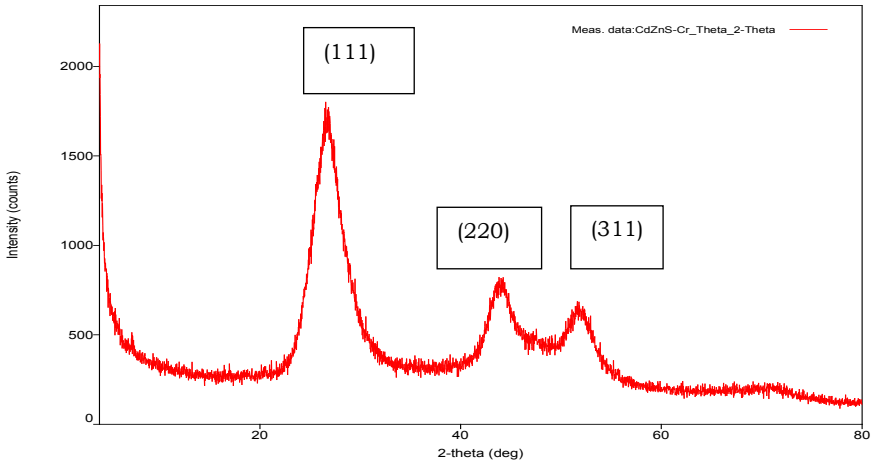

Şekil 1. Cr katkılı CdZnS nanopartiküle ait XRD kırınım desenleri.

Piklerin atamaları JCPDS verileriyle karşılaştırılarak yapılır [11]. Cr katkılı CdZnS (1%) nanopartikülü için ortalama kristalit büyüklüğü Scherer formülü kullanılarak hesaplanmıştır.

$t = 0.9\,\lambda / (\beta \cos\theta)$ (1)

Burada t: nanopartikülün ortalamaboyutu, λ: x-ışınınındalgaboyu, β: radian olarak yarı yükseklikteki tam genişliği (FWHM) ve θ: Bragg'ın difraksiyon açısıdır. Cr katkılı CdZnS nanopartiküllerinin ortalama kristalit boyutu 2-3 nm aralığında hesaplandı.

3.2. Optik Özellikler

CdZnS ve Cr katkılı CdZnS nanopartiküllerininabsorpsiyon spektrumları 300-700 nm aralığında ölçüldü; Filmlerin absorpsiyon spektrumuna dayanan optik bant aralığı Şekil 2'de gösterilmiştir.

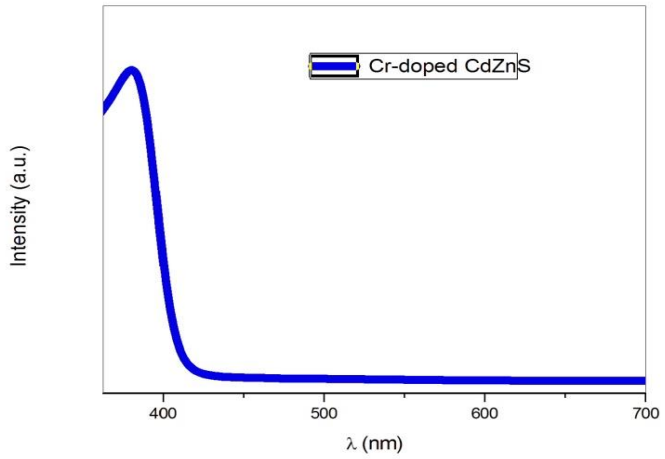

Şekil 2. Cr katkılı CdZnS ve saf CdZnS nanopartiküllere ait optik absorpsiyon spektrumu.

Absorbans tepe pozisyonundan bant aralığı ölçümü, sadece ortalama bant boşluğunun ölçüsünü verir [11]. Elde edilen Şekle göre, Cr katkılı CdZnS nanopartiküllerin absorbsiyon dalga boyu 380.9 nm olarak belirlenmiştir. $E_g = 1240 / \lambda_{absorpsiyon}$ denklemi kullanılarak, Cr katkılı CdZnS nanopartiküller için enerji bant aralığı (E_g) değeri 3,25 eV olarak hesaplanmıştır. Önceki çalışmamızda [12], oda sıcaklığında sentezlenen Cr katkılı CdZnS nanopartikülleri için Eg değeri, aynı yöntem kullanılarak 3.2 eV olarak hesaplandı. Yani Cr katkılı CdZnS nanopartikülleri için elde edilen enerji bandı boşluk değerinin CdZnS nanopartiküllerinden daha yüksek olduğu gözlenmiştir. Cr-katkı materyalinin CdZnS nanopartiküllerin enerji bandı boşluğunu arttırmak için etkili bir faktör olduğu söylenebilir.

4. SONUÇ

Bu çalışma da, kimyasal çökertme tekniği ile oda sıcaklığında hazırlanan saf ve Cr katkılı CdZnS nanopartiküllerinin yapısal ve optik özellikleri sırasıyla x- ray kırınımı (XRD ve UV-Vis ölçümleri yapılarak incelendi. CdZnS ve CdZnS: Crnanopartiküllerinin bant aralığı, 3.91 eV ve 3.2 eV arasında hesaplanmıştır. Cr katkı maddesinin enerji bant aralığını ddeğişştirdiğini söyleyebiliriz. Cr katkılı CdZnSnanopartilünün herhangi bir safsızlık fazı olmayan kübik yapıya sahip olduğu ve kristal boyutu 2-3nmaralığında olduğu hesaplandı. CdZnS nanopartiküllerine Cr ilavesi ile kristalit boyutu artmış, enerji band aralığı düşmüştür.

KAYNAKLAR

[1]. J.R. Tuttle, J.S. Ward, A. Duda, T.A. Berens, M.A. Contreras, K.R.Ramanathan, A.L. Tenant, J. Keane, E.D. Cole, K. Emergy, R. Noufi,Spring MRS Meeting, San Francisco, (1997), p. p. 12.
[2]. T. Ohashi, K. Inakoshi, Y. Hashimoto, K. Ito, Sol. Energy Mater. Sol. Cells50 (1998) 37.
[3]. J. Zhou, X. Wu, G. Teeter, B. To, Y. Yan, R.G. Dhere, T.A. Gessert, Phys.Stat. Sol. (b) 241 (2004) 775.
[4]. S. Chavhan, R.P. Sharma, J. Phys. Chem. Solids 66 (2005) 1721.
[5]. T. Yamaguchi, Y. Yamamoto, T. Tanaka, A. Yoshida, Thin Solid Films 343 (1996) 516.
[6]. L.C. Burton, T.L. Hench, Appl. Phys. Lett. 29 (1976) 612.
[7]. L. P. Deshmukh et al Indian J. Pure Appl. Phys. 35(1997) 428
[8]. A.P. Alivisatos, J. Phys. Chem. 100 (1996) 13226–13239.
[9]. T. Gruszecki, B. Holmstrom, Sol. Ener. Mater. Sol. Cells 31(1993) 227
[10]. X. Wu, Sol. Energy, 77(2004) 803–814.
[11]. G. Sharma, P. Chawl, S. P. Locha, N. Singh, *Radiat. EffectsDefectsSolids,* 164(2009) 763
[12]. https://link.springer.com/article/10.1007/s10854-017-8406-0

ICACChE
2nd International Conference on Applications in Chemistry and Chemical Engineering
10 - 14 October 2018 Belgrade

PbS ve Fe Katkılı PbS İnce Filmlerin Özelliklerinin Karşılaştırılması

Arzu Ekinci[1], Sabit Horoz[2], Ömer Şahin[3]

Özet

Yarı iletken ince film malzemelerinin kalitesini iyileştirmenin en etkili yöntemlerinden biri, metal iyonlar ile ince filmlerin katkılanmasıdır. İnce filmin kristal yapısı, yüzey morfolojisi ve parçacık boyutu katkılama ile kontrol edilebilir. Böylece sentezlenmiş ince filmlerin kimyasal ve fiziksel özellikleri sentez sırasında geliştirilebilir. Farklı çalışmaların yarı iletken ince filmler ürettiği gerçeğine rağmen, mükemmel fiziksel ve kimyasal özelliklere sahip yüksek kaliteli nanoyapılı PBS ince filmlerin sentezlenmesi konusunda hala bir eksiklik söz konusudur. Katkılama işlemindeki en önemli parametrelerden biri, baz metal ve alaşım metal arasındaki kafes eşleşmesidir. Örneğin, Fe iyonik yarıçapı Pb iyonik yarıçapından daha küçüktür. Böylelikle, PbS kafesine kolaylıkla katkılanmış Fe metal iyonları zorlanmaksızın etkileşime girebilir.

Bu çalışmada, PbS ve Fe-katkılı PbS ince filmleri, oda sıcaklığında cam yüzeyler üzerinde maliyet için uygun olan kimyasal banyo çökeltme (CBD) tekniği ile sentezlenmiştir. Sentezlenen ince filmlerin yapısal ve optik özellikleri, X ışını kırınımı (XRD) ve optik absorpsiyon ölçümleri ile karakterize edildi. Fe katkısının PbS yapısını değiştirmemesine rağmen PbS'nin kristal boyutu ve enerji bandı boşluğunu değiştirdiği gözlenmiştir.

Anahtar Kelimeler: İnce filmler, kimyasal banyo çökeltme, optik özellikler, parçacık boyutu

Abstract

One of the most effective methods of improving the quality of semiconductor thin film materials is the alloying of thin films with metal ions. The crystal structure, surface morphology and particle size of the thin film can become controllable by the alloying. Thus, the chemical and physical properties of the synthesized thin films are improved during synthesis. Despite the fact that different studies have produced semiconductor thin films, there is still a shortage to synthesize high quality nanostructured PbS thin films with excellent physical and chemical properties. One of the most important parameters in the alloying process is the lattice matching between the base metal and the alloying metal. For example, the ionic radius of Fe is smaller than the ionic radius of Pb. Thus, it is possible to be easily alloyed Fe metal ions into the PbS lattice with out difficulty. Investigations on the structural, optical and morphological properties of Fe-alloyed PbS thin films have been limited and the photovoltaic properties of Fe-alloyed PbS thin films will be investigated for the first time.

In this study, PbS and Fe-alloyed PbS thin films were synthesized by chemical bath deposition (CBD) technique, which is suitable for cost on glass substrates at room temperature. The structural, elemental and optical properties of the synthesized thin films were characterized by X-ray diffraction (XRD), energy dispersive X-ray (EDX) and optical absorption measurements, respectively. It was observed that Fe dopant alters crystal size and energy bandgap of PbS although it does not change the structure of PbS.

Keywords: Thin films, chemical bath deposition, optical properties, particle size

1. GİRİŞ

Farklı yüzeylerde ve geniş alanlarda sentezlenebilen metal chalcogenide materyalleri son zamanlarda ince film teknolojisinde büyük ilgi görmüştür [1, 2]. Bu malzemeler arasında, kurşun sülfür (PbS), IV-VI grubunun bir üyesidir ve optik ve elektrik özellikleri, oda sıcaklığında 0.41 eV'lik dar bir enerji bandı boşluğuna sahip olduğundan değişebilir [3]. Kızılötesi dedektörler, güneş hücreleri ve gaz dedektörleri gibi çok çeşitli teknolojik alanlarda PbS kullanımı mevcuttur [4-6]. Yarı iletken ince film malzemelerinin kalitesini iyileştirmenin en etkili yöntemlerinden biri, metal iyonları olan ince filmlerin katkılanmasıdır [7, 8]. İnce filmin kristal yapısı, yüzey morfolojisi ve parçacık boyutu katkılama ile kontrol edilebilir. Böylece sentezlenmiş ince filmlerin kimyasal ve fiziksel özellikleri sentez sırasında artmaktadır [9, 10]. Fe-alaşımlı PbS ince filmlerin yapısal, optik ve morfolojik özellikleri ile ilgili araştırmalar sınırlıdır [11, 12].

[1]*Corresponding author: Siirt Üniversitesi Sağlık Yüksek Okulu, 56100 Siirt, aekinci@siirt.edu.tr*
[2]*Siirt Üniversitesi Müh. Mim. Fakültesi Elektrik ve Elektronik Bölümü, 56100 Siirt, sabithoroz@siirt.edu.tr*
[3]*Siirt Üniversitesi Müh. Mim. Fakültesi, Kimya Mühendisliği Bölümü, Siirt University, 56100 Siirt, omersahin@siirt.edu.tr*

Yarıiletken malzemeler darbeli lazer biriktirme (PLD) [13], sprey piroliz [14], ardışık iyonik katman adsorpsiyonu ve reaksiyonu (SILAR) [15], vakum buharlaşması [16] ve kimyasal banyo çökeltme (CBD) [17] gibi çeşitli teknikler kullanılarak sentezlenmektedir. Her biriktirme yönteminin kendine özgü avantajları ve dezavantajları vardır. CBD teknikleri sadeliği, ucuzluğu ve geniş alan kaplamaları elde etme kabiliyeti için tercih edilir. Bu çalışmada, farklı Fe konsantrasyonlarına sahip PbS ve Fe-alaşımlı PbS ince filmleri, oda sıcaklığında cam yüzeyler üzerinde maliyete uygun CBD tekniği ile sentezlenmiştir. Sentezlenen ince filmlerin yapısal ve optik özellikleri, X ışını kırınımı (XRD) ve optik absorpsiyon ölçümleri ile karakterize edildi. Fe katkısının PbS yapısını değiştirmemesine rağmen PbS'nin kristal boyutu ve enerji bandı boşluğunu değiştirdiği gözlenmiştir.

2. MATERYAL VE METOT

Oda sıcaklığında CBD yöntemi kullanılarak farklı Fe konsantrasyonları ile PbSve Fe-katkılı PbS ince filmler sentezlenmesi için gerekli malzemeler kurşun nitrat ($Pb(NO_3)_2$), tiyoasetamid (C_2H_5NS), demir (II) klorür tetrahidrat ($FeCI_24H_2O$), sodyum hidroksit (NaOH) ve trietanolamin (TEA) ($C_6H_{15}NO_3$) kullanıldı. 0.1 M $Pb(N0_3)_2$, 0.1 M C_2H_5NS, 0.5 M NaOH ve belirli bir miktarda TEA, bir cam alt tabaka üzerinde oda sıcaklığında PbS ince filmin sentezlenmesi için 80 mL'lik bir beherde karıştırılmıştır. Karıştırma işlemi, homojen bir çözelti elde edilene kadar sürdürüldü. Daha sonra, iyice temizlenmiş bir cam alt tabaka, çözeltiye dikey bir konumda daldırıldı. Camsubstrat yaklaşık 1 saat süreyle PbS solüsyonunda bırakıldı, daha sonra çıkarıldı, birkaç kez damıtılmış su ile yıkandı ve havada kurutuldu.

Aynı yöntemle, bir cam substrat üzerinde PbS: Fe (% 0.5), PbS: Fe (% 1), PbS: Fe (% 3) ve PbS: Fe (% 5) ince filmler, yukarıda belirtilen çözeltiye sırasıyla 0.005 M $FeCl_24H_20$ ilave edildi ve daha sonra tüm adımlar tekrarlandı.

3. ANALİZLERİN YORUMU

3.1. Yapısal Özellikler

PbS ve farklı konsantrasyonlarda Fe katkılı PbS ince filmlerinin yapısal özelliklerini incelemek için ölçülen XRD sonuçları şekilde 1' de gösterilmiştir.

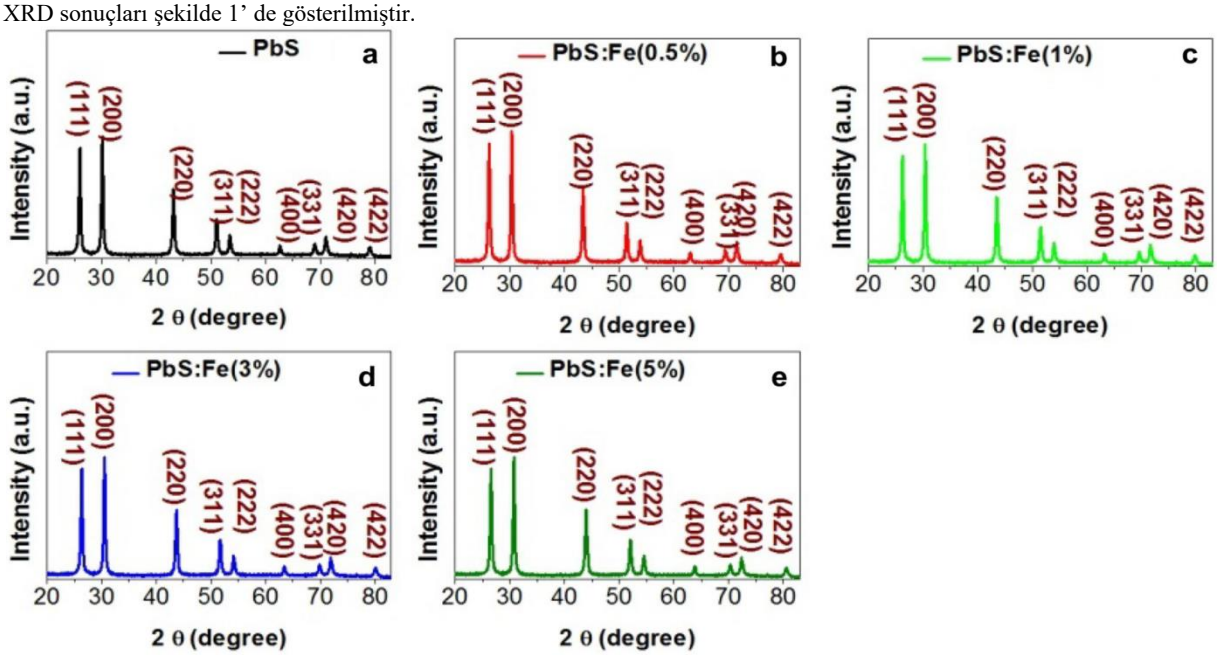

Şekil 1. a) PbS ve b – e) PbS: Fe (% 0,5), PbS: Fe (% 1), PbS: Fe (% 3) ve PbS: Fe (% 5) ince filmler için XRD kırınım desenleri.

Referans verileri kullanılarak, (111), (200), (220), (311), (222), (400), (331), (420) ve (422) düzlemlerine karşılık gelen tüm kırınım modelleri sentezlenmiş ince filmlerin kübik yapıya sahip olduğunu göstermektedir. XRD verilerinde, Fe katkısının neden olabileceği istenmeyen herhangi bir difraksiyon tepelerinin gözlemlenmesi, CBD tekniği ile PbS: Fe (% 0.5), PbS: Fe (% 1), PbS: Fe (% 3) ve PbS: Fe (% 5) ince filmlerin başarılı bir şekilde sentezlendiğinin bir göstergesidir. PbS, PbS: Fe (% 0.5), PbS: Fe (% 1), PbS: Fe (% 3) ve PbS: Fe (% 5) ince filmler için 2θ'ye karşılık gelen (111), (200) ve (220) tepe konumları Tablo 1'de verilmiştir.

Tablo 1. PbS, PbS: Fe (% 0.5), PbS: Fe (% 1), PbS: Fe (% 3) ve PbS: Fe (% 5) için sırasıyla 2θ (derece) değeri

Örnekler (ince film)	Hesaplanan d değerleri (nm)
PbS	25.97
PbS:Fe(0.5%)	24.00
PbS:Fe(1%)	23.29
PbS:Fe(3%)	22.95
PbS:Fe(5%)	21.55

Tablo l'deki sonuç, farklı Fe konsantrasyonlarına sahip Fe-katkılı PbS ince filmlerin tepe pozisyonlarının, saf PbS ince film ile karşılaştırıldığında daha büyük 2θ açı değerlerine kaydırıldığını ve bu değişimin miktarının Fe konsantrasyonuna orantılı olarak arttığını göstermektedir. PbS ve Fe arasındaki yapısal farklılıklar Fe-katkılı PbS ince filmlerinde kafes gerilmesine yol açabilir. Bu, XRD kırınım modellerinde görülen pik kaymasının nedeni olarak açıklanabilir.

3.2. Optik Özellikler

Farklı Fe konsantrasyonlarına sahip PbS ve Fe-alaşımlı PbS ince filmlerin optik absorpsiyon spektrumları, UV-Vis spektroskopisi kullanılarak yapılan ölçümlerin bir sonucu olarak Şekil 2a-e'de gösterilmektedir.

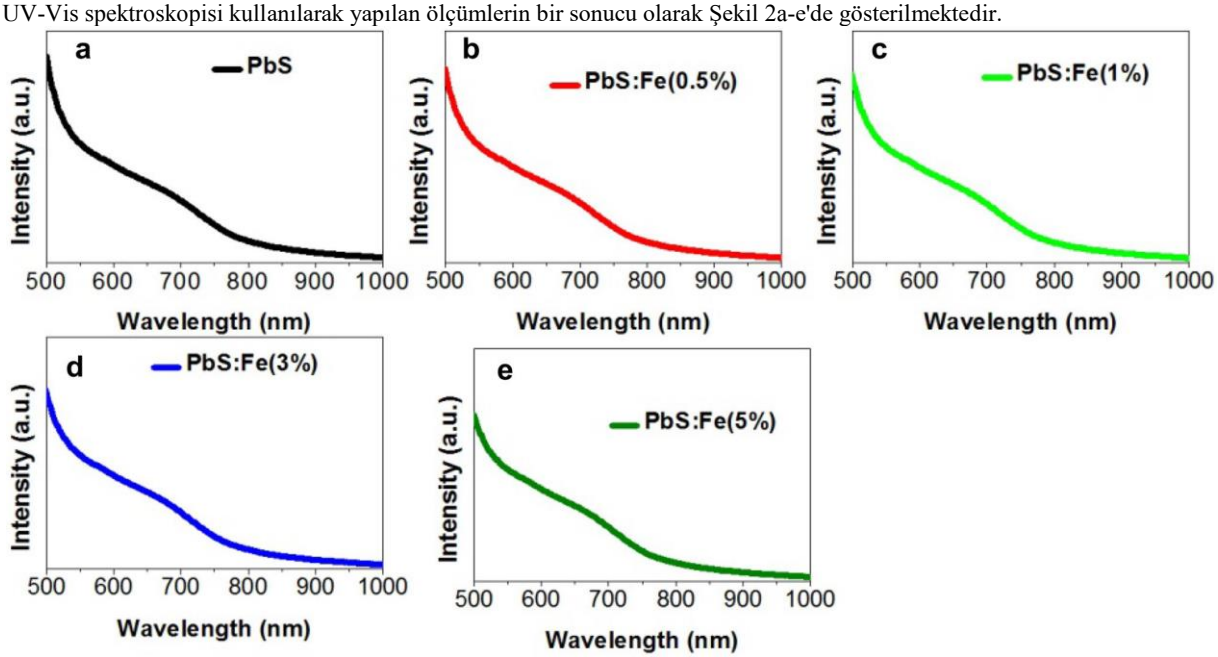

Şekil 2. a) PbS ve b – e) PbS: Fe (% 0,5), PbS: Fe (% 1), PbS: Fe (% 3) ve PbS: Fe (% 5) ince filmler için optik absorpsiyon spektrumları

Bu ölçümler, ince filmlerin enerji bandı boşluğunu belirlemek için gerçekleştirilmiştir. Şekil 2 a-e'de gösterilen verilere dayanarak, Şekil 3a-e'de gösterilen $(\alpha h\nu)^2$'ye karşı hν eğrileri, Tauc denklemi kullanılarak elde edilmiştir.

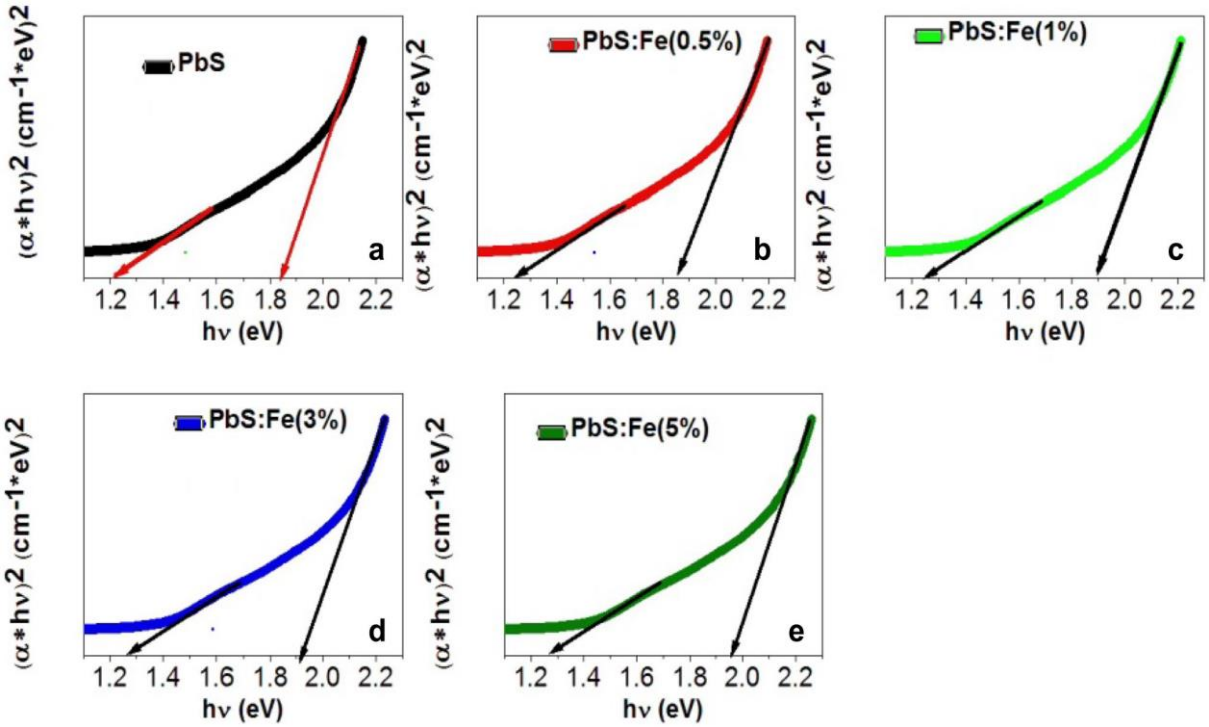

Şekil 3. a) PbS ve b – e) PbS: Fe (% 0,5), PbS: Fe (% 1), PbS: Fe (% 3) ve PbS: Fe (%5) ince filmler için hα'ya karşı (ahν) 2'nin grafikleri.

PbS ve PbS: Fe (% 0.5), PbS: Fe (% 1), PbS: Fe (% 3) ve PbS: Fe (% 5) ince filmler için elde edilen enerji bant aralığı Tablo 2'de gösterilmiştir.

Tablo 3. PbS, PbS: Fe (% 0,5), PbS: Fe (% 1), PbS: Fe (% 3) ve PbS: Fe (% 5) için bant aralığı değerinin belirlenmesi

Örnekler (NPs)	Birinci olsılık enerji band aralığı değerleri (eV)	İkinci olasılık enerji band aralığı değerderleri
PbS	1.22	1.87
PbS:Fe(0.5%)	1.24	1.89
PbS:Fe(1%)	1.25	1.92
PbS:Fe(3%)	1.27	1.94
PbS:Fe(5%)	1.29	1.98

Bu ölçümde iki önemli gözlem elde edildi. (1) Örnekler için iki olası bant aralığı gözlendi. Ayrıca, Fe-katkılı PbS ince filmlerin enerji bandı boşlukları, saf PbS'den daha geniştir. Başka bir deyişle, Fe katkılı PbS ince filmlerin absorbsiyon dalga boyları, PbS'den daha küçük dalga boylarına doğru kaymaktadır. Bu kaymanın nedeni kuantum hapsi etkisiyle ilişkili olabilir. (2) Katkılı konsantrasyonundaki artış, enerji bandı boşluğunun etkisidir. Fe katkılı PbS ince filmlerin enerji bandı boşluklarının Fe katkısının yoğunluğu arttıkça çok daha geniş olduğu görülmüştür. Bant boşluğundaki kademeli artışının nedeni, daha küçük Fe atomlarının malzemeye eklenmesidir.

4. SONUÇ

PbS, PbS: Fe (% 0,5), PbS: Fe (% 1), PbS: Fe (% 3) ve PbS: Fe (% 5) ince filmler, oda sıcaklığında maliyete uygun cam substratlar CBD tekniği üzerinde sentezlendi. Sentezlenen ince filmlerin yapısal ve optik özellikleri, sırasıyla XRD ve optik absorpsiyon ölçümleriyle karakterize edildi. Kübik yapıya sahip PbS, PbS: Fe (% 0,5), PbS: Fe (% 1), PbS: Fe (% 3) ve PbS: Fe (% 5) ince filmlerin hesaplanan kristal boyutları 25.97, 24.00, 23.29, 22.95 ve sırasıyla 21.55 nm olarak hesaplandı. Böylece Fe-katkılı PbS ince filmlerinde Fe katkısının konsantrasyonu arttıkça kristal boyutlarının azaldığı gözlenmiştir. Daha küçük Fe atomlarının

eklenmesiyle, ince filmin enerji bandı boşluğunun kristal boyutu azaldıkça daha geniş hale gelmesi beklenir. Yapılan optik ölçümler sonucunda bu beklenti teyit edilmiştir, çünkü PbS, PbS: Fe (% 0,5), PbS: Fe (% 1), PbS: Fe (% 3) ve (% 5) ince filmler için belirlenen enerji bandı boşlukları sırasıyla 1.89, 1.91, 1.94, 1.96 ve 1.99 eV olarak hesaplandı. Böylece Fe katkısının PbS yapısını değiştirmemesine rağmen PbS'nin kristal boyutu ve enerji bandı boşluğunu değiştirdiği gözlenmiştir.

KAYNAKALAR

[1]. M.R. Gao, Y.F. Xu, J. Jiang, S.H. Yu, Nanostructured metal chalcogenide: synthesis, modification, and applications in energy conversion and storagedevices. Chem. Soc. Rev. 43, 2986–3017 (2013)

[2]. F. Liu, T. Zhu, L. Hu, B. Zhang, J. Yao, M.K. Nazeeruddin, M. Gratzel, S. Dai, Low-temperature solution deposited metal chalcogenide films as highly efficient counter electrodesforsesntized solar cells. J. Mater. Chem. A 3, 6315–6323 (2015)

[3]. M. Suganya, S. Anitha, D. Prabha, S. Balamurugan, J. Srivind, A.R. Balu, Enhanced photocatalytic and antifungal properties of Sr-alloyed PbSn naopowders. Mater. Technol.:Adv. Perform. Mater. 2017, 1–6 (2017)

[4]. S. Kouissa, A. Djemel, M.S. Aida, M.A. Djouida, PbS infarred detectors: experiment and simulation. Sens. Transducers 193, 106–113 (2015)

[5]. L. Hu, A. Mandelis, X. Lan, A. Melnikov, S. Hoogland, E.H. Sargent, Imbalanced charge carriers mobility and Schottky junctioninduced anomalous current-voltage characteristics of excitonic PbS colloidal quantum dot solar cells. Sol. Energy Mater. Sol. Cells 155, 155–165 (2016)

[6]. H. Liu, M. Li, D. Voznyy, L. Hu, Q. Fu, D. Zhou, Z. Xia, E.H. Sargent, J. Tang, Physically flexible, rapid-response gassens orbased on colloidal quantum dot solids. Adv. Mater. 26, 2718–2724 (2014)

[7]. Y. Zhang, J. Hao, Metal-ion alloyed luminescent thin films for optoelectronic applications. J. Mater. Chem. C. 1, 5607–5618 (2013)

[8]. S. Vadivel, G. Rajarajan, Effect of Mg alloying on structural, optical and photocatalytic activity of SnO2 nanostructure thin films. J. Mater. Sci.: Mater. Electron. 26, 3155–3162 (2015)

[9]. S. Ravishankar, A.R. Balu, V.S. Nagarethinam, Effect of Gd3+ions on the thermal behavior, optical, electrical and magnetic properties of PbS thin films. J. Electron. Mater. 47, 1271–1278 (2018)

[10]. B. Touati, A. Gassoumi, N.K. Turki, Structural, optical and electrical properties of Agalloyed PbS thin films: role of Ag concentration. J. Mater. Sci.: Mater. Electron. 28, 18387–18395 (2017)

[11]. K.N.C. Kumar, S.K.K. Pasha, K. Deshmush, K. Chidambaram, G.S. Muhammed, Optical analysis of iron-alloyed lead sulfide thin films for optoelectronic applications. Int. J. Nanosci. 17, 1760004 (2018)

[12]. M.A. Rahma, H.L. Saadon, M.A. Mahdi, All-photonic switching based on selective input pumb polarization states in Fe-alloyed PbS/PVA free standing nanocomposite films. J. Phys. D: Appl. Phys. 50, 110649 (2017)

[13]. M. Frumar, B. Frumarova, P. Nemec, T. Wagner, J. Jedelsky, M. Hrdlicka, Thin chalcogenide films prepared by pulsed laser deposition—new amorphous materials applicable in optoelectronics and chemical sensors. J. Non-Cryst. Solids 352, 544–561 (2006)

[14]. T. Sall, B.M. Soucase, M. Mollar, J.A. Sons, SnS thin films prepared by chemical spray pyrolysis at differentsusbtrate temperatures for photovoltaic applications. J. Mater. Sci. 46, 1714–1719 (2017)

[15]. F. E.Guneri, S. Gode, Cevik, Influence of grain size on structural and opticproperties of PbS thin films produced by SILAR method. Thin solid films. 589, 578–583 (2015)

[16]. N. Memarian, S.M. Rezati, I. Concina, A. Vomiero, Deposition of nanostrucutred CdS thin films by thermal evaporation method: effect of substrate temperature. Materials 10, 773 (2017)

[17]. S. Thirumavalavan, K. Mani, S. Suresh, Investigation on structural, optical, morphological and electrical properties of lead sulfide (PbS) thin films. J. OvonicRes. 11, 123–230 (2015)

ICACCHE

2nd International Conference on Applications in Chemistry and Chemical Engineering

www.icacche.com